

The climatic and environmental conditions during deposition of phosphorites and oil shales in the Late Cretaceous upwelling system of the Negev/Israel

Dissertation
zur Erlangung des Doktorgrades
der Naturwissenschaften

vorgelegt beim Fachbereich Geowissenschaften
der Johann Wolfgang Goethe-Universität
in Frankfurt am Main

von
Heiko Alsenz
aus Bingen

Frankfurt (2014)
(D 30)

Vom Fachbereich Geowissenschaften / Geographie
der Johann Wolfgang Goethe-Universität als Dissertation angenommen.

Dekan: Prof. Dr. Andreas Junge

Gutachter: Prof. Dr. Wilhelm Püttmann
Prof. Dr. Wolfgang Oschmann
Prof. Dr. Silke Voigt
Prof. Dr. Ruprecht Schleyer

Datum der Disputation: 12. März 2015

Table of Contents

List of Tables	6
List of Figures	7
Danksagung	10
Abbreviations	12
Zusammenfassung.....	13
Summary.....	25
Introduction	28
1 Sea surface temperature record of a Late Cretaceous tropical southern Tethys upwelling system.....	40
1.1 Abstract	40
1.2 Introduction.....	40
1.3 Materials and methods	43
1.3.1 Paleogeographical setting	43
1.3.2 Material and study sites	44
1.4 Sample preparation	46
1.5 TEX ₈₆ analysis	47
1.6 Results.....	50
1.7 Discussion	52
1.7.1 Late Cretaceous SSTs and cooling history	52
1.7.2 Late Cretaceous equatorial to polar SST gradient	57
1.7.3 Comparison of SSTs in inner and outer belts of the southern Tethyan upwelling system	58
1.8 Conclusion	60
2 Geochemical evidence for the link between sulfate reduction, sulfide oxidation and phosphate accumulation in a Late Cretaceous upwelling system	61
2.1 Abstract	61
2.2 Introduction.....	62
2.3 Material and methods.....	64
2.3.1 Location and samples	64
2.3.2 Sample preparation and analysis	66

2.4	Results and discussion.....	68
2.4.1	TOC, TFe, TS and TP	68
2.4.2	Correlation of TOC and TS.....	70
2.4.3	Correlation of TOC, TS and TFe	72
2.4.4	Correlation of phosphate precipitation with sulfate reduction.....	75
2.4.5	Fatty acid analysis.....	79
2.5	Summary and conclusions.....	82
3	Geochemical characterization of the Campanian/Maastrichtian upwelling system from Negev (Israel) and influence of natural sulfurization on the preservation of organic matter	84
3.1	Abstract	84
3.2	Introduction	84
3.3	Material and methods	87
3.3.1	Location and samples.....	87
3.3.2	Sample preparation and analysis.....	88
3.4	Results and discussion.....	88
3.4.1	Molecular composition of hydrocarbons	89
3.4.1.1	Straight chain alkanes	89
3.4.1.2	C ₂₇ -C ₂₉ Steranes.....	91
3.4.1.3	Indicators of paleosalinity (chromans)	92
3.4.1.4	Pentacyclic triterpanes	94
3.4.1.5	Straight chain and C ₂₀ -isoprenoid thiophenes	95
3.4.1.6	C ₂₇ -C ₂₉ -Epithiosteranes.....	97
3.4.1.7	Sulfur containing hopanoids.....	99
3.4.1.8	Degree of OM sulfurization.....	104
3.5	Summary and conclusions.....	106
4	Paleoceanographic reconstruction of the Late Cretaceous oil shale of the Negev, Israel: Integration of geochemical, and stable isotope records of the organic matter.....	107
4.1	Abstract	107
4.2	Introduction.....	108

4.2.1	The high-productivity sequence in Israel	108
4.2.2	Background on the foraminiferal assemblages	110
4.3	Materials and methods	111
4.3.1	Location and samples	111
4.3.2	Sample analyses	113
4.4	Results	116
4.4.1	TOC, TON and C/N	116
4.4.2	Pristane/Phytane (Pr/Ph) ratio	117
4.4.3	Organic N and C isotopes	117
4.4.4	Organic petrology	117
4.5	Discussion	118
4.5.1	TOC	118
4.5.2	Organic petrology	118
4.5.3	TON and C/N ratio	119
4.5.4	Pr/Ph ratio	121
4.5.5	$\delta^{13}\text{C}_{\text{org}}$	122
4.5.6	$\delta^{15}\text{N}_{\text{org}}$	125
4.5.7	The depositional environment of the Negev high productivity sequence: integration of geochemical and foraminiferal characteristics	126
4.6	Summary	127
5	Conclusions and future implications	130
5.1	Paleoclimatic changes and paleo sea surface temperature of the upwelling system	130
5.2	Natural sulfurization	131
5.3	Phosphate deposition in the context of sulfate reduction and sulfide oxidation	132
5.4	Bulk geochemical and isotopic implications	133
	References	135
	Appendix	155
	Publications	207
	Curriculum Vitae	209

List of Tables

Table 1	SST ranges of the Shefela basin and the Efe Syncline sampling site calculated using different calibration models.	50
Table 2	Equator-to-pole SST gradients of the modern earth climate system and suggestions for the Late Cretaceous.	56

List of Figures

Figure 1:	Distribution of the continents and oceans during the Cretaceous at 80 Ma and 69 Ma, modified after Hay et al. (1999) and Scotese (2002).	29
Figure 2:	General illustration of the development of upwelling systems at continental margins (modified after Williams (2011)).	32
Figure 3:	Schematic overview of the global phosphorus cycle (modified after Ruttenberg (2003); Paytan and McLaughlin (2007)).	33
Figure 4:	Illustration of the suggested environmental conditions during the deposition of the three different facies types: A) the Phosphate Member, B) the Oil Shale Member and C) the Marl Member.....	36
Figure 5:	Illustration of the geochemical reactions in sulfide oxidizing bacteria populated sediments modified after (Dale et al., 2009; Dale et al., 2013).	37
Figure 6:	Foraminifera and <i>Thioploca</i> filaments in the oxygen minimum zone off Chile.	39
Figure 7:	Location map for the two studied areas.....	45
Figure 8:	Age, stratigraphic data, lithology and sea surface temperature (SST) based on TEX ₈₆ data plotted against depth for studied sections from (A) Aderet 1 borehole and (B) PAMA quarry.	48
Figure 9:	Distribution of reconstructed SSTs covering the Santonian to early Maastrichtian from this study and other published data (all values given in appendix Table A-3).	54
Figure 10:	Location map for the studied area.	65
Figure 11:	Stratigraphy, age, depth and lithological profile (cf. Ashckenazi-Polivoda et al. (2011)).	69
Figure 12:	Plot of TS vs. TOC according to Berner and Raiswell (1983) with modifications adopted from Leventhal (1995).	71

Figure 13:	Ternary plot of TOC, TS and TFe according to Dean and Arthur (1989).	74
Figure 14:	Correlation diagram of TP[%] and TOC/TOC _{OR} ratio.	76
Figure 15:	Schematic illustration of bacterial sulfate reduction and sulfide oxidation under changing redox conditions and the effect on the phosphate deposition (Modified after Brock and Schulz-Vogt (2011) and Dale et al. (2013))	77
Figure 16:	Distribution of the saturated fatty acids C _{16:0} and C _{18:0} and the monounsaturated fatty acid C _{18:1ω9} over the profile. Concentrations are shown in μg/g C _{org}	80
Figure 17:	Location map for the studied area.	87
Figure 18:	Mass chromatogram m/z 57 and total ion current (TIC) with the distribution of n-alkanes, pristane and phytane in the saturated hydrocarbon fraction of sample SAOS 95 (IS = internal standard)	90
Figure 19:	Ternary diagram showing the relative abundances of C ₂₇ -, C ₂₈ - and C ₂₉ -steranes.	91
Figure 20:	Relationship between pristane/phytane and the methyltrimethyltridecyl-chroman (MTTC) ratio in Cretaceous sediments of the Tethys.	92
Figure 21:	Concentration of straight chain and isoprenoid thiophenes along the profile.	96
Figure 22:	Suggested mechanism of the C ₂₈ -epithiosterane formation derived from 24-methyl-5α-cholesta-7,22-dien-3β-ol modified after ten Haven et al. (1986) and (Mackenzie et al., 1982).	98
Figure 23:	The total ion current (TIC) and mass chromatogram m/z 97+111 and m/z 191 of the aromatic hydrocarbon fraction of sample SAOS 189 (Negev/Israel) with the distribution of the sulfur containing hopanoids.	100

Figure 24:	Mass spectra and molecular structures of the two hopanoid thiophenes with molecular ions at m/z 522 observed in the OSM, sample SAOS 189, of the Ghareb Formation.	101
Figure 25:	Stage, formation, depth and profile of the analyzed sediments, proportions of TOC and S are given in percent. The concentration variation along the profile is shown for the hopanoid thiophenes in $\mu\text{g/g}$ TOC.	104
Figure 26:	Paleogeography map shows the upwelling belts developed along the southern Tethys margin during the Late Campanian and Early Maastrichtian. Star marks the inferred position of Negev region within the Levant upwelling belt. From Ashckenazi-Polivoda et al. (2011).	109
Figure 27:	A. Schematic correlation of the Late Cretaceous formations in Israel modified after Reiss et al. (1985).	112
Figure 28:	Stratigraphy, lithology, TOC and P and B-Type assemblages of the studied section at PAMA quarry.	114
Figure 29:	Geological map (1:250,000) of northern Negev modified after Shahar and Wurzbürger (1967). The PAMA quarry is located in the Efe Syncline, where one of the largest oil shale reservoirs of southern Israel occurs. From Ashckenazi-Polivoda et al. (2011).	115
Figure 30:	TOC, TON, Pr/Ph, C/N, $\delta^{13}\text{C}_{\text{org}}$ and $\delta^{15}\text{N}_{\text{org}}$ and foraminiferal assemblage records of the studied sequence.	116
Figure 31:	Selected photos from the organic petrological analysis.	120
Figure 32:	$\delta^{13}\text{C}_{\text{org}}$ vs. C/N ratios.	122
Figure 33:	TON vs. TOC.	123
Figure 34:	$\delta^{15}\text{N}_{\text{org}}$ vs. $\delta^{13}\text{C}_{\text{org}}$	124

Danksagung

Die vorliegende Arbeit entstand im Rahmen des GIF-Projekts (The German-Israeli Foundation for Scientific Research and Development) Nr. 956-38.8/2007 in der Arbeitsgruppe Umweltanalytik von Herrn Prof. Dr. Wilhelm Püttmann am Institut für Atmosphäre und Umwelt der Goethe-Universität Frankfurt am Main.

Herrn Prof. Dr. Wilhelm Püttmann gilt mein ganz besonderer Dank für die überaus interessante und anspruchsvolle Themenstellung. Weiterhin möchte ich ihm ganz besonders für seine intensive Betreuung und wertvolle Hilfe bei der Erstellung der Publikationen und der Anfertigung dieser Arbeit danken. Ganz besonders möchte ich mich für die Ermöglichung der Forschungsaufenthalte in Spanien und Israel bedanken.

Bei Herrn Prof. Dr. Wolfgang Oschmann vom Institut für Geowissenschaften der Goethe-Universität Frankfurt möchte ich mich für die Übernahme des Koreferats bedanken.

Vielen Dank richte ich auch an die gesamte Arbeitsgruppe Umweltanalytik, für das so freundliche Arbeitsklima, dass sie mich mit viel Engagement während meiner Versuche unterstützt, mir stets beigestanden und geholfen haben. Vielen Dank Arlen Adriana Guedez Orozco, Claudia Christ, Julia Regnery, Paola Rua-Gomez, Sri Widodo, Theodoros Potouridis, Apl.-Prof. Dr. Fathi Zereini, Cathrin Wallner, Haris Widayat, Daria Stepien und Claudia Ament für einen doch immer sehr fröhlich gestalteten Laboralltag.

Für den interessanten Forschungsaufenthalt und die Einführung in die Bedienung von Fluoreszenzmikroskopen möchte ich mich bei Dr. Angeles G. Borrego vom Instituto Nacional del Carbón in Oviedo, Spanien bedanken.

Bei Aaron Meilijson, Libby Ron-Yankovich und Sarit Ashckenazi-Polivoda möchte ich mich ganz besonders für die Gastfreundschaft und schöne Zeit während meines Forschungsaufenthalts in Israel bedanken und für die hilfreichen Kommentare, die zum Gelingen unseres Manuskripts beigetragen haben.

Ein besonderer Dank geht an Dr. Sigal Abramovich und Prof. Dr. Shimon Feinstein vom Institut für Geo- und Umweltwissenschaften der Ben-Gurion University of the Negev in Be'er Sheva und Dr. Ahuva Almogi-Labin vom Israelischen Amt für Bodenforschung in Jerusalem für Ihre herzliche Gastfreundschaft während des For-

schungsaufenthalts in Israel und für die vielen konstruktiven Ideen, Hinweise und das sorgfältige Lesen der Manuskripte.

Auch Dr. Zsolt Berner vom Institut für Mineralogie und Geochemie am Karlsruher Institut für Technologie (KIT) möchte ich für seine Unterstützung während des Publikationsprozesses und die nette Kollaboration bedanken.

Besonderer Dank gilt Peter Illner vom Institut für Mineralogie und Geochemie am Karlsruher Institut für Technologie (KIT) für seine stete Bereitschaft zu hilfreichen wissenschaftlichen Diskussionen und für den regen Austausch von Informationen.

Bei Robert Sitals und Werner Haunold möchte ich mich ganz besonders für die Unterstützung bei allen technischen Fragen und Problemen bedanken.

Doris Bergmann-Doerr und Dagmar Schneider vom Institut für Physische Geographie der Goethe-Universität Frankfurt danke ich für die sehr freundliche Unterstützung bei der Messung der organischen Kohlenstoffgehalte.

Ein ganz besonderer Dank gilt meinen Eltern und meiner Schwester, die mich während meines gesamten Studiums immer unterstützt und motiviert und mir das Studium ermöglicht haben.

Ein ganz besonders herzlicher und liebevoller Dank geht an Eva Schweikhard, die mich durch alle Höhen und Tiefen der Promotion begleitet und mich immer unterstützt und motiviert hat.

Abbreviations

ATP	Adenosine triphosphate
CMBE	Campanian/Maastrichtian boundary event
C/N ratio	Carbon-to-nitrogen ratio
DNA	Deoxyribonucleic acid
EAG	Equatorial Atlantic Gateway
GC-MS	Gas chromatography-mass spectrometry
GDGT	Glycerol dialkyl glycerol tetraethers
HPLC-MS/MS	High-performance liquid chromatography-tandem mass spectrometry
JED	Jurf ed Darawish
MM	Marl member
OM	Organic matter
OMZ	Oxygen minimum zone
OSC	Organic sulfur compound
OSM	Oil shale member
PM	Phosphate member
SST	Sea surface temperature
TCC	Tethys Circumglobal Current
TEX ₈₆	TetraEther indeX of tetraethers consisting of 86 carbon atoms
TFe	Total iron
TOC	Total organic carbon
TOC _{OR}	Original TOC
TON	Total organic nitrogen
TP	Total phosphorus
TS	Total sulfur

Zusammenfassung

Im Rahmen dieser Dissertation wurden Untersuchungen an Ölschiefen und Phosphoriten in einem Profil aus dem Tagebau Mishor Rotem (Efe Synkline) in der Wüste Negev und einem Bohrkern aus dem Shefela Becken in Zentralisrael im Rahmen des GIF Projektes Nr. 956-38.8/2007 (GIF The German-Israeli Foundation for Scientific Research and Development) durchgeführt.

In einer multidisziplinären Kooperation von drei wissenschaftlichen Gruppen wurden Untersuchungen an diesen Proben durchgeführt. Die Arbeitsgruppe Mikropaläontologie, am Institut für Geo- und Umweltwissenschaften der Ben-Gurion University of the Negev in Be'er Sheva (Israel), befasste sich mit der Untersuchung der planktischen und benthischen Foraminiferen, um Aussagen über die Produktivität und den Sauerstoffgehalt in der Wassersäule während der Ablagerung der Sedimente zu treffen. Das Auftreten bestimmter benthischer Foraminiferen in den Proben ließ zudem eine grobe Abschätzung der Gewässertiefe zu. Anhand der vorhandenen Foraminiferen war auch eine zeitliche Einordnung der Sedimente mittels Biostratigraphie möglich. Die Arbeitsgruppe Geo- und Umweltwissenschaften am Institut für Mineralogie und Geochemie am Karlsruher Institut für Technologie (KIT) analysierte die Haupt- und Spurenelemente und führte ^{13}C -Isotopenmessungen sowie S-Isotopen-Bestimmungen an verschiedenen Schwefelspezies durch. Die Arbeitsgruppe Umweltanalytik am Institut für Atmosphäre und Umwelt der Goethe-Universität Frankfurt am Main war mit der organisch-geochemischen Analytik der Proben betraut, um aus der Zusammensetzung der Biomarker auf die Sedimentationsbedingungen während der Ablagerung der Sedimente zurückschließen zu können.

Die Ziele der organisch-geochemisch ausgerichteten Arbeitspakete waren:

1. Rekonstruktion der Paläo-Oberflächentemperatur im Wasser des *Upwelling*-Systems während der Ablagerung des analysierten Sedimentprofils aus dem Bohrkern des Shefela Beckens und dem Aufschluss in der Efe Synkline.
2. Mögliche Gründe für die hohe Anreicherung von Phosphat im Sediment und den plötzlichen Übergang von den Phosphoriten zu der Ölschieferfazies zu ermitteln.
3. Eine Erklärung für die hohen Gehalte an Schwefel im Sediment sowie die gute Konservierung der organischen Substanz zu liefern.

Im Rahmen dieser Untersuchungen wurden zwei verschiedene Probensätze bearbeitet. Einerseits Proben aus einem frischen Aufschluss im Tagebau Mishor Rotem (Efe Syncline) und andererseits ein Bohrkern aus dem Shefela Becken. Der erstgenannte Probensatz repräsentiert ein Profil von ca. 50 m Länge, welches in 211 Einzelproben unterteilt wurde. Dieses setzt sich aus drei scharf abgegrenzten Fazies-Typen zusammen, der Phosphorit-Fazies (*Phosphate Member*, PM) an der Basis des Profils (5,4 m mächtig), der zur Mishash Formation gehört, der Ölschiefer-Fazies (*Oil Shale Member*, OSM) im zentralen Bereich des Profils (41 m mächtig) und dem anschließend abgelagerten Mergel (*Marl Member*, MM) (2,8 m mächtig), die beide zur Ghareb Formation gehören. Die analysierten Sedimente wurden insgesamt über einen Zeitraum von ca. 1,8 Millionen Jahren, vom späten Campanium bis zum frühen Maastrichtium (vor etwa 71,6 bis 69,8 Millionen Jahren) abgelagert. Diese Ablagerung fand in einem tropischen küstennahen Auftriebsgebiet in der südlichen Tethys zwischen 8° und 15° nördlicher Breite statt.

Bei dem zweiten Probensatz handelt es sich um einen Bohrkern aus dem Shefela Becken, der bis in eine Tiefe von 600 m erbohrt wurde. Davon wurde der Abschnitt zwischen 265 m Tiefe und 600 m Tiefe (Länge von 335 m) beprobt. Von den insgesamt 339 Proben, die im Abstand von etwa 1 m genommen wurden, wurden 102 Proben mit einem Abstand von 3 m für die vorliegende Arbeit ausgewählt. Das Probenmaterial bestand überwiegend aus einem dunklen, bituminösen Kalk mit wenigen dunklen dünnen Mergellagen, welches zur Ein Zeitim Formation gehört. Unterbrochen wird diese Formation von einem 8 m mächtigen Einschub der Mishash Formation bei einer Tiefe von 530 m. Die biostratigraphischen Untersuchungen am gesamten Kern haben gezeigt, dass die Sedimente über einen Zeitraum von etwa 17 Millionen Jahren, vom Santonium bis zum Maastrichtium (etwa 85–68,3 Mio. Jahre) abgelagert wurden. Diese Probenlokation ist im Vergleich zum Tagebau Mishor Rotem in einem küstenferneren Bereich des ehemaligen Auftriebsgebietes gelegen (im Bereich der Schelfkante oder des Kontinentalhanges).

In Auftriebsgebieten oder *Upwellings* steigen nährstoffreiche, kalte Tiefenwasser an die Oberfläche und führen zu einer Abkühlung der Temperatur im oberflächennahen Meerwasser. Durch die vielen gelösten Nährstoffe, die in diesen aufsteigenden Wassermassen enthalten sind, wird die Bioproduktion enorm angeregt. Der Auftrieb in Küstengebieten wird durch starke Winde parallel zur Küste hervorgerufen, in diesem

Fall Passatwinde aus nordöstlicher Richtung, die am südlichen Rand der Tethys ein hochproduktives Auftriebsgebiet entstehen ließen. Dabei bewegen sich die oberen vom Wind beeinflussten Wasserschichten im rechten Winkel zur Windrichtung und somit von der Küste weg. Es kommen Strömungen zustande, die auf dem sogenannten „Ekman-Transport“ basieren, die nährstoffreiche kühle Tiefenwässer in Küstennähe zur Oberfläche strömen lassen. Ein derartiges *Upwelling* existierte im Untersuchungsgebiet vom Santonium bis zum Maastrichtium über 19 Millionen Jahre lang. Für die Rekonstruktion der Meeresoberflächentemperatur und den Vergleich der Temperaturen innerhalb des Auftriebsgebietes wurden beide Probensätze eingehend untersucht.

Schouten et al. (2002) hat eine auf der Analytik von organischen Biomarkern basierende Methode zur Bestimmung der Meeresoberflächentemperatur entwickelt. Hierbei wird die relative Häufigkeit von Glycerol-Dialkyl-Glycerol-Tetraethern (GDGTs, Strukturen der GDGTs befinden sich im Anhang A1-6) mit Hilfe von HPLC-MS/MS (Hochdruckflüssigkeitschromatographie gekoppelt mit Tandem Massenspektrometrie) ermittelt. Diese Verbindungen stellen Lipide in den Membranen von Archaeen dar. Der Einbau von Cyclopentan- und Hexanringen in das Molekül ist abhängig von den Temperaturbedingungen, unter denen die Archaeen leben. Je höher die Temperatur, desto mehr Cyclopentan-Ringe werden in die GDGTs eingebaut (Schouten et al., 2013). Zur Kalibrierung der Methode wurden 40 Oberflächensedimente aus verschiedenen Klimazonen eines globalen Probensets untersucht. Dabei fand man heraus, dass das Verhältnis der relativen Häufigkeiten der GDGTs (TEX_{86} = Tetraether index of tetraethers consisting of 86 carbon atoms) linear mit der mittleren marinen Jahresoberflächentemperatur im ursprünglichen marinen System korreliert (Schouten et al., 2002). Daher kann man mit Hilfe der Analyse von GDGTs die Oberflächentemperatur von Meerwasser (SST) rekonstruieren. Die Rekonstruktion der Temperatur basiert auf der folgenden von Schouten et al. (2002) vorgeschlagenen Formel:

$$\text{TEX}_{86} = 0,015 \cdot \text{SST} + 0,28 \quad \text{Gl. 1}$$

Die Rekonstruktion der Meeresoberflächentemperatur aus den Sedimenten des Shetland Beckens anhand des TEX_{86} zeigte einen deutlichen Temperaturrückgang am Übergang vom Santonium zum Campanium. Dieser Rückgang um etwa 7 °C wird

mit der Öffnung und Vertiefung der Verbindung zwischen Nord- und Südatlantik und den dadurch geänderten Strömungsverhältnissen der Mittel- und Tiefenwasserströme mit kälteren Wassermassen aus dem Südatlantik erklärt (EAG = Equatorial Atlantic Gateway) (Friedrich et al., 2012). Vor etwa 76 Mio. Jahren kam es dann zu einer weiteren massiven Abkühlung der Oberflächentemperatur des Wassers um etwa 8 °C im Auftriebsgebiet der südlichen Tethys, die zeitlich mit einem starken Anstieg der Primärproduktion zusammenfällt. Eine Verstärkung des aufsteigenden nährstoffreichen Tiefenwasserstroms war vermutlich dafür verantwortlich.

Am Ende des Campaniums vor etwa 70 Mio. Jahren kam es zu einer erneuten weltweiten Abkühlung der Meereswasseroberflächentemperaturen. Dieses Phänomen wird als „Campanian/Maastrichtian boundary event“ (CMBE) bezeichnet (Koch and Friedrich, 2012). Interessanterweise finden sich die Spuren dieser Abkühlung auch in den untersuchten Sedimenten aus dem Shefela Becken, allerdings mit einer Verzögerung von etwa 1 Mio. Jahren, bei etwa 69 Mio. Jahren.

Am Ende des Maastrichtiums, vor etwa 70 Mio. Jahren bis 68 Mio. Jahren kam es zu einer globalen Erwärmung der Ozeane um 2 bis 6 °C (Abramovich et al., 2010), die mittlere jährliche Oberflächentemperatur in der südlichen Tethys stieg von etwa 25 °C auf etwa 31 °C.

Die Kreidezeit gilt in der Erdgeschichte als sehr warme Periode. Frühere Studien zur Oberflächentemperatur des Meerwassers in der Kreidezeit kamen zu dem Ergebnis, dass es zwischen den Oberflächentemperaturen der äquatorialen und polaren Region lediglich einen Unterschied von 15 °C gab bzw. dass dieser sogar noch geringer ausfiel (z.B. Huber et al., 2002; Jenkyns et al., 2004). Der Oberflächentemperaturunterschied des Meerwassers zwischen der Äquator- und der nördlichen Polregion liegt heutzutage bei etwa 30 °C (entsprechend einer Änderung von etwa 0,4 °C/Breitengrad). Die Lufttemperatur unterscheidet sich heute um etwa 0,6 °C/Breitengrad, zwischen dem Äquator und der nördlichen polaren Region (Amiot et al., 2004). Bezüglich des Lufttemperatur-Gradienten zwischen Äquator und Pol in der Kreidezeit geht man beim derzeitigen Forschungsstand von etwa 0,4 °C/Breitengrad aus (Amiot et al., 2004). Unter der Annahme, dass das Verhältnis zwischen der Oberflächentemperatur der Luft und des Meerwassers seit der Kreidezeit gleich geblieben ist, müsste sich daraus ein Temperaturgradient im Meerwasser von etwa 0,26 °C/Breitengrad, zwischen der äquatorialen und polaren Region ergeben. Aufgrund

der im Rahmen der vorliegenden Arbeit ermittelten Daten aus dem Shefela-Becken und Literaturdaten für die polare Region in der Kreidezeit (Amiot et al., 2004; Davies et al., 2009) lässt sich für den Äquator-Pol-Gradienten im Zeitraum zwischen 71,6–69,8 Mio. Jahren ein Temperaturunterschied von 22 °C (0,3 °C/Breitengrad) ableiten, welcher sehr gut mit der Annahme von 0,26 °C/Breitengrad übereinstimmt.

Die Temperaturänderungen in einem Teilbereich der beiden Profile konnten direkt miteinander verglichen werden, da sie im selben Zeitraum im späten Campanium und dem frühen Maastrichtium (71,6–69,8 Mio. Jahren) abgelagert wurden. Diese Proben wurden dazu benutzt, den Temperaturunterschied zwischen dem küstennahen und küstenfernen Bereich des Auftriebsgebietes zu untersuchen. Aufgrund des kühleren, nährstoffreichen Wassers, welches in Küstennähe aufsteigt, sollte das Oberflächenwasser dort eine niedrigere Temperatur besitzen als dies im küstenferneren Bereich der Fall ist. Anhand der TEX₈₆-Daten zeigte sich, dass es einen mittleren Temperaturunterschied zwischen dem inneren und äußeren Schelfbereich des Auftriebsgebietes von 1,5 °C gab. Dies ist durchaus mit modernen Auftriebsgebieten wie dem vor der Küste Kaliforniens oder dem Benguela Auftriebsgebiet vor Namibia vergleichbar (Zaytsev et al., 2003; Santos et al., 2012). Der Temperaturabfall zu dieser Zeit, der sowohl im Shefela Becken als auch im Bereich der Efe Syncline zu beobachten ist, lässt sich vermutlich auf einen intensiveren Auftrieb von kühlem Tiefenwasser zurückführen.

Ein weiterer wichtiger Aspekt dieser Arbeit war es den Zusammenhang zwischen der von Bakterien betriebenen Sulfatreduktion und Sulfidoxidation und der Ablagerung von Phosphat in der PM eingehend zu untersuchen und zu erklären. Diese Vorgänge sind darüberhinaus eng mit der Konservierung von organischem Material durch Schwefel im Bereich des OSM verknüpft.

In dem Sediment des OSM aus der Efe Syncline, führten die anhaltende Sulfatreduktion und anoxische Bedingungen zu einer Anreicherung von Schwefel in der organischen Matrix. Die Auftragung des gesamten organischen Kohlenstoffs (*Total Organic Carbon*, TOC) gegen den Gesamtschwefel (*Total Sulfur*, TS) zeigt eine gute Korrelation von $R^2=0,85$. Empirisch wurden C/S Verhältnisse für verschiedene Ablagerungsmilieus ermittelt. Unterhalb eines C/S Verhältnisses von 2,8 handelt es sich um euxinische Milieus, normal marine Systeme zeichnen sich durch ein C/S-Verhältnis zwischen 2,8 und 3,6 aus. C/S-Verhältnisse über 10 charakterisieren normalerweise

nicht-marine Systeme (Berner and Raiswell, 1983; Berner and Raiswell, 1984; Leventhal, 1995). Die Ölschieferproben aus dem Aufschluss von Mishor Rotem zeigten einen erhöhten C/S Wert von 6,5. Das H₂S, welches durch die Sulfatreduktion entstanden ist, wurde aufgrund des geringen Eisengehaltes im Wasser nur zu einem geringen Teil als Eisenmonosulfid gefällt. Der Eisenmangel führte dazu, dass der Schwefel mit der organischen Substanz im Sediment reagierte und dadurch die weitere Zersetzung des organischen Materials durch Bakterien verhinderte. Dieser Vorgang hat zur weitgehenden Erhaltung des organischen Kohlenstoffs im Sediment beigetragen. Aufgrund der Messdaten und aus der Literatur ist von einem organisch gebundenen Anteil des Schwefel von etwa 60-90 % des Gesamtschwefels im Sediment auszugehen (Dinur et al., 1980; Amrani et al., 2005). Die Korrelation dieser drei Parameter Eisen, Schwefel und organischer Kohlenstoff zeigt deutlich einen Mangel an reaktivem Eisen über den kompletten Ablagerungszeitraum an. Im unteren Bereich der Ölschiefer-Sequenz gab es einen Überschuss an reduzierten Schwefelspezies, die mit der organischen Substanz reagierten. Lediglich während der Ablagerung des Mergels gab es weniger reaktives organisches Material, als zur bakteriellen Sulfatreduktion notwendig gewesen wäre. Aus den Daten zum Schwefelgehalt und dem organischen Kohlenstoff kann die vor der Sulfatreduktion vorhandene ursprüngliche Menge an organischem Kohlenstoff bestimmt werden (*original Total Organic Carbon*, TOC_{OR}). Mit Hilfe der Korrelation des Verhältnisses von TOC/TOC_{OR} und dem Gehalt an Phosphor in dem Sediment wird deutlich, dass im Bereich der höchsten Sulfatreduktion auch die höchsten Konzentrationen an Phosphat zu finden sind. Die modernen Auftriebsgebiete der Ozeane stellen die Hauptentstehungsgebiete von phosphatmineralhaltigen Sedimenten dar. Auch in der Efe Synkline fand Phosphatablagerung statt, in signifikant erhöhter Konzentration sind diese Mineralien aber nur im Bereich der Phosphorite vorhanden. Zur genaueren Charakterisierung der Sedimente wurden der organische Kohlenstoff-, Schwefel-, Eisen- und Phosphorgehalt der Proben aus dem Mishor Rotem (Efe Synkline) bestimmt. Der TOC der Proben zeigt sehr hohe Variationen im Profilverlauf. In den Phosphoriten weist nur eine Probe einen höheren TOC-Gehalt von 17 % auf, alle anderen Werte liegen zwischen 1-4 %. In den Ölschiefen liegen die TOC-Gehalte zwischen 10 und 24 %. Dagegen sinken sie in den Mergeln auf unter 1 %, was vermutlich auf eine vollständige Sauerstoffsättigung der Wassersäule und der Sedimentoberfläche zu-

rückzuführen ist. Aus diesen Daten lässt sich berechnen, dass in den Phosphoriten bis zu einem Drittel der organischen Substanz bei der Sulfatreduktion umgesetzt wurde, in den Ölschiefen reduzierte sich dieser Anteil auf etwa 15 %. Bei neueren Untersuchung an rezenten Sedimenten aus Auftriebsgebieten von Peru und Namibia und fossilen Sedimenten der miozänen Monterey Formation (Kalifornien), wurde ein Zusammenhang zwischen sulfidoxidierenden Bakterien der Gattungen *Beggiatoa*, *Thioploca* oder *Thiomargarita* und der Phosphatdeposition im Sediment entdeckt (Schulz and Schulz, 2005; Arning et al., 2009a; Arning et al., 2009b; Brock and Schulz-Vogt, 2011; Berndmeyer et al., 2012). Diese Bakterien sind allerdings in rezenten und insbesondere fossilen Sedimenten schwierig nachzuweisen, da sie keine hochspezifischen Biomarker produzieren. Hervorzuheben ist jedoch, dass verzweigte, gesättigte und ungesättigte Fettsäuren auf diese Bakterien im Sediment hindeuten (Arning et al., 2008). Aufgrund dessen wurden die Fettsäuren in die Biomarkeranalyse der Proben mit einbezogen. Die höchsten Konzentrationen zeigten die einfach gesättigten Fettsäuren n-C_{16:0} und n-C_{18:0}, die mit 67 µg/g C_{org} und 57 µg/g C_{org} im Phosphorit gefunden wurden. Weiterhin fanden sich Spuren von i-C_{15:0} und die ungesättigten Fettsäuren Ölsäure (C_{18:1ω9}) und Vaccensäure (C_{18:1ω7}). Die hohen Konzentrationen an den einfachen Fettsäuren und das Vorhandensein von einfach gesättigten und verzweigten Fettsäuren können als Indiz für das Vorhandensein von sulfidoxidierenden Bakterien angesehen werden (Arning et al., 2009a).

Die organischen Extrakte der Proben aus der Efe Syncline weisen einen durchschnittlichen Gehalt von 5,8 % an gesättigten Kohlenwasserstoffen, 3,7 % aromatischen Kohlenwasserstoffen und 50 % polare Verbindungen auf. Etwa 40 % entfallen auf die Asphaltene, die bei der Säulenchromatographie auf der Säule verbleiben. Die Gesamtextrakte der Proben aus der Efe Syncline wurden durch Soxhlet-Extraktion über 24 Stunden mit einem Gemisch aus Dichlormethan/Methanol 9:1 erhalten. Die Proben aus dem Shefela Becken wurden mit einem SpeedExtractor (Büchi) bei erhöhtem Druck und Temperatur mit dem gleichen Lösungsmittelgemisch extrahiert. Dieses Verfahren wurde aufgrund der effizienteren Extraktion angewendet, da die Proben nur in geringer Menge vorhanden waren. Die Auftrennung der einzelnen Fraktionen erfolgte durch Säulenchromatographie. Die unpolare Alkanfraktion wurde mit Hexan, die Aromatenfraktion mit Hexan/Dichlormethan (9:1) und die polare Fraktion mit Methanol eluiert. Zur Analyse wurden die Fraktionen der Hetero-

komponenten mit BSTFA [Bis-(trimethylsilyl)-trifluor-acetamid] derivatisiert. Dadurch werden die funktionellen Gruppen in Form von Trimethylsilylestern und -ethern geschützt und eine leichtere Verdampfbarkeit erreicht. Dazu wurde jeweils 1 mg der Probe mit BSTFA sowie Pyridin als Katalysator versetzt und anschließend zwei Stunden bei 60 °C im Heizblock erwärmt. Nachfolgend wurden die einzelnen Fraktionen mittels Gaschromatographie-Massenspektrometrie (GC-MS) analysiert. Bei den n-Alkanen zeigte sich ein bimodales Verteilungsmuster mit einem Maximum zwischen n-C₁₅ und n-C₂₃ und einem zweiten Maximum bei n-C₂₉. Bei den kurzkettigen n-Alkanen dominierten die Verbindungen mit ungeradzahigen Kettenlängen und deuten somit auf einen signifikanten Eintrag von marinem Algenmaterial hin. Die Analyse von C₂₇-C₂₉ Steranen ergab, dass der überwiegende Teil dieser Verbindungen (etwa 90 %) auf planktonischen oder marinen Ursprung zurückgeführt werden kann. Der Beitrag terrestrischen Materials kann anhand der Biomarkeranalyse als sehr gering eingestuft werden. Spiro und Aizenshtat (1977) haben aufgrund der Ergebnisse aus petrographischer Mikroskopie, Röntgendiffraktion, Elektronenstrahlmikroanalyse an Foraminiferen sowie der Analyse der n-Alkane an Ölschieferproben der Ghareb Formation aus dem Maastrichtium von Nebi Musa (Jordan Tal) eine Ablagerung der Sedimente unter anaeroben, sulfatreduzierenden Bedingungen angenommen. In neueren Untersuchungen wurde die relative Häufigkeit von Chromanen in Sedimenten verwendet, um die Salinität des Wassers zur Zeit der Ablagerung der Sedimente zu bestimmen. De Leeuw und Sinninghe Damsté (1990) haben festgestellt, dass das Verhältnis relativer Intensitäten von Methyltrimethyltridecyl-chromanen (MTTC) bei Auftragung gegen das Pristan/Phytan Verhältnis dazu benutzt werden kann, die Salinität des Ablagerungsmilieus zu bestimmen. Normalsaline Umweltbedingungen werden dabei durch MTTC-Verhältnisse > 0,4 in Kombination mit einem Pristan/Phytan Verhältnis > 0,35 beschrieben. Hingegen weisen hypersaline Bedingungen MTTC-Verhältnisse < 0,45 in Kombination mit einem Pristan/Phytan Verhältnis < 0,2 auf. Systeme, die Datenpunkte im Zwischenbereich liefern, bezeichnet man als mesosalin. Die Ablagerung der Ölschiefer aus der Efe Syncline fand überwiegend unter normalsalinen Bedingungen statt (gemessenes MTTC-Verhältnis zwischen 0,51 und 0,86 und Pristan/Phytan Verhältnis zwischen 0,14 und 0,71). Vergleichbare Ergebnisse sind auch von Sedimenten oligozäner und früher miozäner Hochproduktivgebiete der Paratethys aus Aserbaidshans bekannt (Bechtel et al., 2013).

Aus der Häufigkeit und der erhöhten Konzentration pentazyklischer Triterpane kann man ableiten, dass bakterielles Leben eine große Rolle während der Ablagerung der Sedimente gespielt hat. Diese Verbindungen dienen als Membranstabilisatoren in den Zellwänden der Prokaryoten, ähnlich den Steroiden in eukaryotischen Zellen. Zahlreiche Hopane mit 27 bis 35 Kohlenstoffatomen konnten in den Sedimenten nachgewiesen werden. Zu den häufigsten und in den höchsten Konzentrationen pro Gramm organischen Kohlenstoff (TOC) vorliegenden Hopanen gehörten die C₃₀-17 α (H), 21 β (H)-Hopane und C₃₁-17 α (H),21 β (H) bzw. C₃₁-17 β (H), 21 β (H)-Homohopane. Diese Verbindungen konnten vor allem im unteren Teil der Ölschiefer-Fazies nachgewiesen werden und sind ein Indiz für die hohe bakterielle Aktivität in diesem Bereich. In den Phosphoriten und den Mergeln konnten diese Verbindungen dagegen nicht nachgewiesen werden. Der relativ gute Erhaltungsgrad der Verbindungen mit 32–35 Kohlenstoffatomen deutet auf anoxische Bedingungen während der Sedimentation hin. Neuere Untersuchungen haben gezeigt, dass Hopane nicht nur von aeroben Bakterien gebildet werden, sondern auch anaerobe Bakterien (ammoniumoxidierende und sulfatreduzierende) zur Bildung von hopanoiden Verbindungen in der Lage sind (Blumenberg et al., 2006).

Aus der GC-MS Analyse der Aromatenfraktionen wird deutlich, dass „natural vulcanisation“, der Einbau von Schwefel in organische Substanzen während der frühen Diagenese ein wichtiger Prozess während der Ablagerung des Ölschiefers war. Die zahlenmäßig häufigsten Verbindungen in der Fraktion der Aromaten sind Thiophene mit aliphatischer Seitenkette. Diese Verbindungen weisen diagnostische Fragmentionen von m/z 97, 111 und 125 auf. Es konnten Verbindungen mit Seitenkettenlängen zwischen 6 und 23 Kohlenstoffatomen nachgewiesen werden. Besonders häufig waren solche mit 13 bis 18 Kohlenstoffatomen in der Seitenkette. Diese Verbindungen konnten weder in der Phosphorit-Fazies noch in den Mergeln nachgewiesen werden. Von den Verbindungen mit Thiophen-Rest wurde 2-Methyl-5-tridecyl-thiophen mit der höchsten Konzentration (bis zu 38 μ g/g TOC) nachgewiesen. Die isoprenoiden Vertreter dieser Verbindungsklasse sind höchstwahrscheinlich aus der Phytol-Seitenkette des Chlorophylls hervorgegangen und belegen den hohen Eintrag von phytoplanktonischem Material während der Hochphasen der Primärproduktion.

Vermutlich ebenfalls auf planktonischen Ursprung zurückzuführen sind Epithiosterane. Diese schwefelorganischen Verbindungen mit 27 bis 29 Kohlenstoffatomen sind

in allen Proben der Ölschiefer-Fazies vertreten. Sie entstehen bei der Diagenese aus der Reaktion von $\Delta^{8(14),22}$ Steradienen mit Schwefelwasserstoff, die wiederum aus $C_{28}\Delta^{7,22}$ Sterolen entstanden sein können. Diese Sterole sind in marinen Mikroalgen weit verbreitet (Behrens et al., 1997; Volkman, 2003).

Eine weitere Gruppe schwefelorganischer Verbindungen sind die Schwefelhopanoide, die sehr häufig in den Ölschiefersedimenten zu finden sind. Diese Verbindungen wurden von Valisolalao et al. (1984) zum ersten Mal aus kreidezeitlichen Ölschiefer-Sedimenten Angolas (Deep Sea Drilling Project leg 40) beschrieben. Diese Verbindungen sind Bestandteil der Aromatenfraktion und besitzen einen Thiophen- oder Thiolan-Rest in der aliphatischen Seitenkette der Hopane. Sie lassen sich bei der GC/MS-Analyse über das Massenchromatogramm m/z 191 nachweisen und zeigen die für die aus den Thiophenresten der Seitenkette hervorgehenden typischen Fragmentationen bei m/z 97 und 111 (2'-Thienyl- und 2'-(5-Methylthienyl)- Fragmentationen). Von den Thiolanen werden typische Fragmentationen bei m/z 87 und m/z 101 (2'-Thiolanyl- und 2'-(5-Methylthiolanyl)- Fragmentationen) erzeugt. Bis zu zehn verschiedene Verbindungen dieser Gruppe mit einem Thiophenring oder einem Methylthiophen in der Seitenkette konnten in den Proben nachgewiesen werden (Chromatogramm in Kapitel 3.4.1.7, Abbildung 23). Diese Verbindungen hatten Molekülmassen zwischen 494 und 522. Sie gehen aus frühdiagenetischen Reaktionen der Bakteriohopanepolyole mit Schwefelwasserstoff oder Polysulfid unter anoxischen Bedingungen im Sediment hervor.

Des Weiteren, um zusätzliche Informationen über die Redox-Bedingungen während der Sedimentation zu erhalten wurde das Pristan/Phytan-Verhältnis (Pr/Ph) bestimmt. In den Phosphoriten bewegt sich das Pr/Ph-Verhältnis zwischen 0,4 und 0,6, während es in den Ölschiefen zwischen 0,1 und 0,7 schwankt (Schneider-Mor et al., 2012). Aus den Ergebnissen der Pr/Ph-Daten lässt sich eine Ablagerung der Sedimente unter anoxischen Bedingungen im unteren Teil der Ölschiefer-Fazies ableiten. Das ist ein weiterer Grund für die gute Konservierung des organischen Materials. Im Bereich des Mergels beobachtet man einen Anstieg des Pr/Ph-Verhältnisses von 0,45 auf 1,8, was mit einer starken Änderung der Umweltbedingungen vom anoxischen zum suboxischen oder gar oxischen Milieu einhergeht.

Darüber hinaus, um weiteren Aufschluss über den Ursprung des organischen Materials zu erhalten wurde der organisch gebundene Stickstoffgehalt gemessen (TON) und

das organische Kohlenstoff/organische Stickstoffverhältnis (C/N) bestimmt. Die C/N Verhältnisse in den Phosphoriten (24,9–29,8) und den Ölschiefern (24,0–34,5) lagen deutlich höher, als man es von marinen Algen erwarten würde (6–7, Redfield (1958)). Lediglich im Mergel waren die Werte vergleichbar mit anderen marinen Lebensräumen (6,3–6,9). Auch die organisch petrologischen Untersuchungen der Proben bestätigten die vorherigen Ergebnisse, denn 95 % des morphologisch erkennbaren organischen Materials ist marinen Ursprungs. Terrestrisches Material wurde nur zu einem sehr geringen Anteil eingetragen. Ein bevorzugter Abbau der stickstoffreichen Verbindungen über Denitrifikation oder Anammox in den Phosphoriten und den Ölschiefern ist eine mögliche Erklärung für die sehr geringen TON Werte und das sehr hohe C/N Verhältnis (Schneider-Mor et al., 2012). Bei der Denitrifikation wird Nitrat zu molekularem Stickstoff reduziert. Dieser Prozess läuft in mehreren Schritten mit mehreren Zwischenstufen ab (Gl. 2–Gl. 5). In einem ersten Schritt wird Nitrat zu Nitrit reduziert. Dieses wird dann zu Stickstoffmonoxid reduziert und in einer weiteren Reduktion entsteht daraus Distickstoffmonoxid. Im letzten Schritt entsteht aus Distickstoffmonoxid dann molekularer Stickstoff. Bei allen Reduktionsschritten wird der abgespaltene Sauerstoff als Wasser freigesetzt (Cypionka, 2010).



Bei der Anammox Reaktion wird unter anaeroben Bedingungen Ammonium mit Nitrit direkt zu molekularem Stickstoff umgesetzt (Gl. 6).



Die Isotopenanalyse am Bulkmaterial ergab $\delta^{13}\text{C}_{\text{org}}$ Werte von ca. -29 ‰, ein für marines Material sehr ungewöhnlicher Wert, der eher zu Landpflanzenmaterial passen würde. Eine Erklärung hierfür wäre die gezielte Zersetzung von ^{13}C angereicher-

ten Kohlenhydraten und Proteinen durch Bakterien bei einem Sauerstoffdefizit. Forschungsergebnisse haben gezeigt, dass es bei dieser Zersetzung zu einer Veränderung der $\delta^{13}\text{C}$ -Werte hin zu leichterem Kohlenstoff im Vergleich zum Bulkmaterial der Algen kommt (Jenkyns and Clayton, 1986; Hedges et al., 1988; Meyers, 1994). Der im Vergleich zum OSM angestiegene $\delta^{13}\text{C}$ -Wert in den Mergeln ist möglicherweise spezifisch für Degradation unter oxischen Bodenwasserbedingungen. Die durchweg niedrigen $\delta^{13}\text{C}$ Werte im Profil sind vermutlich eine Folge der hohen Konzentration von CO_2 in der Atmosphäre während der Kreide, wodurch es zu einer stärkeren Fraktionierung durch das Phytoplankton kommen kann.

Weiterhin wurden $\delta^{15}\text{N}_{\text{org}}$ Untersuchungen an dem Probenmaterial vorgenommen, um zwischen terrestrischem und marinen Material zu unterscheiden. Während der Proteinhydrolyse kann es zu einer selektiven Anreicherung von ^{15}N und ^{13}C im verbleibenden organischen Material kommen. Allerdings sprechen die Ergebnisse aus dem oberen Bereich der Phosphat- und Ölschiefer-Fazies gegen eine Proteinhydrolyse. Der wahrscheinlichste Mechanismus, der die hohen C/N Verhältnisse und niedrigen $\delta^{15}\text{N}$ Werte erklärt, ist eine selektive Zersetzung der Aminosäuren über Denitrifikation oder Anammox.

Summary

The Late Cretaceous is known to be mostly affected by warm periods interrupted temporarily by a number of cooling events. The atmospheric CO₂ level for the Late Cretaceous is expected to be twice as high as the modern CO₂ level of around 400 ppmV. The reconstruction of the paleoclimatic conditions during a period of high concentration of CO₂ in the atmosphere is of great importance for the creation of future climate models. The reconstruction of sea surface temperatures (SST) during the Late Cretaceous has previously been subject of several studies. Most of the available SST data are based on oxygen isotopic data obtained from foraminifera, but the calcareous shells of the foraminifera are prone to re-mineralization and the resulting SSTs can be cold-biased, especially for the equatorial region. Furthermore, data from the southern Tethys were rarely available and only roughly dated. To prevent problems with the SST calculation, we applied the recently developed method reconstructing the SST from the TEX₈₆ (TEX₈₆, TetraEther index of tetraethers consisting of 86 carbon atoms).

The sample material used for the present study was obtained from the tropical Late Cretaceous southern Tethys upwelling system (paleolatitude 8–15°N, Israel). This upwelling system lasted from the Late Santonian to the Early Maastrichtian (~ 85 to 68 Ma). On the core samples from the Shefela basin, representing the outer belt of the upwelling system and the outcrop profile from the open mine Mishor Rotem (Efe Syncline), representing the inner belt, various bulk geochemical and biomarker studies were performed in this thesis. The outcrop profile from Mishor Rotem covers approximately 50 m and consists of three facies types. The underlying Phosphate Member (PM), belonging to the Mishash Formation and subsequent the Oil Shale Member (OSM) and the overlying Marl Member (MM) belonging to the Ghareb Formation. The core from the Shefela basin covers 335 m and consists mainly of the Ein Zeitim Formation intercalated by a small tongue of the Mishash Formation.

Derived from TEX₈₆ data, a significant long-term SST cooling trend from 36.0 to 29.3 °C is recognized during the Late Santonian and the Early Campanian in the southern Tethys margin. This is consistent with the opening and deepening of the Equatorial Atlantic Gateway (EAG) and the intrusion of cooler deep water from the southern Atlantic Ocean, which had probably influenced the global SSTs and also the

Tethys Ocean. Based on the data from the present study and by comparison with literature data for the SST of the polar region we were able to re-assess the equator to pole SST gradient to 22 °C, which is closer to the modern ocean equator-to-pole SST gradient (30 °C) as suggested from previous studies. Furthermore, the cooler near shore SST usually found in modern upwelling systems could be verified in case of the ancient upwelling system investigated in the present study. The calculated mean SST in the inner belt (27.7 °C) represented in the Efe Syncline was 1.5 °C cooler in comparison to the more seaward located outer belt (Shefela basin).

Moreover, geochemical and biomarker analyses were used to identify both the accumulation of high amounts of phosphate in the PM and good preservation of organic matter (OM) in the lower part of the OSM section. Total organic carbon (TOC) contents are highly variable over the whole profile reaching from 0.6 % in the MM, to 24.5 % in the OSM. Total iron (TFe) varies from 0.1 % in the PM to 3.3 % in the OSM and total sulfur (TS) varies between 0.1 % in the MM and 3.4 % in the OSM. Different correlations of TS, TOC and TFe were used to identify the conditions during the deposition of the different facies types. Natural sulfurization was found to play a key role in the preservation of the OM particularly in the lower part of the OSM. Samples from the OSM and the PM were deposited under dysoxic to anoxic conditions and iron limitation lasted during the deposition of the OSM and the PM, which effected the incorporation of sulfur into OM. Biomarkers indicating photic zone euxinia, could not be detected by GC-MS analyses.

Phosphorus is highly accumulated in the sediments of the PM with a mean proportion of 11.5 % total phosphorus (TP). This proportion is drastically reduced to a mean value of only 0.9 % in the OSM and the MM. From the correlation of the bulk geochemical parameters TOC/TOC_{OR} ratio and TP a major contribution of sulfate reducing bacteria to the phosphate deposition is concluded. This interrelation has previously been investigated in recent coastal upwelling systems off Peru, Chile, California and Namibia. This was further supported by the analysis of branched and monounsaturated fatty acids indicating the occurrence of sulfate reducing and sulfide oxidizing bacteria during the deposition.

According to the results from the analysis of n-alkanes and C₂₇- to C₂₉-steranes there was only a minor contribution of terrestrial material to the sediments. Up to 95 % of the OM was of marine origin.

Organic sulfur compounds (OSC) were a major compound class in the aromatic hydrocarbon fraction. n-Alkyl and isoprenoid thiophenes were the most abundant among the OSC, with highest amounts found for 2-methyl-5-tridecyl-thiophene (28 µg/g TOC). The relatively high abundance of ββ-C₃₅ hopanoid thiophenes and epithiosteranes is equivalent to an incorporation of sulfur during the early stages of diagenesis.

Moreover, the geochemical parameters δ¹³C_{org}, δ¹⁵N_{org}, C/N and the pristane/phytane (Pr/Ph) ratio, were studied for reconstruction of seafloor and water column depositional environments. Our records indicate a gradual decrease with time in surface water productivity in the OSM and a marked weakening at the overlying Marl Member. The high C/N ratio along with relatively low values of δ¹⁵N_{org} (4 ‰ to 6 ‰) and δ¹³C_{org} (-29 ‰ to -28 ‰) are consistent with a significant preferential loss of nitrogen-rich organic compounds during diagenesis. Oxygen-depleted conditions lasted during the deposition of the PM and the bottom of the OSM, reflected by the low Pr/Ph ratio of 0.11–0.7. In the upper part of the OSM and the MM the conditions changed from anoxic to dysoxic or oxic conditions. This environmental trend is consistent with co-occurring foraminiferal assemblages in the studied succession and implies that the benthic species in the Negev sequence were adapted to persistent minimum oxygen conditions by performing complete denitrification as recently found in many modern benthic foraminifera.

Furthermore, the anammox process could have influenced the nitrogen composition of the sediments. In this anaerobically process nitrite and ammonia are converted to molecular nitrogen. In recent studies of e.g. the Benguela upwelling, it was found that this process has a significant influence on the nitrogen cycle in the OMZ of coastal upwelling systems. It accounts for an enormous loss of nitrogen to the atmosphere.

Introduction

Climate

The climate during the Late Cretaceous was highly variable and changed between warm and cold periods (e.g. Barrera and Savin, 1999; Takashima et al., 2006; Moriya, 2011). The Turonian was the warmest period with equatorial sea surface temperatures (SSTs) of 31 to 37 °C (Forster et al., 2007b), possibly even up to 42 °C (Bice et al., 2006). For the polar regions mean annual temperatures above 4 °C were modeled (Sijp et al., 2014). Moreover, from the analysis of the vertebrate assemblage from the high Canadian Arctic a mean annual temperature above 14 °C was suggested (Tarduno et al., 1998). But even in this period of greenhouse conditions there is evidence for a short-term ice shield building in the Antarctic region, approximately 60 % of the modern size. This was suggested from the results of $\delta^{18}\text{O}$ isotopic analyses on planktic foraminifera from an organic-rich marlstone (Turonian to Santonian age) from the western equatorial Atlantic at Demerara Rise (Ocean Drilling Program, ODP Site 1259) (Bornemann et al., 2008). A global cooling trend started in the Santonian and several periods of cooling and warming followed until the Maastrichtian (Barrera and Savin, 1999; Li and Keller, 1999; Abramovich et al., 2010). During the Late Campanian to Middle Maastrichtian the equatorial air temperature was similar to modern conditions and even in the polar region temperatures below 0 °C were limited to paleolatitudes above 80° (Amiot et al., 2004). Figure 1 shows the distribution of the continents and oceans during the Cretaceous at 80 Ma and 69 Ma (according to Hay et al. (1999) and Scotese (2002)). It illustrates the movement of the continental plates with the increasing opening of the connection between the northern and southern Atlantic Ocean together with the location of the study area during the two epochs of the Cretaceous. The changes in the oceanic circulation of the middle and deep waters due to the opening and deepening of the connection between the northern and southern Atlantic Ocean (Equatorial Atlantic Gateway, EAG) during the Late Cretaceous had an enormous influence on the global climate (Friedrich and Erbacher, 2006; Friedrich et al., 2012).

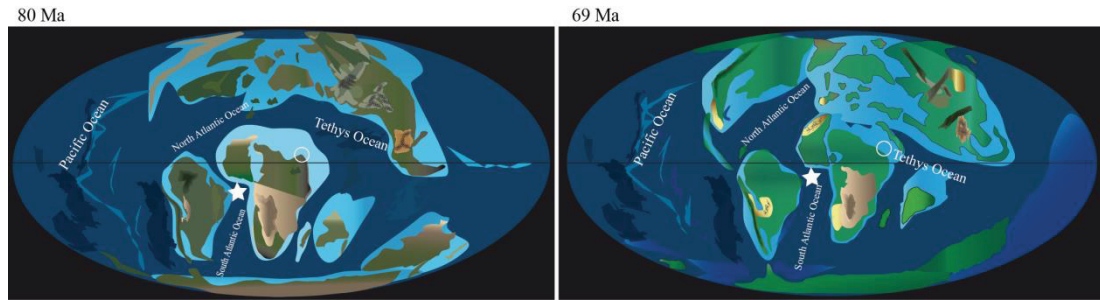


Figure 1: Distribution of the continents and oceans during the Cretaceous at 80 Ma and 69 Ma, modified after Hay et al. (1999) and Scotese (2002). The Equatorial Atlantic Gateway (EAG) is marked with a white asterisk. The location of the study area during the two epochs of the Cretaceous is shown with a white circle.

In the post-Turonian epoch the cooling of the earth's climate lasted until the Maastrichtian (Clarke and Jenkyns, 1999). Several cooling and warming events of global scale occurred during this period. At the end of the Santonian the cooling of the global SST began (e.g. Friedrich et al., 2005; Liu, 2009). Between the Campanian and Maastrichtian a further global cooling event (CMBE = Campanian/Maastrichtian boundary event) occurred with a cooling of 3–4 °C (Jung et al., 2012; Koch and Friedrich, 2012). At the end of the Maastrichtian during a warming period the ocean temperature rose by 3–4 °C (Abramovich et al., 2010). For a better understanding of the global climate in the past it is essential to collect paleoclimatic data from all climate zones. The reconstruction of SSTs is essential for the understanding of ancient marine paleoenvironments and allows detecting climatic changes. Recently a method was developed to reconstruct the SST of ancient marine environments from organic biomarkers called GDGTs (glycerol dialkyl glycerol tetraethers) (Schouten et al., 2002). These are membrane lipids, biosynthesized by archaea such as *Crenarchaeota*, with ether-linkages forming a lipid monolayer in the membrane (Schleper et al., 2005). Archaea are one of three domains of living organisms together with eukaryotes and bacteria (Woese et al., 1990). They were originally thought to live only under extreme conditions (e.g. acidic, anoxic, hypersaline or extremely warm), but they are also widespread distributed in moderate terrestrial, lacustrine and marine habitats (Schleper et al., 2005). The integration of pentane or hexane rings in these molecules is an adaption to the ambient temperature (Macalady et al., 2004). With increasing amounts of cyclopentane moieties archaea are able to live under high temperature conditions. Especially, the integration of the cyclohexane moiety in the crenarchaeol molecule results in a higher flexibility of the structure and allows an adaption to

cooler environments. The molecular composition of the *Crenarchaeota* membrane lipids is highly depending on the ambient temperature (Schouten et al., 2013). The analysis of sediments from different geographic settings showed that the ratio of the relative abundance of the GDGTs defined as TEX₈₆ (TEX₈₆, TetraEther indeX of tetraethers consisting of 86 carbon atoms, Schouten et al. (2002)) is proportional to the annual mean SST (the structures of the GDGTs are given in the Appendix A1 to A6). The TEX₈₆ index is defined as followed (Eq. 1):

$$\text{TEX}_{86} = \frac{A4 + A5 + A6}{A3 + A4 + A5 + A6} \quad \text{Eq. 1}$$

The annual mean SST is linearly correlated with the TEX₈₆ (Eq. 2):

$$\text{TEX}_{86} = 0.015 \cdot \text{SST} + 0.28 \quad \text{Eq. 2}$$

This initial formula from Schouten et al. (2002) was modified several times to better adjust the calculated to the measured SSTs (e.g. Schouten et al., 2003; Kim et al., 2008; Lee et al., 2008; 2010) and to overcome biases resulting from seasonality, depth or terrestrial influence. For description in more detail see Chapter 1.5. This method was applied to determine the SST in ancient oceans up to the middle Jurassic (~160 Ma) due to the relative high stability of these biomarkers during diagenesis (Jenkyns et al., 2012).

Upwelling

During the Late Cretaceous a coastal upwelling established at the southern margins of the Tethys Ocean (Figure 1). Nowadays, the major coastal upwelling systems are located on the western site of North and South America (California, Peru and Chile) and the western coast of North and South Africa (Morocco and Namibia) and the upwelling off Oman and Somalia. Modern coastal upwelling systems with their high biological productivity are of enormous economic and ecological importance. Although they cover only one percent of the ocean surface they contribute to 50 % of the global fisheries landings (Gaines and Airame, 2013). These environments are usually associated with silica-, organic- and phosphate-rich sediments (e.g. Soudry et al., 2006). Ancient upwelling environments are important phosphorite deposits (Parrish and Curtis, 1982), which provide useful resources for the fertilizer industry.

During the formation of the Syrian Arc system NE-SW directed anticlinal ridges and synclinal basins developed (Krenkel, 1924). The upwelling system established within these synclines and anticlines. The Shefela basin was situated in the outer belt of the upwelling system, which is a more open marine environment (Almogi-Labin et al., 1993; Edelman-Furstenberg, 2009). From the Jurassic to the early Cretaceous a strong NNE-SSW depositional trend is observable within the Dead Sea Rift system. The studied sediments of the Efe Syncline belong to the Maastrichtian Ghareb Formation (the Marl Member [MM] and the Oil Shale Member [OSM]), which were deposited in NE-SW directing synclines. Subjacent to the Ghareb Formation the sediments of the Campanian Mishash Formation has been deposited, consisting mainly of phosphorites with intercalated organic rich sediments (Phosphate Member [PM]). The phosphorites belong to the upper Cretaceous-Eocene phosphate belt that developed from South America to North Africa.

A strong westward flowing surface and deep water current, the Tethys Circumglobal Current (TCC) influenced the southern margins of the Tethys during the latest Cretaceous and transported water masses from the Pacific Ocean into the Tethys (Soudry et al., 2006). A cooling in the Late Cretaceous possibly intensified the strength of the easterly trade winds and established an extremely productive upwelling at the southern margin of the Tethys (Almogi-Labin et al., 1993; Pucéat et al., 2005; Soudry et al., 2006). Coastal upwelling is induced when winds are blowing parallel to the shoreline moving the upper water layer (Figure 2). Due to the Coriolis force the resulting Ekman transport moves the water masses in right angles to the wind direction away from the shore, to the right in the northern hemisphere and to the left in the southern hemisphere (Stewart, 2008). This water is replaced by cold nutrient rich deep water and causes a cooling of the water masses near to the shoreline (Figure 2). The transport of nitrate, phosphate, silicate and other nutrients to the photic zone increases the high primary productivity in these upwelling environments.

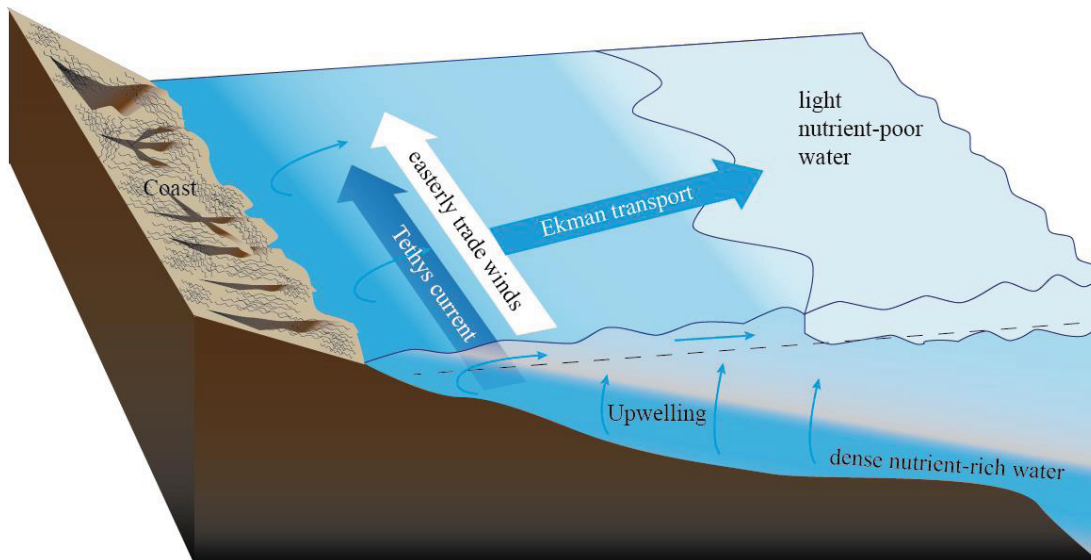


Figure 2: General illustration of the development of upwelling systems at continental margins (modified after Williams (2011)). Easterly trade winds move the upper water layers and due to the Coriolis force the water masses are moved to right angles of the wind direction. The transport of the upper water layer is away from the coast and the warm surface water is replaced by colder, nutrient rich deep water.

Below these high productivity centers, the decomposition of the planktonic biomass by the use of dissolved oxygen proceeds and oxygen minimum zones (OMZ) established (e.g. Schunck et al., 2013). At the continental margins of modern oceans the OMZ occurs between 200 and 700 m (Levin, 2003). The thickness of the OMZ is highly variable and depends on both, the oxygen content of the ocean region and circulation of oxygen rich water. From recent studies variation in thickness between < 400m and over 1000 m are known. There have been fundamental changes in the horizontal and vertical distribution and intensity of the OMZ related to the upwelling over thousands of years (Levin, 2003).

Phosphorous cycle

Phosphorus (P) is an essential element for life as a part of the DNA and in the energy transfer through adenosine triphosphate (ATP) (Ruttenberg, 2003; Paytan and McLaughlin, 2007). In the marine environment P is considered to be the limiting factor of primary production, because it cannot be fixed from the atmosphere. The major source for P is the erosion and (bio-) chemical weathering of continental soil and rocks and it is mainly transported via rivers to the ocean as particulate or dissolved organic and inorganic phosphate (Föllmi, 1996). For a schematic overview of

the phosphorous cycle see Figure 3. Due to the terrigenous influence of coastal waters the continental shelf and slope receives more P. Furthermore, eolian transport of phosphate is of significant importance for marine environments farther away from the shore although the transported amounts are smaller compared to the riverine input (Föllmi, 1996). Most of the riverine transported P is bound to particulate matter and is largely deposited in the estuaries and shelf area. Only up to one third of the total riverine transported P is available for biological uptake (Paytan and McLaughlin, 2007). The major sink for this phosphate is the deep ocean where P is aggregated to organic matter (OM) or as dissolved inorganic phosphate. From these deposits P is mobilized and transported by deep and intermediate currents and comes up to the photic zone in upwelling areas where it is again integrated in the biotic cycle (Föllmi, 1996).

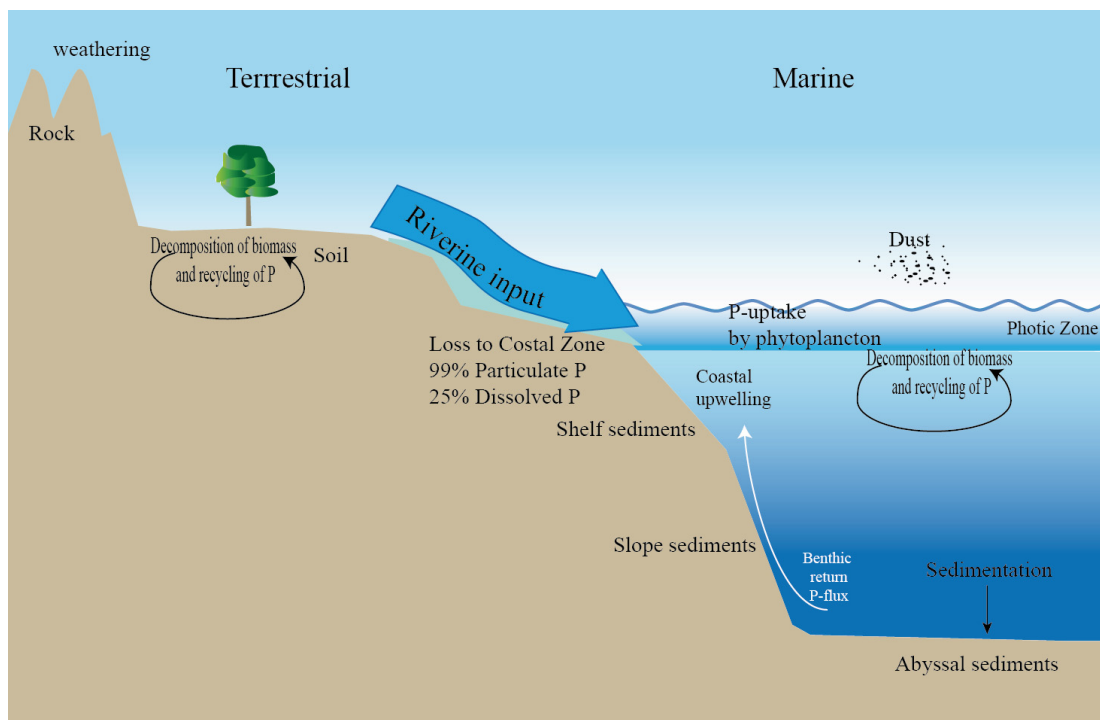


Figure 3: Schematic overview of the global phosphorus cycle (modified after Ruttenberg (2003); Paytan and McLaughlin (2007)). Igneous rocks and terrestrial soils are the main sources of phosphate, which is mobilized by physical and (bio)-chemical weathering. The phosphate is taken up by terrestrial biomass or is mainly transported via rivers to the ocean. Eolian transport is important for offshore oceanic environments. Photoautotrophic organisms take up P and the biomass is decomposed and eventually sedimented in the deep ocean. From the Abyssal sediments, P is reintroduced in the biotic cycle by benthic fluxes to coastal upwelling.

During early diagenesis in the marine environment phosphate is precipitated and forms the mineral francolite (carbonate fluorapatite) which can be represented approximately due to the complex composition with this formula (Jarvis et al., 1994):



A supersaturation of phosphate with respect to phosphate fluorapatite in the porewater of marine sediments is a prerequisite for phosphogenesis (Föllmi, 1996). Phosphorites consist of considerable amounts of authigenic and biogenic phosphate minerals with more than 18 % P_2O_5 (Jarvis et al., 1994).

The carbon, nitrogen and phosphorus cycles are closely related and the growth of the marine phytoplankton depends on these nutrients. Their correlation in the marine phytoplankton is expressed by the Redfield ratio (106C:16N:1P) (Redfield, 1958). Photoautotrophic organisms take up P dissolved in the upper layers of the marine environment. For this reason, the P in upwelling environments is mainly organically bound when the dead biomass is deposited in the sediment. In reducing sediments P cannot be effectively retained in the sediment and is released easily from the OM (Paytan and McLaughlin, 2007). Bacteria influence the precipitation of phosphorus in modern and ancient coastal upwellings. This precipitation mechanism was basis of intensive studies (e.g. Schulz and Schulz, 2005; Arning et al., 2009a; Brock and Schulz-Vogt, 2011; Berndmeyer et al., 2012).

These studies from the modern upwelling systems off Peru, Chile and Namibia have shown that the process of phosphate deposition is closely related to microbial sulfate reducing and sulfide oxidizing activity. P is deposited as carbonate fluorapatite in a microbial mediated process. The large sulfur bacteria *Thiomargarita*, *Thioploca* and *Beggiatoa* are involved in this process and are responsible for the authigenic production of phosphorites in the suboxic to anoxic marine upwelling environments (Föllmi, 1996). Under oxic sediment surface conditions, dissolved phosphate is precipitated as Fe-oxyhydroxide. In the OMZ or oxygen-depleted sediments these Fe-oxyhydroxides are dissolved and reduced. P is then deposited as carbonate fluorapatite. In sediments below high productivity centers reactive OM is ubiquitously available and sulfate reduction is the most important anaerobic degradation process (e.g. Thamdrup and Canfield, 1996). Recent studies on the phosphorite generation from modern upwelling regions show that both sulfate-reducing bacteria and sulfide-

oxidizing bacteria play key roles in the sedimentation of authigenic phosphorites (Arning et al., 2009a). The marine environment is rich in sulfur, mainly present in form of sulfate. Hydrogen sulfide is present in anoxic marine environments or bound in metal complexes and it is rapidly oxidized in seawater via oxygen or iodate (Radford-Knery and Cutter, 1994). The big sulfur bacteria *Beggiatoa* populate the sediment/water interface and are able to live in the oxygen-sulfide interface (Schulz and Jørgensen, 2001). With internally stored sulfur, nitrate and polyphosphate, these large bacteria can overcome sulfide free periods. Nitrate, stored in vacuoles, is used as an electron acceptor for the oxidation of sulfide or internal sulfur to sulfate, during periods of complete anoxia (Schulz and Jørgensen, 2001). If the bottom water is oxygenated and the sulfide concentration in the sediment is low *Beggiatoa* are able to accumulate phosphate as polyphosphate. Under anoxic bottom water conditions with high concentrations of sulfide in the sediment, the polyphosphate is decomposed and released as phosphate to the sediment (Brock and Schulz-Vogt, 2011). As strictly anaerobic organisms *Thioploca* retreat deeper into the sediment and escape higher concentrations of oxygen if the bottom water becomes more oxygenated (Schulz and Jørgensen, 2001). For the oxidation of sulfide they use nitrate, stored in a central vacuole. *Thiomargarita* are the only species that can survive higher concentration of oxygen and use oxygen and nitrate for the oxidation of sulfide or internally stored sulfur. Figure 4 shows the suggested environmental conditions during the deposition of the three different facies types. During the deposition of the PM the sulfide produced by sulfate reducing bacteria was mainly consumed by sulfide oxidizing bacteria and thereby phosphate minerals were deposited. In the OSM, nitrate was not available in sufficient amounts for the sulfide oxidation, possibly due to the competing denitrification/anammox process. The possibly temporal anoxic conditions above the sediment/water interface suppressed the sulfide oxidizing bacteria and the sulfide was scavenged by the OM. Due to the sea level rise during the deposition of the MM the higher bottom water oxygenation results in a decomposition of most of the OM.

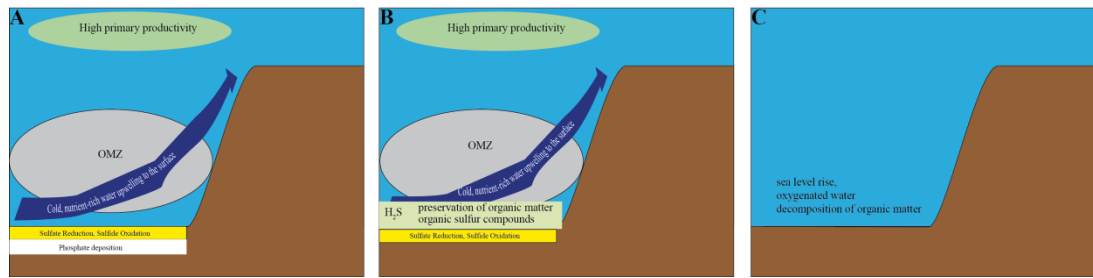
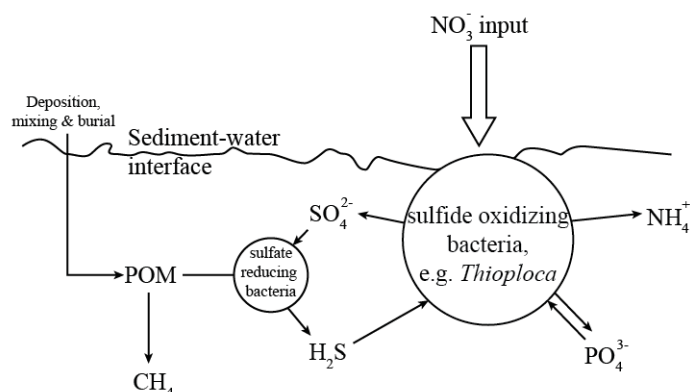


Figure 4: Illustration of the suggested environmental conditions during the deposition of the three different facies types: A) the Phosphate Member, B) the Oil Shale Member and C) the Marl Member. OMZ = oxygen minimum zone

Dale et al. (2009) analyzed the influence of the sulfur bacteria *Thiomargarita namibiensis* in the related C, N and S cycles in the organic-rich sediments of the highly productive upwelling system off Namibia. These bacteria control the sulfur cycle by oxidizing the produced sulfide back to sulfate. The in situ production of SO_4^{2-} also affects the methane production in the sediment and shifts the sulfate-methane transition zone deeper in the sediment. The nitrate in the sediment is almost completely consumed by the sulfide oxidizing bacteria (Dale et al., 2009) and it was previously shown that the denitrification process is of minor importance in sediments populated by *Thioploca* (Thamdrup and Canfield, 1996). The reaction mechanism of the sulfide oxidation is not completely understood. For *Thioploca* a two-step oxidation mechanism is suggested because of the S^0 found in vacuoles in these bacteria (Dale et al., 2009 and references therein). In a recent study by Dale et al. (2013) of sediment samples from the Baltic Sea, the reaction mechanisms influencing the phosphate deposition by sulfide oxidizing bacteria was further analyzed. They concluded that these bacteria “act as phosphorus capacitors in systems with oscillating redox conditions” and they are the driving force in the deposition of phosphate (Dale et al., 2013).



Degradation processes of organic matter:

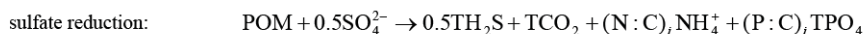
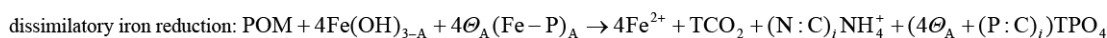
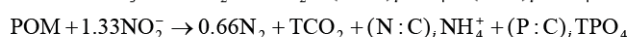
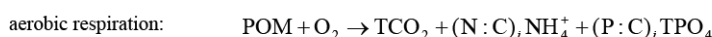


Figure 5: Illustration of the geochemical reactions in sulfide oxidizing bacteria populated sediments modified after (Dale et al., 2009; Dale et al., 2013). POM (particulate organic matter) is according to Dale et al. (2013) a composition of organic C, N and P fractions. $(\text{N}:\text{C})_i$ and $(\text{P}:\text{C})_i$ are the defined ratios of organic N and organic P to particulate organic carbon. The scheme describes possible decomposition reaction pathways for the POM and the role of sulfate reducing and sulfide oxidizing bacteria in this cycle.

Solutes: dissolved inorganic carbon $\text{TCO}_2 = \text{HCO}_3^- + \text{CO}_3^{2-} + \text{CO}_2$

total phosphate $\text{TPO}_4 \approx \text{H}_2\text{PO}_4^- + \text{HPO}_4^{2-}$

total hydrogen sulfide $\text{TH}_2\text{S} \approx \text{H}_2\text{S} + \text{HS}^-$

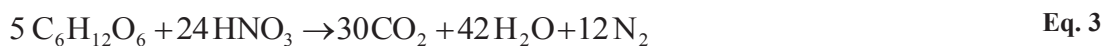
iron-bound P (Fe-P), depth-dependent fraction of Fe-P to $\text{Fe}(\text{OH})_3$ (Θ), reduced during dissimilatory iron reduction and by reaction with dissolved sulfide (Λ)

Microbial mediated processes and early diagenesis

In anoxic marine environments the preservation of OM by incorporation of sulfur is an important, mainly abiotic diagenetic pathway (Sinninghe Damsté and de Leeuw, 1990). The inorganic sulfur species, including sulfate (SO_4^{2-}), sulfide (HS^- and S^{2-}), elemental sulfur (S^0), polysulfides (SO_x^{2-}) and thiosulfate ($\text{S}_2\text{O}_3^{2-}$) involved in these reactions can either be products of abiotic reactions or of microbial activity (Werne et al., 2008). An important process is the oxidation of OM by bacteria by use of sulfate. Sulfate reducing conditions in oxygen-depleted environments with a lack of iron availability and the presence of reactive OM are prerequisite for the formation of organic sulfur compounds. In these environments the OM is an important sink for sulfide. Otherwise, if reactive iron is present in sufficient amounts, sulfide is scav-

enged as iron monosulfide and is further transformed to pyrite (Berner, 1984; Berner et al., 1985). Functional groups of organic compounds can incorporate reduced sulfur species. Even labile organic compounds, like functionalized biolipids or carbohydrates are preserved against microbial decomposition through sulfurization (Sinninghe Damsté et al., 1998b). Low molecular weight organic sulfur compounds (OSCs) with thiolanes or thianes moiety originate from intramolecular reactions. With further diagenesis the more stable thiophenes arise from these compounds. The intermolecular reaction results in large macromolecular compounds cross-linked by sulfide bridges, which are mainly insoluble.

Another important microbial activity in the OMZ beneath the high productivity zones of upwellings is the denitrification. This process accounts for 30–50 % of the total nitrogen loss from the ocean to the atmosphere (Kuypers et al., 2005). In a sequential process nitrate is reduced via nitrite, nitric oxide and nitrous oxide to molecular nitrogen. In the first step of the nitrification ammonium is aerobically oxidized by a microbial process. The reaction can be described as:



This process occurs at the oxic-anoxic interface at the OMZ. In most cases denitrification is a heterotrophic respiratory process and anammox bacteria are autotrophic. Denitrification is primarily controlled by the availability of reactive OM (Capone and Hutchins, 2013). Another very important process in the oceanic nitrogen cycle is the direct oxidation of ammonium to molecular nitrogen, using nitrite under anaerobic conditions (anammox), by bacteria of the order *Planctomycetales* (Eq. 4).



In the major upwellings off Namibia and Peru, anammox is a dominant nitrogen removal process. The nutrient nitrate is removed from the aquatic environment and these organisms compete with the bacteria of the genus *Thioploca* needing the nitrate for sulfide oxidation (Høgslund et al., 2008). In a study of sediment and bottom water samples Høgslund et al. (2008) analyzed population density, nitrate turnover, and oxygen respiration of benthic foraminifera in the OMZ off the Chilean coast. The benthic foraminifera *Nonionella* cf. *stella* and *Stainforthia* sp. strongly accumulate nitrate and were the dominating species in these sediments and additionally OMZs of other upwelling environments (Høgslund et al., 2008 and references

therein). The foraminifera and *Thioploca* share the same living habitat at the sediment/water interface of the upwelling system (Figure 6). The exact way of nitrate uptake by these organisms is still not fully understood (Høgslund et al., 2008).



Figure 6: Foraminifera and *Thioploca* filaments in the oxygen minimum zone off Chile. This picture illustrates the coexistence of foraminifera (illustrated with white arrows) and *Thioploca* bacteria, visible as white filaments at the sediment/water interface of the Chilean upwelling system. Scale bar 500 μm .” Adopted from Høgslund et al. (2008) with permission of Elsevier.

1 Sea surface temperature record of a Late Cretaceous tropical southern Tethys upwelling system

1.1 Abstract

Late Cretaceous sea surface temperatures (SSTs) were reconstructed based on TEX₈₆ data from the unique high productivity upwelling system in the southern Tethys margin, Israel. SSTs were determined from two oil shale sequences of the Santonian–early Maastrichtian (~ 85 to 68 Ma) in southern (Efe Syncline) and central (Shefela basin) Israel (paleolatitude 8–15°N). These two sampling sites represent the inner and outer belts of the upwelling system. Our TEX₈₆ data indicate a significant long-term SST cooling trend from 36.0 to 29.3 °C during the Late Santonian and the Early Campanian in the southern Tethys margin consistent with the opening of the Equatorial Atlantic Gateway (EAG).

Based on our data from the equatorial region and literature data from the polar region we reassessed the equator to pole SST gradient to 22 °C. This value is closer to the modern ocean equator-to-pole SST gradient (30 °C) than suggested from previous studies.

Furthermore, the SST data suggests the presence of cooler surface water in the inner belt (27.7 °C) caused by the upwelling system and warmer surface water (29.2 °C) further seaward in the outer belt.

1.2 Introduction

The climate during the Middle to Late Cretaceous (Aptian to Maastrichtian) experienced significant changes from warm to colder periods with highest sea surface temperatures (SSTs) in the Turonian (Takashima et al., 2006; Moriya, 2011). The Late Cretaceous was characterized by a long-term cooling trend of several degrees that started in the Santonian (86 Ma) and lasted into the Maastrichtian (66 Ma), assumed to be caused by a change in oceanic circulation and a transfer of intermediate to deep water sources to high northern and southern latitudes based on $\delta^{18}\text{O}$ data from foraminifera (Barrera and Savin, 1999; Abramovich et al., 2003; Friedrich et al., 2005; 2012; Koch and Friedrich, 2012). Recently, it has been suggested that this cooling trend is related to the establishment of a deep water passage between the North and

South Atlantic Oceans through the Equatorial Atlantic Gateway (EAG) (Friedrich et al., 2012).

A lot of Late Cretaceous SST records are based on $\delta^{18}\text{O}$ analyses of foraminifera whereby it is essential that their carbonate shells are well preserved (Pearson et al., 2001). However, the $\delta^{18}\text{O}$ composition of foraminifera can be affected by the $\delta^{18}\text{O}$ of the ambient water and by early deep sea diagenetic recrystallization that may introduce biases to SST reconstructions (Schrag et al., 1995; Pearson et al., 2001).

Besides the organic biomarker ratio $U_{37}^{K'}$ (alkenone unsaturation index), based on long-chain unsaturated ketones from haptophyte algae (Brassell et al., 1986a), used for the reconstruction of SST Schouten et al. (2002) established another organic paleo SST proxy. The membrane lipids of marine *Crenarchaeota* were found to consist of glycerol dialkyl glycerol tetraethers (GDGTs) with varying numbers of cyclopentane moieties and one with a cyclohexane moiety. The composition of the GDGTs is a biological adaptation of the archaean to the ambient temperature and has been used to develop the TEX_{86} (TetraEther index of tetraethers consisting of 86 carbon atoms) parameter for the reconstructions of former SSTs (Schouten et al., 2002). Based on the analysis of extracts from more than 40 globally dispersed surface sediments a linear correlation between the TEX_{86} and the annual mean SST was developed as shown in Eq. 5 (Schouten et al., 2002).

$$\text{TEX}_{86} = 0.015 \cdot \text{SST} + 0,28 \quad \text{Eq. 5}$$

The original calibration was further modified and improved for a wide temperature range based on the analysis of 223 core top sediments (Kim et al., 2008). This calibration showed a good correlation of the TEX_{86} with the annual mean water temperature of the upper mixed layer (Kim et al., 2008). For their analysis of eleven sediment samples from various sampling points from Eocene to Oligocene age Liu et al. (2009) used a non-linear TEX_{86} calibration modified after Kim et al. (2008). The development of the TEX_{86} as paleo proxy over the last decade was recently reviewed by Schouten et al. (2013)

In a recent study of suspended particulate matter and core top sediments from the Benguela upwelling system, the SSTs reconstructed from the TEX_{86} were cold biased up to 7 °C compared to in situ measured SSTs (Lee et al., 2008). The discrepancies were explained by a higher production of *Crenarchaeota* lipids below the mixed

layer (Lee et al., 2008) which were uplifted to the surface together with the colder water masses.

Recently, a new proxy based on branched GDGTs (Branched and Isoprenoid Tetraether (BIT) index), was developed for the determination of terrestrial influence on marine systems (Hopmans et al., 2004). Large amounts of terrestrial organic matter, possibly derived from fluvial input, could also bias the TEX_{86} value due to the influence of terrestrially derived isoprenoid GDGTs (Weijers et al., 2006). A further possibility of a seasonal bias on the TEX_{86} value was observed during the analysis of particulate organic matter from different marine settings (Wuchter et al., 2005). The GDGTs show a higher abundance in the winter and spring month which might also affect the TEX_{86} (Wuchter et al., 2005).

In face of these limitations, the TEX_{86} index is thought to be less affected by diagenetic overprinting (e.g. Schouten et al., 2004; Kim et al., 2009) than $\delta^{18}\text{O}$ in carbonatic (Pearson et al., 2001) or phosphatic minerals (Sharp et al., 2000). SST reconstructions based on the $\delta^{18}\text{O}$ of foraminifera of Santonian to Maastrichtian age from equatorial regions are relatively sparse mainly due to the limited number of well-preserved isotopic records from tropical sections (e.g. Maestas et al., 2003; Steuber et al., 2005). Additionally, no TEX_{86} paleotemperature data are available so far from Late Cretaceous sediments of the southern Tethyan Ocean.

Jenkyns et al. (2004) suggested a Late Cretaceous equator-to-pole SST gradient of ca. 15 °C, which is just half of the modern value. Their assumption based on SST data derived from TEX_{86} data obtained from core material of sedimentary rocks from the Late Cretaceous polar ocean (Jenkyns et al., 2004), and SSTs (up to 32 °C) calculated from $\delta^{18}\text{O}$ data of foraminifera from the equatorial Pacific Ocean (Wilson and Opdyke, 1996) which might be a problem because of the biases concerning the evaluation of SSTs from TEX_{86} values determined in sediments from polar regions (Sluijs et al., 2006).

Additionally, we compared our data on tropical SSTs with published data from the polar region that enable a reassessment of the equator-to-pole gradient during the Late Cretaceous.

We studied sediments from two well-dated oil shale sequences located in central and southern Israel. These were obtained from the Aderet 1 borehole in the Shefela basin and the PAMA quarry outcrop in the Efe Syncline (Ashckenazi-Polivoda et al., 2011;

Meilijson et al., 2012) (Figure 7 A, B). Both sequences cover Late Cretaceous sediments deposited in the southern Tethys equatorial region (8–15°N) under the influence of a major upwelling regime (Edelman-Furstenberg, 2009). Within this upwelling system, the sediments from the Aderet 1 borehole and PAMA quarry were deposited in the outer belt and the inner belt, respectively (Almogi-Labin et al., 1993; Ashkenazi-Polivoda et al., 2011; 2012).

The aim of this study was a reconstruction of southern Tethyan equatorial SSTs based on TEX₈₆ from the Late Santonian to the Early Maastrichtian. Trends are discussed in the context to other SST records. Moreover, the availability of sediment profiles from both proximal (PAMA quarry) and distal (Aderet 1 borehole) areas of the upwelling belt may allow to investigate whether TEX₈₆ data detect the occurrence of cold uplifting water more proximal to the coast and warmer water further seawards, similar to common patterns in recent and modern upwelling systems.

1.3 Materials and methods

1.3.1 Paleogeographical setting

The studied sediment samples were deposited during the Late Cretaceous in a highly productive upwelling regime lasting for nearly 20 Myr. from the Santonian to the Late Maastrichtian in the southern part of the Tethys Ocean at a paleolatitudinal position of 8–15°N (Figure 7) (Almogi-Labin et al., 1993; Edelman-Furstenberg, 2009). This upwelling system belongs to the Upper Cretaceous-Eocene phosphate belt which extends from South America (Colombia) over North Africa to the Middle East consisting of organic-rich carbonates, cherts and phosphates (Almogi-Labin et al., 1993; Pufahl et al., 2003).

A driving force of the Late Cretaceous upwelling system was the westward-flowing Tethys Circumglobal Current (Soudry et al., 2006). The prevailing trade winds generated the upwelling systems along the continental margins (Edelman-Furstenberg, 2009).

This study investigates two sequences, which were deposited during the Late Santonian to the Early Maastrichtian (85–66 Ma) in the Shefela basin and the Late Campanian to Early Maastrichtian (ca. 71.8–69.9 Ma) in the Efe Syncline. The sediments from the Shefela basin were deposited at a further seaward located continental slope

(Gvirtzman et al., 1989) or outer belt region of the Late Cretaceous upwelling system (Almogi-Labin et al., 1993; Almogi-Labin et al., 2012; Schneider-Mor et al., 2012). Depending on the faunal composition and abundance of biogenic silica the spatial classification of the depositional environments was expected to be a near open ocean environment (Edelman-Furstenberg, 2009; Ashckenazi-Polivoda et al., 2010). Furthermore, based on this classification the sediments from the Efe Syncline were deposited closer to the shore, representing the inner belt of the upwelling system (Edelman-Furstenberg, 2009; Ashckenazi-Polivoda et al., 2011; Schneider-Mor et al., 2012). The paleodepth of the depositional environment was located between the middle bathyal to upper abyssal according to the analysis of the foraminiferal assemblage (Ashckenazi-Polivoda et al., 2011).

1.3.2 Material and study sites

Samples from Shefela basin near Jerusalem derive from the Aderet 1 borehole, which has been drilled by Israel Energy Initiatives (Figure 7). The oil shale sequence in the Shefela basin is ca. 300 m thick from Late Santonian to Early Maastrichtian age (~85 to 68 Ma) (Meilijson et al., 2012). The core samples cover the depth between 265–600 m. The whole core was divided into 339 pieces of approximately 1 m length. 102 samples were selected to cover the whole length of the core with a sampling interval of 3 m and out of these samples 64 were chosen for the analysis of the TEX₈₆ data with a temporal resolution of approximately 180 ka. The core covers mainly the upper Cretaceous Ein Zeitim Formation (250–520 m and 538–600 m), which is predominantly composed of relatively soft, dark bituminous chalk with few thin lamina of dark marl (Figure 8 A). This formation is interrupted by a small hiatus (~ 8 m) of the upper Cretaceous Mishash Formation (the Mishash tongue) consisting of bituminous chert and phosphate material.

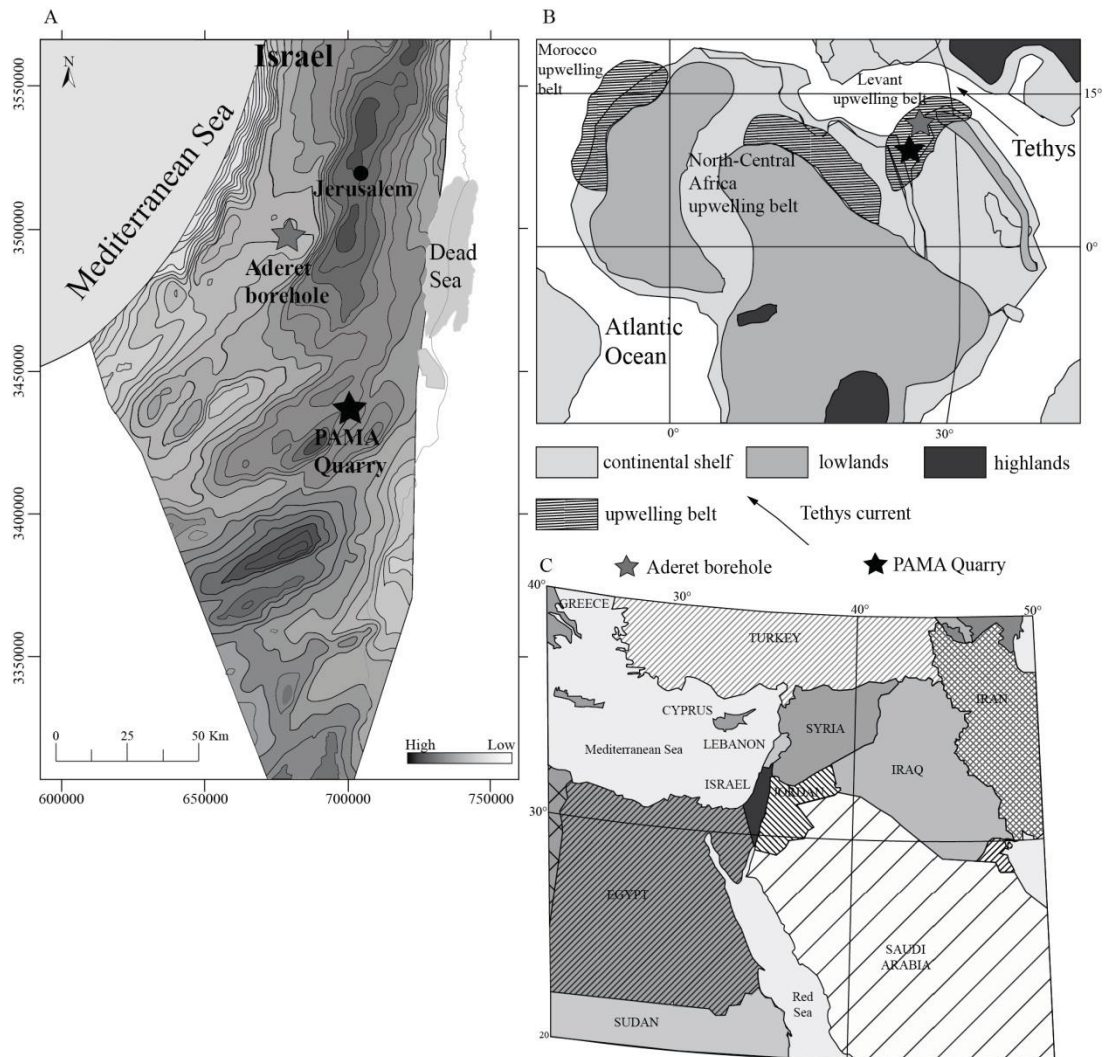


Figure 7: Location map for the two studied areas. A) Position of the PAMA quarry (Efe Syncline) and Aderet 1 borehole (Shefela basin) in a local map of Israel (UTM Coordinate system). Base topography is given in a structural map showing Syrian Arc structures (modified after Gardosh et al. (2008) and Almogi-Labin et al. (2012)). B) Inferred position of the PAMA quarry and Aderet 1 borehole within a paleogeographic map showing the upwelling belts that developed along the southern Tethys margin during the Late Campanian and Early Maastrichtian (from Ashkenazi-Polivoda et al. (2011)). C) Location of Israel shown on a political map of the Middle-East.

Samples from the Efe Syncline ($31^{\circ}04'51.82''\text{N}; 35^{\circ}10'02.85''\text{E}$, northern Negev, Israel) have been obtained from the PAMA quarry outcrop. The sampling material covers ~ 49.6 m and was divided into ~ 220 samples with a length of 0.2 m and a temporal resolution of 20 ka. Out of these samples 111 were selected for the SST reconstructions. The actual distance between the two sampling points is ca. 80 km which would have not changed significantly since the Late Cretaceous. The sample

material was not weathered due to ongoing mining activities. The oil shale section is considerably thinner (~ 40 m) and represents a shorter age interval between Late Campanian and Early Maastrichtian, (~ 71.6–69.8 Ma) (Ashckenazi-Polivoda et al., 2011). The sampled section covers a sequence of about 50 m including a short section of the Mishash Formation representing 3.6 m of the Phosphate Member (PM) and a longer section of the Ghareb Formation composed of 42 m of the Oil Shale Member (OSM) followed upwards by a short sequence (~3 m) of the overlying Marl Member (MM) (Figure 8 B).

The stratigraphic correlation of the profiles is based on biostratigraphic dating from previous studies (Ashckenazi-Polivoda et al., 2011; Meilijson et al., 2012) and is used here for the correlation with global records.

1.4 Sample preparation

20 g of dried and ground rock samples (< 200 µm) from the PAMA quarry were Soxhlet-extracted for 30h using a dichloromethane/methanol mixture (9:1 v/v). For the removal of elemental sulfur, a piece of activated copper (previously activated with 6 N HCl) was added to the extract during the Soxhlet-extraction.

The samples from the Aderet 1 borehole in the Shefela basin were extracted with an accelerated solvent extractor (Büchi SpeedExtractor E-916) because of the limited amounts of available sample material. To verify the equality of the glycerol dialkyl glycerol tetraether (GDGT) composition in the solvent extracts from the SpeedExtractor and the Soxhlet extracts, 20 test extractions of a laboratory internal reference material with known TEX₈₆ values and analyses of the extracts by use of high-performance liquid chromatography (HPLC) coupled with tandem mass spectrometric (MS/MS) detection (HPLC-MS/MS) were carried out and results from the SpeedExtractor were compared with those of the Soxhlet-extraction. The determined TEX₈₆ for 18 samples were within a 2σ confidence band with the known TEX₈₆ value. For the extraction of the samples with the SpeedExtractor, 10 g of dried grounded rock samples (< 200 µm) were mixed with an equal amount of quartz sand (Büchi 0.3-0.9 mm) prior to extraction to avoid clogging of the extraction cells. The sample/sand mixture was filled in a 20 ml stainless steel extraction cell and then heated to 75 °C at 100 bar. Two extraction cycles were performed with a dichloro-

methane/methanol mixture (9:1 v/v). Subsequently the tubes were rinsed for two minutes with dichloromethane/methanol (9:1 v/v) followed by flushing the cells with nitrogen gas for 4 min to remove the solvent mixture. For the removal of elemental sulfur, a piece of activated copper (previously activated with 6 N HCl) was added to the extract which was kept for 12h at 4 °C. After removing the copper by filtration, the solvent mixture was evaporated using a rotary evaporator.

10 mg of the obtained extracts were separated into four fractions by column chromatography using 18 g of silica gel 60 (Merck) and a glass column with 15 mm inside diameter. Fraction F1 was obtained by elution with 80 ml hexane, fraction F2 was eluted with 100 ml hexane/dichloromethane (9:1 v/v), fraction F3 was eluted with 80 ml of dichloromethane/methanol (95:5 v/v) and fraction F4 was eluted with 60 ml methanol. The F3 fraction was further analyzed by HPLC-MS/MS for determination of the TEX₈₆ index.

1.5 TEX₈₆ analysis

The extracts of fraction F3 were dissolved in hexane/isopropanol 99:1 and then filtered through a 0.45µm PTFE filter prior to the measurement with the HPLC-MS/MS. The analyses were performed on a AB Sciex 3200 Q Trap LC/MS/MS system with an autoinjector and Analyst[®] chromatography software. Separation was achieved on a Cyano column (150*2.1 mm, 3µm; Grace, Waukegan, IL, USA), maintained at 30 °C. The GDGTs were eluted isocratically with 99 % hexane and 1 % isopropanol for 5 min, followed by a linear gradient to 10 % isopropanol in 45 min at a flow rate of 0.2 ml/min. After each analysis the column was cleaned by back-flushing hexane/isopropanol (90:10, v/v) at 0.2 mL/min for 10 min.

Detection of the GDGTs was achieved using atmospheric pressure positive ion chemical ionization mass spectrometry (APCI-MS) of the HPLC-eluent. Conditions for APCI-MS were as follows: nebulizer pressure 60 psi, vaporizer temperature 300 °C, drying gas (N₂) flow 6 L/min and temperature 250 °C, capillary voltage 3 kV, corona 5 mA (3.2 kV). Positive ion spectra were generated by scanning m/z 950–1450 in 1.9 s (a representative partial HPLC/MS base peak chromatogram of sample SAOS 27 is given in the appendix Figure A-1 along with the GDGTs and their structures indicated by A1-A6 are shown in the appendix A1-A6, respectively).

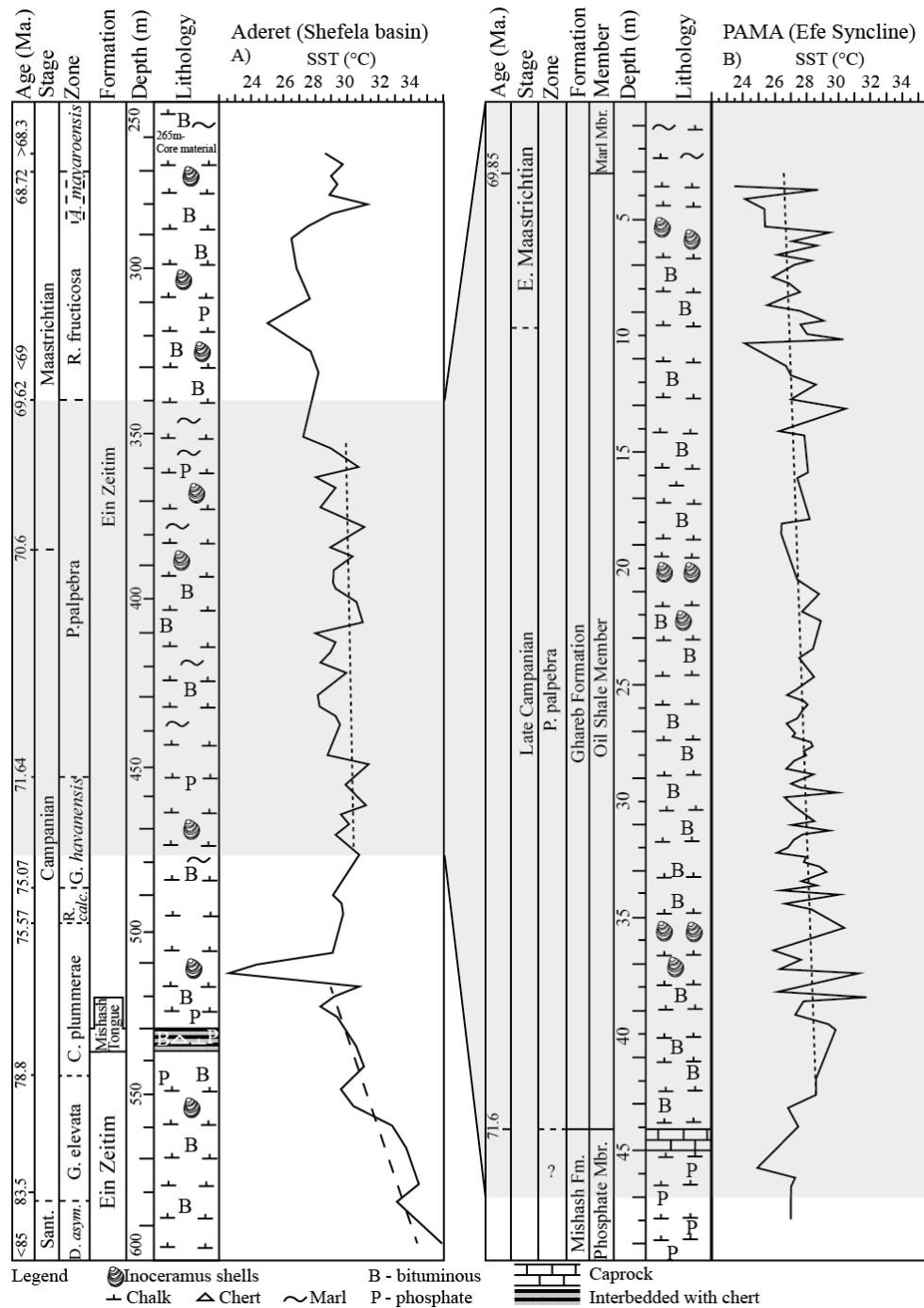


Figure 8: Age, stratigraphic data, lithology and sea surface temperature (SST) based on TEX_{86} data plotted against depth for studied sections from (A) Aderet 1 borehole and (B) PAMA quarry. SSTs are based on TEX_{86} calculated according to equation 12 from Kim et al. (2008) (compilation of all data in Table A-2). The fine dashed line shows the SST trend in the time parallel sequence of the Late Campanian to Early Maastrichtian (column A and B). The coarse dashed line highlights the SST cooling of the Late Santonian to Middle Campanian. Analytical error is ± 0.5 °C. The chronostratigraphy is modified after Meilijson et al. (2012) and Eshet and Almogi-Labin (1996) and in the PAMA quarry section after Ashckenazi-Polivoda et al. (2011).

The analytical method has been adopted from Schouten et al. (2002). For our study, TEX_{86} values were converted to SSTs according to Eq. 6, which is based on the core top calibration of Kim et al. (2008).

$$\text{SST} = -10.78 + 56.2 \cdot \text{TEX}_{86} \quad \text{Eq. 6}$$

We decided on the calibration model developed by Kim et al. (2008) based on the temperature range covered by this equation and the expected SST. Moreover, this calibration provides a low standard error and a good determination coefficient with a great data basis (Kim et al., 2008). We analyzed our data based on different calibration methods to compare these with published data and to further filter the most reasonable results (cf. results in the appendix Table A-2 calculated according to the different calibrations).

Schouten et al. (2003) analyzed sediments from three different locations of the Atlantic Ocean and the Pacific Ocean of Middle Cretaceous age. For their studies they used a modified calibration based on Holocene surface sediments with annual SSTs $> 20 \text{ }^\circ\text{C}$ (Eq. 7).

$$\text{TEX}_{86} = 0.027 \cdot \text{SST} - 0.016 \quad \text{Eq. 7}$$

Another calibration was applied by Jenkyns et al. (2004) for their analysis of Late Cretaceous Arctic Ocean sediments.

$$\text{TEX}_{86} = 0.015 \cdot \text{SST} + 0.29 \quad \text{Eq. 8}$$

The correlation between GDGTs and SST was intensively studied by Kim et al. (2010). Based on 255 samples from various sampling sites, without the subpolar and polar regions, a different calibration model was established. For SSTs between 5 and 30 $^\circ\text{C}$ they suggested a new calibration based on a logarithmic correlation with TEX_{86} .

$$\text{SST} = 68.4 \cdot \log \text{TEX}_{86} + 38.6 \quad \text{Eq. 9}$$

A linear approach with an reciprocal TEX_{86} was used by Liu et al. (2009) for the reconstruction of SSTs from Eocene-Oligocene sediments from 11 globally dispersed sampling sites.

$$\text{SST} = 50.475 - 16.332 \cdot (1 / \text{TEX}_{86}) \quad \text{Eq. 10}$$

Table 1 SST ranges of the Shefela basin and the Efe Syncline sampling site calculated using different calibration models.

Used calibration	a	b	c	d	e	f
Calculated SST (°C)	20.8	22.5	22.5	20.1	23.0	22.9
range Shefela basin	37.0	36.1	31.5	36.3	33.2	30.9
Calculated SST (°C)	22.0	23.5	23.2	21.3	23.9	23.7
range Efe Syncline	32.1	32.0	28.8	31.5	30.5	29.0

^a(Schouten et al., 2002), ^b(Kim et al., 2008), ^c(Schouten et al., 2003), ^d(Jenkyns et al., 2004),
^e(Kim et al., 2010), ^f(Liu et al., 2009)

Our samples were analyzed in duplicate and analytical precision was determined by replicate injections of laboratory internal reference material with known TEX₈₆ values. The analytical error derived from these repeated analysis was < 0.5 °C.

The marine TEX₈₆ index could be biased by GDGTs derived from soil organic material, known as the branched and isoprenoid tetraether (BIT) index (Weijers et al., 2006). This is the case if large amounts of terrestrial material is transported to the marine environment especially by large rivers (Weijers et al., 2006). Even the samples from the proximal Efe Syncline contain only minor amounts of terrigenous material (Schneider-Mor et al., 2012). For the samples from the more distal Shefela basin an even lower influence from terrigenous material can be assumed. Therefore a negative bias from the BIT GDGTs could be excluded.

1.6 Results

For the reconstruction of the SSTs from the two sampling sites of the ancient upwelling systems different calibration models were applied (Schouten et al., 2003; Jenkyns et al., 2004; Kim et al., 2008; Liu et al., 2009; Kim et al., 2010) (cf.

Table 1). We decided to use the calibration developed by Kim et al. (2008) because of the good agreement with other available data for the Late Cretaceous equatorial ocean. Over the whole profile of the Shefela basin core, covering the time from the Late Santonian to the Maastrichtian, the SSTs varied in a range between 22.5 and 36 °C. The sampled profile from the Efe Syncline covers sediments from the Late Campanian to the Early Maastrichtian with a temperature range between 23.5 and 32.0

°C. The variation in the SST recorded in the Shefela basin sequence can be divided into three main sections (Figure 8 A).

The highest SST (36.0 °C) has been determined from Late Santonian sediments at the lowermost part of the Shefela profile (595 m) (Figure 8 A). A significant cooling trend of approximately 7 °C is recorded in the sediments from the Late Santonian and Early Campanian deposited between 85 and 75.57 Ma. The further decreasing temperatures at the Early Maastrichtian and an increasing of SST towards the middle Maastrichtian is reflected in the third interval < 69 Ma.

Subsequently, upwards in the sequence (595–520 m, 84–77 Ma), towards the sediments deposited during the middle Campanian, the SST significantly declines down to 29.3 °C (Figure 8 A). A short-term marked decrease in the SST to 22.5 °C at around 510 m depth (~ 76 Ma) can be observed. This period of cooling passed into a period of relatively stable temperatures with only moderate cooling between 75.57 and 69.62 Ma. During deposition of the sediments (450–265 m), representing Maastrichtian age (~71.5–68 Ma), the SST decreases to a local minimum of 25 °C at a depth of 316 m and finally increases again to ≥ 29 °C in the uppermost part of the studied sequence (Figure 8 A).

For the section analyzed from the PM (48.2 m – 46 m) at the Efe Syncline a mean SST of 26.5 °C was reconstructed. The SSTs of the PM are ~1.5 °C lower compared to the SSTs reconstructed from the sediments of the lower part of the OSM up to approximately 40 m depth. In the upper part of the OSM profile, representing Maastrichtian age sediments (38 m to 3.8 m, 71.4 Ma to 69.85 Ma, Figure 8 B and Table A-2) the TEX₈₆ data provide a mean value of the SST of 27.7 ± 1.3 °C. Within the OSM the SST did not change significantly (indicated by the dotted line Figure 8 B). In the MM GDGTs could not be detected for a reconstruction of SSTs.

For an analysis of the SST difference between the inner and outer belt of the former upwelling system the part of the sequences from both localities representing the period from 71.6 to 69.8 Ma were used (Figure 8). The difference between the mean SST values for the two sampling sites is 1.5 °C, with lower values being obtained from the inner belt sampling site (Figure 8 B).

The temperature shift determined from the time-parallel section of the two sampling locations is close to each other.

1.7 Discussion

1.7.1 Late Cretaceous SSTs and cooling history

The SSTs reconstructed from the sediments of the Shefela basin and the Efe Syncline are in general agreement with the SSTs obtained from other low latitude sampling sites of the Late Cretaceous (Pearson et al., 2001; Wilson and Norris, 2001; Maestas et al., 2003; Steuber et al., 2005; Forster et al., 2007a). From the Late Santonian to the early Maastrichtian the SSTs varied in a range between 23.7 and 36 °C in the Shefela basin and from 23.5 to 32 °C in the Efe Syncline.

Only a few SST data are available for the southern margins of the Tethys in the Late Cretaceous, based on $\delta^{18}\text{O}$ records from the analysis of fish bones and teeth from various locations in Israel, including Efe Syncline (Kolodny and Raab, 1988). These data indicate a prominent decrease in SSTs from 32 °C in the Late Santonian to 20 °C in the early Maastrichtian (Kolodny and Raab, 1988). These data support the observed cooling trend during the early Campanian, although the temperatures are 4–6 °C lower than those calculated in the present study and a detailed correlation along the profile was difficult because of the limited temporal resolution of the index fossils (Kolodny and Raab, 1988).

Tropical SSTs values between 27 to 35 °C, consistent with our data, were obtained from analysis of the $\delta^{18}\text{O}$ isotope composition of shells of rudist bivalves in Mid-Campanian/Maastrichtian sediments from similar paleolatitudes in the northern Atlantic Ocean (8–14°N) (Steuber et al., 2005).

The SSTs up to 36 °C derived from the sediments of the Late Santonian upwelling system are 7–8 °C higher compared to SSTs of the recent tropical region (Dowsett et al., 2012).

In agreement with our data, Clarke and Jenkyns (1999) extrapolated paleo SSTs from $\delta^{18}\text{O}$ data for the low latitudes between 31–36 °C. Additionally, these values are in agreement with TEX_{86} based SSTs of ~35 °C for the Late Santonian reported from Demerara Rise (Ocean Drilling Program Leg 207, Sites 1259) deposited at a similar paleolatitude (Forster et al., 2007a) (Figure 9), although these SSTs were obtained based on different calibration models (Kim et al., 2008). Furthermore, the onset of this significant Late Santonian cooling trend has previously been derived from TEX_{86}

data obtained from the Ocean Drilling Program Leg 207 (site 1259, Demerara Rise, western equatorial Atlantic Ocean (Forster et al., 2007a)). A rapid SST cooling by 2 °C was recorded (Forster et al., 2007a).

Additionally, the recorded cooling trend is in agreement with the cooling previously shown for the Late Santonian to Early Campanian Mooreville Chalk sequence (84.5 to 80 Ma) in the northeastern Gulf of Mexico (Liu, 2009) (Figure 9). Here, SSTs were calculated from $\delta^{18}\text{O}$ measured on bulk material and revealed a continuous decrease of SSTs 31 °C to 24 °C based on the calibration of Erez and Luz (1983). Depending on the calibration models used, the SST varies between 29–23 °C (Epstein et al., 1953) and 28–22 °C (Anderson and Arthur, 1983).

The temperature offset of 5–8 °C (depending on calibration) compared to our data (Figure 9) can be explained by the deposition of the Mooreville Chalk in a more northern paleolatitude (30°N) (Liu, 2009). Furthermore, a difference in the response to the SST between the TEX_{86} and the $\delta^{18}\text{O}$ from bulk carbonates is possible.

Based on Nd isotope studies of fish tooth enamel from various sampling localities within the Tethyan realm, the southern Tethyan margins were suggested to be influenced by a weakening of Pacific Ocean water masses accompanied with a strengthening of a westward Tethys surface current resulting in increased upwelling (Pucéat et al., 2005). This is also supported by a study of Ca and Nd isotopes on phosphatic minerals from the Negev (Soudry et al., 2006). Additionally, a recent study from the Pacific Ocean (Deep Sea Drilling Project Sites 305 and 463; 8°N and 5°S, respectively) and southern high latitudes of the Atlantic Ocean (Deep Sea Drilling Project Site 511, 58°S) (Friedrich et al., 2012) further support the major cooling trend in the Late Santonian (Figure 9). $\delta^{18}\text{O}$ isotope data of benthic foraminifera indicate a cooling of intermediate- to deep water from 20 to 8 °C that occurred from the Santonian to the middle Campanian. This intensive global cooling process has been attributed to the opening and deepening of the EAG and intrusion of cooler Atlantic water masses from higher southern latitudes (Friedrich and Erbacher, 2006; Friedrich et al., 2012).

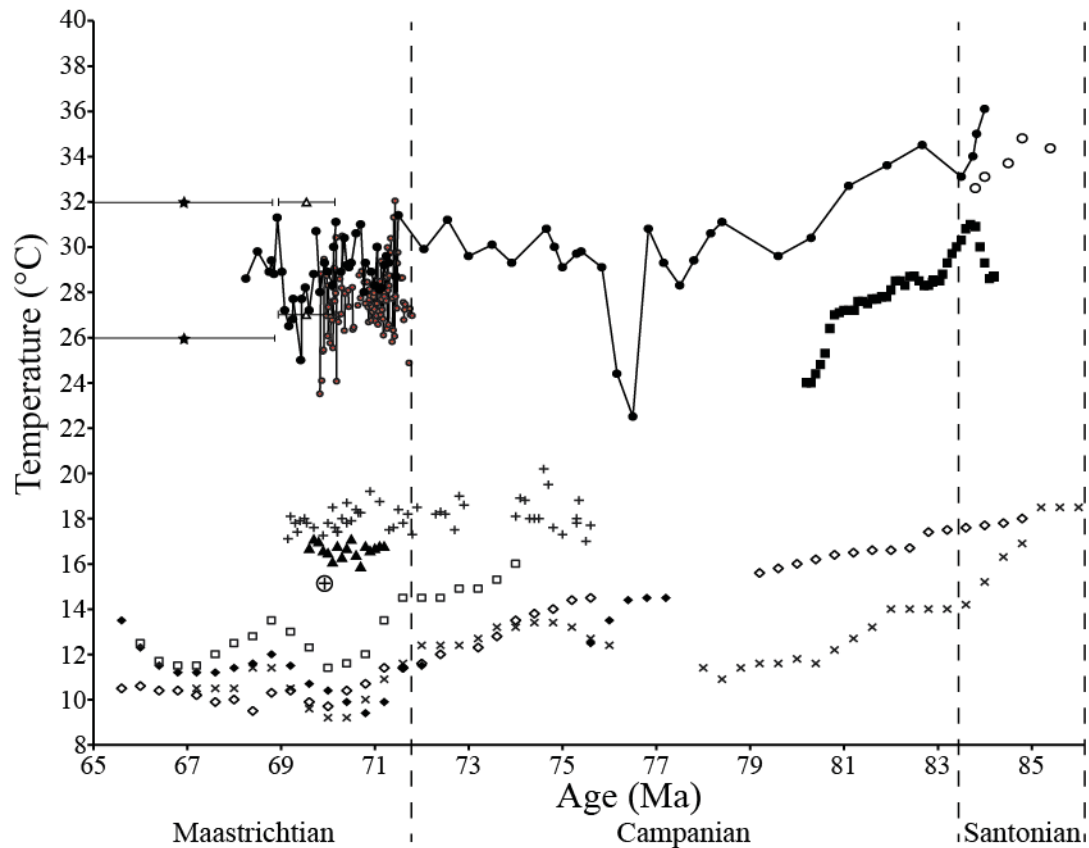


Figure 9: Distribution of reconstructed SSTs covering the Santonian to early Maastrichtian from this study and other published data (all values given in appendix Table A-3).

- This study: PAMA quarry, Efe Syncline (8-15°N; paleo inner belt)
- This study: Aderet 1 borehole, Shefela basin (8-15°N; paleo outer belt)
- Forster et al. (2007a), SST calculated from TEX₈₆ values of samples from western equatorial Atlantic (ODP Leg 207 Site 1259), 5°N
- ⊕ Jenkyns et al. (2004), SST calculated from TEX₈₆ values of samples from the Arctic Ocean (FI-437 and FI-533), 80°N
- Liu (2009), SSTs calculated based on the calibration of Erez and Luz (1983) from δ¹⁸O of bulk material from the Mooreville Chalk of the eastern Gulf Coastal Plain, U.S.A, 30-35°N
- Friedrich et al. (2012), water temperatures from δ¹⁸O values of benthic foraminifera from the subtropical south Atlantic, Walvis Ridge, Deep Sea Drilling Project (DSDP) 525, 30°S
- ◇ Friedrich et al. (2012), water temperatures from δ¹⁸O values of benthic foraminifera from the South Atlantic (Maud Rise, ODP Leg 113 Site 690 C, 65°S; Falkland Plateau DSDP 511, 51°S) and Indian Ocean, Wombat Plateau, ODP Leg 120 Site 750, 57°S
- x Friedrich et al. (2012), SSTs from δ¹⁸O values of benthic foraminifera from the tropical Pacific Ocean at Shatsky Rise and (DSDP 305 and 463), 10°N and 5°S respectively
- ◆ Friedrich et al. (2012), water temperatures from δ¹⁸O values of benthic foraminifera from the North Atlantic, Demerara Rise, 5°N
- ▲ Friedrich et al. (2004), SSTs from δ¹⁸O values of planktic foraminifera from the Blake Plateau western Atlantic DSDP Leg 74 Site 390 A, 30°N
- + Li and Keller (1999), SSTs range calculated from δ¹⁸O values of planktic foraminifera and from the equatorial Pacific DSDP Site 463, 5°S
- △ Wilson and Opdyke (1996) SSTs range calculated from δ¹⁸O values of planktic foraminifera from Leg 144 of the Ocean Drilling Program (ODP), Hole 877A, equatorial Pacific, 8°S
- ★ Pearson et al. (2001), SSTs range calculated from δ¹⁸O values of planktic foraminifera from Lindi, Tanzania (19°S)

Due to the good agreement of this data with the significant cooling of 7 °C resulting from the reconstructed SSTs in the Shefela basin from the Late Santonian/Mid-Campanian we suggest that this change in the circulation of ocean water masses probably also affected the SST of the southern margins of the Tethys.

The significant decline in SST observed in the Aderet 1 borehole profile at 510 m (~76 Ma) correlates with maximum productivity in the upwelling system (Almogi-Labin et al., 1993) and is probably accompanied with an increase of upwelling cool waters. Millennial-scale cooling events up to 3–4 °C have been reported from Holocene upwelling systems off West Africa (20°N, ODP Hole 658C), also caused by an increased upwelling activity (de Menocal et al., 2000). The further moderate decline of the mean SST (by approximately 1 °C) during the Campanian and early Maastrichtian (74 to 69.7 Ma) recorded from the Aderet 1 borehole is much less prominent than the 4–5°C cooling of SST recorded in the Late Campanian (73 to 70 Ma) in the southern Atlantic Ocean DSDP 525A (paleolatitude 36°S) (Li and Keller, 1999). The $\delta^{18}\text{O}$ data from planktic foraminifera in Maastrichtian sediments from Mid-Pacific Mountains (DSDP Site 463), of a paleolatitude (5°S) similar to our study area, provided SSTs in the range from 17 to 19 °C (Li and Keller, 1999) underestimating the SSTs by around 10 °C probably due to early diagenetic overprinting in bottom waters (Figure 9).

At the beginning of the Maastrichtian (316m, ~69 Ma) the SST in the Shefela basin decreased significantly by approximately 3 °C within a relatively short period of time (cf. Figure 9). A comparison with other studies from globally dispersed sampling sites (Figure 9) shows that the ocean water temperatures considerably decrease at the beginning of the Maastrichtian, around 70 Ma. Exemplarily, the bottom water temperatures reconstructed from $\delta^{18}\text{O}$ values of benthic foraminifera from the subtropical south Atlantic, Walvis Ridge, Deep Sea Drilling Project (DSDP) 525, 30°S, show a significant decrease of ca. 3 °C (Friedrich et al., 2012).

The cooling of the SSTs, recorded in the sediments of the Shefela basin, can be interpreted as a delayed response to this globally recognized temperature drop, which is superimposed on the long-term cooling and is known as the Campanian-Maastrichtian Boundary event (CMBE). Recent dating indicates that this event lasted 1.5 million years between 71.5–70 Ma and is marked by a positive excursion in benthic foraminiferal $\delta^{18}\text{O}$ values and coincident change in benthic assemblages from

southern high latitudes near Antarctica (ODP Site 690, Leg 113, south Atlantic Ocean, paleolatitude 65°S) (Koch and Friedrich, 2012). These changes have been attributed to a shift in the sources of intermediate- to deep water masses from low to high latitudes (Koch and Friedrich, 2012).

Table 2 Equator-to-pole SST gradients of the modern earth climate system and suggestions for the Late Cretaceous.

	Modern (Huber et al., 2002)	Previous (Jenkyns et al., 2004)	This study
Equator-to-pole SST gradient (°C/°Latitude)	0.4	0.2	0.3

After this global cooling phase a period of oceanic warming began at ~70 Ma and lasted until ~68 Ma. This is the first of two warming events during the Maastrichtian (Li and Keller, 1998; Li and Keller, 1999). We determined a SST increased from 25 °C to 31 °C in the sediment records from the Shefela basin (approximately 69 to 68.8 Ma, 316–280 m, see Figure 8 A and Figure 9). A sudden increase of ~2 °C – 3 °C in SSTs was reported from the $\delta^{18}\text{O}$ analysis of North Pacific sediments from Shatsky Rise (ODP Leg 198, Sites 1209, 1210 and 1212, ~10°N) (Frank et al., 2005). Furthermore, the SST increase recorded in the sediments of the Shefela basin during the Middle Maastrichtian (< 69 Ma) is supported by the $\delta^{18}\text{O}$ stable isotopic composition of pristine planktic foraminifera in sediment samples from Tanzania (19°S) of Late Maastrichtian age (67±2 Ma) showing high SST between 26–32 °C (Pearson et al., 2001) (Figure 9).

Additionally, a significant SST increase of 6 °C was reported from the analysis of $\delta^{18}\text{O}$ isotopes of planktic foraminifera on Maastrichtian sediments of the North Atlantic (Blake Nose, ODP Site 390 and DSDP Sites 1050 and 1052, paleolatitude 30°N) (MacLeod et al., 2005). It was suggested that the warming was caused by an transport of warm water masses from the South to the North Atlantic (MacLeod et al., 2005). This is in accordance with a similar temperature increase in the Tethys sediments of the Shefela basin, which were probably affected by these warm water masses of the Atlantic Ocean.

1.7.2 Late Cretaceous equatorial to polar SST gradient

We compared our SST data from the equatorial region (71.8–69.8Ma) with published data from the polar region to calculate an equatorial to polar SST gradient. Recently, a mean annual SST of 15 °C (Figure 9) was calculated based on TEX₈₆ data from Campanian to Late Maastrichtian sediment samples of a piston core from the Alpha ridge, northern polar Atlantic Ocean (80°N) (Jenkyns et al., 2004). These data would imply the total absence of polar ice at that time. Jenkyns et al. (2004) uses the $\delta^{18}\text{O}$ data from the western equatorial Pacific Ocean (Wilson and Opdyke, 1996) for their suggestion of an equator-to-pole SST gradient of approximately 15 °C (cf. Table 2). This calculated gradient appears to be too low, compared to the modern SST gradient between these two regions of approximately 30 °C (Dowsett et al., 2012). For the Campanian (75.5–74.5 Ma) an even lower SST gradient of ~ 0.13 °C/° Latitude was calculated by Huber et al. (2002) based on the analysis of $\delta^{18}\text{O}$ data from planktic and benthic foraminifera from the Blake Nose sampling site and the DSDP Sites 511 and 690.

Additionally, these TEX₈₆ and $\delta^{18}\text{O}$ based SSTs are in disagreement with micropaleontological and sedimentological investigations of the Late Campanian sample set from Alpha ridge (CESAR-6 and FI-437) which suggest the occurrence of intermittent sea ice in winter (Davies et al., 2009). Furthermore, statistical studies of plant fossils from northeastern Russia and northern Alaska indicate that the mean air temperature in the Maastrichtian did not exceed 12 °C at higher latitudes (70–80°N) (Spicer and Herman, 2010), from which a SST close to freezing temperature has been estimated (Amiot et al., 2004). These discrepancies may derive from seasonal growth of *Crenarchaeota* resulting in reconstructed SSTs different from the annual mean (Wuchter et al., 2006a; Wuchter et al., 2006b). From Late Paleocene–Early Eocene sediments of the Arctic basin sample site IODP Hole 302-4A (near the North Pole) Sluijs et al. (2006) hypothesize that the TEX₈₆ data provide the summer SST (range 18–23 °C) rather than the annual mean SST in the arctic region.

Wuchter et al. (2006b) analyzed recent sediment trap samples collecting particulate matter from the northeastern Pacific Ocean (33°N and the upwelling area near the California coast (36°N). Additionally, sediment trap samples were taken from the Arabian Sea (17°N). The GDGTs containing the TEX₈₆ signal reaching the deep wa-

ter sediments reflect the annual mean SST, although seasonal variations in SST calculated from TEX_{86} and in situ measured SST were detectable in the upper water layers (Wuchter et al., 2006b). Based on these data we expect that the TEX_{86} derived SSTs from the Shefela basin reflect the annual mean SSTs.

From $\delta^{18}\text{O}$ values of biogenic apatite of continental vertebrates from Late Cretaceous sediments at paleolatitudes ranging from 83°N (Alaska) to 32°S (Madagascar) a terrestrial air temperatures equator to pole gradient of $0.4\text{ }^\circ\text{C} \pm 0.1\text{ }^\circ\text{C}/^\circ\text{Latitude}$ (modern: $0.6\text{ }^\circ\text{C}/^\circ\text{Latitude}$ (Amiot et al., 2004)) was calculated. By comparison, the modern SST gradient is approximately $0.40\text{ }^\circ\text{C}/^\circ\text{Latitude}$ (Huber et al., 2002). From these data a Late Cretaceous SST gradient of $0.26\text{ }^\circ\text{C}/^\circ\text{Latitude}$ can be calculated, based on the assumption that the differences in air temperature between the Late Cretaceous and the present are also valid for SSTs. Based on our TEX_{86} data, from the more seaward located Shefela basin, we calculated a Late Cretaceous ($\sim 71.5\text{--}69.5\text{ Ma}$, sampling interval 450–331 m) equatorial mean SST of $29.2\text{ }^\circ\text{C}$, which is in agreement with zonally averaged SSTs from an ocean general circulation model for the Campanian (80 Ma) (Brady et al., 1998). Amiot et al. (2004) calculated a polar mean SST of $7\text{ }^\circ\text{C}$. Based on these data, we calculate an equator-to-pole gradient of $22\text{ }^\circ\text{C}$ (ca. $0.3\text{ }^\circ\text{C}/^\circ\text{Latitude}$), which is slightly higher than the previous assumption of $0.26\text{ }^\circ\text{C}/^\circ\text{Latitude}$. Additionally, this is further supported by a Late Cretaceous ocean climate model, which indicates an annual mean SST gradient of approximately $26\text{ }^\circ\text{C}$ between the equatorial and polar regions (Otto-Bliesner et al., 2002).

Based on literature data for the polar region and our study, a SST gradient of approximately $0.3\text{ }^\circ\text{C}/^\circ\text{Latitude}$ appears more suitable for the Late Cretaceous, and is in between the modern equator-to-pole SST gradient of $0.4\text{ }^\circ\text{C}/^\circ\text{Latitude}$ (Huber et al., 2002) and the gradient of $0.2\text{ }^\circ\text{C}/^\circ\text{Latitude}$ suggested previously for the Late Cretaceous by (Jenkyns et al., 2004).

1.7.3 Comparison of SSTs in inner and outer belts of the southern Tethyan upwelling system

The sequences representing the period from 71.6 to 69.8 Ma from the two investigated localities were used for the analysis of the SST differences between the inner (Efe Syncline) and outer belts (Shefela basin) of the Tethyan upwelling system (Figure 7).

The SSTs reconstructed from TEX₈₆ data of suspended organic matter from recent studies of the Benguela upwelling system were suggested to reflect mainly colder, deeper water temperatures (Lee et al., 2008). The variances between in situ determined SSTs and the TEX₈₆ based reconstructed temperatures were up to 7 °C. We suggest a relatively minor influence on the TEX₈₆ reconstructed SSTs in both studied locations, because the temperatures are in the range of other tropical locations without upwelling (Wilson and Opdyke, 1996; Wilson and Norris, 2001; Forster et al., 2007a).

The phenomenon of lower SSTs and elevated nutrient concentrations in inner belt areas relative to outer belt areas is the basic principle of upwelling systems and has, for example, been reported for the coastal upwelling system of the Santa Barbara channel south of Point Conception (eg. McPhee-Shaw et al., 2007). The SSTs obtained from high resolution radiometer measurements of the modern California upwelling system also revealed the upwelling of cooler deep water closer to shoreline and higher SSTs at greater distance from the shoreline (Zaytsev et al., 2003). Here, temperature gradients between both areas are in the range of 2–3 °C on a scale of 80–100 km (Zaytsev et al., 2003). From the Benguela upwelling a SSTs differences between inner and outer belts of 3–4 °C on a scale up to 100 km are reported due to the persistent coastal upwelling (Santos et al., 2012). We calculated the SST difference between the outer and inner belt of the Tethyan upwelling system to 1.5 °C, which is more comparable to the California upwelling system. These data were collected between 1970 and 2009 by the UK Meteorological Office (Hadley Center HadISST1 dataset) (Santos et al., 2012). The evaluation has also shown that the temperature of the Benguela coastal waters decreased by 0.13 °C in ten years due to strengthening of the upwelling while the oceanic SST increased by 0.06 °C per decade (Santos et al., 2012). The moderate decrease of the temperature recorded in the inner belt area of the upwelling system in the southern Tethyan margin studied here is probably not associated with an increasing intensity of the upwelling because the intensity and productivity of the upwelling decreased towards the Maastrichtian (Almogi-Labin et al., 1993). The overall decrease of the SST recorded in both, the inner and outer belts is probably related to intensification of the global cooling trend in the Campanian and early Maastrichtian (cf. Figure 9) (Barrera and Savin, 1999; Li and Keller, 1999).

1.8 Conclusion

Our high resolution SST study derived from TEX_{86} data from the southern margins of the Tethys Ocean provide a detailed reconstruction of the paleoceanographic changes from the Late Santonian to Early Maastrichtian. The onset of the Late Santonian cooling is recorded in the sediments from the Shefela basin. The further cooling in the Late Campanian was less prominent as observed in the Atlantic or Pacific Ocean. This cooling is associated with the opening and deepening of the Equatorial Atlantic Gateway. The significant short-time SST decrease in the Shefela basin around 76 Ma can be correlated with an increased productivity and upwelling activity.

Based on our data from the Shefela sequence and published data, we suggest an equatorial to polar SST gradient of about 22 °C for the Late Campanian to Early Maastrichtian that is closer to the modern value than suggested from previous studies of Late Cretaceous sediments.

In the contemporaneous sequences a SST difference documents the influence of the upwelling system. A temperature shift of approximately 1.5 °C reflects the influence of colder water masses closer to the shoreline.

Overall, the reconstruction of the SST record of the Shefela basin sheds light on the evolution of the Late Cretaceous climate. The impact of the changing climate conditions during the Late Cretaceous with global cooling and warming events on the Tethys Ocean is reflected by TEX_{86} data of the present study.

Acknowledgments

Financial support of this study by GIF—The German-Israeli Foundation for Scientific Research and Development, grant no. 956-38.8/2007 and by the LOEWE funding program (Landes-Offensive zur Entwicklung wissenschaftlich-ökonomischer Exzellenz) of Hesses's Ministry of higher Education, Research, and Arts is gratefully acknowledged. The IEI (Israel Energy Initiatives) company is greatly thanked for providing the core from the Aderet 1 borehole, and for the professional and enthusiastic help in sampling the cores and Rotem Amfert Negev Company for their cooperation during the sampling in the PAMA Quarry.

2 Geochemical evidence for the link between sulfate reduction, sulfide oxidation and phosphate accumulation in a Late Cretaceous upwelling system

2.1 Abstract

On Late Cretaceous Tethyan upwelling sediments from the Mishash/Ghareb Formation (Negev, Israel), bulk geochemical and biomarker analyses were performed to explain the high proportion of phosphates in the lower part and of organic matter (OM) preserved in upper parts of the studied section. The profile is composed of three facies types; the underlying Phosphate Member (PM), the Oil Shale Member (OSM) and the overlying Marl Member (MM).

Total organic carbon (TOC) contents are highly variable over the whole profile reaching from 0.6 % in the MM, to 24.5 % in the OSM. Total iron (TFe) varies from 0.1 % in the PM to 3.3 % in the OSM. Total sulfur (TS) ranges between 0.1 % in the MM and 3.4 % in the OSM, resulting in a high C/S ratio of 6.5 in the OSM section. A mean proportion of 11.5 % total phosphorus (TP) in the PM changed abruptly with the facies to a mean value of only 0.9 % in the OSM and the MM.

The TOC/TOC_{OR} ratios argue for a high bacterial sulfate reduction activity and in addition, results from fatty acid analyses indicate that the sulfide-oxidizing activity of bacteria was high during deposition of the PM, while decreasing during the deposition of the OSM.

The upwelling conditions effected a high primary productivity and consequently abundant ability of OM. This, in combination with high sulfate availability in the sediments of the PM resulted in a higher sulfide production due to the activity of sulfate-reducing bacteria. Iron availability was a limiting factor during the deposition of the whole section, affecting the incorporation of S into OM. This effected the preservation of a substantial part of OM against microbial degradation due to naturally-occurring sulfurization processes expressed by the high C/S ratio of 6.5 in the OSM.

Further, the abundant sulfide supported the growth of sulfide-oxidizing bacteria promoting the deposition of P, which amounted to as much as 15 % in the PM. These

conditions changed drastically from the PM to the OSM, resulting in a significant reduction of the apatite precipitation and a high concentration of reactive S species reacting with the OM.

2.2 Introduction

In most anoxic environments, hydrogen sulfide (H_2S) originating from sulfate reduction will preferentially react with reduced iron (Fe) to form Fe monosulfides, which are transformed during diagenesis to pyrite (Berner, 1970). However, when the supply of reduced Fe in the water column and pore water of the sediments is limited and organic matter (OM) is abundantly available, both sulfate reduction by one part of the OM and quenching of the reduced sulfur (S) species by the remaining part of the OM will occur, leading to formation of S-rich sedimentary OM (Hartgers et al., 1997; Schaeffer et al., 2006). Such conditions are typical of highly productive upwelling systems on continental margins with restricted inputs of Fe from terrigenous systems (Eglinton and Repeta, 2011).

Many studies have been carried out to elucidate the mechanism of S reactions with OM in sediments (e.g. Werne et al., 2000). Bacterially-produced inorganic S species, like H_2S , polysulfides or elemental S, are potential agents for the reaction with the OM (e.g. Adam et al., 1993; Aizenshtat et al., 1995; Amrani and Aizenshtat, 2004). Incorporation of elemental S and polysulfides into OM is known to occur in association with two types of chemolithotrophic organisms, the green and purple sulfur bacteria living in photic zone euxinia (e.g. Tang et al., 2009) and sulfide-oxidizing bacteria such as *Thiomargarita*, *Thioploca* and *Beggiatoa* living at sediment surfaces in upwelling areas (e.g. Arning et al., 2008; Arning et al., 2009a; Goldhammer et al., 2010). Upon reaction of these S species with the biomass during early diagenesis, low amounts of S are able to preserve high amounts of OM from microbial degradation. Therefore, incorporation of reduced S into the humic matrix of anoxic sediments will result in an increase of the C/S ratios compared to sediments deposited under normal marine conditions (Nissenbaum and Kaplan, 1972; Francois, 1987).

Dinur et al. (1980) investigated oil shale samples from the Ghareb Formation from different sites in Israel and found that 50-95 % of the total S was organically bound. More recently, Amrani et al. (2005) found a similar value (85 %) for an immature

organic-rich limestone from the Ghareb Formation containing Type-II-S kerogen. Upon hydrous pyrolysis of these samples the early released H₂S formed secondary pyrite, which was isotopically 21‰ lighter than the bulk organic S, indicating that the system was not in equilibrium (Amrani et al., 2005). Large S-isotopic discrimination comparing S incorporated in the oil and in its source kerogen indicated more open system conditions (Amrani et al., 2005), meaning that fresh sulfate was introduced while sulfate reduction proceeded (Schwarcz and Burnie, 1973).

Results from elemental analysis (C and S) of sediments from the Ghareb Formation, which have been reported in several studies before (e.g. Bein et al., 1990; Minster et al., 1992), are rather characteristic of freshwater sediments, despite the fact that deposition took place in a marine environment. Two different reasons were given to explain this discrepancy. The deposition of the Ghareb Formation took place under normal marine conditions and the H₂S generated in the sediment escaped partly into the atmosphere (Minster et al., 1992). This would imply that the water column was entirely euxinic. Bein et al. (1990) provided a different explanation by proposing that deposition of the oil shale took place in the marine environment under a limited flux of sulfate into the sediment, which served to limit the availability of sulfate for OM consumption during sulfate reduction.

More recently, the importance of the chemolithoautotrophic bacteria such as *Thiomargarita*, *Thioploca* and *Beggiatoa* for S cycling in upwelling environments was recognized (Sievert et al., 2007; Zopfi et al., 2008). These organisms, which obtain their energy from oxidizing sulfide by using either molecular oxygen or nitrate (Schulz and Jørgensen, 2001), accumulate elemental S in their biomass and are enriched particularly in anoxic sediments, characterized by a high rate of sulfate reduction (Schulz et al., 2005; Arning et al., 2008).

In sediments from the Namibian shelf, large populations of the sulfide-oxidizing bacteria *Thiomargarita* were found, which are also responsible for the accumulation of phosphorite in the sediments (Schulz and Schulz, 2005). Recently, the accumulation and deposition of phosphate of a marine *Beggiatoa* strain was documented under laboratory conditions (Brock and Schulz-Vogt, 2011). The investigation of shelf sediments from central Chile showed that *Thioploca* influenced the mineralization of P in coastal upwelling systems (Holmkvist et al., 2010). A close relationship between phosphorite formation and sulfate-reducing and sulfide-oxidizing bacteria has also

been shown for other phosphogenic sediments, phosphatic laminites and phosphorites (Schulz and Schulz, 2005; Arning et al., 2008; Arning et al., 2009a). The greater availability of P in coastal upwelling regions has been associated with their higher biological productivity (Ruttenberg, 2003). Modern phosphogenesis is predominantly located in the upwelling regions off Namibia, Chile, Peru, in the Gulf of California and the Arabian Sea (Föllmi, 1996) under suboxic to anoxic conditions.

The biomarker pattern of the sulfide-oxidizing bacteria is not very specific (mono-unsaturated n-C₁₆ and n-C₁₈ fatty acids are dominant) and, as such, it is difficult to trace back their presence in ancient sediments (Arning et al., 2008; Arning et al., 2009a).

In the present study, the proportions of several elements (C, S, Fe and P) and the fatty acid composition were determined in Late Cretaceous sediments from the Mishash/Ghareb Formation (Negev/Israel), covering the facies types of phosphate, oil shale and marls to distinguish between the different depositional environments and explain the facies changes in the upwelling system.

2.3 Material and methods

2.3.1 Location and samples

During the Late Cretaceous, a highly productive upwelling regime existed along the southern margins of the Tethys, lasting nearly 20 million years (Myr) from the Santonian to the late Maastrichtian (Almogi-Labin et al., 1993). The sampled sedimentary profile was deposited during the late Campanian to the early Maastrichtian (71.6 to 69.85 Ma). The sediments, consisting of organic-rich carbonates and phosphorites, belong to the Upper Cretaceous-Eocene phosphate belt, which extends from South America (Colombia) over North Africa to the Middle East (Almogi-Labin et al., 1993; Pufahl et al., 2003).

The samples were obtained from a fresh section within the PAMA quarry at Mishor-Rotem in the northern Negev, Israel (Efe Syncline; 31°04'51.82"N; 35°10'02.85"E). The samples, unaltered by weathering, were obtained during mining activities. The sampling site is shown on a local map of Israel with topographical information (Figure 10 A) and a paleogeographical reconstruction shows the settings during the Cretaceous (Figure 10 B).

The sampled profile (Figure 11) of ca. 50 m is composed of a short sequence of the Mishash Formation [phosphate member (PM) 5.6 m] and the Ghareb Formation, mostly belonging to the oil shale member (OSM, 42 m) and a short sequence of the overlying marl member (MM, ca. 3 m).

The brownish-gray PM is mainly composed of peloids, bone fragments and fecal pellets (Ashckenazi-Polivoda et al., 2011; Meilijson et al., 2014). The condensed layer consists of approximately 20 % dolomite, 45 % fluorapatite, 30 % calcite, and 1–2 wt.% TOC, previously reported in Bein et al. (1990). The OSM is composed of dark gray organic-rich carbonate mudstone with decreasing TOC content from the base to the top.

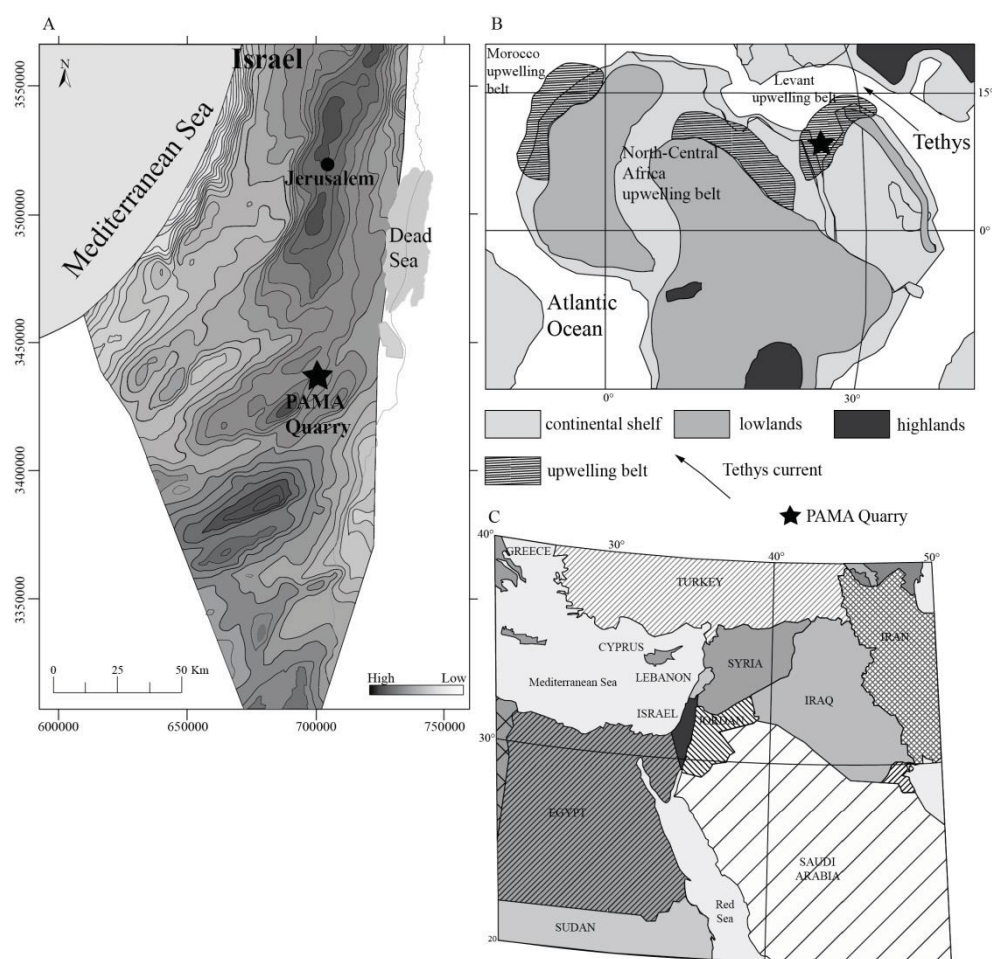


Figure 10: Location map for the studied area. A) Position of the PAMA Quarry (Efe Syncline) in a local map of Israel (UTM Coordinate system). Base topography is given in a structural map showing Syrian Arc structures (modified after Gardosh et al. (2008) and Almogi-Labin et al. (2012)). B) Inferred position of the PAMA Quarry within a paleogeography map showing the upwelling belts that developed along the southern Tethys margin during the late Campanian and early Maastrichtian (from Ashckenazi-Polivoda et al. (2011)). C) Location of Israel shown on a political map of the Middle-East

The MM is a light-yellow marly chalk with TOC values below 1.0 wt.%. The lithology of the whole section has been described in detail by Ashckenazi-Polivoda et al. (2011) and Meilijson et al. (2014).

The TOC, total S (TS), total Fe (TFe) and total P (TP) values were determined on up to 211 samples of the profile.

2.3.2 Sample preparation and analysis

For the measurement of TOC, the samples were analyzed using a LECO RC-412 carbon analyzer. Total Carbon (TC) was determined by combustion of the untreated sample material and TOC was determined after removing carbonate by acidification with hydrochloric acid (10 %). The instrument was calibrated with the synthetic carbon standard 502-029 from LECO Corp. and an in-house CaCO₃ standard. Approximately 100 mg of finely ground sample (< 200µm) were weighed into a quartz glass vessel before combustion.

The TS, TFe and TP contents were determined by means of energy dispersive X-ray fluorescence spectrometry (ED-XRF) on a selected set of samples (ca. every 0.2 m; 197 samples) at the Institute of Mineralogy and Geochemistry of the Karlsruhe Institute of Technology, Germany. For this, ca. 5 g of powdered sample material (<63 µm) was loaded into a Spectro-cup before sealing with 6 µm Mylar film. As radiation source, the instrument (Epsilon 5, PANalytical) used a tungsten X-ray tube, whereas detection and quantification was carried out with a Ge-detector. Detection limit for S was 100 mg kg⁻¹. Analytical precision, based on repeated measurement of reference materials (AGV-1P, GXR-2, GXR-3, GXR-4, GXR-5, GXR-6, SCO-1, SDO-1P, SCO-1, SL1, SOIL V, SOIL VII) was generally better than ±5 % for S and P and ±0.6 % for TFe content (expressed as Fe₂O₃), respectively.

The TOC and TS values were used to calculate the TOC_{OR}. The TOC_{OR} can be used for the estimation of the TOC before the loss of OM via sulfate reduction during diagenesis. It is calculated from Eq. 11 according to Vetó et al. (1994).

$$\text{TOC}_{\text{OR}} = \text{TOC} + \text{TOC}_{\text{SR}} \quad \text{Eq. 11}$$

TOC_{SR} is the loss of TOC by sulfate reduction and has been calculated using Eq. 12 (Vetó et al., 1994):

$$\text{TOC}_{\text{SR}} = \frac{\text{TS} \cdot 0.75}{(1 - q\text{H}_2\text{S})} \quad \text{Eq. 12}$$

The value $q\text{H}_2\text{S}$ describes the reoxidation by sulfide oxidizing bacteria or escape of H_2S . With a value of 0.35 an intense sulfide re-oxidation by chemolithotrophic bacteria such as *Thioploca* spp. is assumed (Ferdelman et al., 1997).

Bacterial sulfate reduction can be simplified described by Eq. 13:



A reduction of 1 % of S is equivalent to a loss of 0.75 % of TOC.

For the analysis of lipid biomarker 20 g dried grounded rock sample ($< 200 \mu\text{m}$) were Soxhlet extracted for 30 h with dichloromethane/methanol (DCM/MeOH) 9:1. The solvent was evaporated using a rotary evaporator. An aliquot (10 mg) of the extract was separated into fractions of saturated hydrocarbons, aromatic hydrocarbons and polar N-, S-, O-containing compounds via column chromatography (20 g silica gel 60, Merck; glass column, 15 mm i.d). The composition of saturated and aromatic hydrocarbon fractions will not be discussed in the present paper. The fatty acids in the polar fractions were derivatized to trimethylsilylestere using 35 μl N,O-bis(trimethylsilyl)trifluoroacetamide (BSTFA) and 7 μl pyridine at 70 °C for 1 h. The polar fractions were analyzed using gas chromatography-mass spectrometry (GC-MS) with a Trace GC Ultra gas chromatograph coupled to a dual stage quadrupole (DSQ II) mass spectrometer (Thermo Fisher Scientific). The system was equipped with a TR5-MS column (30 m, 0.25 mm i.d., 0.25 μm film thickness; Thermo Fisher Scientific). The diluted fractions were injected in splitless mode with a splitless time of 1 min. The GC oven temperature was programmed from 40 to 320 °C at 3 °C min^{-1} .

The mass spectrometer was operated in electron ionization (EI, 70 eV) and full scan mode. Helium was used as carrier gas. The data were recorded, processed and quantified with Xcalibur[®] software. As internal standard 3 μl of 1,1-binaphthyl ($1 \mu\text{g} \mu\text{l}^{-1}$) was added to the polar fraction.

2.4 Results and discussion

2.4.1 TOC, TFe, TS and TP

TOC was determined in 211 samples and the data are shown in Figure 11 (all data are compiled in appendix Table A-4).

Within the PM, the mean value of TOC was 2.7 %. At 48.2 m a thin section with a very high TOC value of 17.2 % is intercalated (Figure 11 a). The transition from the Ghareb Formation to the Mishash Formation is represented by a substantial hiatus visible as a condensed interval of 1 m thickness, which separates the PM from the OSM. A sharp increase in TOC from 1.9 % to 17.7 % is apparent between the condensed layer and OSM. Within the OSM the TOC values tend to decrease from the bottom to the top of the section. In the lower part of the OSM section (42.8–35 m), the mean TOC values tends to decrease from 18.0 % at the bottom to 10.3 % at the top. One exceptional high value is observed at 35.6 m depth (24.5 %). The facies change from the OSM to the MM is characterized by a sharp decrease of the TOC to 1.4 %. In the MM section the TOC values are in a range between 0.6 to 1.4 % (Figure 11 a).

The TOC/TOC_{OR} ratio reflects the proportion of remaining TOC after bacterial sulfate reduction. The original TOC (TOC_{OR}) and the TOC/TOC_{OR} ratios are plotted in Figure 11 b and c together with the contents of TFe (Figure 11 d), TS (Figure 11 e) and TP (Figure 11 f) determined in 197 samples. The TOC_{OR} (Figure 11 b) varies largely parallel with the TOC content along the total profile. The lowest TOC/TOC_{OR} ratios, with a mean value of 0.72, are observed in the PM, indicative of a higher degree of sulfate reduction here compared to the OSM and MM sections. In the OSM, the TOC/TOC_{OR} is very homogeneous, with values varying between 0.68 and 0.88 (mean 0.85), implying stable environmental conditions during sedimentation. Furthermore, this indicates an intensive bacterial consumption of the originally deposited OM for sulfate reduction during deposition of most parts of the OSM. Similar reduction rates were reported from the recent upwelling system in the northeastern Arabian Sea (Lückge et al., 1999). In the MM the ratio of TOC/TOC_{OR} (Figure 11 c) varies between 0.75 and 0.99, with high fluctuation indicating changing environmen-

tal conditions. The effect of sulfate reduction on the precipitation of phosphate is discussed later.

The TFe content along the profile shows a trend largely opposite to that observed for TOC (Figure 11 d). The lowest abundance is in the PM (between 0.1 % and 0.2 %), interrupted by only one sharp maximum of 0.7 % at 48.2 m. Within the hiatus the TFe content increases from 0.1 % to 0.6 %. The TFe content varies between 0.5 and 3.1% for the OSM and between 1.4 and 2.4 % for the MM, demonstrating a slightly increasing trend in concentrations towards the OSM.

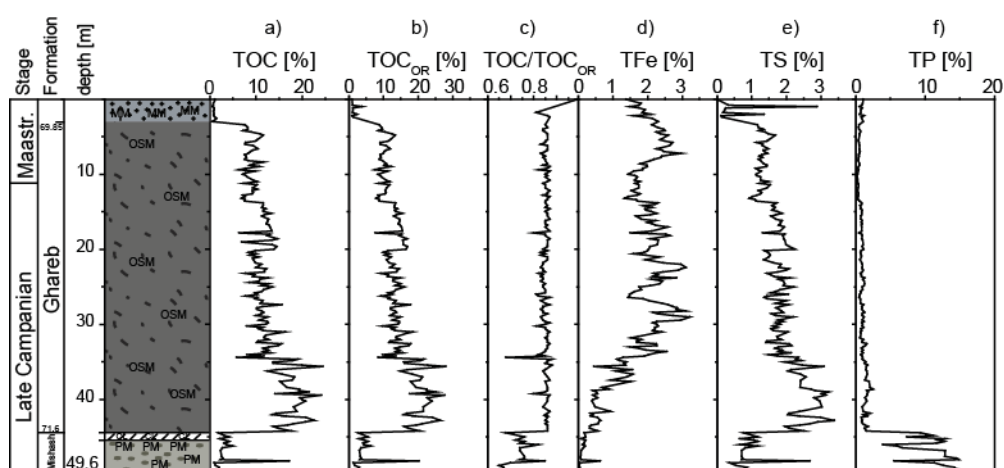


Figure 11: Stratigraphy, age, depth and lithological profile (cf. Ashckenazi-Polivoda et al. (2011)). MM, Marl Member; OSM, Oil Shale Member; CL, condensed layer; PM, Phosphate Member) of the sampled section with (a) variation in TOC, (b) calculated original TOC (TOC_{OR}), (c) TOC/TOC_{OR} ratio, (d) TFe, (e) TS and (f) TP.

Within the PM, the TS content (Figure 11 e) fluctuates slightly around a mean value of 0.8 %, with the exception of one sample at 48.2m, which also shows a maximum in TOC and TFe content. At the transition to the adjacent OSM, the TS content increases significantly from 1.1 to 2.5 %. The TS values vary somewhat in parallel with the TOC values. Within the OSM it follows the same trend as observed for TOC. The proportion of TS is higher in the lower part of the profile (mean value 2.6 %) compared to the upper part (mean value 1.5 %). The TS content (Figure 11 e) in the MM fluctuates between 0.1 % and 2.9 %, with two high outlier values at 1 m (2.9 %) and 2 m (1.4 %).

TP is significantly enriched in the PM and fluctuates between 3.9 % and 15.0 % with a mean proportion of 11.5 % (Figure 11 f). With the facies change from the PM/h hiatus to the OSM the proportion of TP in the sediments decreases drastically.

Further upwards along the profile, the amount of TP is low with a mean value of only 0.9 % in the OSM and the MM.

2.4.2 Correlation of TOC and TS

Figure 12 (all data in appendix Table A-4) shows the correlation diagram of TOC and TS, which was previously introduced by Berner and Raiswell (1983) and Leventhal (1995). The dashed lines indicate the field for sediments deposited under normal marine conditions, with C/S values between 2.8 (Berner and Raiswell, 1983) and 3.6 (Leventhal, 1995). C/S values for freshwater sediments will plot close to the dotted lines, with values between 10 (Berner and Raiswell, 1984) and 25 (Leventhal, 1995). As expected, the values obtained for samples from the three different facies types plot in different areas of the diagram. The values from the PM plot between the lines of 2.8 and 3.6, suggestive of normal marine conditions (Berner and Raiswell, 1984).

These results are in contrast to organic geochemical and micropaleontological investigations of this section. According to the very low pristane/phytane ratio (Schneider-Mor et al., 2012) and investigations based on the foraminifera assemblage (Ashkenazi-Polivoda et al., 2011), this part of the sequence should have been deposited under oxygen deficient conditions. These conditions would imply a higher TOC content of the sediment and hence resulting in a higher C/S ratio. This discrepancy in the C/S ratio may be attributed to an intensive bacterial decomposition of the OM, due to sulfate reduction and sulfide oxidation, in combination with the deposition of phosphate in the PM (e.g. Schulz and Schulz, 2005; Algeo and Ingall, 2007; Arning et al., 2009a; Berndmeyer et al., 2012; Dale et al., 2013).

The TS values for the OSM correlate strongly ($R^2 = 0.85$) with TOC values and provide a slope of 0.12. In general, this is a characteristic value for euxinic environments (Minster et al., 1992). However, biomarkers such as aryl isoprenoids, indicating photic zone euxinia were absent in the GC-MS analyses of all sediment extracts. The samples from the OSM plot between the freshwater and normal marine field had a mean C/S ratio of 6.5. Similar C/S ratios have previously been reported for samples from the Ghareb and the Mishash Formation in Mishor Rotem (Minster et al., 1992) and boreholes from the Zin Valley and Shefela (Bein et al., 1990). This reflects the

higher primary productivity (Almogi-Labin et al., 1993) and preservation of the OM during deposition of this section. C/S ratios previously found in sediments from the Benguela, Peru and Oman upwelling zones are 1.3, 1.8 and sometimes even 2.8 times higher, compared to C/S ratios determined from sediments deposited under normal marine conditions (Morse and Emeis, 1990).

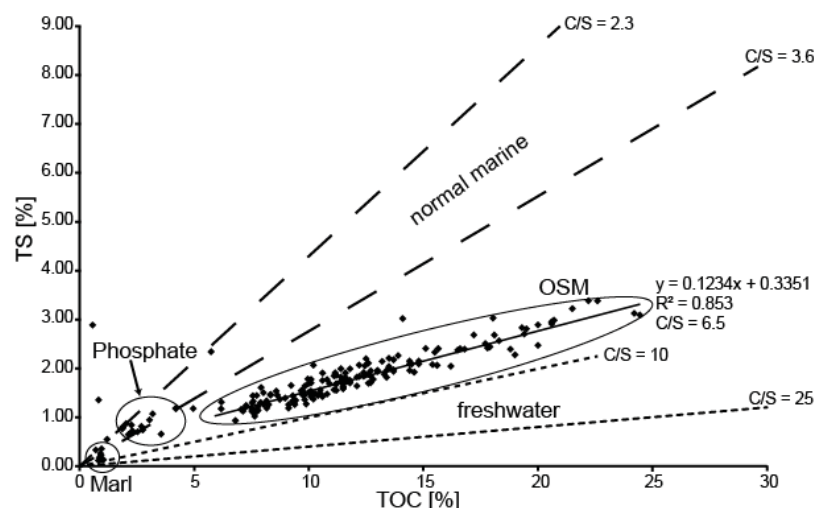


Figure 12: Plot of TS vs. TOC according to Berner and Raiswell (1983) with modifications adopted from Leventhal (1995). The fine dotted line indicates non-marine (freshwater) environments of deposition. Data points from normal marine environments usually plot between both dashed lines. The samples from the MM and the PM plot along the line indicating normal marine conditions, whereas data points of the OSM plot in the field between normal marine and freshwater conditions. This provides further evidence for

an enhanced preservation of OM in upwelling environments, due to naturally occurring sulfurization processes. The C/S ratio of the OSM in the present study is between that of the Peru and Oman upwelling system (2.3 times higher than expected for normal marine conditions as shown in Figure 12). Comparable results with C/S values of more than twice as high as expected from normal marine sediments were also reported for marine upwelling sediments from the Arabian Sea (Lückge et al., 1999; Schenau et al., 2002).

The low amount of TFe, particularly in the PM and the lower section of OSM (Figure 11 d), also supports that a significant proportion of TS has been fixed in the organic matrix, due to the limited Fe availability in the depositional environment. The OM becomes more resistant against microbial degradation, whereupon high amounts of OC can be preserved by low amounts of reduced S (Sinninghe Damsté et al., 1989b; Morse and Emeis, 1990). This was previously attributed to a low tempera-

ture vulcanization process, in which macromolecular organic compounds are generated through sulfide bridges, preserving the OM in environments where reduced S is not rapidly consumed by Fe^{2+} in the water column or porewater (Adam et al., 1993). This is well reflected by the geochemical data in Figure 11 showing an inverse trend for S/C and Fe in the OSM.

This is largely consistent with the previously reported proportion of 85 % organically bound S in the Ghareb Formation (Amrani et al., 2005). Consequential, OSM samples with ca. 15 % TOC contain about 2 % organically bound S. This gives a TOC/S_{org} ratio of 7.5, which can be compared with TOC/S_{org} values for kerogen from the Peruvian upwelling system (6.6 to 33; Mossman et al. (1991)) and from the Monterey oil shale (15 to 50; Orr (1986)). The degree of OM sulfurization in the Mishash/Ghareb Formation therefore tends to be slightly higher than in recent sediments from the Peruvian upwelling area and much higher than in the Miocene Monterey Formation, which was also deposited in an upwelling environment.

However, the excess H₂S in Fe-limited environments might not only react with organic compounds but might also be re-oxidized. According to Goldhaber et al. (1977) and Jørgensen (1978), up to 90 % of the H₂S produced in the shelf sediments with concomitant high rates of bioproduction and high bioturbation might be lost due to re-oxidation after transport to the surface.

2.4.3 Correlation of TOC, TS and TFe

Figure 13 (data shown in appendix Table A-4) shows a ternary correlation diagram for TOC, TS and TFe introduced by Dean and Arthur (1989) for the reconstruction of paleoenvironmental conditions during deposition of sediments. Fine dotted lines were used to illustrate environments of sediment deposition under oxic, dysoxic and anoxic conditions (Ross and Bustin, 2009). Samples plotting below the line of 100 % Fe fixation as pyrite are characterized by an excess of S and organically bound S compounds (OSC) (Dean and Arthur, 1989; Arthur and Sageman, 1994). The data from the MM samples plot with two exceptions in the field of oxic conditions, which is consistent with the low amount of organic carbon in this section. In contrast, data from the OSM samples argue for deposition under dysoxic to anoxic conditions (see Figure 13). Samples from the base of the OSM plot in the field indicating excess of S

during sedimentation. This is consistent with the observations from the analysis of the pristane/phytane ratio (Schneider-Mor et al., 2012) and micropaleontological investigations (Ashckenazi-Polivoda et al., 2011) of this section indicating a low sea floor aeration.

Also included in Figure 13 is the empirically found relationship between TOC and TS for sediments deposited under "normal" marine conditions (Berner and Raiswell, 1983), shown by the fine dashed line indicating a C/S ratio of 2.8. For the three different facies types three different trends in the diagram are apparent. The samples from the PM show a fluctuating C/S ratio between 2.8 and 6.5. The PM samples clearly plot in the field below the pyrite line, indicating Fe limitation and an excess of S availability. OM is still available, but in highly biodegraded form, as indicated by results from GC-MS analysis of the saturated hydrocarbon fraction of samples from those sections. Short to long chain n-alkanes in the PM section are completely degraded, while in the OSM section these n-alkanes are present.

In accordance with Dean and Arthur (1989), the mean C/S ratio of 6.5 in the OSM, indicated by the coarse dashed line, suggests that a high proportion of S is not present as pyrite. Similar values were found by Lückge et al. (1996) in samples from the Oman upwelling region, likely due to an increased incorporation of S into OM as a result of iron-limiting conditions. An abundance of reactive OM is associated with highly productive upwelling systems, which increases the rate of sulfate reduction to H₂S (Berner and Raiswell, 1983). This, in combination with a limited incursion of Fe increases the amount of organically bound S.

In the ternary diagram (Figure 13), the OSM samples neither plot along the 100 % pyrite line nor along the C/S 2.8 line; instead the data points crosscut the 100 % pyrite line, with samples from the OSM base plotting below, and samples from the OSM top plotting above, this line. However, this cannot be interpreted as a result of changing environmental conditions from Fe-limited conditions to OM-limited conditions during deposition of the sediments going from the bottom to the top of the profile. Instead, Fe-limited conditions prevailed throughout deposition of the whole section but were more apparent during deposition of the bottom part of the OSM compared to the upper part. This particular situation will develop when the highly abundant OM in upwelling sediments is degraded by sulfate-reducing bacteria and more H₂S is generated than can be quenched by the reduced Fe in the sediment. In this

case, refractory sulfurized OM is produced, which cannot be utilized by sulfate-reducing bacteria.

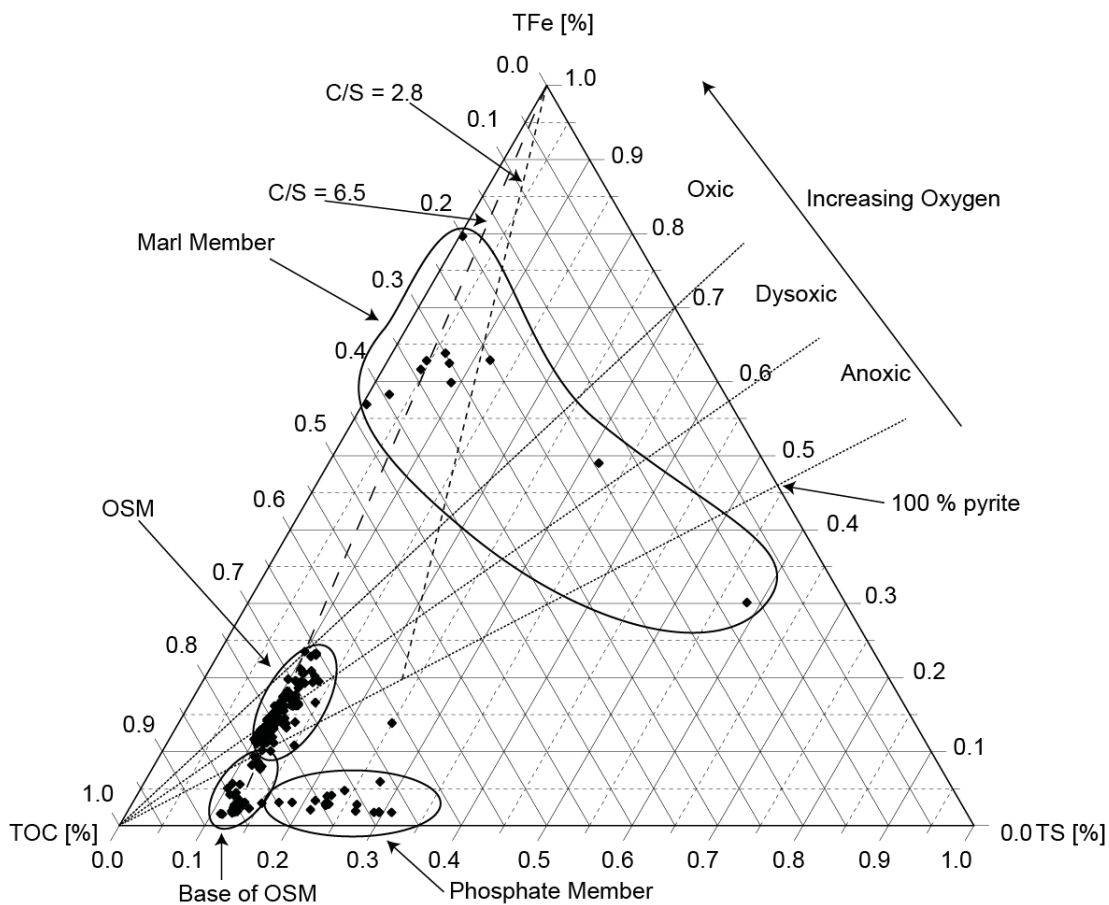


Figure 13: Ternary plot of TOC, TS and TFe according to Dean and Arthur (1989). The fine dashed line represents a C/S ratio of 2.8 which is indicative for samples deposited under normal marine conditions according to Berner and Raiswell (1983). The coarse dashed line results from the measured data on samples from the OSM with a mean C/S ratio of 6.5. The different facies types are marked with elliptical labels. The OSM samples are separated in an upper part of the section labeled as OSM and a lower part of the section labeled “Base of OSM”. The fine dotted line (100 % pyrite) represents conditions where all reactive iron in the sediment would be present as pyrite. Fine dotted lines are further used to separate different oxygenation levels according to Ross and Bustin (2009)

A similar situation has been found in Late Albian samples from the North Atlantic studied by Hofmann et al. (2000), by way of TOC-TS-TFe relationships comparable to those in the OSM facies.

The samples from the MM also show high variability in the C/S ratio. A mean C/S ratio cannot be derived from these data. With one exception, the samples plot above the pyrite line which indicates restricted availability of degradable OM during sedi-

ment deposition. This was probably effected on the one hand by the reduced productivity in the upwelling system and on the other hand by an increasing sea floor aeration (Ashckenazi-Polivoda et al., 2011). Such OM-limited conditions were previously described by Hofmann et al. (2000) from the western North Atlantic drilling Site 386.

2.4.4 Correlation of phosphate precipitation with sulfate reduction

In recent publications it was demonstrated that sulfate-reducing and sulfide-oxidizing bacteria force the precipitation of phosphate in ancient and modern upwelling systems (e.g. Schulz and Schulz, 2005; Algeo and Ingall, 2007; Arning et al., 2009a; Arning et al., 2009b; Brock and Schulz-Vogt, 2011; Berndmeyer et al., 2012; Lepland et al., 2014).

Figure 14 (data shown in appendix Table A-4) shows the correlation of the TOC/TOC_{OR} ratio and the proportion of TP [%] according to Lückge et al. (1999). The correlation of TOC/TOC_{OR} and TP was used to determine whether the phosphate deposition was influenced by the sulfate reducing process. Sulfate reduction and sulfide oxidation played a crucial role in the accumulation of phosphate in modern upwelling systems, like those of Peru and Namibia (Brock, 2011).

This close relation between the precipitation of phosphate and the reduction of sulfate is reflected by the geochemical data of the analyzed profile. The mean TOC/TOC_{OR} ratio of 0.73 in the PM section indicates an intensive sulfate-reducing process and is in accordance with the accumulation of TP up to 15% (Figure 11 c and 11 f). The PM and OSM sections were analyzed separately because of the clearly different environmental conditions which prevailed during their sedimentation. In contrast to the OSM section, the phosphates in the PM segment significantly correlate with the TOC/TOC_{OR} ratio ($R^2=0.53$).

Further support for the interaction between sulfide oxidation and phosphate precipitation comes from Schulz and Schulz (2005), who analyzed Namibian shelf sediments, populated by the sulfide-oxidizing bacterium *Thiomargarita*. They found a correlation between the occurrence of these sulfide-oxidizing bacteria and increased deposition of phosphate. Goldhammer et al. (2010) used organic rich sediments from the Benguela upwelling system to analyze the role of sulfide-oxidizing bacteria in the

sequestration of P. With ^{33}P radiotracer the accumulation of P in these bacteria was observed and the release of inorganic phosphate under anoxic conditions from which apatite can precipitate. Goldhammer et al. (2010) found that the large sulfide-oxidizing bacteria gain their energy from nitrate which directly influences the precipitation of P under anoxic conditions.

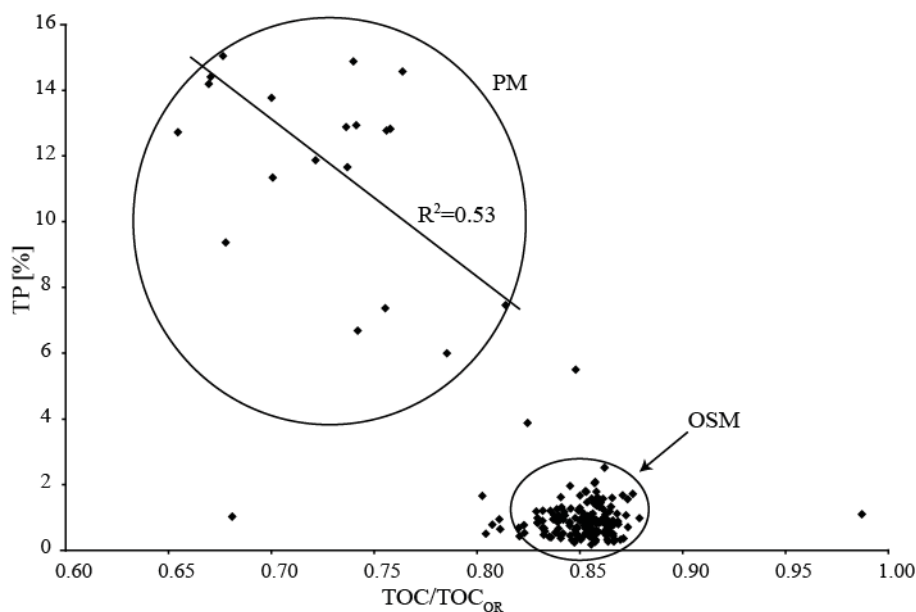


Figure 14: Correlation diagram of TP[%] and TOC/TOC_{OR} ratio. The data points belonging to the OSM and PM are marked. The sulfate reduction and proportion of TP show a strong correlation ($R^2 = 0.53$).

Brock and Schulz-Vogt (2011) cultivated sulfide-oxidizing bacteria of the species *Beggiatoa* and demonstrated that these bacteria store large amounts of phosphate under oxic conditions. These bacteria live at the oxygen-sulfide interface of the sediment (Schulz and Jørgensen, 2001). The sulfide is produced in the deeper sediment by bacteria reducing sulfate and oxidizing organic material to gain their energy. The large sulfide-oxidizing bacteria use oxygen or nitrate to re-oxidize the sulfide to sulfate and gain energy out of this process (Schulz and Jørgensen, 2001; Arning et al., 2009a). The nitrate is stored in vacuoles which is used under the euxinic conditions in the sediment for the oxidation of sulfide (Schulz and Jørgensen, 2001). Under conditions of low sulfide concentrations, bacteria like *Beggiatoa* store polyphosphates in vacuoles within their cells (e.g. Arning et al., 2009a; Brock and Schulz-Vogt, 2011; Brock et al., 2012). When switching from oxic to anoxic conditions with high sulfide concentrations, the stored polyphosphate is hydrolyzed by these bacteria

and phosphate is released to the sediment and precipitates as apatite (Brock and Schulz-Vogt, 2011) (Figure 15).

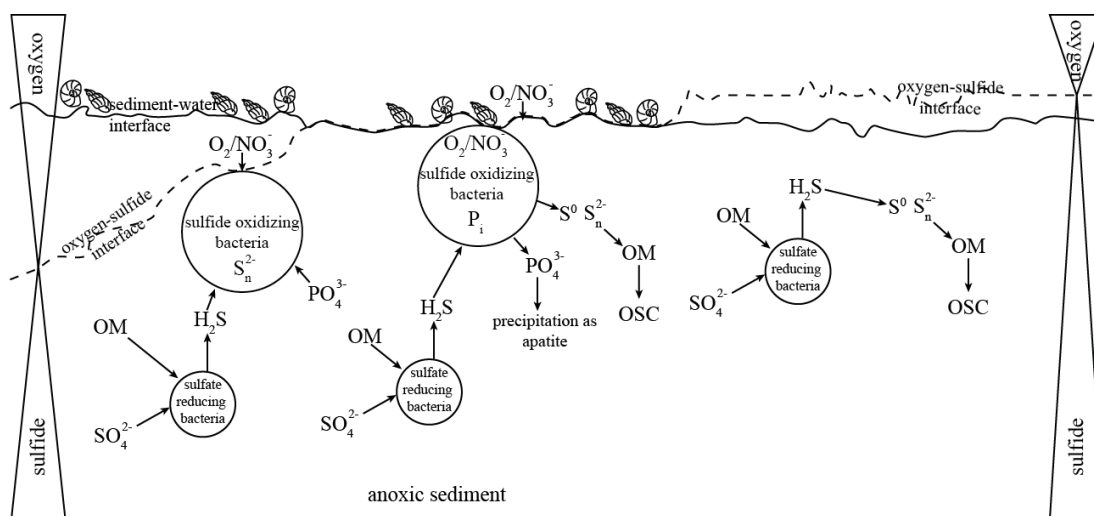


Figure 15: Schematic illustration of bacterial sulfate reduction and sulfide oxidation under changing redox conditions and the effect on the phosphate deposition (Modified after Brock and Schulz-Vogt (2011) and Dale et al. (2013))

Figure 15 illustrates the link between the interaction of sulfate reduction, sulfide oxidation and phosphate precipitation during the deposition of the PM and the OSM. The left side of Figure 15 shows the conditions that prevail in Fe-poor sediments when the oxygen-sulfide interface is below the sediment-water interface. In this case the availability of sulfate for sulfate-reducing bacteria is low since diffusion of sulfate from the sea water into the porewater of the sediment is hindered. As a consequence, H_2S production and the activity of sulfide-oxidizing bacteria will also be low due to the restricted availability of oxygen and nitrate deeper in the sediment. Under these conditions sulfide-oxidizing bacteria re-oxidize H_2S to sulfate will take up phosphate and accumulate polyphosphate in their cell walls for energy storage (e.g. Schulz and Schulz, 2005; Goldhammer et al., 2010; Brock and Schulz-Vogt, 2011). Abundant benthic foraminifera will colonize the sediment-water interface. When the oxygen-sulfide interface interferes with the sediment-water interface, the situation shown in the middle of Figure 15 will establish. More sulfate will be available in the sediment and sulfate reduction will increase. High sulfide concentrations in the sediments will force the sulfide-oxidizing bacteria to release S and polysulfides as well as phosphate into the sediment (Berg et al., 2014) and the phosphate will be precipi-

tated as apatite. Benthic foraminifera can survive under these conditions and will co-exist with sulfide-oxidizing bacteria (Høgslund et al., 2008). The elemental S and the polysulfides will react with OM in the sediment under formation of OSC (Brassell et al., 1986b; Vairavamurthy and Mopper, 1987; de Graaf et al., 1992). When the oxygen-sulfide interface is moving further upwards into the water column (Figure 15 right side) sulfide-oxidizing bacteria cannot survive in the sediment due to the absence of molecular oxygen. The H₂S from sulfate reduction generates sulfidic bottom water conditions and accounts for the increasing amounts of OSC generated in the Fe-poor depositional environment.

During deposition of the PM the situation shown on the left side and in the middle of Figure 15 prevailed with the oxygen-sulfide interface moving temporarily from the surface into the sediment which is in accordance with the high abundance of benthic foraminifera (Ashckenazi-Polivoda et al., 2011). Under these oscillating redox conditions the sulfide-oxidizing bacteria have their greatest phosphate storing ability (Dale et al., 2013). This forced an accumulation of P, which is 7 to 10 times higher in concentration compared to the OSM.

During deposition of the OSM the oxygen sulfide interface remained close to the sediment interface and the abundance of both sulfide-oxidizing bacteria and benthic foraminifera decreased. The data obtained in the present study do not support the establishment of an euxinic water column during deposition of the OSM (Figure 15 right side) since benthic foraminifera are still present throughout the whole section although in lower abundance compared to the PM. Within the OSM sea floor aeration was lower in the bottom section and increased towards the top of the OSM section and even further in the MM section according the composition of planktic and benthic foraminifera (Ashckenazi-Polivoda et al., 2011).

The elevated primary productivity of the upwelling system supports the development of an OMZ in the mean water (Almogi-Labin et al., 1993). During the deposition of the OSM, conditions in the sediment became anoxic due to the expansion of the OMZ to the sediment-water interface, as indicated by the accumulation of OM and the high abundance of organically bound S (up to 90 %) in this section (Dinur et al., 1980; Bein et al., 1990). The more anoxic and sulfidic conditions during the sedimentation of the OSM lead to more resistant OM being preserved as organic S compound (OSC). Various of these compounds like thiophenes, thiolanes, hopanoid thio-

phenes and further compounds originating from these environmental conditions were detected by our GC-MS analyses. The diagenetic pathways and conditions of their origin were in detail described previously by different authors from the geologically corresponding Jurf ed Darawish in Jordan (e.g. Sinninghe Damsté et al., 1989b; Kohnen et al., 1990b; Hofmann et al., 1992; Sinninghe Damsté et al., 1995b; Sinninghe Damsté et al., 1998a).

The large sulfide-oxidizing bacteria decreased in abundance compared to the PM and were not further able to accumulate polyphosphate for energy storage. The deposition of P would no longer be promoted by these bacteria. This is reflected by the comparably low amounts of P (ca. 1%) in this section, values which are common for marine sediments (Ruttenberg, 1992).

Soudry and Champetier (1983) analyzed Campanian phosphorite sediments from the Negev/Israel with microscopic and SEM techniques. They found filamentous, tubular structures in the phosphatic matrix and suggested an algal or cyanobacterial origin. However, similar structures are also known from sulfur bacteria like *Beggiatoa* and *Thioploca* living in upwelling environments of the modern oceans (Jørgensen and Gallardo, 1999) and it seems very likely that the intertwined filamentous structures described by Soudry and Champetier (1983) derive from sulfide-oxidizing bacteria like *Beggiatoa* or *Thioploca*. In recent studies the sulfide-oxidizing bacteria were described as colorless filaments (Schulz and Jørgensen, 2001; Schulz and Schulz, 2005; Arning et al., 2008; Brock, 2011).

More recently, Soudry et al. (2006) analyzed sediments from the Negev of Mid-Cretaceous to Eocene age and demonstrated that the P accumulation rates reach their maximum during the Campanian/Maastrichtian, which is in agreement with our data. The major source of the P was located in the Northern Pacific ocean indicated by the analysis of Nd isotopes (Soudry et al., 2006).

2.4.5 Fatty acid analysis

The analysis of the polar fraction after derivatization was further used to provide evidence for the influence of sulfate-reducing and sulfide-oxidizing bacteria in the sediments of the former upwelling system. The polar fraction of the sediment extracts contains fatty acids in the range from C₉ to C₃₀. They are mostly the dominat-

ing compound class of the polar fraction. Over the whole profile several samples show a sigmoidal distribution of the fatty acids with a first maximum at $C_{16:0}$ or $C_{18:0}$ and a second at $C_{24:0}$. In most cases the $C_{16:0}$ and $C_{18:0}$ fatty acids are the dominating compounds (concentration of the saturated fatty acids $C_{16:0}$ and $C_{18:0}$ and the mono-unsaturated fatty acids $C_{18:1\omega7}$ and $C_{18:1\omega9}$ over the profile are shown in the appendix Table A-5), although long chain fatty acids (C_{20} – C_{30}) show a greater resistance towards degradation (Arning et al., 2008). Generally, the even numbered fatty acids predominate.

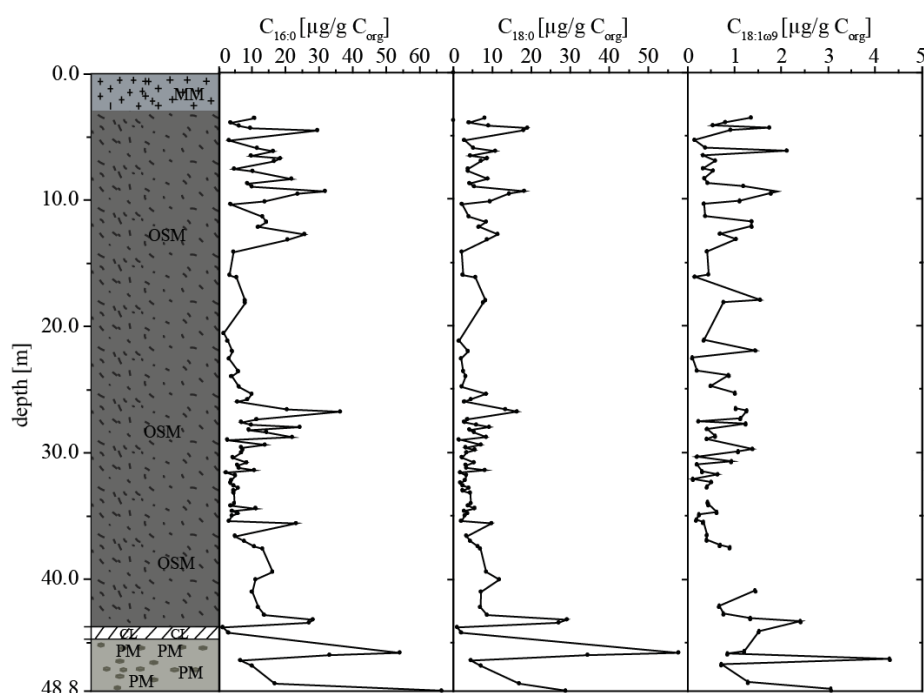


Figure 16: Distribution of the saturated fatty acids $C_{16:0}$ and $C_{18:0}$ and the monounsaturated fatty acid $C_{18:1\omega9}$ over the profile. Concentrations are shown in $\mu\text{g/g } C_{\text{org}}$.

The longest of these fatty acids (C_{26} – C_{30}) were present in low to trace amounts and could be determined in a few samples over the whole profile. This further supports the previous suggestion of a minor contribution of terrestrial organic matter to the upwelling sediments derived from the low total organic nitrogen (TON) content and high C/N ratios (Schneider-Mor et al., 2012). The $C_{24:0}$ fatty acid shows the highest abundance among the long chain fatty acids. The source of this fatty acid is widespread in marine sediments and likely originates from phytoplankton in upwelling environments, as other, especially land plant derived biomarkers are missing.

The most dominating components in the polar fraction are the n-C_{16:0} and n-C_{18:0} fatty acids (mass spectra and structures in appendix Figure A-3 and Figure A-6) with highest amounts of 67 µg/g TOC and 57 µg/g TOC determined in the PM section (Figure 16). The abundant appearance of these lipids reflects the phytoplanktonic origin and the very high productivity in the upwelling system during the sedimentation of the PM. This is supported by the results of micropaleontological analyses on the foraminiferal assemblages (Almogi-Labin et al., 1993; Ashckenazi-Polivoda et al., 2011), whereupon the high productivity was derived from the planktonic foraminifers. Recently, the molecular biomarker and elemental composition of phosphorites from the Miocene Monterey Formation were investigated (Berndmeyer et al., 2012). In accordance with our results, the fatty acid composition was also dominated by C_{16:0} and C_{18:0} fatty acids (Berndmeyer et al., 2012). Further support comes from a recent study of the fatty acid composition from sediments of the Chilean coastal upwelling (Niggemann and Schubert, 2006). The analyzed sediments showed a comparable composition of fatty acids and a predominance of the C_{16:0} (Niggemann and Schubert, 2006).

Trace amounts of the branched fatty acid *i*-C_{15:0} determined in several samples of the PM and OSM section indicate the expected activity of sulfate-reducing bacteria during the sedimentation. The occurrence of this branched fatty acid in phosphatic laminites from *Beggiatoa* populated sediments was previously reported from the Peru upwelling (Arning et al., 2009a) and from phosphorites from the Miocene Monterey Formation where their appearance was also explained with the occurrence of sulfate-reducing bacteria (Berndmeyer et al., 2012). This further supports our conclusion from the bulk geochemical data and the TOC/TOC_{OR} ratio that abundant OM was consumed by sulfate-reducing bacteria. Additionally, it supports the co-occurrence of phosphate deposition and sulfate-reducing and sulfide-oxidizing processes as reported in previous studies (Schulz and Schulz, 2005; Arning et al., 2008; Arning et al., 2009a; Brock and Schulz-Vogt, 2011).

Moreover, the detection of the monounsaturated fatty acids oleic acid (C_{18:1 ω 9}) and vaccenic acid (C_{18:1 ω 7}), which were detected over the whole profile except in the condensed layer (Figure 16), provides additional evidence that the sedimentation of the PM and OSM was influenced by *Beggiatoa* and *Thioploca*. These monounsaturated

rated fatty acids were previously reported from the *Beggiatoa* and *Thioploca* populated sediments from the upwelling regions off Namibia, Peru and Chile (McCaffrey et al., 1989; Arning et al., 2008) and recently from the Miocene Monterey Formation (Berndmeyer et al., 2012). Highest concentrations of these substances in the PM are in accordance with highest intensities of sulfate reduction derived from the geochemical data (Figure 11 & 16). Upwards in the profile, the concentration of these fatty acids decreased significantly.

Recent analysis of sediments from the Chilean upwelling shows that the concentration of these monounsaturated fatty acids decreased significantly with depth, due to the habitat of these sulfur bacteria in the upper sediment level. The relatively low amounts of the detected unsaturated fatty acids is possibly due to their increased sensitivity towards degradation (Niggemann and Schubert, 2006).

The analysis of the fatty acid composition of the PM and OSM samples supports the suggestion that these sediments were deposited under the influence of both sulfate-reducing bacteria and sulfide-oxidizing bacteria.

2.5 Conclusions

The geochemical analyses of the phosphorites and oil shales from the Late Cretaceous Tethyan Ghareb and Mishash Formation provide evidence for a link between sulfate reduction, sulfide oxidation and phosphate accumulation during the sedimentation process. Changing environmental conditions influence the uptake and release of phosphate via sulfide-oxidizing bacteria. When anoxic conditions prevail deeper in the sediment, less sulfide will be available in the pore water and bacteria like *Beggiatoa* will store polyphosphates in vacuoles within their cells. When the oxygen-sulfide interface approaches the sediment-water interface, more oxygen and nitrate become available for sulfide-oxidizing bacteria, which then store large amounts of nitrate to further oxidize the sulfide produced by sulfate-reducing bacteria. This will cause the liberation of phosphate into the pore water followed by its precipitation as apatite.

The high abundance of benthic foraminifers present in the PM provides evidence that the oxygen-sulfide interface did not expand beyond the sediments into the water during the deposition of this section.

The oscillating redox conditions present during the deposition of the PM changed to permanently anoxic porewater conditions and the activity of sulfide-oxidizing bacteria became locally restricted to the area close to the sediment-water interface. An expansion of the anoxic zone over the upper zone of the sediment into the water column and displacement of the oxygen would result in the complete extinction of the sulfide-oxidizing bacteria. This did not happen for longer times during deposition of the OSM. The low abundance of Fe avoided the effective scavenge of sulfide and reduced S species played a crucial role in the sedimentation process.

The OM was the only available sink for the excess sulfide produced, resulting in an accumulation of S in the organic matrix and a preservation of this material against microbial degradation. This process, known as natural vulcanization, is mainly responsible for the high accumulation of organic material in the sediments of the OSM and the abundant appearance of organic S compounds.

Acknowledgments

Financial support of this study by GIF—The German-Israeli Foundation for Scientific Research and Development, grant no. 956-38.8/2007 is gratefully acknowledged. We thank Rotem Amfert Negev Company for their cooperation during the sampling in the PAMA Quarry.

3 Geochemical characterization of the Campanian/Maastrichtian upwelling system from Negev (Israel) and influence of natural sulfurization on the preservation of organic matter

3.1 Abstract

Late Cretaceous Tethyan sediments from the Mishash/Ghareb Formation (Negev, Israel), deposited in an upwelling environment, were investigated using geochemical methods to explain the high proportion of organic matter (OM) preserved in parts of the study section. Geochemical analyses were performed on 99 samples from three facies, the overlying Marl Member (MM), the Oil Shale Member (OSM) and the underlying Phosphate Member (PM). The abundance and distribution patterns of n-alkanes and C₂₇- to C₂₉-steranes indicating an input of mainly marine OM into the sediments with a minor contribution of terrestrial material. The most abundant organic sulfur compounds in the analyzed sediments were the n-alkyl and isoprenoid thiophenes. Highest amounts were found for 2-methyl-5-tridecyl-thiophene with up to 28 µg/g TOC. The distribution and abundance of these compounds is comparable and often observed in modern and ancient marine upwelling systems. Up to 60 % of the total sedimentary sulfur is organically bound. The relatively high occurrence of ββ-C₃₅ hopanoid thiophenes and epithiosteranes is equivalent to an incorporation of sulfur during the early stages of diagenesis. The abundance of C₃₅ hopanoid thiophenes along the profile is independent of the total sulfur abundance, which is indicative for a diagenetic origin and emphasized the significant contribution of bacteria to the OM of the sediments.

3.2 Introduction

Besides reactive iron species, organic matter (OM) is an important sink for sulfur in the environment (Aizenshtat et al., 1995). Incorporation of reduced sulfur into the humic matrix of anoxic sediments has been reported by Nissenbaum and Kaplan (1972) and later by Francois (1987) using bulk analysis (C/S values). An enormous amount of organically bound sulfur in ancient sediments was generated via diagenet-

ic and catagenetic pathways (Aizenshtat et al., 1995). The first molecular investigations, using gas chromatography-mass spectrometry (GC-MS), provided further evidence for the incorporation of sulfur into OM during early diagenesis (Valisolalao et al., 1984; Brassell et al., 1986b; Sinninghe Damsté et al., 1989b). Reactive inorganic sulfur species like the sulfide anion HS^- and polysulfides S_x^{2-} were recognized as sulfurizing agents in inter- and intramolecular sedimentary sulfurization processes during diagenesis (Kohnen et al., 1990b; ten Haven et al., 1990; Kohnen et al., 1991a; Kohnen et al., 1992; Aizenshtat et al., 1995). Many investigations have been carried out to elucidate the mechanism of reaction of sulfur with OM in sediments. At first only functionalized lipid hydrocarbons were suggested to be susceptible to reaction with reduced sulfur species in a process called “natural sulfurization” (Sinninghe Damsté et al., 1986; Kohnen et al., 1991a). Through intramolecular reaction of polyunsaturated hydrocarbons with H_2S and polysulfides, cyclic products such as thianes, thiolanes and thiophenes are generated (Sinninghe Damsté et al., 1989a), while intermolecular reactions link different molecules by sulfide and polysulfide bridges (Kohnen et al., 1991b). Organic molecules react with H_2S or polysulfides and resulted in complex macromolecular molecules, prone against microbial degradation (Sinninghe Damsté et al., 1989a). Later, carbohydrates were also suggested to be sulfurized in anoxic sediments, based on pyrolysis–GC-MS studies and measurements of $\delta^{13}\text{C}$ -values of individual thiophenes in pyrolysates from an experimentally sulfurized alga (*Phaeocystis* sp.) and in the Jurassic Kimmeridge Clay Formation (Sinninghe Damsté et al., 1998a). Dinur et al. (1980) investigated oil shale samples from the Ghareb Formation from different sites in Israel and found that 50–95 % of the total sulfur was organically bound. More recently, Amrani et al. (2005) found a similar value (85 %) for an immature organic-rich limestone from the Ghareb Formation containing Type-II-S kerogen. Upon hydrous pyrolysis of these samples Amrani et al. (2005) found that the early released H_2S forms secondary pyrite, which was isotopically 21 ‰ lighter than the bulk organic sulfur, indicating that the system was not in equilibrium. Large isotopic discrimination between the oil and its source kerogen indicated more open system conditions (Amrani et al., 2005), meaning that fresh sulfate was introduced to the system while sulfate reduction proceeds (Schwarcz and Burnie, 1973).

Organic geochemical studies of the Maastrichtian oil shale sequence of the Ghareb Formation (Negev, Israel) are scarce. The depositional environment has been suggested to be anoxic and non-euxinic, based on C/S ratio and pristane/phytane ratio (Bein and Amit, 1982). Moreover the predominance of even numbered *n*-alkanes in extracts was suggested to be indicative of deposition of the bituminous Ghareb oil shale in a hypersaline environment (Spiro and Aizenshtat, 1977). Biomarker ratios (hopanes and steranes) were used to interpret the maturity of the shale as “low” (Rullkötter et al., 1984a). Spiro et al. (1983) investigated the tetrapyrrole pigments (Ni and V=O) in the Ghareb Formation from various locations and found regional differences in the concentration of the porphyrins, probably caused by variation in the redox conditions during sedimentation.

More detailed organic geochemical investigations were carried out on the Maastrichtian Jurf ed Darawish (JED) Formation in Jordan, the stratigraphic equivalent of the Ghareb Formation. The JED oil shale was revealed to be very rich in organic sulfur compounds (OSCs), which were identified as alkyl thiophenes, alkyl thiolanes and alkyl thianes (Kohnen et al., 1990a; 1990b). Additionally, more complex compounds such as benzothiophene hopanoids (van Kaam-Peters et al., 1995), thiophene and thiolane hopanes (de las Heras et al., 1997) and alkyl thiochromanes (Schouten et al., 1995) were found. These compounds can be explained as resulting from the early diagenetic sulfurization of biohopanoids, phytol or highly branched isoprenoids. Moreover, the incorporation of sulfur into the side chain of C₃₅ hopanoids increases significantly the preservation of the C₃₅ carbon skeleton (Sinninghe Damsté et al., 1995b).

Until now, JED samples were analyzed with the aim of identifying individual OSCs but only few sections of the sequence have been studied to investigate compositional changes along the sequence.

The aims of the present study were to (I) determine whether the OSCs found in JED were also present in the Ghareb Formation (Negev, Israel) and (II) study their concentration variations along a profile of the Ghareb oil shale, including the underlying Campanian phosphorites and the overlying Maastrichtian marls, both separated from the oil shale by a sharp facies change.

3.3 Material and methods

3.3.1 Location and samples

The samples were obtained from the PAMA quarry at Mishor Rotem in the northern Negev, Israel (Efe Syncline; 31°04'51.82"N; 35°10'02.85"E, Figure 17 shows a detailed presentation of the sampling area). The samples were obtained from a profile (Figure 21) of ca. 50 m, which is composed of a short sequence of the Mishash Formation [Phosphate Member (PM) 5.6 m] and the Ghareb Formation mostly belonging to the Oil Shale Member (OSM, 42 m) and a short sequence of the overlying Marl Member (MM, ca. 3 m). Sampling was carried out at a fresh quarry, not altered by weathering, during mining activities. From 211 samples of the profile 99 were collected at ca. 20 cm to 1 m intervals for organic-geochemical investigation.

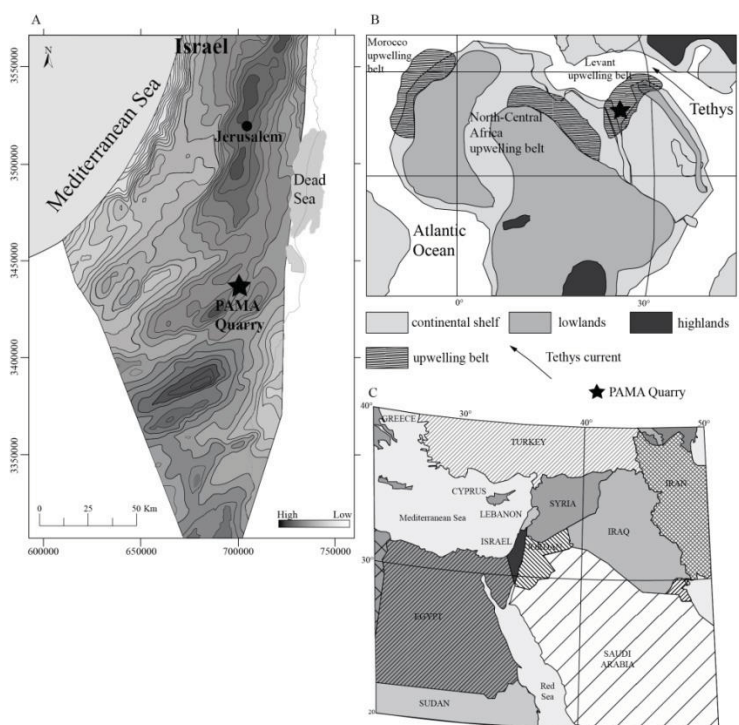


Figure 17: Location map for the studied area. A) Detailed map of Israel in UTM Coordinate system with the position of the PAMA quarry (Efe Syncline). Base topography is given in a structural map showing Syrian Arc structures (modified after Gardosh et al. (2008) and Almogi-Labin et al. (2012)). B) Inferred position of the PAMA quarry within a paleogeography map showing the upwelling belts that developed along the southern Tethys margin during the Late Campanian and Early Maastrichtian (from Ashckenazi-Polivoda et al. (2011)). C) Location of Israel shown on a political map of the Middle-East.

3.3.2 Sample preparation and analysis

20 g dried grounded rock sample (< 200 μm) were Soxhlet extracted for 30 h with dichloromethane/methanol (DCM/MeOH) 9:1. The solvent was evaporated using a rotary evaporator and an aliquot of the solvent extract (10 mg) was separated into three fractions, saturated hydrocarbons (F1), aromatic hydrocarbons (F2) and polar hydrocarbons (F3) via column chromatography (20 g silica gel 60, Merck; glass column, 15 mm i.d). The F1 fraction was obtained by elution with 40 ml hexane. F2 was eluted with 100 ml hexane/DCM (9:1) and F3 with 40 ml MeOH. The F1 and F2 fractions were analyzed using gas chromatography-mass spectrometry (GC-MS) with a Trace GC Ultra gas chromatograph coupled to a dual stage quadrupole (DSQ II) mass spectrometer (Thermo Fisher Scientific). The system was equipped with a TR5-MS column (30 m, 0.25 mm i.d., 0.25 μm film thickness; Thermo Fisher Scientific). The diluted F1 and F2 fractions were injected in splitless mode with a splitless time of 1 min. The GC oven temperature was programmed from 40 to 320 $^{\circ}\text{C}$ at 3 $^{\circ}\text{C}/\text{min}$. The mass spectrometer was operated in electron ionization (EI, 70 eV) and full scan mode. Helium was used as carrier gas. The data were recorded, processed and quantified with Xcalibur[®] software. As internal standards, 3 μl of perdeuterated tetracosane (1 $\mu\text{g } \mu\text{l}^{-1}$) were added to the F1 fraction and 3 μl of 1,1-binaphthyl (1 $\mu\text{g } \mu\text{l}^{-1}$) to the F2 fraction, respectively.

3.4 Results and discussion

According to a study by Rullkötter et al. (1983) maturity parameters such as vitrinite reflectance and spore coloration measurements could not be determined on samples from the oil shale due to the absence of terrigenous OM, but the level of maturity was suggested to be low, based on the distribution of biological markers like hopanes and steranes. The C_{29} sterane 20S/20S+20R ratio obtained by Rullkötter et al. (1984a) with values between 0.35 and 0.40 would be equivalent to a vitrinite reflectance of 0.65 using the proposed correlation diagram of Mackenzie (1984) for calculating vitrinite reflectance from biomarker ratios. However, a calculated vitrinite reflectance of 0.65 is too high and not in accordance with the low maturity of the study samples here. Vitrinite reflectance measurements of a limestone from the Ghareb

Formation at El Lajjun, Jordan provided a value of 0.39 % R_o (Koopmans et al., 1998), which coincides with the expected maturity for the section studied here.

3.4.1 Molecular composition of hydrocarbons

On average the fractions of the saturated hydrocarbons have an amount of 5.8 % of the total extractable organic matter, the aromatic hydrocarbon fractions were 3.7 % on average and the polar hydrocarbon fractions 50 %.

3.4.1.1 Straight chain alkanes

n-Alkanes are the most abundant compound class in the saturated hydrocarbon fraction of all extracts of the OSM. Their distribution ranges in C-chain length from C_9 to C_{43} . They also appear in some extracts of the MM and PM, but most of these samples do not show an n-alkane distribution comparable to the OSM section probably due to biodegradation or oxidation of the OM. The total ion current of sample SAOS 95 shows exemplarily the bimodal distribution of the n-alkanes in the sediments of the OSM section (Figure 18). The analysis of the mass chromatograms shows that most of the samples have a maximum at C_{15} – C_{23} and a second maximum at C_{29} . The short chain n-alkanes show an odd-over-even predominance demonstrating the predominant contribution of algal material to the OM. Bein and Amit (1982) also mentioned a major contribution of marine algal matter derived from their analysis of Upper Cretaceous phosphorites from the Negev. Nevertheless there was a minor contribution from terrestrial material to the sediments. This is demonstrated by the strong odd-over-even predominance of the long chain alkanes. The carbon preference index (CPI) (calculated after Bray and Evans (1961), appendix Eq.-A1) fluctuates between 1.5 and 4.4 with a mean value of 3.0 ± 0.4 (appendix, Table A-4). These values are significantly higher compared to those previously reported from the Zin Valley (CPI values between 1.1 and 3.4 (mean 1.5)) by Bein et al. (1990). The results further emphasize the thermally immature character of the analyzed sediments (Peters et al., 2007). Input of terrestrial higher plant material is indicated by CPI values exceeding 4.0 according to Sinnighe Damsté et al. (1995a and references therein). The dominant C_{29} n-alkane is mostly located in samples from the lower parts of the OSM profile between 42.8 and 20.6 m. Eolian dust is a probable source of this leaf wax n-

alkanes. Although, Rullkötter et al. (1984b) reported elevated CPI values from their analysis of sediment samples of Albian–Cenomanian to Early Pliocene age from DSDP Hole 530A in the Angola Basin. They suggested that bacterial reworking was responsible for the higher CPI values. This would be in accordance with the hopanoid biomarkers identified in the sediments of the Ghareb Formation (chapter 3.4.1.4). Furthermore, biomarker evidence for higher terrestrial plants, neither saturated nor aromatic hydrocarbons like cadalene were found in the samples of the analyzed profile.

Spiro and Aizenshtat (1977) analyzed the mineralogical and chemical composition of bituminous shales of the Ghareb Formation of Maastrichtian age from the Jordan Valley.

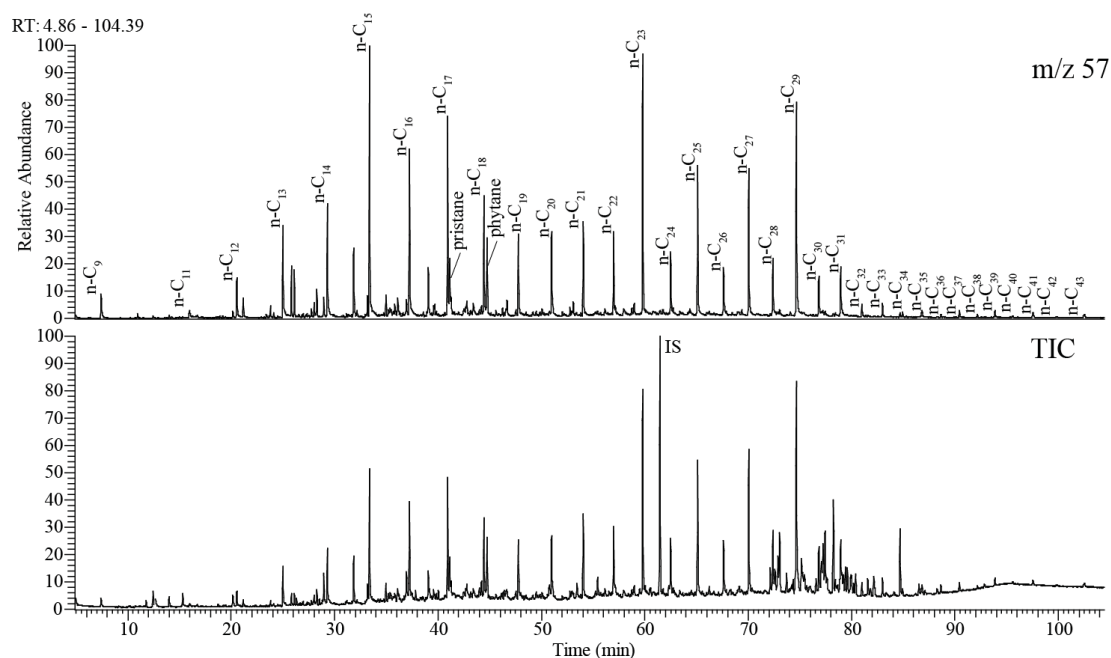


Figure 18: Mass chromatogram m/z 57 and total ion current (TIC) with the distribution of n-alkanes, pristane and phytane in the saturated hydrocarbon fraction of sample SAOS 95 (IS = internal standard)

In contrast to our results they found a predominance of even numbered n-alkanes in the range between C₂₈ and C₃₀ and suggested a hypersaline environment. They further concluded a high activity of sulfate reducing bacteria (Spiro and Aizenshtat, 1977). For the sediments of the present study a high sulfate reducing and sulfide oxidizing bacterial activity could be derived from the bulk geochemical data and the high occurrence of OSC. But the clear odd over even predominance of the alkanes

and a domination of n-C₂₉ among the long chain n-alkanes is in contrast to the results of Spiro and Aizenshtat (1977).

The missing n-alkanes in the MM can be explained by the high sulfate reduction rate derived from the TOC/TOC_{OR} ratio. Caldwell et al. (1998) analyzed the effect of sulfate reduction on the n-alkane distribution in a marine sediment and found, that the C₁₅–C₃₄ alkanes were completely removed within 200 days. Higher sulfide concentrations in the lower part of the OSM favor the incorporation of sulfur into the OM and the occurrence of OSCs.

3.4.1.2 C₂₇–C₂₉ Steranes

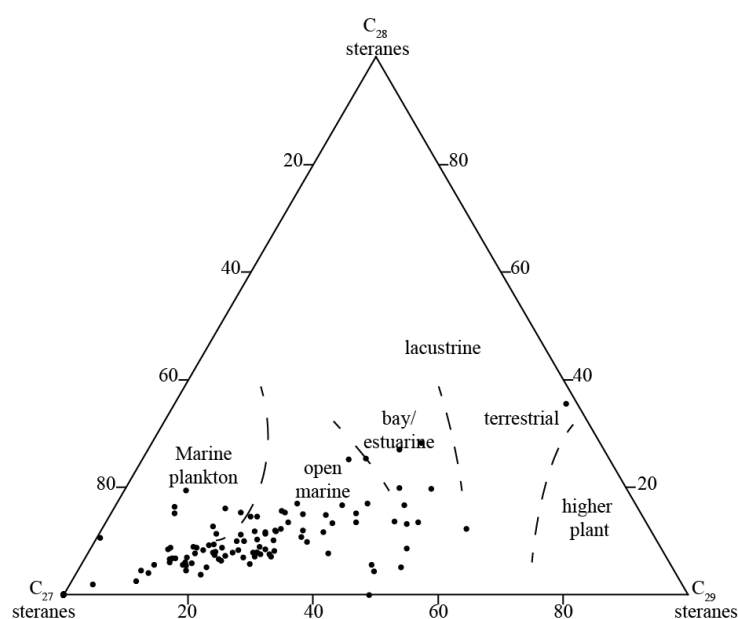


Figure 19: Ternary diagram showing the relative abundances of C₂₇-, C₂₈- and C₂₉-steranes. The relative abundance of the steranes allows a differentiation between the depositional environments which are labeled with dashed lines in the diagram (derived from Huang and Meinschein (1979)).

Based on the study of C₂₇–C₂₉ sterols obtained from different environments Huang and Meinschein (1979) developed a ternary diagram to distinguish between different depositional environments. They found an empiric relationship between the relative abundance of C₂₇–C₂₉ sterols and the ecosystems where the samples derived from. These diagram was used in a modified form by Follows and Tyson (1998) and Banga et al. (2011). They used the ternary correlation of C₂₇–C₂₉ steranes to determine the source of the OM input to the sediments. In this study the correlation (Figure 19,

concentration of the used steranes is given in the appendix Table A-6) was used to get further information of the main source of OM input. Resulting from the ternary diagram more than 90 % of the OM derived from marine plankton or other marine organisms as can be expected for a marine upwelling system. These data support the previously presented results derived from the n-alkane distribution. Based on the results from the correlation diagram (Figure 19) it can be further concluded that the contribution of terrestrial higher plant material was rather low. Moreover, this is in accordance with previous studies by Schneider-Mor et al. (2012). The steranes distribution in the OSM samples from the Ghareb Formation is comparable to the previously reported from the three different facies types of the Cretaceous JED oil shale (Kohnen et al., 1990b). In contrast to the appearance of the steranes in all three facies types of the JED, namely the bituminous limestone, bituminous calcareous marl and phosphorite (Kohnen et al., 1990b), the steranes are not present in the samples from the PM or the MM probably due to the consumption of the OM by sulfate reducing bacteria in the phosphorites and the oxidation of the OM in the marls due to the exposure to oxygen.

3.4.1.3 Indicators of paleosalinity (chromans)

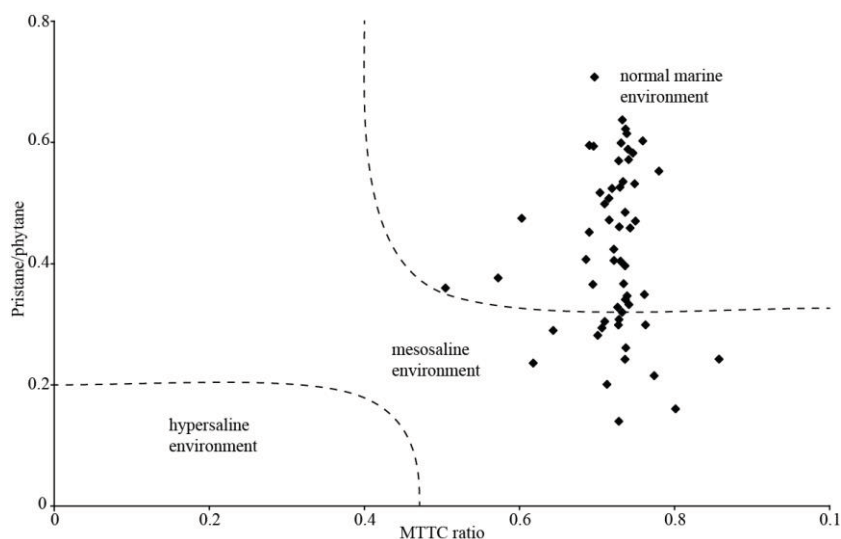


Figure 20: Relationship between pristane/phytane and the methyltrimethyltridecyl-chroman (MTTC) ratio in Cretaceous sediments of the Tethys. The MTTC ratio was calculated according to de Leeuw and Sinninghe Damsté (1990).

The origin of the methylated methyltrimethyltridecyl-chromans (MTTCs, structures in appendix Figure A-2) is still under debate but an eu- or archaeobacterial derived

precursor has been proposed (Sinninghe Damsté et al., 1987a; de Leeuw and Sinninghe Damsté, 1990). Moreover, a condensation reaction pathway of phenols with phytols during early diagenesis is discussed (Li et al., 1995). Within the aromatic hydrocarbon fraction, the MTTCs belong to the most abundant compound classes. MTTCs can be found in most of the samples from the OSM, but they are absent in the MM. A possible reason for this observation is on the one hand a change of the environmental conditions during the deposition of the sediments of the MM with the effect that the biological precursor disappeared and on the other hand an oxidation of the OM and removal of these molecules. In three samples of the PM the MTTCs were detected which is probably due to the degradation of the OM in this section. The ratio of these compounds has been used for assessing the salinity of paleoenvironments (Sinninghe Damsté et al., 1987a; de Leeuw and Sinninghe Damsté, 1990). In normal marine environments the 5,7,8-triMe-MTTC dominates whereas the 8-Me-MTTC is the most abundant in hypersaline environments. Sinninghe Damsté et al. (1989a) investigated a plot of the pristane/phytane ratio vs. the MTTC ratio to determine whether the sediments were deposited under normal marine or hypersaline conditions. The di- and tri-methylated MTTC are present in sufficient amounts to calculate the di-/tri-MTTC ratio. The MTTC ratio was calculated based on the equation (Eq. 14) suggested by de Leeuw and Sinninghe Damsté (1990).

$$\text{MTTCratio} = \frac{[5,7,8 - \text{triMe-MTTC}]}{[\text{total methylated MTTC}]} \quad \text{Eq. 14}$$

The most abundant of all MTTC over the whole OSM profile is the 5,7,8-triMe-MTTC. Most of the samples plot in the field of normal marine salinity but some of them, mostly belonging to the lower part of the OSM section, plot in the field of mesosaline conditions. 72 % of the samples plot in a range between 0.7 and 0.8 (Figure 20). This is comparable to results from the analysis of sediment extracts from organic rich silty claystone samples from the Maikop Formation deposited in eastern Azerbaijan under high productivity conditions during the Oligocene and early Miocene (Bechtel et al., 2013). A similar value for the MTTC-ratio was reported from the analysis of oil shale sediment extracts from the Cretaceous JED which were suggested to derive from an hypersaline environment (de Leeuw and Sinninghe Damsté, 1990). In accordance with the results from our analysis of the methylated chromans,

Kolonic et al. (2002) found 5,7,8-triMe-MTTC as dominating component of the methylated chromans in sediment extracts from samples of three exploration wells of the Cenomanian/Turonian Tarfaya basin, Southwest Morocco. These sediments were deposited in a nutrient-rich upwelling system. 5,7,8-triMe-MTTC was significantly present in sediments of ancient upwelling systems (Sinninghe Damsté et al., 1987a; Sinninghe Damsté et al., 1989a; Bechtel et al., 2013), which seems to be a favorable environment for the biological precursor of these compounds. MTTC are structurally related to tocopherols but seem not to be the precursor molecules of the methylated chromans (Wang et al., 2011 and references therein).

3.4.1.4 Pentacyclic triterpanes

According to Neunlist et al. (1988) bacteriohopanetetrol (BHT) is preferentially biosynthesized by aerobic bacteria to stabilize the membranes of their cell walls, similar to the steroids in eukaryotic organisms (Ourisson et al., 1987). However, more recently the capability of BHT synthesis has also been found for strictly anaerobic bacteria such as *Planctomycetes* producing N_2 by anaerobic oxidation of NH_3 (Sinninghe Damsté et al., 2004) and for sulfate-reducing bacteria (Blumenberg et al., 2006).

The bacterial influence on the sediment is represented by the various saturated and unsaturated triterpanes. The occurrence of significant amounts of $17\beta(H),21\beta(H)$ hopanes and neohop-13(18)-ene in the OSM section of the studied profile further indicates the microbial activity (Barouxis et al., 1988). The hopanes and hop-17(21)-enes were determined over the whole profile. Besides the alkanes, the hopanoids were the most abundant compounds in the saturated hydrocarbon fraction. The C_{30} - C_{35} -hop-17(21)-enes (m/z 231) were identified by comparison of their mass spectral data and retention time with those previously published (ten Haven et al., 1985; McEvoy and Giger, 1986). The most abundant compound of this group is the hop-17(21)-ene and in comparison to that, the extended hopenes are present in significant lower amounts. In the lower part of the OSM section the C_{31} - C_{35} hop-17(21)-enes are more abundant compared to the upper part of the OSM section, indicating a high microbial alteration of labile OM. The hopanes show predominantly the $17\beta(H),21\beta(H)$ configuration in the OSM sediments, significant for the low maturity of the samples. The hopanes range from C_{27} to C_{35} carbon atoms, with highest concentrations of the C_{30} - $17\alpha(H),21\beta(H)$ -hopane and the C_{31} - $17\alpha(H),21\beta(H)$ and C_{31} -

17 β (H),21 β (H)-homohopane. The highest amounts of the hopanes were measured in the lower part of the OSM. In the PM and in the MM these compounds were absent. The relatively good preservation of the long-chain homologues with 32–35 carbon atoms, especially the relatively high amounts of C₃₅-hopanes in the lower parts of the OSM indicate anoxic conditions present during the deposition of these sediments (Köster et al., 1997). These results are in agreement with the low pristane/phytane ratio in this section (Schneider-Mor et al., 2012) and the high amounts of preserved organic carbon. The analysis of recent and ancient sediments from the Benguela upwelling system shows that an increase of the productivity and higher amounts of TOC in the sediment did effect the proportion of hopanoids in the sediments (Blumenberg et al., 2010). High amounts of sulfur co-occur with high concentration of hopanoids at the same positions in the sediment, probably indicating the preserving influence of the sulfur on the OM. Recently, Blumenberg et al. (2006) reported the biosynthesis of hopanoids by sulfate reducing bacteria in anoxic environments. An input of hopanoids through ammonium oxidizing bacteria and sulfate reducing bacteria is very likely because of the very low C/N ratio of the OSM section (Schneider-Mor et al., 2012) and further bulk-geochemical and biomarker evidence for the sulfate reducing activity (e.g. Figure 14 and Figure 16).

3.4.1.5 Straight chain and C₂₀-isoprenoid thiophenes

The most frequent compound class of the aromatic hydrocarbon fractions in the solvent extracts from sediment samples of the OSM are the alkylthiophenes with diagnostic fragment ions at m/z 97, m/z 111 or m/z 125 indicating the presence of no methyl substituent at the thiophene ring, one or two respectively. For identification the mass spectra and retention time of the thiophenes were compared to literature data (Sinninghe Damsté et al., 1986).

The alkyl side chain length ranges between C₆ and C₂₃ and the alkylthiophenes with a tridecyl-sidechain are the most abundant of all thiophenic compounds (C₁₈). Thiophenes with chain length shorter than 13 and longer than 18 are less abundant. The 2-methyl-5-alkyl-thiophenes do not show any preference of odd or even numbered side chain length.

The concentrations of thiophenic compounds 1-6 (Figure 21) tend to decrease towards the upper part of the OSM section. In the MM these compounds are complete-

ly absent or below detection limit. Only the 2-methyl-5-tridecyl-thiophene and 2-methyl-5-pentadecyl-thiophene were found in the PM (compounds 1 and 6 in Figure 21). The straight chain and isoprenoid thiophenes show a relatively similar distribution along the profile. The 2-methyl-5-tridecyl-thiophene is the compound with the highest abundance of this group.

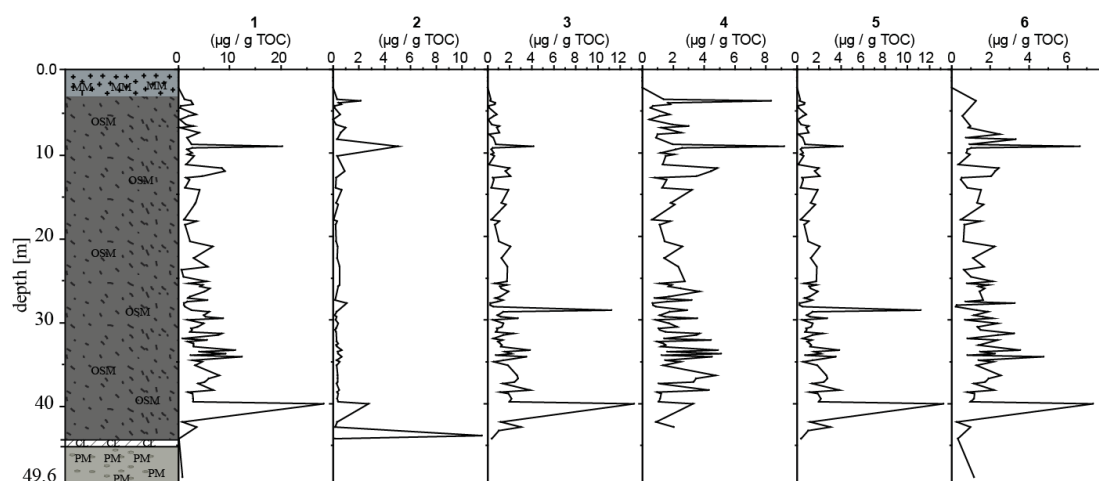


Figure 21: Concentration of straight chain and isoprenoid thiophenes along the profile. 1 2-methyl-5-tridecyl-thiophene (MW 280), **2** 2,3-dimethyl-5-(2,6,10-trimethylundecyl)-thiophene (MW 308), **3** 3-methyl-2-(3,7,11-trimethyldodecyl)-thiophene (MW 308), **4** 3-(4,8,12-trimethyltridecyl)-thiophene (MW 308), **5** 2-methyl-5-tetradecyl-thiophene (MW 294), **6** 2-methyl-5-pentadecyl-thiophene (MW 308)

The likely source of the C_{20} -isoprenoid thiophenes (2–4 in Figure 21) is according to Fukushima et al. (1992) and Aizenshtat et al. (1995) from chlorophyll-derived phytol via phytadiene intermediates. A maximum in concentration for all compounds correlates well with a maximum proportion of TOC at 40m indicating a good preservation of OM due to natural sulfurization. This is in accordance with a very high biological productivity in the water column during this period of maximum upwelling and high amounts of chlorophyll derived from planktonic organisms (Almogi-Labin et al., 1993). This biomass was probably preserved under the anoxic sedimentary conditions with H_2S in the sediment and probably the sediment-water interface. Biomarkers for photic zone euxina were absent in the analysis of the solvent extracts indicating that H_2S did not reach the photic zone. Under these conditions the chlorophyll-derived phytol from the phytoplankton reacted with H_2S , S_x^{2-} or HS^- at the earliest stages of diagenesis to form these isoprenoid thiophenes. HS^- and S_x^{2-} are

the main sulfurizing agents in marine sedimentary environments (Amrani and Aizenshtat, 2004), with latter is more reactive and therefore the most important. In laboratory experiments by Fukushima et al. (1992) these compounds were generated at low temperatures of 50 °C under mild reaction conditions. The occurrence of these compounds further supports the suggestion of a very low maturity of the sediments and high concentration of H₂S in the sediments during the deposition of the OSM.

3.4.1.6 C₂₇–C₂₉-Epithiosteranes

C₂₇–C₂₉-epithiosteranes are quite abundant in the aromatic hydrocarbon fraction. These compounds have been reported from the Miocene Monterey Formation in California, the Timahdite bituminous shale in Morocco and the Messinian Gibellina sediments (Behrens et al., 1997 and references therein). Cabrera et al. (2002) reported these compounds from the biomarker analysis of samples from the lacustrine Oligocene Mequinenza Formation.

The epithiosteranes have been identified from their mass spectral data, which were compared to previously published data (Behrens et al., 1997; Cabrera et al., 2002). These compounds were determined in the solvent extracts from the PM and the OSM but were absent in the MM. In all analyzed data two stereoisomeric C₂₈-epithiosteranes are present and a single C₂₇ and C₂₉ epithiosterane. The epithiosteranes show diagnostic ions at m/z 317 and m/z 331. The C₂₇-epithiosterane was identified by these characteristic ions and the base peak at m/z 115 as well as the molecular ion peak at m/z 402.

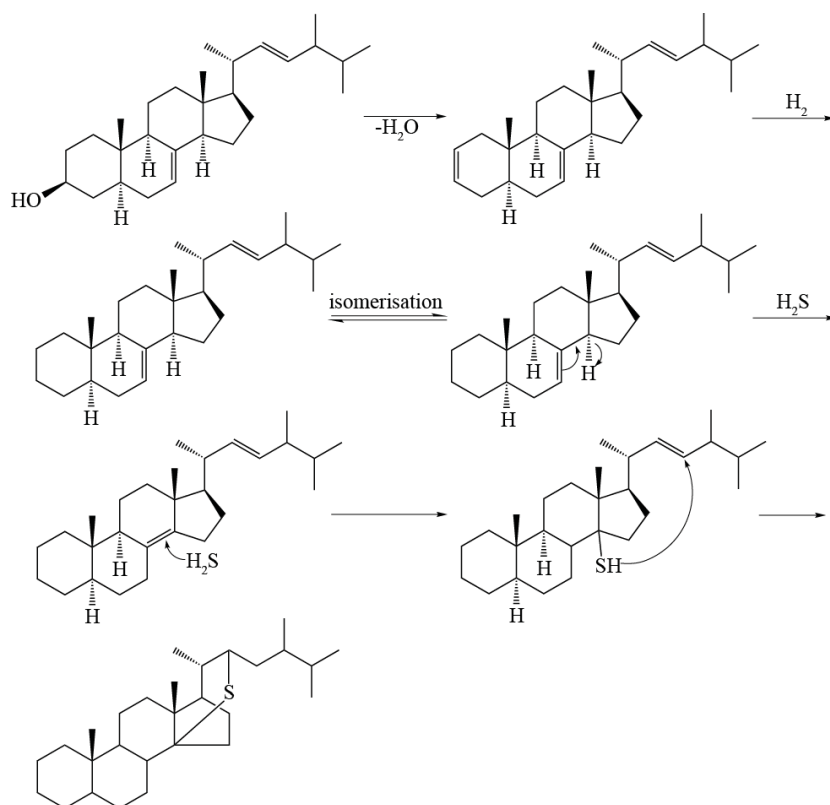


Figure 22: Suggested mechanism of the C_{28} -epithiosterane formation derived from 24-methyl- 5α -cholesta-7,22-dien- 3β -ol modified after ten Haven et al. (1986) and (Mackenzie et al., 1982).

Trace amounts of this compound could be determined in the samples of the OSM and PM. The two stereoisomers of the C_{28} -epithiosterane were present in higher abundance compared to the C_{27} -epithiosterane. These compounds were identified by their base peak at m/z 129 and the two diagnostic peaks at m/z 317 and 331, respectively. The molecular peak is at m/z 416. The C_{29} epithiosterane has a molecular peak at m/z 430 and a base peak at m/z 143. These compounds were suggested to originate from phytoplankton (Behrens et al., 1997; Cabrera et al., 2002). A possible precursor molecule originates from $\Delta^{8(14),22}$ steradienes which might be diagenetically derived from $\Delta^{7,22}$ sterols (Behrens et al., 1997). $C_{28}\Delta^{7,22}$ sterols, like 24-methyl- 5α -cholesta-7,22-dien- 3β -ol are common in microalgae of the genus Chlorophyceae (Volkman, 2003). These algae are ubiquitously present in upwelling systems. ten Haven et al. (1986) predicted a pathway for the diagenetic alteration of Δ^7 -sterols. The isomerization between Δ^7 and $\Delta^{8(14)}$ was suggested to occur at the early stages of diagenesis (ten Haven et al., 1986). The $C_{28}\Delta^{7,22}$ or $C_{28}\Delta^{5,7,22}$ sterols are common in marine phytoplankton therefore it is not surprising that among the epithiosteranes the C_{28} stereoi-

somers are the most abundant. The rather unlikely appearance of $C_{27}\Delta^{7,22}$ or $C_{27}\Delta^{5,7,22}$ sterols in microorganisms (Volkman, 2003) explains the very low amounts of the C_{27} -epithiosterane. A diagenetic pathway for the formation of C_{28} -epithiosteranes is shown in Figure 22. The highest concentration of epithiosteranes is found in the samples with the highest amounts of sulfur, but there is no further correlation between the concentration of the epithiosteranes and the proportion of sulfur. This further indicates the incorporation of sulfur into the OM during the early stages of diagenesis and moreover emphasized the fact that the OM was the major sink for the H_2S in the sediments of this depositional environment due to the limited availability of reactive iron.

3.4.1.7 Sulfur containing hopanoids

A sulfur containing hopanoid with a thiophene moiety was first reported from Cretaceous black shale samples from the Angola basin, collected during Deep Sea Drilling Project leg 40 (Valisolalao et al., 1984). Later, a wide variety of hopanoid thiophenes and thiolanes were characterized and reported from lacustrine, marine, hypersaline and upwelling environments from the Triassic to the Miocene, including the Miocene Monterey Shale, the Cretaceous JED oil shale, Paleocene and Cretaceous shales from the Morocco Shelf and Cretaceous claystones from the Gulf of California (e.g. Sinninghe Damsté et al., 1989a; ten Haven et al., 1990; de las Heras et al., 1997). The C_{35} -hopanoid thiophene, as a product of early diagenesis, has been proposed to derive from bacteriohopanetetrol (Valisolalao et al., 1984).

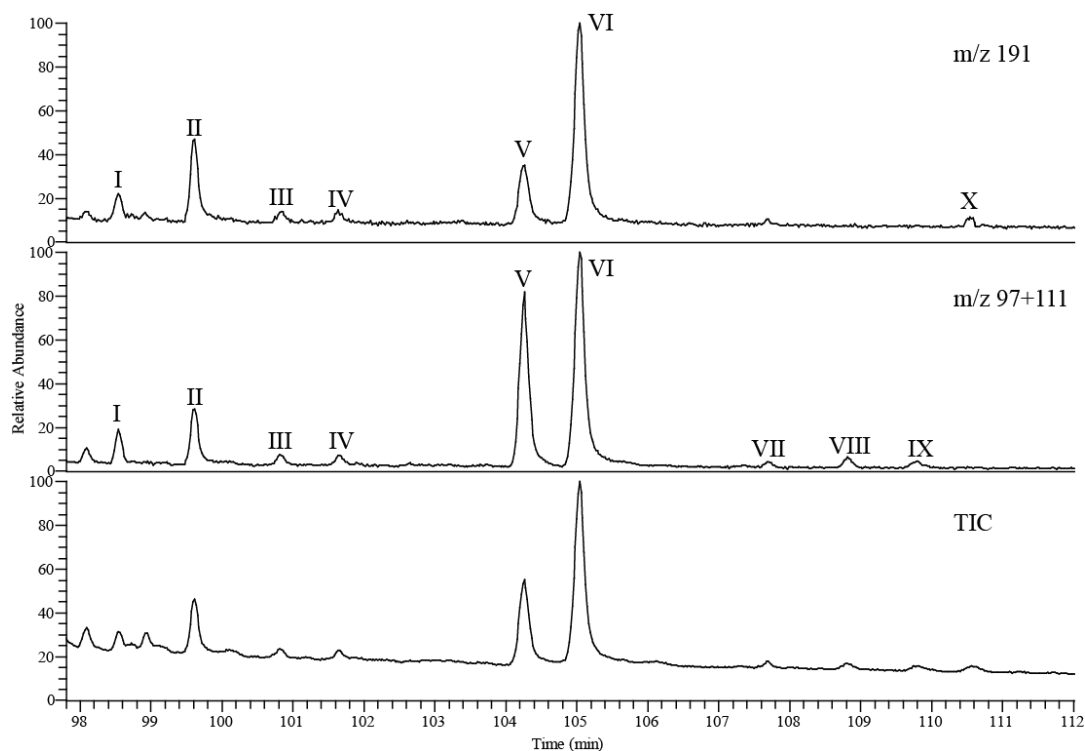


Figure 23: The total ion current (TIC) and mass chromatogram m/z 97+111 and m/z 191 of the aromatic hydrocarbon fraction of sample SAOS 189 (Negev/Israel) with the distribution of the sulfur containing hopanoids. **I** 30-[2'-(5'-methylthienyl)-17 α (H), 21 β (H)-hopane, **II** 31-(2'-thienyl)-17 α (H),21 β (H)-homohopane, **III** 31-(2'-thienyl)-17 β (H),21 α (H)-homohopane, **IV** 30-(2'-thienyl)-17 β (H),21 β (H)-hopane, **V** 30-[2'-(5'-methylthienyl)-17 β (H),21 β (H)-hopane, **VI** 31-(2'-thienyl)-17 β (H),21 β (H)-homohopane, **VII** 31-[2'-(5'-methylthienyl)-17 α (H),21 β (H)-homohopane, **VIII** 31-[2'-(5'-methylthienyl)-17 β (H), 21 α (H)-homohopane, **IX** 32-(2'-thienyl)-17 β (H), 21 α (H)-bishomohopane, **X** 3-methyl-31-(2'-thiolanyl)-homohopane

In Figure 23, a part of the total ion current and two mass chromatograms m/z 97+111 and m/z 191 obtained by the GC-MS analysis of the aromatic hydrocarbon fraction of sample SAOS 189 are shown, representing the typical distribution of the sulfur containing hopanoids in the studied section of the Ghareb Formation. The partial chromatogram shows the 2'-thienyl, 2'-(5'-methylthienyl) and 2'-thiolanyl derivatives of the C₃₅ sulfur containing hopanoids and the C₃₆ homologues with the 2'-thienyl and 2'-(5'-methylthienyl) moiety. Compounds with all three variations of the stereoisomeric configuration of the hopane structure, the 17 α (H), 21 β (H), 17 β (H),21 α (H) and 17 β (H),21 β (H) are present in the samples. These compounds were identified by comparison of their mass spectral data and the retention time with published data from de las Heras et al. (1997).

(Structural information and mass spectra for these compounds are given in Figure 24 and in the appendix in Figures A-26 to A-33). The sulfur containing hopanoids are present in the mass range between m/z 494 and 522. The C_{36} -hopanoid thiophenes have a molecular ion at m/z 522.

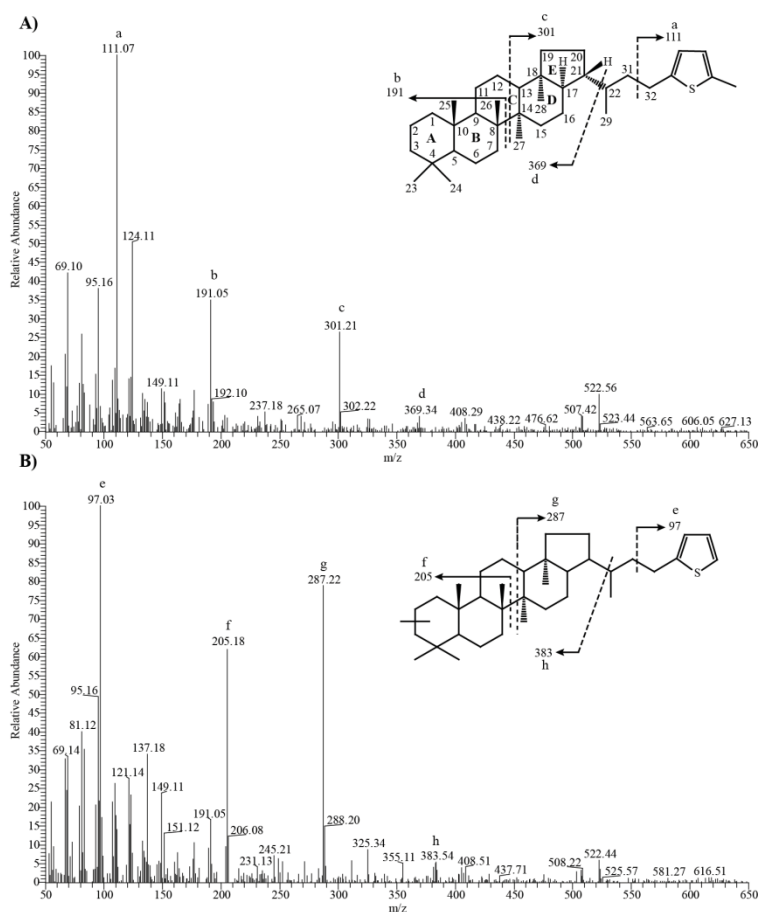


Figure 24: Mass spectra and molecular structures of the two hopanoid thiophenes with molecular ions at m/z 522 observed in the OSM, sample SAOS 189, of the Ghareb Formation. A) 31-[2'-(5'-methylthienyl)-17 α (H),21 β (H)-homohopane (VII) with numbering and notation of the hopanoid skeleton and characteristic fragment ions; B) methyl-31-(2'-thienyl)-homohopane (IX) with characteristic fragment ions.

Stereoisomers of C_{36} -hopanoid thiophenes (m/z 522) have been previously reported from the analysis of oil shale samples from the Cretaceous JED Formation in Jordan with their characteristic fragment ions (Sinninghe Damsté et al., 1989a). A homohopane (compound VII) and a 3-methylhopane (compound IX) skeleton was derived from the comparison of the fragmentation pattern of the mass spectra of the two C_{36} -hopanoid thiophenes (compounds VII and IX Figure 24) in the samples of the OSM

with the literature data of de las Heras et al. (1997) and Sinninghe Damsté et al. (1989a).

The characteristic ion m/z 111 (fragment a in Figure 24 A), indicative for the 2'-(5'-methylthienyl) moiety, results from the cleavage in the side chain of the homohopane molecule between C-30 and C-31. The cleavage in the C ring results in the characteristic fragment ion m/z 191 (fragment b in Figure 24 A) containing the A/B rings of the hopanoid structure. The cleavage in the C ring gives rise to the fragment molecule m/z 301 (fragment c in Figure 24 A) containing the D/E ring of the hopanoid and the side chain. The cleavage between C-21 and C-22 (fragment d, Figure 24 A) gives rise to the hopanoid characteristic fragment at m/z 369.

Sinninghe Damsté et al. (1989a) tentatively identified the compound shown in Figure 24 B based on the characteristic ions as 3-methyl-31-(2'-thienyl)-homohopane. 3-Methyl hopanoids are produced for example by methanotrophic bacteria which use methane, derived from the degradation of OM, in the oxic zone to gain their energy (Neunlist and Rohmer, 1985; Summons and Jahnke, 1990). A methylhopane from a methanotrophic origin would be detectable by a very depleted $\delta^{13}\text{C}$ value (Summons et al., 1994). These measurements have to be conducted. A 2-methyl derivative cannot be fully excluded based on the mass spectral data. 2-methyl-hopanoids are generally believed to derive from cyanobacterial organisms and are an indicator of oxygenic photosynthesis (e.g. Summons et al., 1999). These organisms have been reported for example from the upper boundary of the OMZ in the coastal upwelling system off Chile (Cuevas and Morales, 2006). Although in a recent study by Rashby et al. (2007) on cultured organisms of the anoxygenic phototroph *Rhodospseudomonas palustris*, it was shown that these organisms produce significant amounts of 2-methylbacteriohopanepolyols. However, methylhopanes without a thiophenic moiety in the side chain were not detected in either of the samples. This is a further support for an early diagenetic incorporation of sulfur into the OM.

However, the cleavage in the side chain between C-31 and C-32 give rise to the characteristic fragment ion m/z 97 (fragment e in Figure 24 B) of the 2'-thienyl moiety. The addition of the methyl group to the A/B ring of the hopanoid skeleton increases the fragment ion from m/z 191 to m/z 205 (fragment f in Figure 24 B). Cleavage of the C ring (fragment g= m/z 287, Figure 24 B) results in the moiety containing the D/E ring and the side chain. The fragmentation between C-21 and C-22

gives rise to the fragment h (m/z 383, Figure 24 B), which is characteristic of the methyl hopanes structure.

Furthermore, a thiolane was detected in the solvent extracts of the sediment samples and co-occurs together with the thiophenes mainly in the OSM and in very low amounts in some parts of the PM (compound X in Figure 23, mass spectrum and structure in appendix Figure A-33). This compound is absent in the sediments of the MM.

Thiolanes show a molecular ion at m/z 512. Based on the analysis of immature bituminous calcareous marl stones from the Cretaceous JED Formation Sinninghe Damsté et al. (1989c) suggested that thiophenes derive diagenetically from thiolanes via dehydrogenation. The less stable thiolane is more abundant in the upper part of the profile and a further thiolane hopanoid with a molecular ion at m/z 512 occurs which allows to assume that these sediments are slightly more immature compared to the bottom part of the OSM section.

The C_{35} -hopanoids with the 2'-thienyl and 2'-5'-methylthienyl moiety (compounds I, II, V and VI in Figure 23) are the most abundant of the sulfur containing hopanoids and were quantified along the profile. All hopanoid thiophenes show nearly the same variation along the profile. In the MM these thiophenes are absent. The compounds I and II show the lowest concentration (0.02 to 0.43 $\mu\text{g/g}$ TOC, mean 0.09 $\mu\text{g/g}$ TOC for I and 0.05 to 0.66 $\mu\text{g/g}$ TOC, mean 0.20 $\mu\text{g/g}$ TOC for II), in comparison to that the two compounds with the biogenic $\beta\beta$ configuration (compounds V and VI, Figure 23) show a considerably higher concentration in the range between 0.08 and 1.6 $\mu\text{g/g}$ TOC (mean 0.45 $\mu\text{g/g}$ TOC) for compound V and a concentration between 0.24 to 3.8 $\mu\text{g/g}$ TOC (mean, 1.16 $\mu\text{g/g}$ TOC) for compound VI. This further supports the previous suggestion that the sulfurization starts at the early stages of diagenesis.

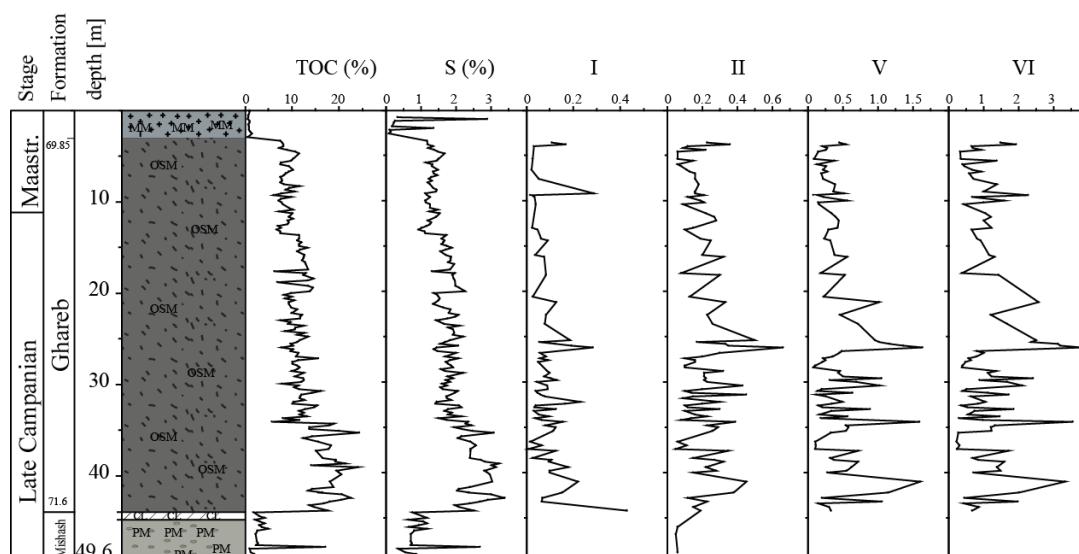


Figure 25: Stage, formation, depth and profile of the analyzed sediments, proportions of TOC and S are given in percent. The concentration variation along the profile is shown for the hopanoid thiophenes in $\mu\text{g/g}$ TOC. I 30-[2'-(5'-methylthienyl)-17 α (H),21 β (H)-hopane, II 31-(2'-thienyl)-17 α (H),21 β (H)-homohopane, V 30-[2'-(5'-methylthienyl))-17 β (H),21 β (H)-hopane, VI 31-(2'-thienyl)-17 β (H),21 β (H)-homohopane.

According to Kohnen et al. (1990b), the hopanoid thiophenes can be used as biomarkers for bacterial reworking in the sediment. This corresponds with the observed peaks in the concentration of the thiophenes and the corresponding dent in the abundance of the TOC (e.g. at 24.2 m, 34.4 m and 41m in Figure 23). This is in accordance with the high bacterial activity assumed for the OSM derived from the biomarker analyses. However, the concentration of the thiophenes correlates neither with the TOC nor the TS content. There is no significant enrichment of these compounds present e.g. in the lower part of the OSM which was deposited under more oxygen deficient conditions than the upper part of the section. This allows us to assume that the organisms producing bacteriohopantetrol, the precursor of the C₃₅-hopanoid thiophenes, were rather present in the water column than in the sediment. Thus, an origin from heterotrophic bacteria feeding on primary producers in the water column is more likely than an origin from sulfate-reducing bacteria or *Planctomycetes*.

3.4.1.8 Degree of OM sulfurization

A previous analysis of OM-rich sediments from the Ghareb Formation from the Zin valley shows that up to 80 % of the sedimentary sulfur is organically bound (Bein et

al., 1990). Comparable results with 85 % of the total sulfur organically bound were reported from a limestone of the Cretaceous Ghareb Formation from Mishor Rotem, (Amrani et al., 2005). These data are in agreement with results from the upwelling sediments from the Peruvian margin (ODP Leg 112) where up to 46 % of the total sedimentary sulfur were found to be organically bound (Mossmann et al., 1991). Moreover, similar values have been reported for the more deeply buried petroleum source rocks of the Miocene Monterey Formation (Orr, 1986). Eglinton et al. (1994) analyzed a ca. 100 m sediment core from the Peru margin obtained during ODP Leg 112 (Hole 681 C) and found increasing C/S values and organic sulfur contents up to 70 % of the total sulfur. Moreover, the analysis of OM-rich upwelling sediments from the Pakistan margin a comparable value of up to 60 % of the total sulfur content was found to be organically bound (Lückge et al., 2002).

In the ancient and recent upwelling sediments high amounts of organic carbon coincide with a high amount of organic bound sulfur. This is reflected by the elevated C/S ratios in the analyzed samples of these environments e.g. a C/S ratio of 6.6 in this study and a comparable C/S ratio of 6.6 to 33 from the Peruvian upwelling system (Mossmann et al., 1991). From the Monterey oil shale a C/S ratio of 15 to 50 was previously reported (Orr, 1986). The degree of OM sulfurization therefore tends to be slightly higher in the Mishash/Ghareb Formation than in recent sediments from the Peruvian upwelling area and much higher than in the Miocene Monterey Formation.

This high degree of OM sulfurization is reflected by the occurrence of straight chain and isoprenoid alkylthiophenes, which are the most abundant OSCs in the analyzed sediments, comparable to the distribution of alkylthiophenes e.g. from the Miocene Messinian Peticara basin sediments (Sinninghe Damsté et al., 1986) or the sediments from the highly productive surface waters in the northeastern Arabian Sea off Pakistan (Lückge et al., 2002). The occurrence of various thiophene hopanoids of which the compounds I, II, V, VI shown in Figure 23 are the most abundant reaching concentrations of up to $6.4 \mu\text{g g}^{-1}$ TOC (sum of the four isomers) in the extracts. For comparison, in sediments from the Benguela Upwelling System (BUS) (latest 80 ka) S-bound C₃₅ homohopane was present at only $1 \mu\text{g g}^{-1}$ TOC, contributing < 3 % of the total hopanoid content and the concentration tends to increase with sediment age

(Blumenberg et al., 2010). Sinninghe Damsté et al. (1995b) found C₃₅-hopanoid thiophene in the apolar fraction at 30 to 70 $\mu\text{g g}^{-1}$ TOC (sum of four isomers), indicating an even higher sulfurization rate of the OM in the JED. High sulfurization of the OM is a common feature in upwelling sediments due to the special environmental conditions with high sulfate reduction and sulfide oxidation and it played a key role in the preservation of the OM of the OSM facies.

3.5 Summary and conclusions

The OM of the sample material derived almost exclusively from marine organisms, mainly algae, with a minor contribution of terrestrial material evident from the analysis of the n-alkanes and C₂₇- to C₂₉-steranes. The high amounts of n-alkyl and isoprenoid thiophenes is comparable to recent and ancient upwelling environments indicating the incorporation of sulfur during the early stages of diagenesis. Furthermore, a ¹³C isotopic analysis of the methylated sulfur containing hopanoid will give information about the source of this compound and with NMR analysis the structure can be solved. The high abundance of C₃₅ hopanoid thiophenes in the OSM is consistent with an origin from heterotrophic bacteria living in the aerobic water column rather than from sulfate reducing bacteria or anaerobic *Planctomyces*. Biomarkers for photic zone euxinia were absent in the analyzed sediments and argue for the precipitation or re-oxidation of the excess H₂S within the sediment or beneath the photic zone. The degree of sulfurization of the organic matter seems to be generally elevated in upwelling systems due to the special conditions in these environments and ranges between 60 and 85 % of the total sedimentary sulfur.

The natural vulcanization of OM in upwelling sediments deposited under Fe limited conditions will result in the preservation of abundant organic carbon by comparable low amounts of sulfur.

Acknowledgments

Financial support of this study by GIF—The German-Israeli Foundation for Scientific Research and Development, grant no. 956-38.8/2007 is gratefully acknowledged. We thank Rotem Amfert Negev Company for their cooperation during the sampling in the PAMA Quarry.

4 Paleocceanographic reconstruction of the Late Cretaceous oil shale of the Negev, Israel: Integration of geochemical, and stable isotope records of the organic matter

4.1 Abstract

The Levantine high productivity system was an extensive coastal upwelling that operated in the Late Cretaceous along the SE Tethyan margin. This study focuses on the top Phosphate Member (PM) of the Mishash Formation and the Oil Shale Member (OSM) of the Ghareb Formation (latest Campanian-Early Maastrichtian), which represent the last phase of this high productivity system in the Negev, Israel. Bulk organic matter (TOC), $\delta^{13}\text{C}_{\text{org}}$, $\delta^{15}\text{N}_{\text{org}}$, C/N and pristane/phytane (Pr/Ph) ratios, were studied for reconstruction of seafloor and water column depositional environments. Our records indicate a gradual decrease with time in surface water productivity in the OSM and a marked weakening at the overlying Marl Member (MM). High C/N ratio along with relatively low $\delta^{15}\text{N}_{\text{org}}$ (4 ‰ to 6 ‰) and $\delta^{13}\text{C}_{\text{org}}$ (-29 ‰ to -28 ‰) probably reflect significant diagenetic preferential loss of nitrogen-rich organic compounds enriched with ^{15}N and ^{13}C isotopes (e.g. proteins). This along with the low Pr/Ph values (0.11–0.7), indicate oxygen depleted bottom water (anoxia-dysoxia) during the deposition of the top PM and the OSM. The moderate gradual upward increase in $\delta^{15}\text{N}_{\text{org}}$, and in Pr/Ph values and the decrease of TOC and C/N values from the top PM through the OSM indicate transition from anoxic (Phosphate-lower OSM) to dysoxic (middle-upper OSM) conditions. This environmental trend is consistent with co-occurring foraminiferal assemblages in the studied succession and implies that the benthic species in the Negev sequence were adapted to persistent minimum oxygen conditions by performing complete denitrification as recently found in many modern benthic foraminifera.

4.2 Introduction

4.2.1 The high-productivity sequence in Israel

The Upper Cretaceous succession in Israel, enriched in Si–C–P, was described in numerous studies as a product of a coastal high productivity upwelling regime that persisted in the southern margins of the Tethys (e.g. Bein et al., 1990; Almogi-Labin et al., 1993; Kolodny and Garrison, 1994; Soudry et al., 2006; Edelman-Furstenberg, 2008; 2009, Figures 25, 26 A and B). Such marine high-productivity systems, characterized by high nutrient levels usually supplied by upwelling and associated oxygen deficient bottom water, are recognized by the accumulation of cherts, porcelanites, phosphates, and organic rich carbonates (Parrish and Curtis, 1982; Suess and Thiede, 1983; Thiede and Suess, 1983; Summerhayes et al., 1992). Although upwelling induced productivity reached its peak in the SE Tethyan margins, other high productivity deposits appeared globally in the Upper Cretaceous along continental margins and the Tethyan Circular Current (TCC) pointing to similar modes of occurrences connected with upwelling regimes (Parrish, 1998; Erlich et al., 2000; Rey et al., 2004; Soudry et al., 2006, see Figure 25). The organic rich sequence in Israel spans from the Santonian into the Maastrichtian (Bein et al., 1990; Almogi-Labin et al., 1993, Figure 26 A) with the most intense upwelling phase occurring during the Middle-Late Campanian. During this time interval, the inner belt (e.g. southern Israel, Negev basins) was distinctly more productive than the outer, offshore belt (central Israel) as is also reflected in the significantly different lithological associations, i.e. mainly chert and phosphorite in the Negev compared to organic-rich carbonate in offshore belt (Figure 27 A and B).

The Mishash Formation rocks in southern Israel were deposited in a series of recurring sedimentary cycles. The Mishash Formation is distinguished by thick chert beds, silicified carbonates, and porcelanites, overlain with beds of brecciated chert, and thick Phosphate Member (PM) (Soudry et al., 1985). Total organic carbon content (TOC) in organic rich layer in the PM is as high as 24 wt.% (Bein et al., 1990).

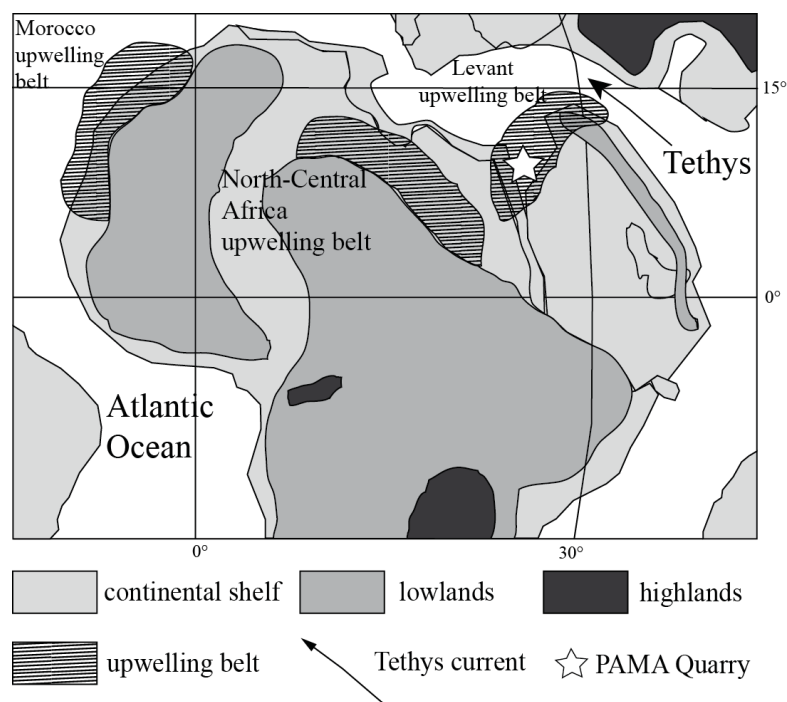


Figure 26: Paleogeography map shows the upwelling belts developed along the southern Tethys margin during the Late Campanian and Early Maastrichtian. Star marks the inferred position of Negev region within the Levant upwelling belt. From Ashckenazi-Polivoda et al. (2011).

At the top of the Mishash Formation the lithology changes dramatically into a monotonous sequence of organic rich carbonates, locally referred as the Oil Shale Member (OSM) containing up to 15–20 wt.% TOC (Bein et al., 1990; Minster, 1996). This change is ascribed to a shift of the upwelling system southeastward, leaving the Negev area at a still productive, more distal position (Almogi-Labin et al., 1993).

The OSM comprises the lower part of the Ghareb Formation and was recently dated as latest Campanian–Early Maastrichtian, spanning from 71.6 to 69.85 Ma (Ashckenazi-Polivoda et al., 2011, Figure 27). The thickness of the OSM in the Negev varies significantly: it is, up to 40–45 m in the Efe syncline, central Negev, and disappearing towards the flanks of the higher structures (Minster, 1996). The Maastrichtian pelagic marl and chinks of the middle and upper parts of the Ghareb Formation mark the end of the upwelling activity and the return of more normal oceanic conditions in this region. The deposition of the oil shale sequence signifies a major change in the dynamics of the Late Cretaceous southern Tethys upwelling system.

The mechanisms that drive such change and the paleoenvironmental history of this upwelling regime are still not well understood and are of great scientific interest.

4.2.2 Background on the foraminiferal assemblages

The foraminiferal assemblages of the OSM in the Negev at the PAMA quarry, Israel (Figure 29) were studied in detail by Ashckenazi-Polivoda et al. (2011). Five distinct planktic (P-Types) and benthic (B-Type) foraminiferal assemblages were identified based on statistical clustering of the relative abundance of the planktic and benthic foraminiferal genera (Figure 28). The cosmopolitan and ecologically generalist genera *Globigerinelloides*, *Heterohelix* and *Hedbergella* were found to be the main contributors to clustering of the five planktic foraminiferal assemblages.

Assemblage P-Type 5 characterizes only the PM, and exhibits the highest occurrences of *Globigerinelloides* (87 %), lowest occurrences of *Heterohelix* (9 %) and an absence of the ecologically specialized keeled globotruncanid species. An overall change from assemblage P-Types 4 to P-Type 1 was observed along the OSM, reflected by an increase in the abundance of *Heterohelix* (from 44 % to 73 %) and coinciding decrease in the abundance of *Globigerinelloides* (from 32 % to 5 %). This change reflects a clear decrease in surface water productivity in time (Figure 28).

The main contributors to the clustering of the five benthic foraminiferal assemblages (B-Type) are infaunal triserial buliminids (*Praebulimina* and *Neobulimina*) typical to anoxic pore water, and rotaliids (mainly *Gyroidinoides* and *Gavelinella*) that are more common in aerated seafloor environments. Assemblage B-Type 5 represented only in the PM, and characterizes by dominance of the triserial buliminids (98 %). A clear transition is observed from assemblage B-Types 4 at the base of the OSM to assemblage B-Type 1 at the top of the OSM and the MM. This transition marks an increase in the abundance of *Gyroidinoides* (from 17 % to 35 %) and decrease in the abundance of *Gavelinella* (from 29 % to 12 %) and the triserial buliminids (from 42 % to 10 %), and reflects an increase in bottom water aeration (Figure 28). At the base of the OSM, the establishment of planktic foraminifera, including appearances of intermediate-water dwellers keeled globotruncanids, and the establishment of benthic rotaliid fauna, marks the most prominent change and a transition to a pelagic outer shelf-upper slope environment. Further deepening probably occurred during deposi-

tion of the middle part of the OSM (~32 m), when rotaliids became predominant in the benthic foraminiferal assemblage (Figure 28). The paleodepth of the OSM is estimated to be several hundred meters (upper-middle bathyal) based on the dominance of the deep sea *Gyroidinoides* spp. and the appearance of the deep sea species *Nuttallides truempyi*.

The upward changes in the P-types and B-Types coincide with a decline in TOC content, from ~20 wt.% to 0.1 wt.% (Figure 28). This correspondence indicates a strong linkage between foraminiferal assemblage composition and upper-water-column productivity, and oxygen levels at the seafloor and within the sediment. The present study was aimed to create a complementary high-resolution geochemical characterization of this sequence that will allow us to further explore the significance of this linkage and its paleoceanographic implications. This study is based on integration of foraminiferal assemblages with organic C and N concentrations and their stable isotope composition that were used for detailed reconstruction of fluctuations in primary production levels and nutrient availability in the water column and the sea-floor during the accumulation of the oil shale succession and during the transition from the underlying phosphorites to the overlying MM.

4.3 Materials and methods

4.3.1 Location and samples

The extended lithological sequence of the high-productivity succession, exposed at the open PAMA quarry, was chosen for this study as a representative section of the Late Cretaceous southern Tethyan upwelling regime (Figure 30). This quarry is operated by Rotem Amfert Negev Company and is located at Mishor Rotem (Efe Syncline; 31°04'51.82"N; 35°10'02.85"E), where one of the largest oil shale reservoirs in Israel is found. Unlike most of the Negev OSM outcrops, the sequence exposed at PAMA quarry is fresh, unaltered with low thermal maturity (see Section 4.4.4) and contains well-preserved fossils, and is considered of high quality similar to that found in deep sea cores.

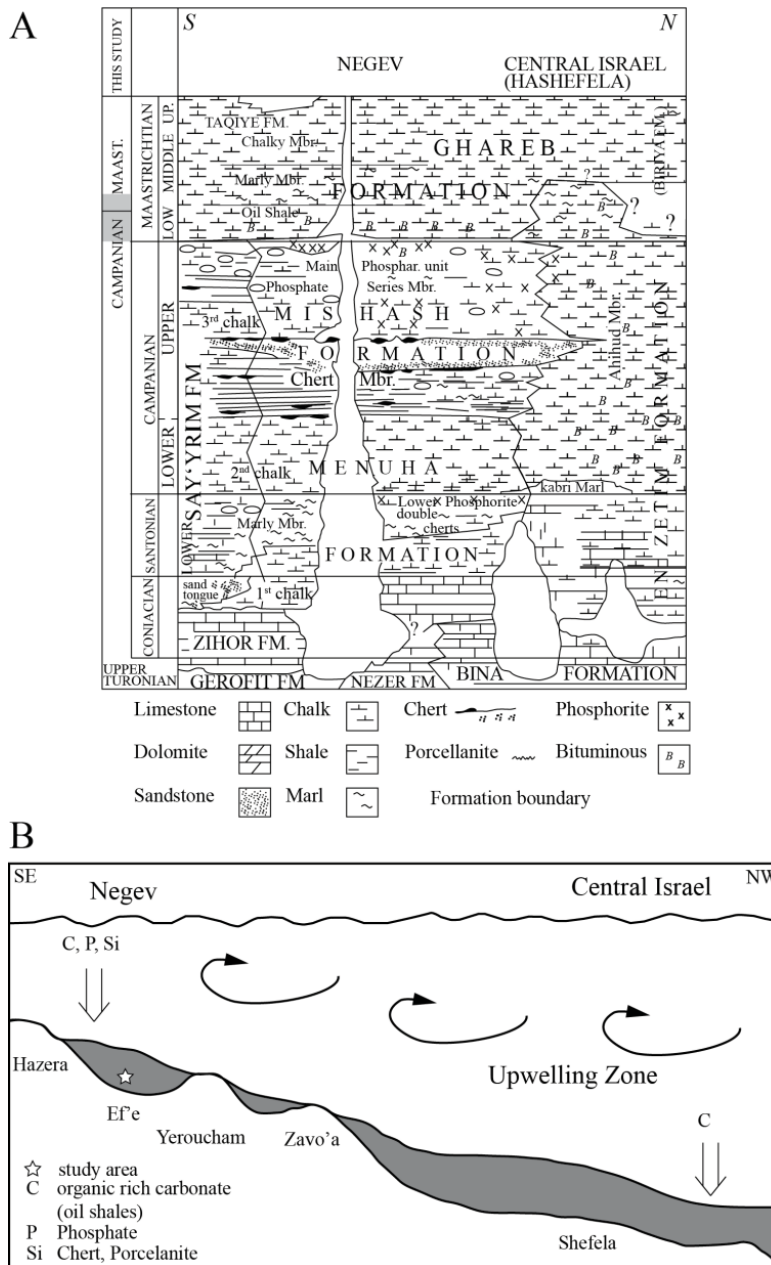


Figure 27: A. Schematic correlation of the Late Cretaceous formations in Israel modified after Reiss et al. (1985). White intervals indicate hiatus. The high productivity system is represented by the accumulation of cherts, porcellanites, organic-rich carbonates, and phosphorites during the Middle-Late Campanian Mishash Formation and Oil Shale Member of the Late Campanian-Early Maastrichtian Ghareb Formation (modified age after Gradstein et al. (2005)). The transition to pelagic marls and chalks marks the return of normal marine conditions. **B. SE-NW schematic cross-section (not to scale) across the Syrian Arc, from the Negev to central Israel, with Mishash and Ghareb Formation filling synclines (gray area).** Upwelling zone extends across the entire traverse, with organic-rich carbonate (C), phosphorite (P), and siliceous sediment as chert and porcellanite (Si) deposited in varying proportions in the synclines. Modified after Almogi-Labin et al. (2012).

The same sample set that was used by Ashckenazi-Polivoda et al. (2011) for the micropaleontological analysis of the planktic and benthic foraminiferal assemblages was used in this study. This set consists of fifty samples that were taken at approximately 1 m intervals (~50 m) and include the uppermost part of the PM of the Mishash Formation (5.8 m) the entire OSM (42 m) and the base of the MM (~3 meters) of the Ghareb Formation (see in Ashckenazi-Polivoda et al. (2011) details on the lithology and biostratigraphy, and Figure 28).

4.3.2 Sample analyses

For the analysis of the organic carbon and nitrogen content 1–2 g of dried powdered rock samples were treated with 2 M HCl, to dissolve the carbonate matrix. The treated samples were shaken with a vortex to achieve complete dissolution. The residue was thereafter washed several times with double distilled water until no Cl^- ions were detected, using silver nitrate. The washed samples were used to measure wt% carbon and nitrogen and their isotopic composition. Total organic carbon (TOC) and total organic nitrogen (TON) were calculated from the measured % C and % N values, which were corrected for the removed % CaCO_3 fraction. The bulk organic carbon and the C and N isotope measurements were performed on Carlo Erba EA1110 elemental analyzer in line with Finnigan MAT252 stable isotope ratio mass spectrometer at the Department of Environmental Sciences and Energy Research at Weizmann Institute of Science in Israel. The carbon and nitrogen isotopes were measured simultaneously from the same sample by peak jumping with mean standard deviation of 0.19 ‰ and 0.28 ‰ for $\delta^{13}\text{C}_{\text{org}}$ and $\delta^{15}\text{N}_{\text{org}}$, respectively. All results are reported relative to PDB for $\delta^{13}\text{C}_{\text{org}}$ and relative to air for $\delta^{15}\text{N}_{\text{org}}$. In addition, an internal standard of lignin was used every 6 to 8 samples to ensure stable measurement without drifts. For the analysis of saturated hydrocarbons in solvent extracts of the organic matter (OM), 20 g of dried powdered rock samples (< 200 μm) were Soxhlet extracted for 30 h with dichloromethane/methanol 9:1. The solvent mixture was evaporated using a rotary evaporator. 10 mg of the obtained extracts were separated into three fractions, saturated hydrocarbons (F1), aromatic hydrocarbons (F2) and polar hydrocarbons (F3) by column chromatography using 15 g of silica gel 60 (Merck) and a glass column with 15 mm inside diameter. The F1 fraction was ob-

tained by elution with 40 ml hexane, F2 was eluted with 100 ml hexane/dichloromethane 9:1 and F3 with 40ml of methanol. The F1 fraction was further analyzed by gas chromatography–mass spectrometry (GC–MS) for determination of the pristane/phytane (Pr/Ph) ratio. GC–MS analyses were performed on a Trace GC Ultra gas chromatograph coupled to a dual stage quadrupole (DSQ II) mass spectrometer (Thermo Fisher).

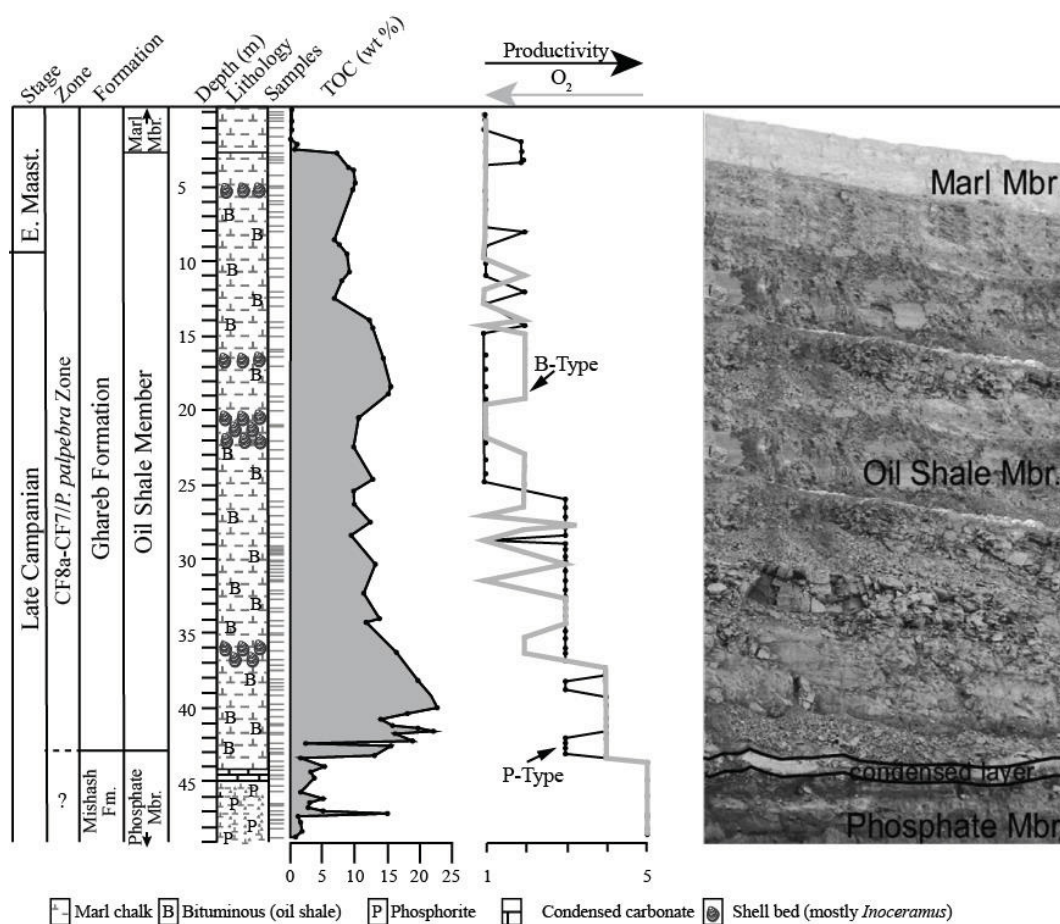


Figure 28: Stratigraphy, lithology, TOC and P and B-Type assemblages of the studied section at PAMA quarry. Modified after (Ashckenazi-Polivoda et al., 2011).

The GC–MS system was equipped with a TR5-MS column (30 m, 0.25 mm ID) with 0.25 μm film thickness from Thermo Fisher. The diluted F1 fractions were injected in splitless mode with a splitless time of 1 min. The GC oven temperature was programmed from 40 to 320 $^{\circ}\text{C}$ at a rate of 3 $^{\circ}\text{C}/\text{min}$. The mass spectrometer was operated in EI mode (70 eV) and in full scan mode. Helium was used as carrier gas. The data were recorded, processed and quantified with Xcalibur[®] software. To the extracts of the saturated hydrocarbon fraction 3 μL of perdeuterated tetracosane

(1 $\mu\text{g}/\mu\text{L}$) was added as internal standard.

An organic petrological analysis was carried out on four representative samples (2.6 m, 26.6 m, 42.6 m, and 43.8 m) at Core Lab Houston. This analysis was carried out in order to identify the type of kerogen present in the samples, particularly if it is dominantly marine or terrestrial origin. The analysis was performed by reflected and transmitted white light and reflected UV fluoresces.

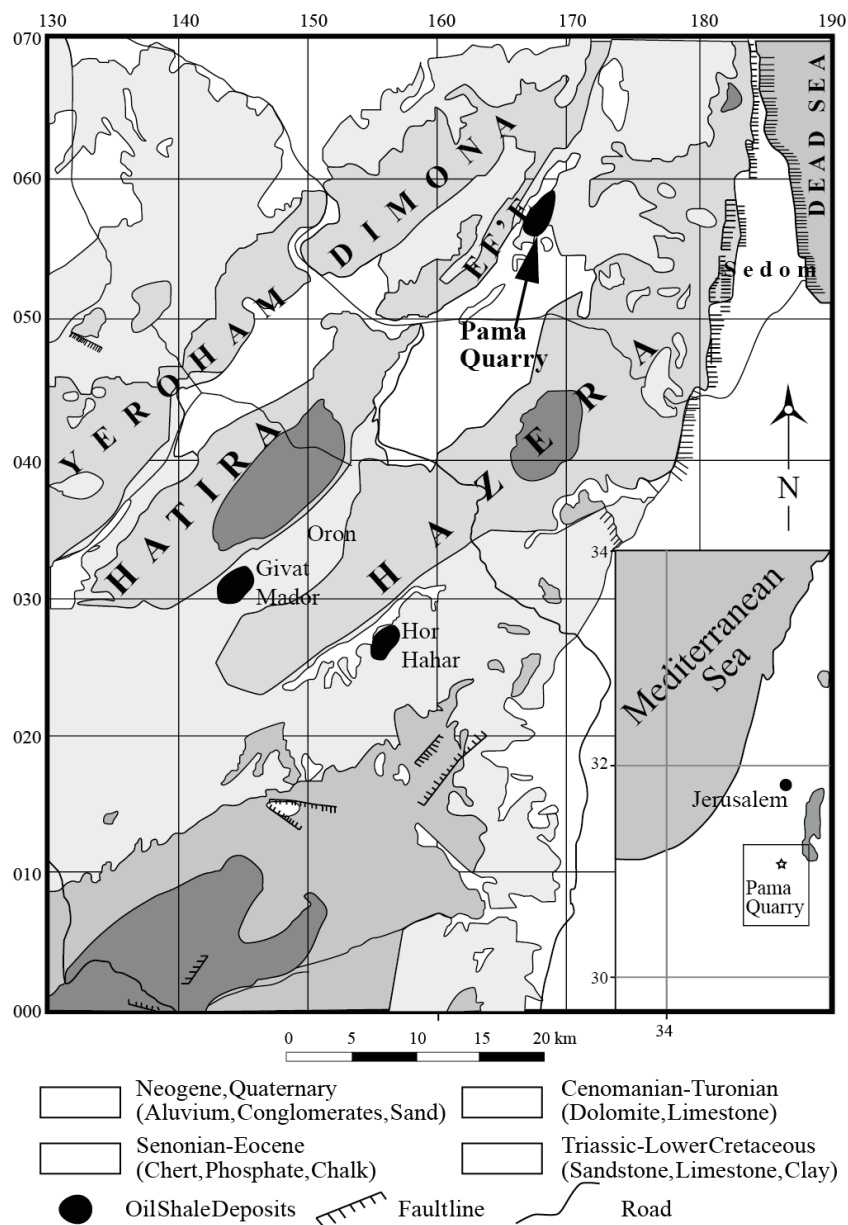


Figure 29: Geological map (1:250,000) of northern Negev modified after Shahar and Wurzburger (1967). The PAMA quarry is located in the Efe Syncline, where one of the largest oil shale reservoirs of southern Israel occurs. From Ashkenazi-Polivoda et al. (2011).

4.4 Results

4.4.1 TOC, TON and C/N

The TOC record shows clear difference between the OSM and its transitions with the underlying top of the PM and the overlying MM with OSM values being significantly higher than in the other two units (Figure 30). At the top of the PM TOC values mostly range between 1 and 4 wt.%. However these low values do not represent the whole PM that at certain intervals showed values up to 24 wt.% (Bein et al., 1990). There is a distinct step-wise decrease in the TOC content from the base to the top of the OSM (Figure 30). The highest TOC values (up to 18 wt.%) are found in the lower part (43.8–37.0 m), intermediate values (mostly 9–11 wt.%) at 37.0 to 13.0 m and a further drop to mostly 5.5–8.0 wt.% in the upper part of the OSM between 13.0 and 3.0 m.

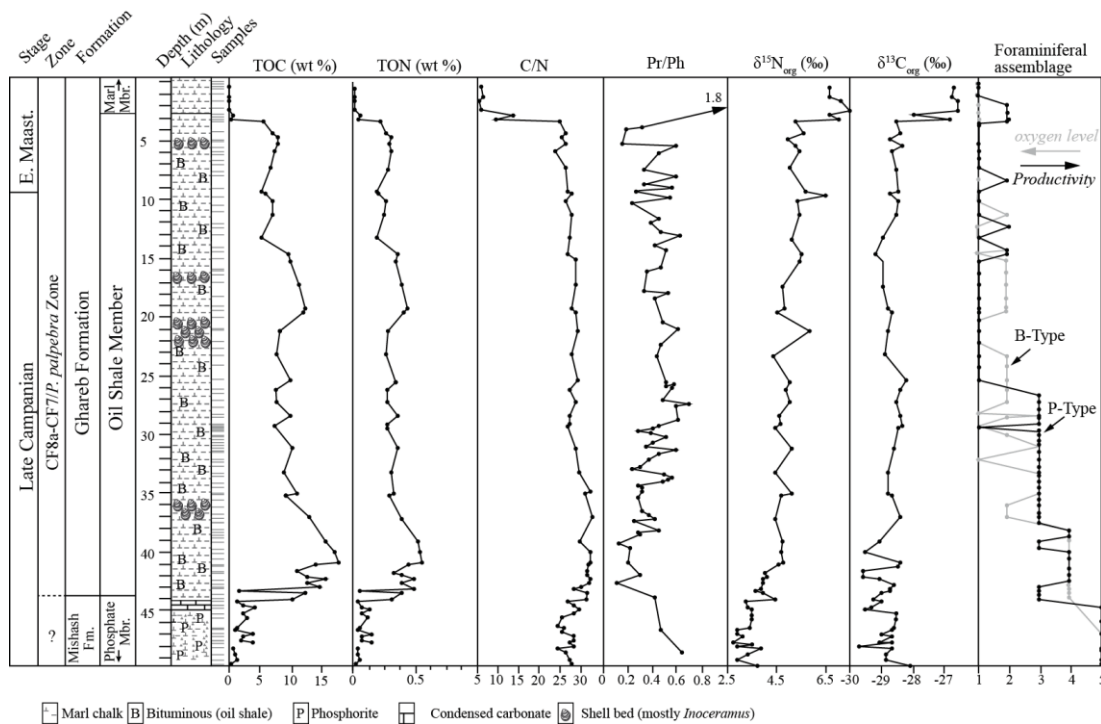


Figure 30: TOC, TON, Pr/Ph, C/N, $\delta^{13}\text{C}_{\text{org}}$ and $\delta^{15}\text{N}_{\text{org}}$ and foraminiferal assemblage records of the studied sequence. Note: 1. The very low TON content and high C/N ratios along the OSM. 2. The gradual decrease in TOC and TON, and increase in Pr/Ph, $\delta^{15}\text{N}_{\text{org}}$ and $\delta^{13}\text{C}_{\text{org}}$ along the OSM. 3. The sharp change at the transition to the MM. 4. The change in foraminiferal P and B- Types assemblages that follows the change in TOC and TON records and are opposite to the $\delta^{15}\text{N}_{\text{org}}$ trend (all values in appendix, Table A-8).

The contact with the overlying MM is marked by a sharp decrease in TOC values below 1.0 wt.%. TON values in the studied sequence are low and ranged between 0.02 wt.% and 0.56 wt.%. Highest TON values are recorded at the lower part of the OSM (up to 37 m) and generally decrease upward by a half (Figure 30). TON values of the top of the PM and the MM are considerably lower than the OSM and vary between 0.02 wt.% and 0.15 wt.%. C/N values at the top of the PM and throughout the OSM are high and range from 25 to 32 (Figure 30). At the transition from the top of the PM to the OSM C/N values increase from 28 to 32 and gradually decline to ~25 at the upper OSM. The transition to the MM shows a sharp decrease to values of 6–7.

4.4.2 Pristane/Phytane (Pr/Ph) ratio

A relatively high Pr/Ph ratio of 1.8 is only observed in the MM. The Pr/Ph ratios (appendix, Table A-8) generally vary from 0.43 to 0.65 within the PM and between 0.11 and 0.7 in the OSM. The lowest Pr/Ph value (0.11) is observed only in the base of the OSM and is followed by gradual increase upwards up to the center of the OSM profile. In the upper part of the OSM sequence the Pr/Ph remains nearly on the same level (around 0.44) with some fluctuations (Figure 30).

4.4.3 Organic N and C isotopes

The $\delta^{15}\text{N}_{\text{org}}$ record (appendix, Table A-8) shows an enrichment trend with a shift from values of 2.8–3.9 ‰ at the top of the PM to 4.5–6 ‰ within the OSM and another enrichment of up to 7.5 ‰ at the MM (Figure 30). A secondary features observed within the OSM are fluctuations in the order of 0.6–1.5 ‰, superimposed on the general trend. The $\delta^{13}\text{C}_{\text{org}}$ record shows little variation within the top of the PM and the OSM where it fluctuates from -29.6 to -28 ‰. The transition to the overlying MM is marked by increase to -26.5 ‰ (Figure 30).

4.4.4 Organic petrology

All samples include fluorescing amorphous matrix bituminite (kerogen type II), dinoflagellate cysts, marine fossil fragments (mostly pelagic foraminifera, bivalves, and minor bryozoans), trace amounts (< 5 %) of terrestrial kerogen types III and IV (al-

lochthonous inertinite and vitrinite), calcareous and siliceous mineral matrix, and framboidal pyrite (Figure 29). Discrete or laminated unicellular marine algal bodies (*Tasmanales*) were seen in two of the samples. White light reflectance (% Ro) measured on sporadic vitrinite-like particles found in two samples is ~0.3 % Ro indicating very low maturity level.

4.5 Discussion

4.5.1 TOC

The bulk OM can be used as a proxy for changes in surface productivity and in burial processes in the sediments (e.g. Jenkyns et al., 2002). Moreover, the combination of TOC with foraminiferal assemblage data can be used to infer the relative contribution of surface water productivity, burial efficiency and diagenetic processes (see Ashckenazi-Polivoda et al., 2011).

In the Late Cretaceous Negev high productivity succession, the high TOC content of the OSM (18.0–5.5 wt.%) indicates both high organic input and burial efficiency and preservation (Figure 30). This is evident from the planktic and benthic foraminiferal assemblages indicating high productivity at the surface water and relatively low-oxygen bottom water during the deposition of the OSM (Ashckenazi-Polivoda et al., 2011). The upward decrease in TOC content within the OSM coincides with changes in the benthic and planktic foraminiferal assemblages implying a gradual decrease in surface water productivity from highly eutrophic to mesotrophic and at the same time a contemporaneous shift from an anoxic to a dysoxic-suboxic seafloor (Figure 28).

The low TOC content of the top PM that underlies the OSM is a local diagenetic feature, typical to the studied outcrop. Elsewhere in the Negev, this unit can be enriched in organic carbon by as much as 20 wt.% (Rotem Amphart Ltd, personal communication). In contrast, the low TOC content of the MM that overlies the OSM is a regional phenomenon, indicating that this unit experienced diagenetic indurations and OM oxidation (Figure 30).

4.5.2 Organic petrology

The samples analyzed appear to be marine oil shale composed of lipid-rich OM derived from marine algae, dinoflagellate cysts, and amorphous fluorescing bituminite

of sapropelic origin (sapropelinite). The very small amount (< 5 %) of allochthonous vitrinite and inertinite indicates a minor contribution of terrestrial OM (Figure 31). Similarly, Eshet and Almogi-Labin (1996) and Eshet et al. (1994) found abundant and diverse dinoflagellate and calcareous nannofossil assemblages throughout the high productivity sequence of the Negev that indicate a dominant marine source for the OM. The low maturity, 0.3 % Ro, is consistent with the low maturity suggested in earlier studies of the OSM (Bein and Amit, 1982; Bein et al., 1990).

4.5.3 TON and C/N ratio

TON and C/N ratios of OM have been widely used as a reliable parameter to distinguish between algal and land-plant origins of sedimentary OM (Hedges et al., 1986; Twichell et al., 2002). Marine plankton typically have on average C/N ratios between 6 and 7 (“Redfield ratio”), whereas vascular land plants have C/N ratios of 20 and greater (Hedges et al., 1986; Meyers, 1994; Hedges et al., 1997). C/N ratios of the top PM and OSM are considerably higher than typical marine algal values, whereas the values of the MM are more similar to the latter (Figures 30 and 32). The very low TON values and high C/N ratios of the OSM may appear to record an input of vascular land plants. However, the organic petrology analysis clearly indicates that the majority of the OM is of marine origin (Figure 31). Twichell et al. (2002) observed an increase in C/N ratio values from 5 to 15 in OM in sediments from the Middle Miocene to latest Miocene and Pliocene deposited under the Benguela current upwelling system. Meyers et al. (2006) reported similar elevated C/N values (20–40) in the Albian to Santonian black shale sequences from Demerara Rise. These authors suggested that the high C/N ratio resulted from greater recycling rates of nitrogen-rich, relative to carbon-rich OM components as the flux of total OM to the seafloor increased. van Mooy et al. (2002) showed that when the modern marine OM is degraded under suboxic to anoxic conditions via denitrification it preferentially decomposes nitrogen-rich amino acids resulting in a reduction of the TON content. A similar preferential degradation by denitrification and release of gaseous nitrogen (N₂ and NO₂) was previously discussed by Altabet et al. (1995).

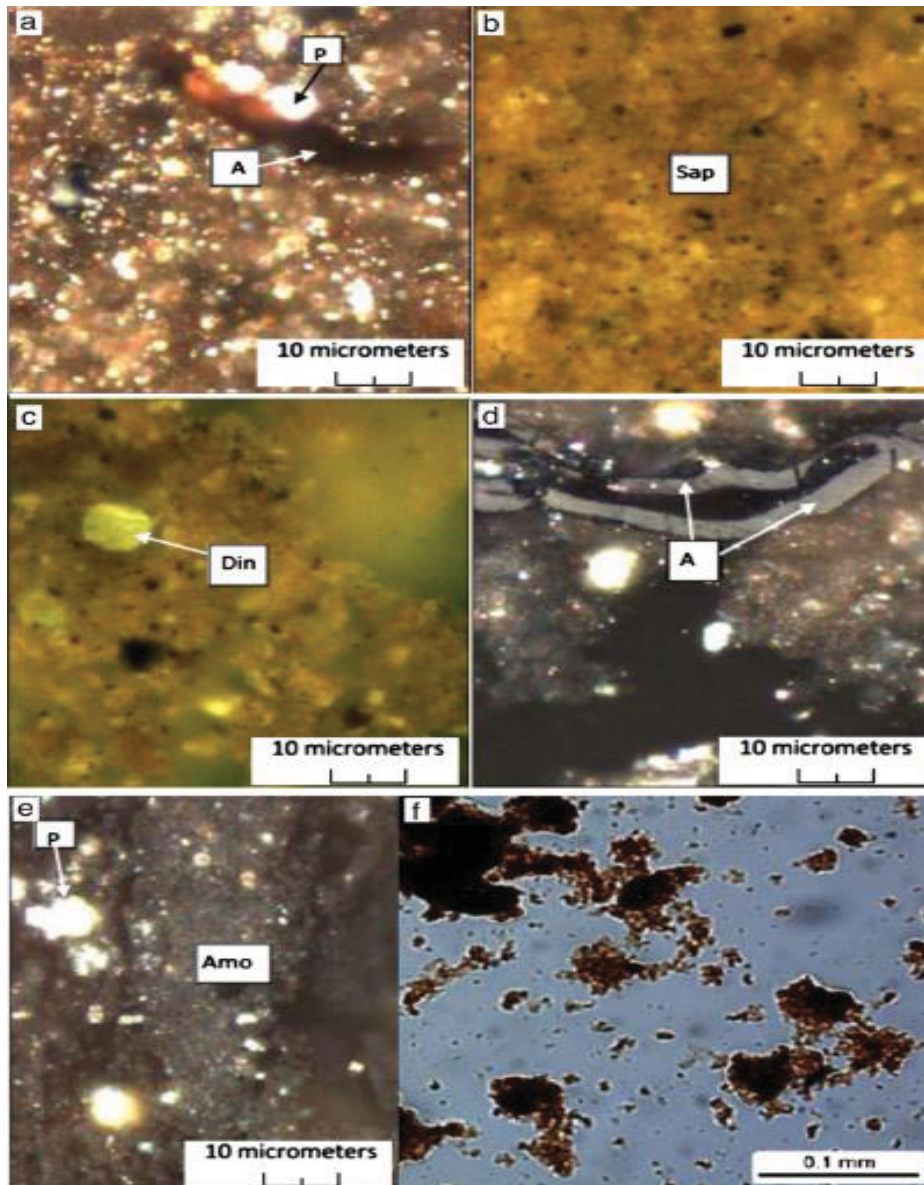


Figure 31: Selected photos from the organic petrological analysis. (a) Sample 3.6 m, photo of kerogen concentrate under reflected light; unicellular marine Tasmanales alginite (A), mineral matter and pyrite (P). (b,c) Sample 26.6 m, photos were taken under reflected UV light; fluorescing spropelinite (Sap), dinoflagellate cyst (Din) in fluorescing matrix. (d) Sample 42.6m, photo of kerogen concentrate under reflected light; broken fragment of Tasmanales alginite (A). (e) Sample 43.8 m, photo of kerogen concentrate under reflected light; amorphinite (Amo) and framboidal pyrite (P). (f) Sample 43.8 m, photo taken under transmitted light; amorphous kerogen type II.

We postulate that the very low TON values and high C/N ratios at the top of the PM and the OSM signify a similar mechanism of enhanced preferential degradation of nitrogen-rich components of the OM under depleted oxygen conditions due to high surface water productivity and flux of OM to the bottom. These relations are further

substantiated by the very good linear correlation between the TON and the TOC ($r^2=0.98$, Figure 33). If we assume a typical averaged algal C/N value of ~6–7 as an initial ratio for the 15 wt.% TOC of the lower OSM, an increase to the observed C/N ratio of ~30, would have required a selective removal of about 70 % of the initial nitrogen content. This percentage is considerably higher than the loss of nitrogen from preferential degradation presented in van Mooy et al. (2002) experiments (i.e., 9 %). The significantly high % N loss in the OSM may to some extent reflect the differences between geological degradation processes and experimental time. However, there might be other reasons that require further investigation.

4.5.4 Pr/Ph ratio

The C₁₉ and C₂₀ isoalkane molecules, respectively pristane (Pr) and phytane (Ph), are very common constituents of oil and solvent extract of the organic fraction in hydrocarbon source rocks. The ratio of Pr to Ph is widely attributed mainly to the redox conditions at the depositional environment of the source rock (e.g. Didyk et al., 1978). This notion stems from the initial assumption that both Pr and Ph are mainly diagenetic products of phytyl side chain of chlorophyll due to differential reactions which are dependent on the depositional redox conditions (Maxwell et al., 1972; Powell and Mc Kirdy, 1973). However, several other factors (e.g. thermal maturity, variable biomolecules sources, diagenetic effects) have been shown to influence the level of the Pr/Ph ratio determined from crude oils, coal and sedimentary OM and suggest that its use as an indicator for the oxicity of the depositional environment should be in conjunction with other paleoenvironmental proxies (e.g. ten Haven et al., 1987; Rowland, 1990; Kohnen et al., 1991a; Peters et al., 2007). Nevertheless, the low Pr/Ph ratio obtained (≤ 0.7) in this study (Figure 30), the consistency of the Pr/Ph records with implications of other chemical and stable isotope characteristics and the improbable significant thermal maturity effect suggest that the Pr/Ph ratios of the studied section mainly reflect the redox depositional conditions. This interpretation is further corroborated by the inverse trends of the Pr/Ph and TOC (Figure 30) which is consistent with higher OM input, better preservation and anoxia during deposition of the OM in the lower part of the section.

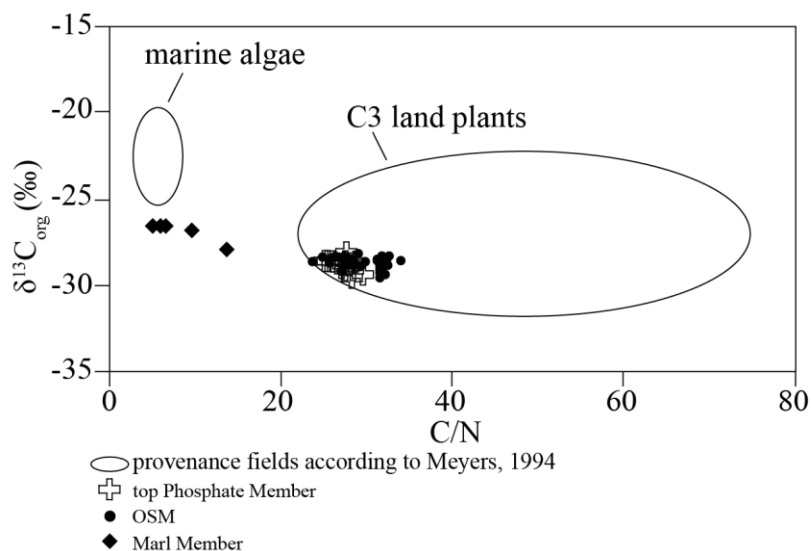


Figure 32: $\delta^{13}\text{C}_{\text{org}}$ vs. C/N ratios. Note that the records of OM from the top PM and the OSM are more similar to those of C3 land plants than to algal marine source.

The low Pr/Ph ratios (0.11–0.7) within the upper PM and the OSM (Figure 30) can be interpreted to reflect anoxic to dysoxic conditions throughout the entire OSM with increasing anoxicity towards the bottom of the OSM (terms used are according to Kaiho, 1994). The Pr/Ph ratios obtained from samples of the top PM are similar to those values derived from the upper OSM section (ca. 0.48). This feature is somewhat discordant with the implication of the benthic foraminiferal assemblages of the top PM that indicate anoxic conditions (Figure 30). These differences may be the results of a local diagenetic partial oxidation of the OM within this unit observed in the studied outcrop (see discussion in Section 4.5.1). The significant increase of the Pr/Ph ratio from around 0.45 to 1.8 is consistent with a drastic change of the depositional environment from suboxic to oxic conditions of deposition.

4.5.5 $\delta^{13}\text{C}_{\text{org}}$

$\delta^{13}\text{C}_{\text{org}}$ records of the top PM and the OSM are considerably depleted in ^{13}C compared to modern marine OM and are more similar to those characterizing terrestrial OM (Wefer et al., 1994; Meyers, 1997) (Figures 32 and 34). However, as discussed in Section 4.5.2, the source of the OM in the organic rich succession of the Negev is most definitely algal marine. Moreover, values as low as ~ -29 ‰ are lighter even if the kerogen was consisted entirely of land plant material (Figures 32 and 34) (Meyers, 1994). The low $\delta^{13}\text{C}_{\text{org}}$ values of the top PM and the OSM values may rep-

resent a diagenetic effect of differential removal of ^{13}C -enriched fraction (Meyers, 1994; Lehmann et al., 2002). Selective removal of ^{13}C -enriched carbohydrates and proteins fractions which are more susceptible to decomposition, and fortification of the ^{13}C depleted lipid fraction can lead to decrease in the $\delta^{13}\text{C}$ compared to the bulk algal tissue (Jenkyns and Clayton, 1986; Hedges et al., 1988; Meyers, 1994).

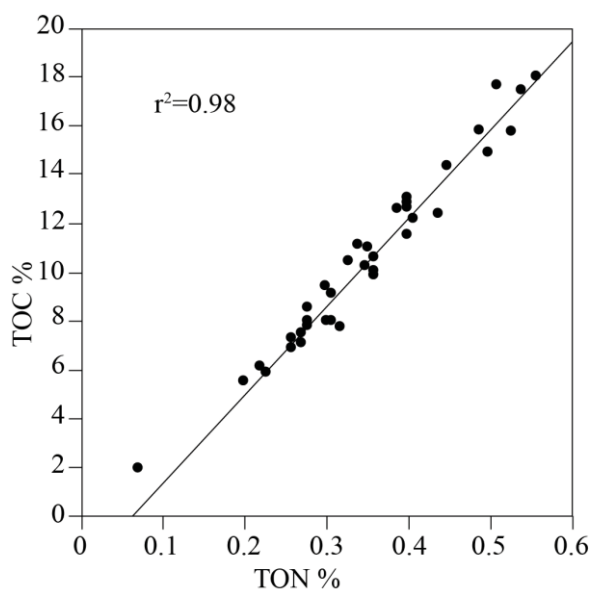


Figure 33: TON vs. TOC. Note the perfect correlation between the TON and TOC content.

Jenkyns and Clayton (1986), suggested this mechanism to account for the low $\delta^{13}\text{C}_{\text{org}}$ values recorded from lower Jurassic (Toarcian) Tethyan black shale. Under certain conditions, this mechanism may selectively remove isotopically heavy organic components from the sediment (e.g. carbohydrates). It is likely, therefore, that very low $\delta^{13}\text{C}_{\text{org}}$ values of the top PM and the OSM was in part the result of an early mineralization and selective decomposition of the proteins fraction via denitrification under reduced oxygen conditions in bottom waters that persisted throughout the deposition of these units. The ~ 2 ‰ increase of the $\delta^{13}\text{C}_{\text{org}}$ at the base of the MM represents a small amount of organic content (~ 0.5 %) (Figures 30 and 33), that may reflect a residual fraction that was protected from late diagenesis by being attached to the clay fraction, or alternatively an original signal of enhanced degradation under oxic condition at the bottom water. Another possible explanation for the very low $\delta^{13}\text{C}_{\text{org}}$ values of the top PM and the OSM may be related to elevated levels of atmospheric CO_2 during the Cretaceous.

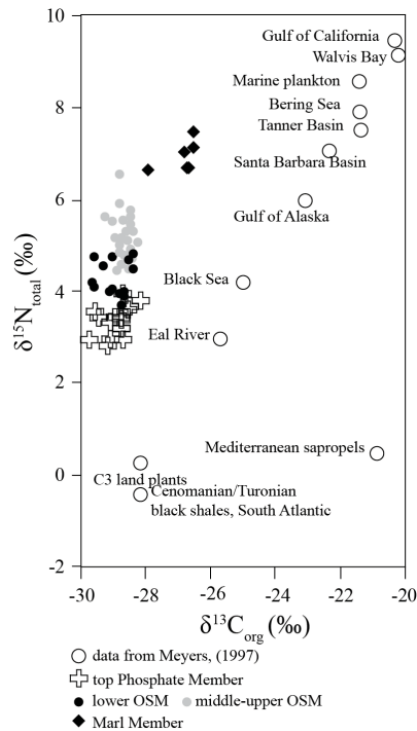


Figure 34: $\delta^{15}\text{N}_{\text{org}}$ vs. $\delta^{13}\text{C}_{\text{org}}$. Note the relatively low $\delta^{13}\text{C}_{\text{org}}$ values of the OSM and top Phosphate compared to records from modern marine environments. Also note the strong correlation in $\delta^{15}\text{N}_{\text{org}}$ from the top PM through the lower–upper part of the OSM to the MM. The subdivision of the OSM (lower/middle-upper) was determined at ~35 m where both TOC and foraminiferal assemblages exhibit a significant change.

Dean et al. (1986) claimed that marine Cretaceous organic rich sediments consistently have $\delta^{13}\text{C}$ values lower than Cretaceous terrestrial OM and ~5 ‰ lower compared to those of modern marine sediments. They suggested that out of the 5 ‰ negative shift, diagenetic processes can account for 1–2 ‰, whereas the rest is due to the high concentration of CO_2 in the atmosphere. The Late Cretaceous atmospheric CO_2 levels were estimated to be around ~550 ppm based on stomata index or higher based on modeling results (Kump and Arthur, 1999; Royer, 2006; Quan et al., 2009). High CO_2 levels could affect carbon isotopes in different ways: 1. The high availability of CO_2 could cause a shift to larger fractionation due to higher selectivity of the phytoplankton to ^{12}C (Dean et al., 1986). 2. If the isotopic composition of the atmospheric CO_2 was depleted thereby affecting the values of dissolved inorganic carbon and organic carbon (i.e. Suess effect, Gruber et al., 1999; Olsen et al., 2006; Liu et al., 2007). 3. Volcanic input (Méhay et al., 2009) or release of methane (Weissert and Erba, 2004). Since the $\delta^{13}\text{C}_{\text{org}}$ record did not vary considerably along the OSM ($\Delta <$

0.5 ‰), the low values suggest that it could have been established under stable atmospheric environment with high CO₂ levels.

4.5.6 $\delta^{15}\text{N}_{\text{org}}$

$\delta^{15}\text{N}_{\text{org}}$ can be used to distinguish between terrestrial vs. marine algal source, in the case that the primary composition is preserved. This is due to the fact that the $\delta^{15}\text{N}$ value of atmospheric N₂ is about 0 ‰, whereas the values of dissolved nitrate generally range between +7 ‰ and +10 ‰ (Meyers, 1997) (Figure 34). However, diagenesis of the marine OM could cause a significant deviation from its original signal. The influence of diagenetic processes seems to be reflected by the $\delta^{15}\text{N}_{\text{org}}$ records of the top PM and the OSM that are both relatively depleted in ¹⁵N compared to marine algal records that are similar to that of the dissolved nitrate (Figure 34). Kinetic isotope fractionation during protein hydrolysis can lead to selective release of both ¹⁵N-depleted and ¹²C-depleted compounds and enrichment of ¹⁵N and ¹³C in the residual organic fraction (Silfer et al., 1992; Macko et al., 1994; Lehmann et al., 2002). The depleted $\delta^{13}\text{C}_{\text{org}}$ and $\delta^{15}\text{N}_{\text{org}}$ values of the top PM and the OSM are in contrast to the expected isotopic signature of protein hydrolysis and thus suggest the involvement of a different diagenetic process (Figures 30 and 34). In some phytoplankton and bacterial cultures, the total protein within a cell has been found to be enriched in $\delta^{15}\text{N}$ (~3 ‰) relative to bulk nitrogen (Macko et al., 1987). Libes and Deuser (1988) showed a decrease of $\delta^{15}\text{N}_{\text{org}}$ with depth below the oxycline in OM sinking through the water in the Peru upwelling system and inferred that it could be due to selective decomposition of ¹⁵N enriched proteins. They also proposed that in addition to mineralization, bacterial ingrowth supplies $\delta^{15}\text{N}$ -depleted compounds to the OM, which enhances the negative shift of $\delta^{15}\text{N}$. A similar mechanism was suggested by Lehmann et al. (2002) from the study of sediments in Lake Lugano. However, addition of bacterial ingrowth is expected to yield lower C/N ratios compared to those of normal marine values, in contrast to the relatively high values that were recorded at the top PM and the OSM. Therefore, it is not likely that bacterial ingrowth had been a dominant mechanism in the early diagenesis processes. Meyers (1997) suggested that the low $\delta^{15}\text{N}$ values of Cenomanian-Turonian black shales from the South Atlantic and Plio-Pleistocene sapropels from the Mediterranean may reflect utilization of dissolved N₂

by nitrogen-fixing bacteria that are possibly responsible for these anomalous isotopic values, or alternatively episodes of enhanced nitrate availability that allowed greater algal discrimination in favor of ^{14}N . Still, these two mechanisms cannot alone account for the very high C/N ratio in the marine OM of the top PM and the OSM which appear to reflect selective removal of nitrogen. The combination of high C/N ratios and relatively low $\delta^{15}\text{N}$ values of the top PM and the OSM implies that the main mechanism that determined the values of these records was selective decomposition of amino acids via denitrification and/or anammox. The observed differences between the $\delta^{15}\text{N}_{\text{org}}$ values of the top PM and lower OSM (2.8–3.9 ‰) and the middle-upper OSM values (4.5–6 ‰, Figure 34) could reflect a decrease of the effect of preferential removal of N-rich organic compounds as a result of a change from anoxic to somewhat more aerated conditions (dysoxic) of the bottom water. This notion is further supported by the differences in the foraminiferal (B-Type 1–5) assemblages between these units (Figures 28 and 30; (Ashckenazi-Polivoda et al., 2011)). The $\delta^{15}\text{N}_{\text{org}}$ increase to 7.5 ‰ at the base of the MM, which resembles marine algal values (Figure 34), could reflect an original signal of relic OM preserved under more oxic conditions. However, we cannot rule out the possibility that other factors may contribute to the relative depletion of the $\delta^{15}\text{N}$ values of these units.

4.5.7 The depositional environment of the Negev high productivity sequence: integration of geochemical and foraminiferal characteristics

Twichell et al. (2002) and van Mooy et al. (2002) suggested that the selective removal of nitrogen and increase in C/N ratio in marine OM could occur early in the sinking process within the water column. In such a case, the processes that caused the increase in C/N ratio and possibly the lowering of TON, $\delta^{15}\text{N}$, $\delta^{13}\text{C}$ and Pr/Ph values were not only associated with anoxia in the pore water of the seafloor sediments but also with low-oxygen conditions (anoxic- dysoxic) in the lower part of the water column throughout the time interval of the deposition of the top PM and the OSM (Figures 32 and 34). The presence of abundant infaunal triserial bulimind benthic foraminifera species typical to anoxic/dysoxic conditions (B-Types 5–4) at the top of the PM and at the base of the OSM (Ashckenazi-Polivoda et al., 2011) supports this model. The upward change from *Globigerinelloides* dominating P-Type 5 to *Hetero-*

helix dominating P-Type 1 along the OSM correlates with a distinct decrease in TOC content (18–5 wt.%), and signifies an upward decline in surface productivity (Figure 30). Based on this relation, it was inferred that *Globigerinelloides* species are the best tracers for extreme eutrophic surface water, whereas heterohelicids are associated with more mesotrophic conditions (Ashckenazi-Polivoda et al., 2011). The transition in time from assemblages B-Type 5 to 1 mainly reflects a change from the predominance of praebuliminids and neobuliminids to a more diversified rotaliid-dominated assemblage, indicating an increase in bottom water aeration (Ashckenazi-Polivoda et al., 2011). This change is not proportionally expressed by the C/N ratios, which record an upward decrease from 32 to 25 from the bottom to the top of the OSM, but remain considerably high compared to a typical algal ratio (Figure 32). The persistence of high C/N ratios at the upper part of the OSM implies that the seafloor sediments and perhaps bottom water conditions remained low in oxygen (i.e. dysoxic) throughout deposition of the OSM.

This model challenges the proposed oxic-suboxic bottom water conditions along the deposition of the OSM (Ashckenazi-Polivoda et al., 2011), which is based on our traditional interpretations of the requirement of oxygen for the microhabitats of the Cretaceous benthic foraminifera species. Certainly, the recent findings that benthic foraminifera can carry out complete denitrification to N₂ in the absence of oxygen (i.e. Risgaard-Petersen et al., 2006; Høglund et al., 2008) call for reevaluations of this concept. This possibility is particularly stressed by the study of Piña-Ochoa et al. (2010) showing that denitrification is in fact a widespread phenomena shared by many benthic foraminifera of different phylogenetic origins. This adaptation may have existed also in many of the Cretaceous benthic foraminiferal groups that allowed them to survive conditions in the absence of oxygen at the seafloor and within the sediments. Testing this hypothesis is beyond the scope of this study but surely will shed light on our knowledge of foraminiferal microhabitats from Cretaceous organic rich environments such as in the Negev.

4.6 Summary

1. The top PM and OSM (Late Campanian) are part of a high productivity sequences that resulted from a coastal upwelling system that operated along the south-

eastern Tethyan margins. The high TOC content of the OSM, which is mainly of marine algal source, indicates both high organic input and increase burial efficiency and preservation. The upward decrease in TOC content within the OSM implies a gradual decrease in surface water productivity with time.

2. The low TON content and high C/N ratios of the OM at the top of the PM and the OSM are atypical of marine algal source and indicate a significant diagenetic loss of nitrogen organic compounds (e.g. proteins).
3. Pr/Ph ratios determined from solvent extracts indicate moderate variation in the redox conditions during the upper PM and OSM deposition, with anoxic conditions in the lower part of the section and decreasing anoxicity towards the top of the profile. A sharp increase in the Pr/Ph ratio at the transition to the overlying MM suggests substantial change in the redox potential and its deposition under oxic conditions.
4. The low $\delta^{13}\text{C}_{\text{org}}$ values of the top PM and the OSM probably reflect the high concentration of CO_2 in the atmosphere in the Late Cretaceous and perhaps additional depletion by preferential decomposition of the ^{13}C enriched proteins fraction via denitrification under oxygen deficient sediment and bottom water environment.
5. The relatively low $\delta^{15}\text{N}_{\text{org}}$ values of the top PM and the OSM seem to indicate similar effect of selective removal of N-rich organic compounds, as proposed for the C/N and $\delta^{13}\text{C}_{\text{org}}$ records. We further suggest that the upward increase in $\delta^{15}\text{N}_{\text{org}}$ values from the top PM through the OSM and the prominent increase in the MM, indicating transition from anoxic (Phosphate-lower OSM) to dysoxic (middle-upper OSM) to suboxic (Marl) bottom water environment. This environmental change is consistent with the foraminiferal data presented by Ashckenazi-Polivoda et al. (2011).
6. Our interpretation that the deposition of the top PM and the OSM had been associated with low-oxygen conditions in the bottom and pore water challenges the conventional model on the microhabitats of the Cretaceous benthic foraminifera species. It suggests that some of the benthic species that were found in the Negev may have had a preconditioned adaptation to survive the lack of oxygen on the seafloor, perhaps by carrying out complete denitrification. This possibility is consistent with the recent findings on modern benthic foraminifera that shows that

denitrification is in fact a widespread phenomena shared by many benthic foraminifera of different phylogenetic origins.

Acknowledgments

We wish to express our gratitude to S. Volin and Amir Eyal, from Rotem Amfert Negev Company for their cooperation, to M. Kitin from the Geological Survey of Israel for his assistance in the laboratory procedures, and to Dr. Thomas Gentzis from Core Laboratories, Houston for the organic petrology analysis. We thank Alon Amrani for his helpful comments on this manuscript. We greatly thank reviewers Mark R. Leckie and Philip A. Meyers for their significant contribution towards improvement of this paper. The research was supported by GIF - The German-Israeli Foundation for Scientific Research and Development - grant no. 956-38.8/2007, the Israeli Ministry of National Infrastructure grant no. 27-17-005 and the Robin and Harold Vinegar contribution.

5 Conclusions and future implications

Two sets of samples from the inner belt (Efe Syncline) and the outer belt (Shefela basin) of the Late Cretaceous upwelling at the southern Tethys margin were investigated in this study. Interestingly, the climatic and paleoenvironmental changes during the deposition of these sediments could be elucidated. Furthermore, the geochemical implications concerning the phosphate deposition and the sulfur incorporation into the organic matter were in the focus of this work.

5.1 Paleoclimatic changes and paleo sea surface temperature of the upwelling system

An HPLC-MS/MS method has been applied to determine the TEX₈₆ values from both sample sets at high resolution for the reconstruction of SST variations during the Late Cretaceous. Notably, these are the first high resolution SST data for the southern margin of the Tethys revealed from two distinct profiles representing different distances of the sediment deposition from the former shoreline. Previously, only some SST data derived from isotope measurement on foraminifera were available from several sampling sites in Israel with rough temporal resolution. The new data set allows a detailed insight into the local paleoceanographic conditions and the local climate. Furthermore, we used these data to classify these local climatic conditions into the context of the global climate conditions of the Late Cretaceous. Importantly, the TEX₈₆ data obtained from the Shefela basin core facilitates to reconstruct the climatic changes in the Late Cretaceous over a time interval of 17 million years, from the Late Santonian to the Early Maastrichtian (~ 85 to 68 Ma). The response of this environment to the global climatic changes and local variations in SST were preserved in the GDGT composition of the sediments. During the Late Santonian to Early Campanian the SST in the Shefela basin decreased by 7 °C. This was the end of the extremely warm Late Cretaceous epoch, with highest temperatures in the Turonian, which lasted till to the Santonian. Interestingly, the data shed light onto a previously observed extremely high productivity event (~ 76 Ma) derived from the analysis of the foraminiferal assemblage in the sediments of the Shefela basin. Now, this could be correlated to a massive and relatively short termed temperature drop of almost 7 °C, probably caused by an intensification of upwelling of nutrient rich and

cold deep waters. Tectonic plate movement opened the connection between the North and South Atlantic Ocean (EAG) starting in the Albian. The separation of the two continents, namely South America and Africa proceeds and the connection between the North and South Atlantic becomes wider and deeper (Friedrich and Erbacher, 2006 and references therein). The resulting changes in the oceanic circulation and the development of new oceanic currents enormously influenced the SSTs of the Atlantic and Pacific Ocean. In comparison to these oceans the influence on the SST of the Tethys was rather moderate and so the further cooling in the Late Campanian was less prominent. The TEX₈₆ data from the Shefela basin were also used to reevaluate the equatorial to polar SST gradient of the Late Campanian to Early Maastrichtian by comparison with data from previous studies on the polar region. According to these calculations, the equatorial to polar SST gradient is about 22 °C and therefore closer to the modern value of 30 °C than suggested in previous studies.

The phenomenon of upwelling is based on the uplifting of cold water near to the shore, so that the near shore SST is lower in comparison to the more offshore located SST. Notably, the TEX₈₆ data from the two locations reflect this temperature difference between the inner and outer belt of the ancient upwelling system. The distance between the inner and the outer belt was nearly 80 km and a temperature shift of approximately 1.5 °C in the mean SST reflects the influence of colder water masses closer to the shoreline.

5.2 Natural sulfurization

The nutrient richness in upwelling environments promotes the primary production. Under these high productivity conditions areas of oxygen minimum develop in the sediment and sulfate-reducing bacteria consume the available reactive OM for the sulfide production, which is further oxidized again by sulfide oxidizing bacteria. Under these particular environmental conditions with either high sulfide concentration in the sediment or in the sediment/water interface combined with a limited availability of reduced iron in the pore water an effect called “natural vulcanization” becomes very important. Under these conditions the OM deposited in the sediment is preserved by the intermolecular or intramolecular reaction with reduced sulfur species. This results in a higher resistance of these molecules against microbial decomposi-

tion and explain the high amounts of preserved organic carbon. Furthermore, different correlation methods of geochemical proxies have been applied in the present study to distinguish between the different depositional environments. For the interpretation of the high sulfur content we used a TS vs. TOC diagram and identified that the C/S ratio of upwelling systems is two to three times higher compared to normal marine environments. Consequently, the mean C/S ratio from the OSM section is comparable to those for sediments from modern upwelling areas like the Peruvian or Benguela upwelling systems.

The iron-limited conditions during the sedimentation of the OSM and PM section were illustrated by the use of a ternary correlation diagram of Fe, S and TOC. Due to the high primary production the supply of reactive OM was not limited except for the MM. The high supply of H₂S due to sulfate reduction in combination with the lack of effective scavenging of the reduced sulfur by Fe promotes the incorporation of sulfur into the OM.

The OM derived mainly from marine algal material with a minor contribution of terrestrial material evident from biomarkers like n-alkanes and C₂₇- to C₂₉-steranes. OSCs are present in various compound classes like thiophenes with an n-alkyl or isoprenoid side chain, sulfur-containing derivatives of steranes and hopanoids with thiophene and thiolane moieties. The occurrence of these compounds argues for the incorporation of sulfur during the early stages of diagenesis. The degree of sulfurization of the OM seems to be generally elevated in upwelling systems due to the special conditions in these environments and ranges between 60 and 85 % of the total sedimentary sulfur.

5.3 Phosphate deposition in the context of sulfate reduction and sulfide oxidation

Compared to the OSM an enormous amount of OM was consumed by sulfate reducing bacteria during deposition of the PM. Together with the sulfate reducing bacteria sulfide oxidizers were present in the sediment/water interface yielding an increased sedimentation of phosphorus. The sulfide oxidizers *Thioploca*, *Beggiatoa* and *Thiomargarita* are able to store large amounts of intracellular polyphosphates, sulfur and nitrate. Under anoxic conditions with high concentrations of sulfide, phosphate is released by these bacteria and precipitated as carbonate fluorapatite. Interestingly,

the accumulation of phosphorus in the PM was 7 to 10 times higher compared to the OSM. The occurrence of these sulfate reducing and sulfide oxidizing bacteria was indirectly determined by the detection of branched and monounsaturated fatty acids. After a drastically change of the environmental conditions the phosphate deposition decreased to level observed in normal marine environments.

5.4 Bulk geochemical and isotopic implications

The PM and OSM show atypical low TON contents and high C/N ratios for marine algal source and indicate a significant diagenetic loss of nitrogen via denitrification and/or anammox. The redox conditions during the deposition of the upper PM and the OSM changed only moderately, reflected by the Pr/Ph ratios. A deposition under anoxic conditions in the lower part of the profile and only slightly aerated conditions towards the top of the profile can be suggested. The strong increase of the Pr/Ph ratio indicates a significant change of the depositional environment at the transition to the MM and probably a deposition of the sediments under oxic conditions.

The high atmospheric CO₂ concentration of the Late Cretaceous is probably reflected by the low $\delta^{13}\text{C}_{\text{org}}$ values of OM at the top of the PM and in the OSM. Additionally, the decomposition of ¹³C-enriched proteins via denitrification may also contribute to the low $\delta^{13}\text{C}_{\text{org}}$ values.

The low $\delta^{15}\text{N}_{\text{org}}$ values at the top of the PM and in the OSM were probably influenced by a selective removal of N-rich organic compounds. The changes of the paleoceanographic conditions reflected by the three different facies types correlate with the changing $\delta^{15}\text{N}_{\text{org}}$ values indicating transition from anoxic (Phosphate-lower OSM) to dysoxic (middle-upper OSM) to suboxic (Marl) bottom water environment. These data are supported by the results obtained from the analysis of the foraminiferal assemblage.

A special adaptation of the benthic foraminifera to survive the lack of oxygen on the seafloor, most likely by carrying out complete denitrification, is in accordance with the results of recent studies on modern benthic foraminifera showing that denitrification is a widespread phenomenon shared by many benthic foraminifera.

An interesting topic for future studies could be the analysis of the compound specific carbon isotopic composition of the fatty acids to determine their source. Furthermore,

the $\delta^{34}\text{S}$ compound specific isotopic analysis on compounds of the aromatic fraction might be used to further clarify the pathway of early diagenetic sulfurization of molecules. For structural analysis of unknown compounds, like the methylhopanoid thiophene in the aromatic fraction, a HPLC separation of these compounds with subsequent NMR structural analysis might be worth to be investigated. This would give some further insights into the OM sulfurization pathway. Moreover, the geochemical composition of the Shefela basin core could be further examined with respect to changes in the composition of the organic biomarkers from the Santonian to the Maastrichtian using sampling at high resolution.

References

- Abramovich, S., Keller, G., Stüben, D., Berner, Z. 2003. Characterization of Late Campanian and Maastrichtian planktonic foraminiferal depth habitats and vital activities based on stable isotopes. *Paleogeogr. Paleoclimatol. Paleoecol.* 202: 1-29.
- Abramovich, S., Yovel-Corem, S., Almogi-Labin, A., Benjamini, C. 2010. Global climate change and planktic foraminiferal response in the Maastrichtian. *Paleoceanography*. 25: PA2201.
- Adam, P., Schmid, J.C., Mycke, B., Strazielle, C., Connan, J., Huc, A., Riva, A., Albrecht, P. 1993. Structural investigation of nonpolar sulfur cross-linked macromolecules in petroleum. *Geochim. Cosmochim. Ac.* 57: 3395-3419.
- Aizenshtat, Z., Krein, E.B., Vairavamurthy, M.A., Goldstein, T.P. 1995. Role of sulfur in the transformations of sedimentary organic matter: a mechanistic overview. *In Geochemical Transformations of Sedimentary Sulfur*. Vol. 612. M.A. Vairavamurthy, M.A.A. Schoonen, T.I. Eglinton, G.W. Luther III and B. Manowitz, editors. American Chemical Society, Washington. 16-37.
- Algeo, T.J., Ingall, E. 2007. Sedimentary C_{org}:P ratios, paleocean ventilation, and Phanerozoic atmospheric pO₂. *Paleogeogr. Paleoclimatol. Paleoecol.* 256: 130-155.
- Almogi-Labin, A., Bein, A., Sass, E. 1993. Late Cretaceous upwelling system along the southern Tethys margin (Israel): interrelationship between productivity, bottom water environments, and organic matter preservation. *Paleoceanography*. 8: 671-690.
- Almogi-Labin, A., Ashkenazi-Polivoda, S., Edelman-Furstenberg, Y., Benjamini, C. 2012. Anoxia-dysoxia at the sediment-water interface of the southern Tethys in the Late Cretaceous: Mishash Formation, southern Israel. *In Anoxia: Evidence for Eukaryote Survival and Paleontological Strategies, Cellular Origin, Life in Extreme Habitats and Astrobiology*. Vol. 21. A.V. Altenbach, J.M. Bernhard and J. Seckbach, editors. Springer Netherlands, Heidelberg, Dordrecht, London, New York. 553-572.
- Altabet, M.A., Francois, R., Murray, D.W., Prell, W.L. 1995. Climate-related variations in denitrification in the Arabian Sea from sediment ¹⁵N/¹⁴N ratios. *Nature*. 373: 506-509.
- Amiot, R., Lécuyer, C., Buffetaut, E., Fluteau, F., Legendre, S., Martineau, F. 2004. Latitudinal temperature gradient during the Cretaceous upper Campanian–middle Maastrichtian: δ¹⁸O record of continental vertebrates. *Earth. Planet. Sci. Lett.* 226: 255-272.
- Amrani, A., Aizenshtat, Z. 2004. Mechanisms of sulfur introduction chemically controlled: δ³⁴S imprint. *Org. Geochem.* 35: 1319-1336.
- Amrani, A., Lewan, M.D., Aizenshtat, Z. 2005. Stable sulfur isotope partitioning during simulated petroleum formation as determined by hydrous pyrolysis of Ghareb limestone, Israel. *Geochim. Cosmochim. Ac.* 69: 5317-5331.
- Anderson, T.F., Arthur, M.A. 1983. Stable isotopes of oxygen and carbon and their application to sedimentologic and paleoenvironmental problems *In Stable Isotopes in Sedimentary*

References

- Geology. Vol. 10. M.A. Arthur, T.F. Anderson, I.R. Kaplan, J. Veizer and L.S. Land, editors. SEPM, Tulsa. 1-151.
- Arning, E.T., Birgel, D., Schulz-Vogt, H.N., Holmkvist, L., Jørgensen, B.B., Larson, A., Peckmann, J. 2008. Lipid biomarker patterns of phosphogenic sediments from upwelling regions. *Geomicrobiol. J.* 25: 69-82.
- Arning, E.T., Birgel, D., Brunner, B., Peckmann, J. 2009a. Bacterial formation of phosphatic laminites off Peru. *Geobiology*. 7: 295-307.
- Arning, E.T., Lückge, A., Breuer, C., Gussone, N., Birgel, D., Peckmann, J. 2009b. Genesis of phosphorite crusts off Peru. *Mar. Geol.* 262: 68-81.
- Arthur, M.A., Sageman, B.B. 1994. Marine black shales: depositional mechanisms and environments of ancient-deposits. *Annu. Rev. Earth Pl. Sci.* 22: 499-551.
- Ashckenazi-Polivoda, S., Edelman-Furstenberg, Y., Almogi-Labin, A., Benjamini, C. 2010. Characterization of lowest oxygen environments within ancient upwelling environments: benthic foraminifera assemblages. *Paleogeogr. Paleoclimatol. Paleoecol.* 289: 134-144.
- Ashckenazi-Polivoda, S., Abramovich, S., Almogi-Labin, A., Schneider-Mor, A., Feinstein, S., Püttmann, W., Berner, Z. 2011. Paleoenvironments of the latest Cretaceous oil shale sequence, southern Tethys, Israel, as an integral part of the prevailing upwelling system. *Paleogeogr. Paleoclimatol. Paleoecol.* 305: 93-108.
- Banga, T., Capuano, R.M., Bissada, K.K. 2011. Petroleum generation in the southeast Texas basin: implications for hydrocarbon occurrence at the South Liberty salt dome. *AAPG Bull.* 95: 1257-1291.
- Barouxis, A., Scribe, P., Dagaut, J., Saliot, A. 1988. Free and bound lipids from equatorial surficial sediments separated as a function of particle size. *Org. Geochem.* 13: 773-783.
- Barrera, E., Savin, S.M. 1999. Evolution of Late Campanian-Maastrichtian marine climates and oceans. *Geol. S. Am. S.* 332: 245-282.
- Bechtel, A., Movsumova, U., Strobl, S.A.I., Sachsenhofer, R.F., Soliman, A., Gratzner, R., Püttmann, W. 2013. Organofacies and paleoenvironment of the Oligocene Maikop series of Angeharan (eastern Azerbaijan). *Org. Geochem.* 56: 51-67.
- Behrens, A., Schaeffer, P., Albrecht, P. 1997. 14 β ,22R-Epithiosteranes, a novel series of fossil steroids widespread in sediments. *Tetrahedron Lett.* 38: 4921-4924.
- Bein, A., Amit, O. 1982. Depositional environments of the Senonian chert, phosphorite and oil shale sequence in Israel as deduced from their organic matter composition. *Sedimentology*. 29: 81-90.
- Bein, A., Almogi-Labin, A., Sass, E. 1990. Sulfur sinks and organic carbon relationships in Cretaceous organic-rich carbonates; implications for evaluation of oxygen-poor depositional environments. *Am. J. Sci.* 290: 882-911.
- Berg, J.S., Schwedt, A., Kreutzmann, A.-C., Kuypers, M.M.M., Milucka, J. 2014. Polysulfides as intermediates in the oxidation of sulfide to sulfate by *Beggiatoa* spp. *Appl. Environ. Microbiol.* 80: 629-636.

- Berndmeyer, C., Birgel, D., Brunner, B., Wehrmann, L.M., Jöns, N., Bach, W., Arning, E.T., Föllmi, K.B., Peckmann, J. 2012. The influence of bacterial activity on phosphorite formation in the Miocene Monterey Formation, California. *Paleogeogr. Paleoclimatol. Paleoecol.* 317–318: 171-181.
- Berner, R.A. 1970. Sedimentary pyrite formation. *Am. J. Sci.* 268: 1-23.
- Berner, R.A., Raiswell, R. 1983. Burial of organic carbon and pyrite sulfur in sediments over phanerozoic time: a new theory. *Geochim. Cosmochim. Ac.* 47: 855-862.
- Berner, R.A. 1984. Sedimentary pyrite formation: an update. *Geochim. Cosmochim. Ac.* 48: 605-615.
- Berner, R.A., Raiswell, R. 1984. C/S method for distinguishing freshwater from marine sedimentary rocks. *Geology.* 12: 365-368.
- Berner, R.A., de Leeuw, J.W., Spiro, B., Murchison, D.G., Eglinton, G. 1985. Sulphate reduction, organic matter decomposition and pyrite formation. *Philos. Trans. R. Soc. Lond. A.* 315: 25-38.
- Bice, K.L., Birgel, D., Meyers, P.A., Dahl, K.A., Hinrichs, K.-U., Norris, R.D. 2006. A multiple proxy and model study of Cretaceous upper ocean temperatures and atmospheric CO₂ concentrations. *Paleoceanography.* 21: PA2002.
- Blumenberg, M., Krüger, M., Nauhaus, K., Talbot, H.M., Oppermann, B.I., Seifert, R., Pape, T., Michaelis, W. 2006. Biosynthesis of hopanoids by sulfate-reducing bacteria (genus *Desulfovibrio*). *Environ. Microbiol.* 8: 1220-1227.
- Blumenberg, M., Mollenhauer, G., Zabel, M., Reimer, A., Thiel, V. 2010. Decoupling of bio- and geohopanoids in sediments of the Benguela Upwelling System (BUS). *Org. Geochem.* 41: 1119-1129.
- Bornemann, A., Norris, R.D., Friedrich, O., Beckmann, B., Schouten, S., Sinninghe Damsté, J.S., Vogel, J., Hofmann, P., Wagner, T. 2008. Isotopic evidence for glaciation during the Cretaceous supergreenhouse. *Science.* 319: 189-192.
- Brady, E.C., DeConto, R.M., Thompson, S.L. 1998. Deep water formation and poleward ocean heat transport in the warm climate extreme of the Cretaceous (80 Ma). *Geophys. Res. Lett.* 25: 4205-4208.
- Brassell, S.C., Eglinton, G., Marlowe, I.T., Pflaumann, U., Sarnthein, M. 1986a. Molecular stratigraphy: a new tool for climatic assessment. *Nature.* 320: 129-133.
- Brassell, S.C., Lewis, C.A., de Leeuw, J.W., de Lange, F., Sinninghe Damsté, J.S. 1986b. Isoprenoid thiophenes: novel products of sediment diagenesis? *Nature.* 320: 160-162.
- Bray, E.E., Evans, E.D. 1961. Distribution of n-paraffins as a clue to recognition of source beds. *Geochim. Cosmochim. Ac.* 22: 2-15.
- Brock, J., 2011. Impact of sulfide-oxidizing bacteria on the phosphorus cycle in marine sediments. Ph.D.-Thesis.Bremen.
- Brock, J., Schulz-Vogt, H.N. 2011. Sulfide induces phosphate release from polyphosphate in cultures of a marine *Beggiatoa* strain. *ISME J.* 5: 497-506.

References

- Brock, J., Rhiel, E., Beutler, M., Salman, V., Schulz-Vogt, H. 2012. Unusual polyphosphate inclusions observed in a marine *Beggiatoa* strain. *A. van Leeuw. J. Microb.* 101: 347-357.
- Cabrera, L., Cabrera, M., Gorchs, R., de las Heras, F.X.C. 2002. Lacustrine basin dynamics and organosulphur compound origin in a carbonate-rich lacustrine system (Late Oligocene Mequinenza Formation, SE Ebro Basin, NE Spain). *Sediment. Geol.* 148: 289-317.
- Caldwell, M.E., Garrett, R.M., Prince, R.C., Suflita, J.M. 1998. Anaerobic biodegradation of long-chain n-alkanes under sulfate-reducing conditions. *Environ. Sci. Technol.* 32: 2191-2195.
- Capone, D.G., Hutchins, D.A. 2013. Microbial biogeochemistry of coastal upwelling regimes in a changing ocean. *Nature Geosci.* 6: 711-717.
- Clarke, L.J., Jenkyns, H.C. 1999. New oxygen isotope evidence for long-term Cretaceous climatic change in the southern hemisphere. *Geology.* 27: 699-702.
- Cuevas, L.A., Morales, C.E. 2006. Nanoheterotroph grazing on bacteria and cyanobacteria in oxic and suboxic waters in coastal upwelling areas off northern Chile. *J. Plankton. Res.* 28: 385-397.
- Cypionka, H. 2010. Grundlagen der Mikrobiologie. Springer, Heidelberg, Dordrecht, London, New York. 340 pp.
- Dale, A.W., Brüchert, V., Alperin, M., Regnier, P. 2009. An integrated sulfur isotope model for Namibian shelf sediments. *Geochim. Cosmochim. Ac.* 73: 1924-1944.
- Dale, A.W., Bertics, V.J., Treude, T., Sommer, S., Wallmann, K. 2013. Modeling benthic–pelagic nutrient exchange processes and porewater distributions in a seasonally hypoxic sediment: evidence for massive phosphate release by *Beggiatoa*? *Biogeosciences.* 10: 629-651.
- Davies, A., Kemp, A.E.S., Pike, J. 2009. Late Cretaceous seasonal ocean variability from the Arctic. *Nature.* 460: 254-258.
- de Graaf, W., Sinningh Damsté, J.S., de Leeuw, J.W. 1992. Laboratory simulation of natural sulfurization: I. formation of monomeric and oligomeric isoprenoid polysulfides by low-temperature reactions of inorganic polysulfides with phytol and phytadienes. *Geochim. Cosmochim. Ac.* 56: 4321-4328.
- de las Heras, X.F.C., Grimalt, J.O., Lopez, J.F., Albaigés, J., Sinninghe Damsté, J.S., Schouten, S., de Leeuw, J.W. 1997. Free and sulfurized hopanoids and highly branched isoprenoids in immature lacustrine oil shales. *Org. Geochem.* 27: 41-63.
- de Leeuw, J.W., Sinninghe Damsté, J.S. 1990. Organic sulfur compounds and other biomarkers as indicators of palaeosalinity. In *Geochemistry of Sulfur in Fossil Fuels*. Vol. 429. American Chemical Society. 417-443.
- de Menocal, P., Ortiz, J., Guilderson, T., Sarnthein, M. 2000. Coherent high- and low-latitude climate variability during the Holocene warm period. *Science.* 288: 2198-2202.
- Dean, W.E., Arthur, M.A., Claypool, G.E. 1986. Depletion of ¹³C in Cretaceous marine organic matter: source, diagenetic, or environmental signal? *Mar. Geol.* 70: 119-157.
- Dean, W.E., Arthur, M.A. 1989. Iron-sulfur-carbon relationships in organic-carbon-rich sequences I: Cretaceous Western Interior Seaway. *Am. J. Sci.* 289: 708-743.

- Didyk, B.M., Simoneit, B.R.T., Brassell, S.C., Eglinton, G. 1978. Organic geochemical indicators of palaeoenvironmental conditions of sedimentation. *Nature*. 272: 216-222.
- Dinur, D., Spiro, B., Aizenshtat, Z. 1980. The distribution and isotopic composition of sulfur in organic-rich sedimentary rocks. *Chem. Geol.* 31: 37-51.
- Dowsett, H.J., Robinson, M.M., Haywood, A.M., Hill, D.J., Dolan, A.M., Stoll, D.K., Chan, W.-L., Abe-Ouchi, A., Chandler, M.A., Rosenbloom, N.A., Otto-Bliesner, B.L., Bragg, F.J., Lunt, D.J., Foley, K.M., Riesselman, C.R. 2012. Assessing confidence in Pliocene sea surface temperatures to evaluate predictive models. *Nature Clim. Change*. 2: 365-371.
- Edelman-Furstenberg, Y. 2008. Macrobenthic community structure in a high-productivity region: Upper Campanian Mishash Formation (Israel). *Paleogeogr. Paleoclimatol. Paleocol.* 261: 58-77.
- Edelman-Furstenberg, Y. 2009. Cyclic upwelling facies along the Late Cretaceous southern Tethys (Israel): taphonomic and ichnofacies evidence of a high-productivity mosaic. *Cretaceous Res.* 30: 847-863.
- Eglinton, T.I., Irvine, J.E., Vairavamurthy, A., Zhou, W., Manowitz, B. 1994. Formation and diagenesis of macromolecular organic sulfur in Peru margin sediments. *Org. Geochem.* 22: 781-799.
- Eglinton, T.I., Repeta, D.J. 2011. Organic matter in the contemporary ocean. In *Geochemistry of Earth Surface Systems: From the Treatise on Geochemistry*. H.D. Holland and K.K. Turekian, editors. Elsevier/Academic Press, Amsterdam, Boston. 389-425.
- Elvert, M., Hopmans, E.C., Treude, T., Boetius, A., Suess, E. 2005. Spatial variations of methanotrophic consortia at cold methane seeps: implications from a high-resolution molecular and isotopic approach. *Geobiology*. 3: 195-209.
- Epstein, S., Buchsbaum, R., Lowenstam, H.A., Urey, H.C. 1953. Revised carbonate-water isotopic temperature scale. *Geol. Soc. Am. Bull.* 64: 1315-1326.
- Erez, J., Luz, B. 1983. Experimental paleotemperature equation for planktonic foraminifera. *Geochim. Cosmochim. Ac.* 47: 1025-1031.
- Erlich, R.N., Macsotay I, O., Nederbragt, A.J., Antonieta Lorente, M. 2000. Birth and death of the Late Cretaceous “La Luna Sea”, and origin of the Tres Esquinas phosphorites. *J. S. Am. Earth Sci.* 13: 21-45.
- Eshet, Y., Almogi-Labin, A., Bein, A. 1994. Dinoflagellate cysts, paleoproductivity and upwelling systems: a Late Cretaceous example from Israel. *Mar. Micropaleontol.* 23: 231-240.
- Eshet, Y., Almogi-Labin, A. 1996. Calcareous nannofossils as paleoproductivity indicators in Upper Cretaceous organic-rich sequences in Israel. *Mar. Micropaleontol.* 29: 37-61.
- Ferdelman, T.G., Lee, C., Pantoja, S., Harder, J., Bebout, B.M., Fossing, H. 1997. Sulfate reduction and methanogenesis in a *Thioploca*-dominated sediment off the coast of Chile. *Geochim. Cosmochim. Ac.* 61: 3065-3079.
- Föllmi, K.B. 1996. The phosphorus cycle, phosphogenesis and marine phosphate-rich deposits. *Earth-Sci. Rev.* 40: 55-124.

References

- Follows, B., Tyson, R.V. 1998. Organic facies of the Asbian (Early Carboniferous) Queensferry Beds, Lower Oil Shale Group, South Queensferry, Scotland, and a brief comparison with other Carboniferous North Atlantic oil shale deposits. *Org. Geochem.* 29: 821-844.
- Forster, A., Schouten, S., Baas, M., Sinninghe Damsté, J.S. 2007a. Mid-Cretaceous (Albian–Santonian) sea surface temperature record of the tropical Atlantic Ocean. *Geology.* 35: 919-922.
- Forster, A., Schouten, S., Moriya, K., Wilson, P.A., Sinninghe Damsté, J.S. 2007b. Tropical warming and intermittent cooling during the Cenomanian/Turonian oceanic anoxic event 2: sea surface temperature records from the equatorial Atlantic. *Paleoceanography.* 22: PA1219.
- Francois, R. 1987. A study of sulphur enrichment in the humic fraction of marine sediments during early diagenesis. *Geochim. Cosmochim. Ac.* 51: 17-27.
- Frank, T.D., Thomas, D.J., Leckie, R.M., Arthur, M.A., Bown, P.R., Jones, K., Lees, J.A. 2005. The Maastrichtian record from Shatsky Rise (northwest Pacific): a tropical perspective on global ecological and oceanographic changes. *Paleoceanography.* 20: PA1008.
- Friedrich, O., Herrle, J.O., Köbller, P., Hemleben, C. 2004. Early Maastrichtian stable isotopes: changing deep water sources in the North Atlantic? *Paleogeogr. Paleoclimatol. Paleoecol.* 211: 171-184.
- Friedrich, O., Herrle, J.O., Hemleben, C. 2005. Climatic changes in the Late Campanian–Early Maastrichtian: micropaleontological and stable isotopic evidence from an epicontinental sea. *J. Foramin. Res.* 35: 228-247.
- Friedrich, O., Erbacher, J. 2006. Benthic foraminiferal assemblages from Demerara Rise (ODP Leg 207, western tropical Atlantic): possible evidence for a progressive opening of the Equatorial Atlantic Gateway. *Cretaceous Res.* 27: 377-397.
- Friedrich, O., Norris, R.D., Erbacher, J. 2012. Evolution of Middle to Late Cretaceous oceans—a 55 m.y. record of Earth's temperature and carbon cycle. *Geology.* 40: 107-110.
- Fukushima, K., Yasukawa, M., Muto, N., Uemura, H., Ishiwatari, R. 1992. Formation of C₂₀ isoprenoid thiophenes in modern sediments. *Org. Geochem.* 18: 83-91.
- Gaines, S., Airame, S. 2013. Ocean Explorer. National Oceanic and Atmospheric Administration, U.S. Department of Commerce. <http://oceanexplorer.noaa.gov/explorations/02quest/background/upwelling/upwelling.html>
- Gardosh, M., Druckman, Y., Buchbinder, B., Rybakov, M. 2008. The Levant basin offshore Israel: stratigraphy, structure, tectonic evolution and implications for hydrocarbon exploration. Geological Survey of Israel. 118 pp.
- Goldhaber, M.B., Aller, R.C., Cochran, J.K., Rosenfeld, J.K., Martens, C.S., Berner, R.A. 1977. Sulfate reduction, diffusion, and bioturbation in Long Island Sound sediments; report of the FOAM group. *Am. J. Sci.* 277: 193-237.
- Goldhammer, T., Brüchert, V., Ferdelman, T.G., Zabel, M. 2010. Microbial sequestration of phosphorus in anoxic upwelling sediments. *Nature Geosci.* 3: 557-561.

- Gradstein, F.M., Ogg, J.G., Smith, A.G. 2005. A geologic time scale 2004. Cambridge University Press, New York 610 pp.
- Gruber, N., Keeling, C.D., Bacastow, R.B., Guenther, P.R., Lueker, T.J., Wahlen, M., Meijer, H.A.J., Mook, W.G., Stocker, T.F. 1999. Spatiotemporal patterns of carbon-13 in the global surface oceans and the oceanic suess effect. *Global Biogeochem. Cy.* 13: 307-335.
- Gvirtzman, G., Almogi-Labin, A., Moshkovitz, S., Lewy, Z., Honigstein, A., Reiss, Z. 1989. Upper Cretaceous high-resolution multiple stratigraphy, northern margin of the Arabian platform, central Israel. *Cretaceous Res.* 10: 107-135.
- Hartgers, W.A., López, J.F., Sinninghe Damsté, J.S., Reiss, C., Maxwell, J.R., Grimalt, J.O. 1997. Sulfur-binding in recent environments: II. speciation of sulfur and iron and implications for the occurrence of organo-sulfur compounds. *Geochim. Cosmochim. Ac.* 61: 4769-4788.
- Hay, W.W., DeConto, R.M., Wold, C.N., Wilson, K.M., Voigt, S., Schulz, M., Wold, A.D., Dullo, W.-C., Ronov, A.B., Balukhovskiy, A.N., Söding, E. 1999. Alternative global Cretaceous paleogeography. *Geol. S. Am. S.* 332: 1-47.
- Hedges, J.I., Clark, W.A., Quay, P.D., Richey, J.E., Devol, A.H., Santos, U.D. 1986. Compositions and fluxes of particulate organic material in the Amazon river. *Limnol. Oceanogr.* 31: 717-738.
- Hedges, J.I., Clark, W.A., Cowie, G.L. 1988. Fluxes and reactivities of organic matter in a coastal marine bay. *Limnol. Oceanogr.* 33: 1137-1152.
- Hedges, J.I., Keil, R.G., Benner, R. 1997. What happens to terrestrial organic matter in the ocean? *Org. Geochem.* 27: 195-212.
- Hofmann, I.C., Hutchison, J., Robson, J.N., Chicarelli, M.I., Maxwell, J.R. 1992. Evidence for sulphide links in a crude oil asphaltene and kerogens from reductive cleavage by lithium in ethylamine. *Org. Geochem.* 19: 371-387.
- Hofmann, P., Ricken, W., Schwark, L., Leythaeuser, D. 2000. Carbon-sulfur-iron relationships and $\delta^{13}\text{C}$ of organic matter for Late Albian sedimentary rocks from the North Atlantic Ocean: paleoceanographic implications. *Paleogeogr. Paleoclimatol. Paleoecol.* 163: 97-113.
- Høgslund, S., Revsbech, N.P., Cedhagen, T., Nielsen, L.P., Gallardo, V.A. 2008. Denitrification, nitrate turnover, and aerobic respiration by benthic foraminiferans in the oxygen minimum zone off Chile. *J. Exp. Mar. Biol. Ecol.* 359: 85-91.
- Holmkvist, L., Arning, E.T., Küster-Heins, K., Vandieken, V., Peckmann, J., Zabel, M., Jørgensen, B.B. 2010. Phosphate geochemistry, mineralization processes, and *Thioploca* distribution in shelf sediments off central Chile. *Mar. Geol.* 277: 61-72.
- Hopmans, E.C., Weijers, J.W.H., Schefuß, E., Herfort, L., Sinninghe Damsté, J.S., Schouten, S. 2004. A novel proxy for terrestrial organic matter in sediments based on branched and isoprenoid tetraether lipids. *Earth. Planet. Sci. Lett.* 224: 107-116.
- Huang, W.-Y., Meinschein, W.G. 1979. Sterols as ecological indicators. *Geochim. Cosmochim. Ac.* 43: 739-745.

- Huber, B.T., Norris, R.D., MacLeod, K.G. 2002. Deep-sea paleotemperature record of extreme warmth during the Cretaceous. *Geology*. 30: 123-126.
- Jarvis, I., Burnett, W., Nathan, Y., Almbaydin, F., Attia, A., Castro, L., Flicoteaux, R., Hilmy, M., Husain, V., Qutawnah, A., Serjani, A., Zanin, Y. 1994. Phosphorite geochemistry: state-of-the-art and environmental concerns. *Eclogae Geol. Helv.* 87: 643-700.
- Jenkyns, H.C., Clayton, C.J. 1986. Black shales and carbon isotopes in pelagic sediments from the Tethyan Lower Jurassic. *Sedimentology*. 33: 87-106.
- Jenkyns, H.C., Jones, C.E., Gröcke, D.R., Hesselbo, S.P., Parkinson, D.N. 2002. Chemostratigraphy of the Jurassic System: applications, limitations and implications for palaeoceanography. *J. Geol. Soc. London*. 159: 351-378.
- Jenkyns, H.C., Forster, A., Schouten, S., Sinninghe Damsté, J.S. 2004. High temperatures in the Late Cretaceous Arctic Ocean. *Nature*. 432: 888-892.
- Jenkyns, H.C., Schouten-Huibers, L., Schouten, S., Sinninghe Damsté, J.S. 2012. Warm Middle Jurassic–Early Cretaceous high-latitude sea-surface temperatures from the southern Ocean. *Clim. Past*. 8: 215-226.
- Jørgensen, B.B. 1978. A comparison of methods for the quantification of bacterial sulfate reduction in coastal marine sediments. *Geomicrobiol. J.* 1: 49-64.
- Jørgensen, B.B., Gallardo, V.A. 1999. *Thioploca* spp.: filamentous sulfur bacteria with nitrate vacuoles. *FEMS Microbiol. Ecol.* 28: 301-313.
- Jung, C., Voigt, S., Friedrich, O. 2012. High-resolution carbon-isotope stratigraphy across the Campanian–Maastrichtian boundary at Shatsky Rise (tropical Pacific). *Cretaceous Res.* 37: 177-185.
- Kaiho, K. 1994. Benthic foraminiferal dissolved-oxygen index and dissolved-oxygen levels in the modern ocean. *Geology*. 22: 719-722.
- Kim, J.-H., Schouten, S., Hopmans, E.C., Donner, B., Sinninghe Damsté, J.S. 2008. Global sediment core-top calibration of the TEX₈₆ paleothermometer in the ocean. *Geochim. Cosmochim. Ac.* 72: 1154-1173.
- Kim, J.-H., Huguet, C., Zonneveld, K.A.F., Versteegh, G.J.M., Roeder, W., Sinninghe Damsté, J.S., Schouten, S. 2009. An experimental field study to test the stability of lipids used for the TEX₈₆ and U^{K37} palaeothermometers. *Geochim. Cosmochim. Ac.* 73: 2888-2898.
- Kim, J.-H., van der Meer, J., Schouten, S., Helmke, P., Willmott, V., Sangiorgi, F., Koç, N., Hopmans, E.C., Sinninghe Damsté, J.S. 2010. New indices and calibrations derived from the distribution of crenarchaeal isoprenoid tetraether lipids: implications for past sea surface temperature reconstructions. *Geochim. Cosmochim. Ac.* 74: 4639-4654.
- Koch, M.C., Friedrich, O. 2012. Campanian–Maastrichtian intermediate- to deep-water changes in the high latitudes: benthic foraminiferal evidence. *Paleoceanography*. 27: PA2209.
- Kohnen, M.E.L., Peakman, T.M., Sinninghe Damsté, J.S., de Leeuw, J.W. 1990a. Identification and occurrence of novel C₃₆–C₅₄ 3,4-dialkylthiophenes with an unusual carbon skeleton in immature sediments. *Org. Geochem.* 16: 1103-1113.

- Kohnen, M.E.L., Sinninghe Damsté, J.S., Rijpstra, W.I.C., de Leeuw, J.W. 1990b. Alkylthiophenes as sensitive indicators of palaeoenvironmental changes. *In Geochemistry of Sulfur in Fossil Fuels*. Vol. 429. American Chemical Society. 444-485.
- Kohnen, M.E.L., Sinninghe Damsté, J.S., de Leeuw, J.W. 1991a. Biases from natural sulphurization in palaeoenvironmental reconstruction based on hydrocarbon biomarker distributions. *Nature*. 349: 775-778.
- Kohnen, M.E.L., Sinninghe Damsté, J.S., Kock-van Dalen, A.C., de Leeuw, J.W. 1991b. Di- or polysulphide-bound biomarkers in sulphur-rich geomacromolecules as revealed by selective chemolysis. *Geochim. Cosmochim. Ac.* 55: 1375-1394.
- Kohnen, M.E.L., Schouten, S., Sinninghe Damsté, J.S., de Leeuw, J.W., Merritt, D.A., Hayes, J.M. 1992. Recognition of paleobiochemicals by a combined molecular sulfur and isotope geochemical approach. *Science*. 256: 358-362.
- Kolodny, Y., Raab, M. 1988. Oxygen isotopes in phosphatic fish remains from Israel: paleothermometry of tropical Cretaceous and Tertiary shelf waters. *Paleogeogr. Paleoclimatol. Paleoecol.* 64: 59-67.
- Kolodny, Y., Garrison, R.E. 1994. Sedimentation and diagenesis in paleo-upwelling zones of epeiric sea and basinal settings: a comparison of the Cretaceous Mishash Formation of Israel and the Miocene Monterey Formation of California. *In Siliceous, Phosphatic and Glauconitic Sediments of the Tertiary and Mesozoic*. A. Iijima, A.M. Abed and R.E. Garrison, editors. Proc. 29th Int. Geol. Congr. Part C., Utrecht. 133-158.
- Kolonic, S., Sinninghe Damsté, J.S., Böttcher, M.E., Kuypers, M.M.M., Kuhnt, W., Beckmann, B., Scheeder, G., Wagner, T. 2002. Geochemical characterization of Cenomanian/Turonian black shales from the Tarfaya Basin (SW Morocco) - relationships between palaeoenvironmental conditions and early sulphurization of sedimentary organic matter. *J. Petrol. Geol.* 25: 325-350.
- Koopmans, M.P., Rijpstra, W.I.C., de Leeuw, J.W., Lewan, M.D., Sinninghe Damsté, J.S. 1998. Artificial maturation of an immature sulfur- and organic matter-rich limestone from the Ghareb Formation, Jordan. *Org. Geochem.* 28: 503-521.
- Köster, J., van Kaam-Peters, H.M.E., Koopmans, M.P., de Leeuw, J.W., Sinninghe Damsté, J.S. 1997. Sulphurisation of homohopanoids: effects on carbon number distribution, speciation, and 22S/22R epimer ratios. *Geochim. Cosmochim. Ac.* 61: 2431-2452.
- Krenkel, E. 1924. Der Syrische Bogen. *ZBL Mineral. Geol. Paläont.*: B9, 274-281 and 210, 301-313.
- Kump, L.R., Arthur, M.A. 1999. Interpreting carbon-isotope excursions: carbonates and organic matter. *Chem. Geol.* 161: 181-198.
- Kuypers, M.M.M., Lavik, G., Woebken, D., Schmid, M., Fuchs, B.M., Amann, R., Jørgensen, B.B., Jetten, M.S.M. 2005. Massive nitrogen loss from the Benguela Upwelling System through anaerobic ammonium oxidation. *Proc. Natl. Acad. Sci. U.S.A.* 102: 6478-6483.

- Lee, K.E., Kim, J.-H., Wilke, I., Helmke, P., Schouten, S. 2008. A study of the alkenone, TEX₈₆, and planktonic foraminifera in the Benguela Upwelling System: implications for past sea surface temperature estimates. *Geochem. Geophys. Geosyst.* 9: Q10019.
- Lehmann, M.F., Bernasconi, S.M., Barbieri, A., McKenzie, J.A. 2002. Preservation of organic matter and alteration of its carbon and nitrogen isotope composition during simulated and in situ early sedimentary diagenesis. *Geochim. Cosmochim. Ac.* 66: 3573-3584.
- Lepland, A., Joosu, L., Kirsimäe, K., Prave, A.R., Romashkin, A.E., Črne, A.E., Martin, A.P., Fallick, A.E., Somelar, P., Üpraus, K., Mänd, K., Roberts, N.M.W., van Zuilen, M.A., Wirth, R., Schreiber, A. 2014. Potential influence of sulphur bacteria on Palaeoproterozoic phosphogenesis. *Nature Geosci.* 7: 20-24.
- Leventhal, J.S. 1995. Carbon-sulfur plots to show diagenetic and epigenetic sulfidation in sediments. *Geochim. Cosmochim. Ac.* 59: 1207-1211.
- Levin, L.A. 2003. Oxygen minimum zone benthos: adaption and community response to hypoxia. *In* Oceanography and Marine Biology: an Annual Review. Vol. 41. R.N. Gibson and R.J.A. Atkinson, editors. Taylor & Francis, London. 1-45.
- Li, L., Keller, G. 1998. Maastrichtian climate, productivity and faunal turnovers in planktic foraminifera in South Atlantic DSDP sites 525A and 21. *Mar. Micropaleontol.* 33: 55-86.
- Li, L., Keller, G. 1999. Variability in Late Cretaceous climate and deep waters: evidence from stable isotopes. *Mar. Geol.* 161: 171-190.
- Li, M., Larter, S.R., Taylor, P., Jones, D.M., Bowler, B., Bjorøy, M. 1995. Biomarkers or not biomarkers? A new hypothesis for the origin of pristane involving derivation from methyltrimethyltridecyl-chromans (MTTCs) formed during diagenesis from chlorophyll and alkylphenols. *Org. Geochem.* 23: 159-167.
- Libes, S.M., Deuser, W.G. 1988. The isotope geochemistry of particulate nitrogen in the Peru upwelling area and the Gulf of Maine. *Deep-Sea Res.* 35: 517-533.
- Liu, K.-K., Kao, S.-J., Wen, L.-S., Chen, K.-L. 2007. Carbon and nitrogen isotopic compositions of particulate organic matter and biogeochemical processes in the eutrophic Danshuei estuary in northern Taiwan. *Sci. Total Environ.* 382: 103-120.
- Liu, K. 2009. Oxygen and carbon isotope analysis of the Mooreville Chalk and Late Santonian-Early Campanian sea level and sea surface temperature changes, northeastern Gulf of Mexico, U.S.A. *Cretaceous Res.* 30: 980-990.
- Liu, Z., Pagani, M., Zinniker, D., DeConto, R., Huber, M., Brinkhuis, H., Shah, S.R., Leckie, R.M., Pearson, A. 2009. Global cooling during the Eocene-Oligocene climate transition. *Science.* 323: 1187-1190.
- Lückge, A., Boussafir, M., Lallier-Vergès, E., Littke, R. 1996. Comparative study of organic matter preservation in immature sediments along the continental margins of Peru and Oman. Part I: results of petrographical and bulk geochemical data. *Org. Geochem.* 24: 437-451.

- Lückge, A., Ercegovac, M., Strauss, H., Littke, R. 1999. Early diagenetic alteration of organic matter by sulfate reduction in Quaternary sediments from the northeastern Arabian Sea. *Mar. Geol.* 158: 1-13.
- Lückge, A., Horsfield, B., Littke, R., Scheeder, G. 2002. Organic matter preservation and sulfur uptake in sediments from the continental margin off Pakistan. *Org. Geochem.* 33: 477-488.
- Macalady, J., Vestling, M., Baumler, D., Boekelheide, N., Kaspar, C., Banfield, J. 2004. Tetraether-linked membrane monolayers in *Ferroplasma* spp: a key to survival in acid. *Extremophiles.* 8: 411-419.
- Mackenzie, A.S., Brassell, S.C., Eglinton, G., Maxwell, J.R. 1982. Chemical fossils: the geological fate of steroids. *Science.* 217: 491-504.
- Mackenzie, A.S. 1984. Applications of biological markers in petroleum geochemistry. In *Advances in Petroleum Geochemistry*. Vol. 1. J. Brooks and D.H. Welte, editors. Academic Press, New York. 115-214.
- Macko, S.A., Fogel, M.L., Hare, P.E., Hoering, T.C. 1987. Isotopic fractionation of nitrogen and carbon in the synthesis of amino acids by microorganisms. *Chem. Geol. : Isotope Geosci. Sect.* 65: 79-92.
- Macko, S.A., Engel, M.H., Qian, Y. 1994. Early diagenesis and organic matter preservation - a molecular stable carbon isotope perspective. *Chem. Geol.* 114: 365-379.
- MacLeod, K.G., Huber, B.T., Isaza-Londoño, C. 2005. North Atlantic warming during global cooling at the end of the Cretaceous. *Geology.* 33: 437-440.
- Maestas, Y., MacLeod, K.G., Douglas, R., Self-Trail, J., Ward, P.D. 2003. Late Cretaceous foraminifera, paleoenvironments and paleoceanography of the Rosario Formation, San Antonio del Mar, Baja California, Mexico. *J. Foramin. Res.* 33: 179-191.
- Maxwell, R.E., Cox, R.G., Ackman, R.G., Hooper, S.N. 1972. The diagenesis and maturation of phytol. The stereochemistry of 2,6,10,14-tetramethylpentadecane from an ancient sediment. In *Advances in Organic Geochemistry*. H.R. von Gaertner and H. Wehner, editors. 177-291.
- McCaffrey, M.A., Farrington, J.W., Repeta, D.J. 1989. Geochemical implications of the lipid composition of *Thioploca* spp. from the Peru upwelling region—15°S. *Org. Geochem.* 14: 61-68.
- McEvoy, J., Giger, W. 1986. Origin of hydrocarbons in Triassic Serpiano oil shales: hopanoids. *Org. Geochem.* 10: 943-949.
- McPhee-Shaw, E.E., Siegel, D.A., Washburn, L., Brzezinski, M.A., Jones, J.L., Leydecker, A., Melack, J. 2007. Mechanisms for nutrient delivery to the inner shelf: observations from the Santa Barbara Channel. *Limnol. Oceanogr.* 52: 1748-1766.
- Méhay, S., Keller, C.E., Bernasconi, S.M., Weissert, H., Erba, E., Bottini, C., Hochuli, P.A. 2009. A volcanic CO₂ pulse triggered the Cretaceous Oceanic Anoxic Event 1a and a biocalcification crisis. *Geology.* 37: 819-822.
- Meilijson, A., Ashckenazi-Polivoda, S., Ron, L., Alsenz, H., Illner, P., Abramovich, S., Almogil-Labin, A., Feinstein, S., Speijer, R.P. 2012. Paleocyanography and depositional environment

- of a Late Cretaceous oil shale deposit in the Shefela basin, central Israel. *In* TMS Foraminifera and Nannofossil Group Joint Meeting, Edinburgh, Scotland.
- Meilijson, A., Ashckenazi-Polivoda, S., Ron-Yankovich, L., Illner, P., Alsenz, H., Speijer, R.P., Almogi-Labin, A., Feinstein, S., Berner, Z., Püttmann, W., Abramovich, S. 2014. Chronostratigraphy of the Upper Cretaceous high productivity sequence of the southern Tethys, Israel. *Cretaceous Res.* 50: 187-213.
- Meyers, P.A. 1994. Preservation of elemental and isotopic source identification of sedimentary organic matter. *Chem. Geol.* 114: 289-302.
- Meyers, P.A. 1997. Organic geochemical proxies of paleoceanographic, paleolimnologic and paleoclimatic processes. *Org. Geochem.* 27: 213-250.
- Meyers, P.A., Bernasconi, S.M., Forster, A. 2006. Origins and accumulation of organic matter in expanded Albian to Santonian black shale sequences on the Demerara Rise, South American margin. *Org. Geochem.* 37: 1816-1830.
- Minster, T., Nathan, Y., Raveh, A. 1992. Carbon and sulfur relationships in marine Senonian organic-rich, iron-poor sediments from Israel - a case study. *Chem. Geol.* 97: 145-161.
- Minster, T., 1996. Basin reconstruction in the Senonian sequence, northern Negev - a contribution to the understanding of anoxic events. Ph.D.-Thesis. Tel-Aviv, Israel.
- Moriya, K. 2011. Development of the Cretaceous greenhouse climate and the oceanic thermal structure. *Paleontol. Res.* 15: 77-88.
- Morse, J.W., Emeis, K.C. 1990. Controls on C/S ratios in hemipelagic upwelling sediments. *Am. J. Sci.* 290: 1117-1135.
- Mossman, J.R., Aplin, A.C., Curtis, C.D., Coleman, M.L. 1991. Geochemistry of inorganic and organic sulphur in organic-rich sediments from the Peru margin. *Geochim. Cosmochim. Ac.* 55: 3581-3595.
- Neunlist, S., Rohmer, M. 1985. Novel hopanoids from the methylotrophic bacteria *Methylococcus capsulatus* and *Methylomonas methanica*. (22S)-35-aminobacteriohopane-30,31,32,33,34-pentol and (22S)-35-amino-3 β -methylbacteriohopane-30,31,32,33,34-pentol. *Biochem. J.* 231: 635-639.
- Neunlist, S., Bissere, P., Rohmer, M. 1988. The hopanoids of the purple non-sulfur bacteria *Rhodospseudomonas palustris* and *Rhodospseudomonas acidophila* and the absolute configuration of bacteriohopanetetrol. *Eur. J. Biochem.* 171: 245-252.
- Niggemann, J., Schubert, C.J. 2006. Fatty acid biogeochemistry of sediments from the Chilean coastal upwelling region: sources and diagenetic changes. *Org. Geochem.* 37: 626-647.
- Nissenbaum, A., Kaplan, I. 1972. Chemical and isotopic evidence for the in situ origin of marine humic substances. *Limnol. Oceanogr.*: 570-582.
- Olsen, A., Omar, A.M., Bellerby, R.G.J., Johannessen, T., Ninnemann, U., Brown, K.R., Olsson, K.A., Olafsson, J., Nondal, G., Kivimäe, C., Kringstad, S., Neill, C., Olafsdottir, S. 2006. Magnitude and origin of the anthropogenic CO₂ increase and ¹³C Suess effect in the Nordic seas since 1981. *Global Biogeochem. Cy.* 20: GB3027.

- Orr, W.L. 1986. Kerogen/asphaltene/sulfur relationships in sulfur-rich Monterey oils. *Org. Geochem.* 10: 499-516.
- Otto-Bliesner, B.L., Brady, E.C., Shields, C. 2002. Late Cretaceous ocean: coupled simulations with the National Center for Atmospheric Research Climate System Model. *J. Geophys. Res.* 107: 4019.
- Ourisson, G., Rohmer, M., Poralla, K. 1987. Prokaryotic hopanoids and other polyterpenoid sterol surrogates. *Annu. Rev. Microbiol.* 41: 301-333.
- Parrish, J.T., Curtis, R.L. 1982. Atmospheric circulation, upwelling, and organic-rich rocks in the Mesozoic and Cenozoic eras. *Paleogeogr. Paleoclimatol. Paleoecol.* 40: 31-66.
- Parrish, J.T. 1998. Interpreting Pre-Quaternary climate from the geologic record. Columbia University Press, New York. 338 pp.
- Paytan, A., McLaughlin, K. 2007. The oceanic phosphorus cycle. *Chem. Rev.* 107: 563-576.
- Pearson, P.N., Ditchfield, P.W., Singano, J., Harcourt-Brown, K.G., Nicholas, C.J., Olsson, R.K., Shackleton, N.J., Hall, M.A. 2001. Warm tropical sea surface temperatures in the Late Cretaceous and Eocene epochs. *Nature.* 413: 481-487.
- Peters, K.E., Walters, C.C., Moldowan, J.M. 2007. The Biomarker Guide, Volume 2. Biomarkers and Isotopes in Petroleum Systems and Earth History. Cambridge University Press, New York. 1155 pp.
- Philp, R.P. 1985. Fossil fuel biomarker: Applications and spectra. Elsevier, Amsterdam. 294 pp.
- Piña-Ochoa, E., Høgslund, S., Geslin, E., Cedhagen, T., Revsbech, N.P., Nielsen, L.P., Schweizer, M., Jorissen, F., Rysgaard, S., Risgaard-Petersen, N. 2010. Widespread occurrence of nitrate storage and denitrification among foraminifera and *Gromiida*. *Proc. Natl. Acad. Sci. U.S.A.* 107: 1148-1153.
- Powell, T.G., Mc Kirdy, D.M. 1973. Relationship between ratio of pristane to phytane, crude oil composition and geological environment in Australia. *Nature.* 243: 37-39.
- Pucéat, E., Lécuyer, C., Reisberg, L. 2005. Neodymium isotope evolution of NW Tethyan upper ocean waters throughout the Cretaceous. *Earth. Planet. Sci. Lett.* 236: 705-720.
- Pufahl, P.K., Grimm, K.A., Abed, A.M., Sadaqah, R.M.Y. 2003. Upper Cretaceous (Campanian) phosphorites in Jordan: implications for the formation of a south Tethyan phosphorite giant. *Sediment. Geol.* 161: 175-205.
- Quan, C., Sun, C., Sun, Y., Sun, G. 2009. High resolution estimates of paleo-CO₂ levels through the Campanian (Late Cretaceous) based on *Ginkgo* cuticles. *Cretaceous Res.* 30: 424-428.
- Radford-Knery, J., Cutter, G.A. 1994. Biogeochemistry of dissolved hydrogen sulfide species and carbonyl sulfide in the western North Atlantic Ocean. *Geochim. Cosmochim. Ac.* 58: 5421-5431.
- Rashby, S.E., Sessions, A.L., Summons, R.E., Newman, D.K. 2007. Biosynthesis of 2-methylbacteriohopanepolyols by an anoxygenic phototroph. *Proc. Natl. Acad. Sci. U.S.A.* 104: 15099-15104.

References

- Redfield, A.C. 1958. The biological control of chemical factors in the environment. *Am. Sci.* 46: 205-221.
- Reiss, Z., Almogi-Labin, A., Honigstein, A., Lewy, Z., Lipson-Benitah, S., Moskovitz, S., Zak, Y. 1985. Late Cretaceous multiple stratigraphic framework of Israel. *Israel J. Earth Sci.* 34: 147-166.
- Rey, O., Simo, J.A., Lorente, M.A. 2004. A record of long- and short-term environmental and climatic change during OAE3: La Luna Formation, Late Cretaceous (Santonian–Early Campanian), Venezuela. *Sediment. Geol.* 170: 85-105.
- Rhead, M.M., Eglinton, G., Draffan, G.H. 1971. Hydrocarbons produced by the thermal alteration of cholesterol under conditions simulating the maturation of sediments. *Chem. Geol.* 8: 277-297.
- Risgaard-Petersen, N., Langezaal, A.M., Ingvardsen, S., Schmid, M.C., Jetten, M.S.M., Op den Camp, H.J.M., Derksen, J.W.M., Pina-Ochoa, E., Eriksson, S.P., Peter Nielsen, L., Peter Revsbech, N., Cedhagen, T., van der Zwaan, G.J. 2006. Evidence for complete denitrification in a benthic foraminifer. *Nature.* 443: 93-96.
- Ross, D.J.K., Bustin, R.M. 2009. Investigating the use of sedimentary geochemical proxies for paleoenvironment interpretation of thermally mature organic-rich strata: examples from the Devonian–Mississippian shales, Western Canadian Sedimentary Basin. *Chem. Geol.* 260: 1-19.
- Rowland, S.J. 1990. Production of acyclic isoprenoid hydrocarbons by laboratory maturation of methanogenic bacteria. *Org. Geochem.* 15: 9-16.
- Royer, D.L. 2006. CO₂-forced climate thresholds during the Phanerozoic. *Geochim. Cosmochim. Ac.* 70: 5665-5675.
- Rullkötter, J., Vuchev, V., Hinz, K., Winterer, E.L., Baumgartner, P.O., Bradshaw, M.L., Channel, J.E.T., Jaffrezo, M., Jansa, L.F., Leckie, R.M., Moore, J.M., Schaftenaar, C., Steiger, T.H., Wiegand, G.E. 1983. Potential deep sea petroleum source beds related to coastal upwelling. In Coastal Upwelling, its Sediment Record; Part B, Sedimentary Records of Ancient Coastal Upwelling. J. Thiede and E. Suess, editors. Plenum Press, New York. 467-483.
- Rullkötter, J., Aizenshtat, Z., Spiro, B. 1984a. Biological markers in bitumens and pyrolyzates of Upper Cretaceous bituminous chalks from the Ghareb Formation (Israel). *Geochim. Cosmochim. Ac.* 48: 151-157.
- Rullkötter, J., Mukhopadhyay, P., Welte, D. 1984b. Geochemistry and petrography of organic matter in sediments from Hole 530A, Angola Basin, and Hole 532, Walvis Ridge, Deep Sea Drilling Project. *Init. Repts. DSDP.* 75: 1069–1087.
- Rullkötter, J., Landgraf, M., Disko, U. 1988. Gas chromatographic and mass spectrometric characterization of isomeric alkylthiophenes (C₂₀) and their occurrence in deep sea sediments. *J. High. Resolut. Chromatogr.* 11: 633-638.
- Ruttenberg, K.C. 1992. Development of a sequential extraction method for different forms of phosphorus in marine sediments. *Limnol. Oceanogr.* 37: 1460-1482.

- Ruttenberg, K.C. 2003. The global phosphorus cycle. *In* Treatise on Geochemistry. D.H. Heinrich and K.T. Karl, editors. Pergamon, Oxford. 585-643.
- Santos, F., Gomez-Gesteira, M., deCastro, M., Alvarez, I. 2012. Differences in coastal and oceanic SST trends due to the strengthening of coastal upwelling along the Benguela current system. *Cont. Shelf. Res.* 34: 79-86.
- Schaeffer, P., Adam, P., Philippe, E., Trendel, J.M., Schmid, J.-C., Behrens, A., Connan, J., Albrecht, P. 2006. The wide diversity of hopanoid sulfides evidenced by the structural identification of several novel hopanoid series. *Org. Geochem.* 37: 1590-1616.
- Schenau, S.J., Passier, H.F., Reichart, G.J., de Lange, G.J. 2002. Sedimentary pyrite formation in the Arabian Sea. *Mar. Geol.* 185: 393-402.
- Schleper, C., Jurgens, G., Jonuscheit, M. 2005. Genomic studies of uncultivated archaea. *Nat. Rev. Micro.* 3: 479-488.
- Schneider-Mor, A., Alsenz, H., Ashckenazi-Polivoda, S., Illner, P., Abramovich, S., Feinstein, S., Almogi-Labin, A., Berner, Z., Püttmann, W. 2012. Paleooceanographic reconstruction of the Late Cretaceous oil shale of the Negev, Israel: integration of geochemical, and stable isotope records of the organic matter. *Paleogeogr. Paleoclimatol. Paleoecol.* 319-320: 46-57.
- Schouten, S., Sinninghe Damsté, J.S., de Leeuw, J.W. 1995. A novel triterpenoid carbon skeleton in immature sulphur-rich sediments. *Geochim. Cosmochim. Ac.* 59: 953-958.
- Schouten, S., Hopmans, E.C., Schefuß, E., Sinninghe Damsté, J.S. 2002. Distributional variations in marine crenarchaeotal membrane lipids: a new tool for reconstructing ancient sea water temperatures? *Earth. Planet. Sci. Lett.* 204: 265-274.
- Schouten, S., Hopmans, E.C., Forster, A., van Breugel, Y., Kuypers, M.M.M., Sinninghe Damsté, J.S. 2003. Extremely high sea-surface temperatures at low latitudes during the Middle Cretaceous as revealed by archaeal membrane lipids. *Geology.* 31: 1069-1072.
- Schouten, S., Hopmans, E.C., Sinninghe Damsté, J.S. 2004. The effect of maturity and depositional redox conditions on archaeal tetraether lipid palaeothermometry. *Org. Geochem.* 35: 567-571.
- Schouten, S., Hopmans, E.C., Sinninghe Damsté, J.S. 2013. The organic geochemistry of glycerol dialkyl glycerol tetraether lipids: a review. *Org. Geochem.* 54: 19-61.
- Schrag, D.P., DePaolo, D.J., Richter, F.M. 1995. Reconstructing past sea surface temperatures: correcting for diagenesis of bulk marine carbonate. *Geochim. Cosmochim. Ac.* 59: 2265-2278.
- Schulz, H.M., Bechtel, A., Sachsenhofer, R.F. 2005. The birth of the Paratethys during the Early Oligocene: from Tethys to an ancient Black Sea analogue? *Global Planet. Change.* 49: 163-176.
- Schulz, H.N., Jørgensen, B.B. 2001. Big bacteria. *Annu. Rev. Microbiol.* 55: 105-137.
- Schulz, H.N., Schulz, H.D. 2005. Large sulfur bacteria and the formation of phosphorite. *Science.* 307: 416-418.

- Schunck, H., Lavik, G., Desai, D.K., Großkopf, T., Kalvelage, T., Löscher, C.R., Paulmier, A., Contreras, S., Siegel, H., Holtappels, M., Rosenstiel, P., Schilabel, M.B., Graco, M., Schmitz, R.A., Kuypers, M.M.M., LaRoche, J. 2013. Giant hydrogen sulfide plume in the oxygen minimum zone off Peru supports chemolithoautotrophy. *PLoS ONE*. 8: e68661.
- Schwarcz, H.P., Burnie, S.W. 1973. Influence of sedimentary environments on sulfur isotope ratios in clastic rocks: a review. *Miner. Deposita*. 8: 264-277.
- Scotese, C.R. 2002. Paleomap Project. <http://www.scotese.com>
- Shahar, Y., Wurzbarger, U. 1967. A new oil shale deposit in the Northern Negev, Israel. In *The Proceedings of the Seventh World Petroleum Congress, Mexico*. 719-728.
- Sharp, Z.D., Atudorei, V., Furrer, H. 2000. The effect of diagenesis on oxygen isotope ratios of biogenic phosphates. *Am. J. Sci.* 300: 222-237.
- Sievert, S.M., Kiene, R.P., Schultz-Vogt, H.N. 2007. The sulfur cycle. *Oceanography*. 20: 117-123.
- Sijp, W.P., von der Heydt, A.S., Dijkstra, H.A., Flögel, S., Douglas, P.M.J., Bijl, P.K. 2014. The role of ocean gateways on cooling climate on long time scales. *Global Planet. Change*. 119: 1-22.
- Silfer, J.A., Engel, M.H., Macko, S.A. 1992. Kinetic fractionation of stable carbon and nitrogen isotopes during peptide bond hydrolysis: experimental evidence and geochemical implications. *Chem. Geol. : Isotope Geosci. Sect.* 101: 211-221.
- Sinninghe Damsté, J.S., ten Haven, H.L., de Leeuw, J.W., Schenck, P.A. 1986. Organic geochemical studies of a Messinian evaporitic basin, northern Apennines (Italy)-II. Isoprenoid and *n*-alkyl thiophenes and thiolanes. *Org. Geochem.* 10: 791-805.
- Sinninghe Damsté, J.S., Kock-van Dalen, A.C., de Leeuw, J.W., Schenck, P.A., Guoying, S., Brassell, S.C. 1987a. The identification of mono-, di- and trimethyl 2-methyl-2-(4,8,12-trimethyltridecyl)-chromans and their occurrence in the geosphere. *Geochim. Cosmochim. Ac.* 51: 2393-2400.
- Sinninghe Damsté, J.S., Kock -van Dalen, A.C., de Leeuw, J.W., Schenck, P.A. 1987b. The identification of 2,3-dimethyl-5-(2,6,10-trimethylundecyl)thiophene, a novel sulphur containing biological marker. *Tetrahedron Lett.* 28: 957-960.
- Sinninghe Damsté, J.S., Rijpstra, W.I.C., de Leeuw, J.W., Schenck, P.A. 1989a. The occurrence and identification of series of organic sulphur compounds in oils and sediment extracts: II. Their presence in samples from hypersaline and non-hypersaline palaeoenvironments and possible application as source, palaeoenvironmental and maturity indicators. *Geochim. Cosmochim. Ac.* 53: 1323-1341.
- Sinninghe Damsté, J.S., Rijpstra, W.I.C., Kock-van Dalen, A.C., de Leeuw, J.W., Schenck, P.A. 1989b. Quenching of labile functionalised lipids by inorganic sulphur species: evidence for the formation of sedimentary organic sulphur compounds at the early stages of diagenesis. *Geochim. Cosmochim. Ac.* 53: 1343-1355.
- Sinninghe Damsté, J.S., van Koert, E.R., Kock-van Dalen, A.C., de Leeuw, J.W., Schenck, P.A. 1989c. Characterisation of highly branched isoprenoid thiophenes occurring in sediments and immature crude oils. *Org. Geochem.* 14: 555-567.

- Sinninghe Damsté, J.S., de Leeuw, J.W. 1990. Analysis, structure and geochemical significance of organically-bound sulphur in the geosphere: state of the art and future research. *Org. Geochem.* 16: 1077-1101.
- Sinninghe Damsté, J.S., Frewin, N.L., Kenig, F., de Leeuw, J.W. 1995a. Molecular indicators for paleoenvironmental change in a Messinian evaporitic sequence (Vena-Del-Gesso, Italy). I: Variations in extractable organic matter of ten cyclically deposited marl beds. *Org. Geochem.* 23: 471-483.
- Sinninghe Damsté, J.S., van Duin, A.C.T., Hollander, D., Kohnen, M.E.L., de Leeuw, J.W. 1995b. Early diagenesis of bacteriohopanepolyol derivatives: formation of fossil homohopanoids. *Geochim. Cosmochim. Ac.* 59: 5141-5157.
- Sinninghe Damsté, J.S., Kohnen, M.E.L., Horsfield, B. 1998a. Origin of low-molecular-weight alkylthiophenes in pyrolysates of sulphur-rich kerogens as revealed by micro-scale sealed vessel pyrolysis. *Org. Geochem.* 29: 1891-1903.
- Sinninghe Damsté, J.S., Kok, M.D., Köster, J., Schouten, S. 1998b. Sulfurized carbohydrates: an important sedimentary sink for organic carbon? *Earth. Planet. Sci. Lett.* 164: 7-13.
- Sinninghe Damsté, J.S., Rijpstra, W.I.C., Schouten, S., Fuerst, J.A., Jetten, M.S.M., Strous, M. 2004. The occurrence of hopanoids in planctomycetes: implications for the sedimentary biomarker record. *Org. Geochem.* 35: 561-566.
- Sluijs, A., Schouten, S., Pagani, M., Woltering, M., Brinkhuis, H., Sinninghe Damsté, J.S., Dickens, G.R., Huber, M., Reichart, G.-J., Stein, R., Matthiessen, J., Lourens, L.J., Pedentchouk, N., Backman, J., Moran, K., Expedition-302-Scientists. 2006. Subtropical Arctic Ocean temperatures during the Palaeocene/Eocene thermal maximum. *Nature.* 441: 610-613.
- Soudry, D., Champetier, Y. 1983. Microbial processes in the Negev phosphorites (southern Israel). *Sedimentology.* 30: 411-423.
- Soudry, D., Nathan, Y., Roded, R. 1985. The Ashosh-Haroz facies and their significance for the Mishash palaeogeography and phosphorite accumulation in northern and central Negev, southern Israel. *Israel J. Earth Sci.* 34: 211-220.
- Soudry, D., Glenn, C.R., Nathan, Y., Segal, I., Vonderhaar, D. 2006. Evolution of Tethyan phosphogenesis along the northern edges of the Arabian-African shield during the Cretaceous-Eocene as deduced from temporal variations of Ca and Nd isotopes and rates of P accumulation. *Earth-Sci. Rev.* 78: 27-57.
- Spicer, R.A., Herman, A.B. 2010. The Late Cretaceous environment of the Arctic: a quantitative reassessment based on plant fossils. *Paleogeogr. Paleoclimatol. Paleoecol.* 295: 423-442.
- Spiro, B., Aizenshtat, Z. 1977. Bacterial sulphate reduction and calcite precipitation in hypersaline deposition of bituminous shales. *Nature.* 269: 235-237.
- Spiro, B., Dinur, D., Aizenshtat, Z. 1983. Evaluation of source, environments of deposition and diagenesis of some israeli "oil shales" - *n*-Alkanes, fatty acids, tetrapyrroles and kerogen. *Chem. Geol.* 39: 189-214.

- Steuber, T., Rauch, M., Masse, J.-P., Graaf, J., Malkoc, M. 2005. Low-latitude seasonality of Cretaceous temperatures in warm and cold episodes. *Nature*. 437: 1341-1344.
- Stewart, R.H. 2008. Introduction to physical oceanography. Department of Oceanography Texas A & M University, http://oceanworld.tamu.edu/home/course_book.htm. 353 pp.
- Suess, E., Thiede, J. 1983. Coastal upwelling, its sediment records. Part A, responses of the sedimentary regime to present coastal upwelling. Springer, New York. 604 pp.
- Summerhayes, C.P., Prell, W.L., Emeis, K.C. 1992. Evolution of upwelling system since the Early Miocene. *In* Upwelling System: Evolution of Upwelling System since the Early Miocene. Vol. 64. C.P. Summerhayes, W.L. Prell and K.C. Emeis, editors. Geological Society Special Publication. 1-5.
- Summons, R.E., Jahnke, L.L. 1990. Identification of the methylhopanes in sediments and petroleum. *Geochim. Cosmochim. Ac.* 54: 247-251.
- Summons, R.E., Jahnke, L.L., Roksandic, Z. 1994. Carbon isotopic fractionation in lipids from methanotrophic bacteria: relevance for interpretation of the geochemical record of biomarkers. *Geochim. Cosmochim. Ac.* 58: 2853-2863.
- Summons, R.E., Jahnke, L.L., Hope, J.M., Logan, G.A. 1999. 2-Methylhopanoids as biomarkers for cyanobacterial oxygenic photosynthesis. *Nature*. 400: 554-557.
- Takashima, R., Nishi, H., Huber, B.T., Leckie, R. 2006. Greenhouse world and the Mesozoic ocean. *Oceanography*. 19: 82-92.
- Tang, K., Baskaran, V., Nemati, M. 2009. Bacteria of the sulphur cycle: an overview of microbiology, biokinetics and their role in petroleum and mining industries. *Biochem. Eng. J.* 44: 73-94.
- Tarduno, J.A., Brinkman, D.B., Renne, P.R., Cottrell, R.D., Scher, H., Castillo, P. 1998. Evidence for extreme climatic warmth from Late Cretaceous Arctic vertebrates. *Science*. 282: 2241-2243.
- ten Haven, H.L., de Leeuw, J.W., Schenck, P.A. 1985. Organic geochemical studies of a Messinian evaporitic basin, northern Apennines (Italy) I: hydrocarbon biological markers for a hypersaline environment. *Geochim. Cosmochim. Ac.* 49: 2181-2191.
- ten Haven, H.L., de Leeuw, J.W., Peakman, T.M., Maxwell, J.R. 1986. Anomalies in steroid and hopanoid maturity indices. *Geochim. Cosmochim. Ac.* 50: 853-855.
- ten Haven, H.L., de Leeuw, J.W., Rullkötter, J., Sinninghe Damsté, J.S. 1987. Restricted utility of the pristane/phytane ratio as a palaeoenvironmental indicator. *Nature*. 330: 641-643.
- ten Haven, H.L., Rullkötter, J., Sinninghe Damsté, J., S., de Leeuw Jan, W. 1990. Distribution of organic sulfur compounds in Mesozoic and Cenozoic sediments from the Atlantic and Pacific oceans and the Gulf of California. *In* Geochemistry of Sulfur in Fossil Fuels. Vol. 429. W.L. Orr and C.M. White, editors. American Chemical Society, Washington. 613-632.
- Thamdrup, B., Canfield, D.E. 1996. Pathways of carbon oxidation in continental margin sediments off central Chile. *Limnol. Oceanogr.* 41: 1629-1650.
- Thiede, J., Suess, E. 1983. Coastal upwelling, its sediment records; Part B, sedimentary records of ancient coastal upwelling. Springer, New York. 604 pp.

- Twichell, S.C., Meyers, P.A., Diester-Haass, L. 2002. Significance of high C/N ratios in organic-carbon-rich Neogene sediments under the Benguela Current Upwelling System. *Org. Geochem.* 33: 715-722.
- Vairavamurthy, A., Mopper, K. 1987. Geochemical formation of organosulphur compounds (thiols) by addition of H₂S to sedimentary organic matter. *Nature.* 329: 623-625.
- Valisolalao, J., Perakis, N., Chappe, B., Albrecht, P. 1984. A novel sulfur containing C₃₅ hopanoid in sediments. *Tetrahedron Lett.* 25: 1183-1186.
- van Kaam-Peters, H.M.E., Köster, J., de Leeuw, J.W., Sinninghe Damsté, J.S. 1995. Occurrence of two novel benzothiophene hopanoid families in sediments. *Org. Geochem.* 23: 607-616.
- van Mooy, B.A.S., Keil, R.G., Devol, A.H. 2002. Impact of suboxia on sinking particulate organic carbon: enhanced carbon flux and preferential degradation of amino acids via denitrification. *Geochim. Cosmochim. Ac.* 66: 457-465.
- Vető, I., Hetényi, M., Demény, A., Hertelendi, E. 1994. Hydrogen index as reflecting intensity of sulphidic diagenesis in non-bioturbated, shaly sediments. *Org. Geochem.* 22: 299-310.
- Volkman, J.K. 2003. Sterols in microorganisms. *Appl. Microbiol. Biotechnol.* 60: 495-506.
- Wang, L., Song, Z., Yin, Q., George, S.C. 2011. Paleosalinity significance of occurrence and distribution of methyltrimethyltridecyl-chromans in the Upper Cretaceous Nenjiang Formation, Songliao Basin, China. *Org. Geochem.* 42: 1411-1419.
- Wefer, G., Heinze, P.M., Berger, W.H. 1994. Clues to ancient methane release. *Nature.* 369: 282.
- Weijers, J.W.H., Schouten, S., Spaargaren, O.C., Sinninghe Damsté, J.S. 2006. Occurrence and distribution of tetraether membrane lipids in soils: implications for the use of the TEX₈₆ proxy and the BIT index. *Org. Geochem.* 37: 1680-1693.
- Weissert, H., Erba, E. 2004. Volcanism, CO₂ and palaeoclimate: a Late Jurassic–Early Cretaceous carbon and oxygen isotope record. *J. Geol. Soc. London.* 161: 695-702.
- Werne, J.P., Hollander, D.J., Behrens, A., Schaeffer, P., Albrecht, P., Sinninghe Damsté, J.S. 2000. Timing of early diagenetic sulfurization of organic matter: a precursor-product relationship in Holocene sediments of the anoxic Cariaco Basin, Venezuela. *Geochim. Cosmochim. Ac.* 64: 1741-1751.
- Werne, J.P., Lyons, T.W., Hollander, D.J., Schouten, S., Hopmans, E.C., Sinninghe Damsté, J.S. 2008. Investigating pathways of diagenetic organic matter sulfurization using compound-specific sulfur isotope analysis. *Geochim. Cosmochim. Ac.* 72: 3489-3502.
- Wiley Registry. 2008. 8th Edition/NIST. Mass Spectral Library. Hoboken, New Jersey
- Williams, R.G. 2011. Ocean eddies and plankton blooms. *Nature Geosci.* 4: 739-740.
- Wilson, P.A., Opdyke, B.N. 1996. Equatorial sea-surface temperatures for the Maastrichtian revealed through remarkable preservation of metastable carbonate. *Geology.* 24: 555-558.
- Wilson, P.A., Norris, R.D. 2001. Warm tropical ocean surface and global anoxia during the Mid-Cretaceous period. *Nature.* 412: 425-429.
- Woese, C.R., Kandler, O., Wheelis, M.L. 1990. Towards a natural system of organisms: proposal for the domains archaea, bacteria, and eucarya. *Proc. Natl. Acad. Sci. U.S.A.* 87: 4576-4579.

References

- Wuchter, C., Schouten, S., Wakeham, S.G., Sinninghe Damsté, J.S. 2005. Temporal and spatial variation in tetraether membrane lipids of marine *Crenarchaeota* in particulate organic matter: Implications for TEX₈₆ paleothermometry. *Paleoceanography*. 20: PA3013.
- Wuchter, C., Abbas, B., Coolen, M.J.L., Herfort, L., van Bleijswijk, J., Timmers, P., Strous, M., Teira, E., Herndl, G.J., Middelburg, J.J., Schouten, S., Sinninghe Damsté, J.S. 2006a. Archaeal nitrification in the ocean. *Proc. Natl. Acad. Sci. U.S.A.* 103: 12317-12322.
- Wuchter, C., Schouten, S., Wakeham, S.G., Sinninghe Damsté, J.S. 2006b. Archaeal tetraether membrane lipid fluxes in the northeastern Pacific and the Arabian Sea: implications for TEX₈₆ paleothermometry. *Paleoceanography*. 21: PA4208.
- Yang, F.Q., Feng, K., Zhao, J., Li, S.P. 2009. Analysis of sterols and fatty acids in natural and cultured *Cordyceps* by one-step derivatization followed with gas chromatography–mass spectrometry. *J. Pharm. Biomed. Anal.* 49: 1172-1178.
- Zaytsev, O., Cervantes-Duarte, R., Montante, O., Gallegos-Garcia, A. 2003. Coastal upwelling activity on the Pacific shelf of the Baja California peninsula. *J. Oceanogr.* 59: 489-502.
- Zopf, J., Böttcher, M.E., Jørgensen, B.B. 2008. Biogeochemistry of sulfur and iron in *Thioploca*-colonized surface sediments in the upwelling area off central Chile. *Geochim. Cosmochim. Ac.* 72: 827-843.

Appendix

Structures of GDGTs

A1	Crenarchaeol.....	159
A2	GDGT-0.....	159
A3	GDGT-1.....	159
A4	GDGT-2.....	159
A5	GDGT-3.....	159
A6	Crenarchaeol, regioisomer.....	159

List of Figures

Figure A-1	Typical partial HPLC/MS base peak chromatogram obtained from the analysis of sample SAOS 27 from the Ghareb Formation, Negev/Israel. A1-A6 indicate the structures of the GDGTs.	160
Figure A-2	Structures of Chromanes	161
Figure A-3	Mass spectrum of hexadecanoic acid (Wiley Registry, 2008)	161
Figure A-4	Mass spectrum of oleic acid (18:1 ω 9) (Elvert et al., 2005; Yang et al., 2009).....	162
Figure A-5	Mass spectrum of vaccenic acid (18:1 ω 7) (Elvert et al., 2005)	162
Figure A-6	Mass spectrum of octadecanoic acid (Wiley Registry, 2008)	162
Figure A-7	Mass spectrum of 5 β (H)-cholestane (Rhead et al., 1971)	163
Figure A-8	Mass spectrum of 5 α (H)-cholestane (Rhead et al., 1971)	163
Figure A-9	Mass spectrum of 24-methyl-5 β (H)-cholestane (Philp, 1985).....	163
Figure A-10	Mass spectrum of 24-methyl-5 α (H)-cholestane (Philp, 1985).....	164
Figure A-11	Mass spectrum of 24-ethyl-5 β (H)-cholestane (Philp, 1985)	164
Figure A-12	Mass spectrum of 24-ethyl-5 α (H)-cholestane (Philp, 1985)	164

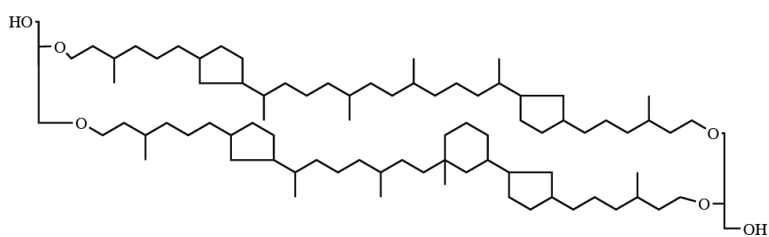
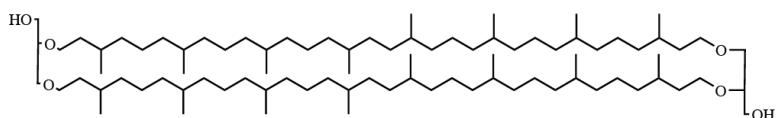
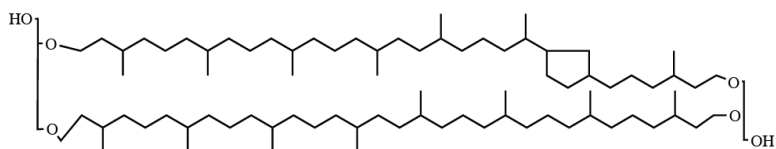
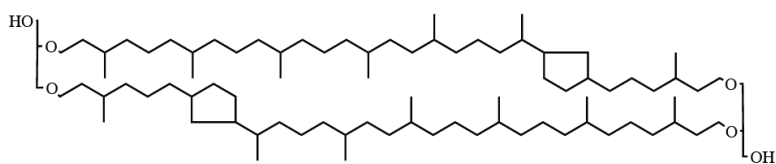
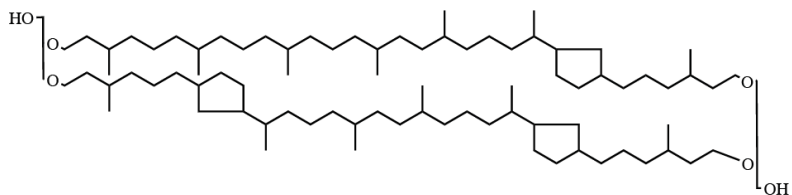
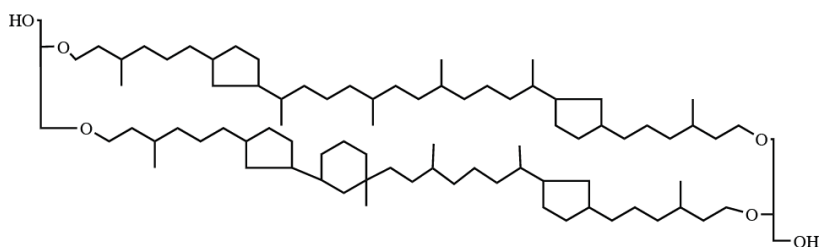
Figure A-13	Mass spectrum of 2,8-dimethyl-2-(4,8,12-trimethyltridecyl)-chroman	165
Figure A-14	Mass spectrum of 2,5,8-trimethyl-2-(4,8,12-trimethyltridecyl)-chroman (5,8-diMe-MTTC) (Sinninghe Damsté et al., 1987a).....	165
Figure A-15	Mass spectrum of 2,7,8-trimethyl-2-(4,8,12-trimethyltridecyl)-chroman (7,8-diMe-MTTC) (Sinninghe Damsté et al., 1987a).....	165
Figure A-16	Mass spectrum of 2,5,7,8-tetramethyl-2-(4,8,12-trimethyltridecyl)-chroman (5,7,8-triMe-MTTC) (Sinninghe Damsté et al., 1987a)	166
Figure A-17	Mass spectrum of 2-methyl-5-tridecyl-thiophene (Wiley Library).....	166
Figure A-18	Mass spectrum of 2,3-dimethyl-5-(2,6,10-trimethylundecyl)-thiophene	166
Figure A-19	Mass spectrum of 3-methyl-2-(3,7,11-trimethyldodecyl)-thiophene (Rullkötter et al., 1988).....	167
Figure A-20	Mass spectrum of 3-(4,8,12-trimethyltridecyl)-thiophene (Rullkötter et al., 1988).....	167
Figure A-21	Mass spectrum of 2-methyl-5-tetradecyl-thiophene (Kohnen et al., 1990a)	167
Figure A-22	Mass spectrum of 2-methyl-5-pentadecyl-thiophene (Kohnen et al., 1990a)	168
Figure A-23	Mass spectrum of C ₂₇ -epithiosterane (Behrens et al., 1997)	168
Figure A-24	Mass spectrum of C ₂₈ -epithiosterane (Behrens et al., 1997)	168
Figure A-25	Mass spectrum of C ₂₉ -epithiosterane (Behrens et al., 1997)	169
Figure A-26	Mass spectrum of 30-[2'-(5'-methylthienyl)-17 α (H),21 β (H)-hopane (de las Heras et al., 1997).....	169
Figure A-27	Mass spectrum of 31-(2'-thienyl)-17 α (H),21 β (H)-homohopane (de las Heras et al., 1997)	169

Figure A-28	Mass spectrum of 31-(2'-thienyl)-17 β (H),21 α (H)-homohopane (de las Heras et al., 1997).....	170
Figure A-29	Mass spectrum of 30-(2'-thienyl)-17 β (H),21 β (H)-hopane (de las Heras et al., 1997).....	170
Figure A-30	Mass spectrum of 30-[2'-(5'-methylthienyl)]-17 β (H),21 β (H)-hopane (de las Heras et al., 1997).....	170
Figure A-31	Mass spectrum of 31-(2'-thienyl)-17 β (H),21 β (H)-homohopane (de las Heras et al., 1997).....	171
Figure A-32	Mass spectrum of 31-[2'-(5'-methylthienyl)]-17 β (H),21 α (H)-homohopane (Sinninghe Damsté et al., 1989a).....	171
Figure A-33	Mass spectrum of 31-(2'-thiolanyl)-17 β (H),21 β (H)-homohopane (Sinninghe Damsté et al., 1989a).....	171

List of Tables

Table A-1	Sample name and corresponding sample depth [m].....	172
Table A-2	Sampling depth, TEX ₈₆ , log TEX ₈₆ and resulting SST (°C) calculated according to 1) Schouten et al. (2002) 2) Kim et al. (2008) 3) Schouten et al. (2003) 4) Jenkyns et al. (2004) 5) Kim et al. (2010) 6) Liu et al. (2009) for the Shefela Basin and the Efe Syncline (n.a. not analyzed, n.d. not detected).	173
Table A-3	Distribution of reconstructed SSTs covering the Santonian to early Maastrichtian from this study and other published data.....	180
Table A-4	Depth and variation in TOC, calculated original TOC (TOC _{OR}), TOC/TOC _{OR} ratio, TFe, TS, TP and CPI (n.d. not detected, n.a. not analyzed).	185
Table A-5	Distribution of the saturated fatty acids C _{16:0} and C _{18:0} and the monounsaturated fatty acids C _{18:1ω7} and C _{18:1ω9} over the profile in μ g/g TOC.....	190
Table A-6	Distribution and proportion of sum of C ₂₇ –C ₂₉ steranes along the Efe Syncline profile.....	192

Table A-7	Concentration of hopanoid thiophenes along the profile in $\mu\text{g/g}$ TOC I 30-[2'-(5'-methylthienyl)-17 α (H),21 β (H)-hopane, II 31-(2'-thienyl)-17 α (H),21 β (H)-homohopane, V 30-[2'-(5'-methylthienyl))-17 β (H),21 β (H)-hopane, VI 31-(2'-thienyl)-17 β (H),21 β (H)-homohopane.....	196
Table A-8	Depth, TON, Pr/Ph, C/N, $\delta^{15}\text{N}_{\text{org}}$ and $\delta^{13}\text{C}_{\text{org}}$ records of the studied sequence.....	201

Structures of GDGTs**A1 Crenarchaeol****A2 GDGT-0****A3 GDGT-1****A4 GDGT-2****A5 GDGT-3****A6 Crenarchaeol, regioisomer**

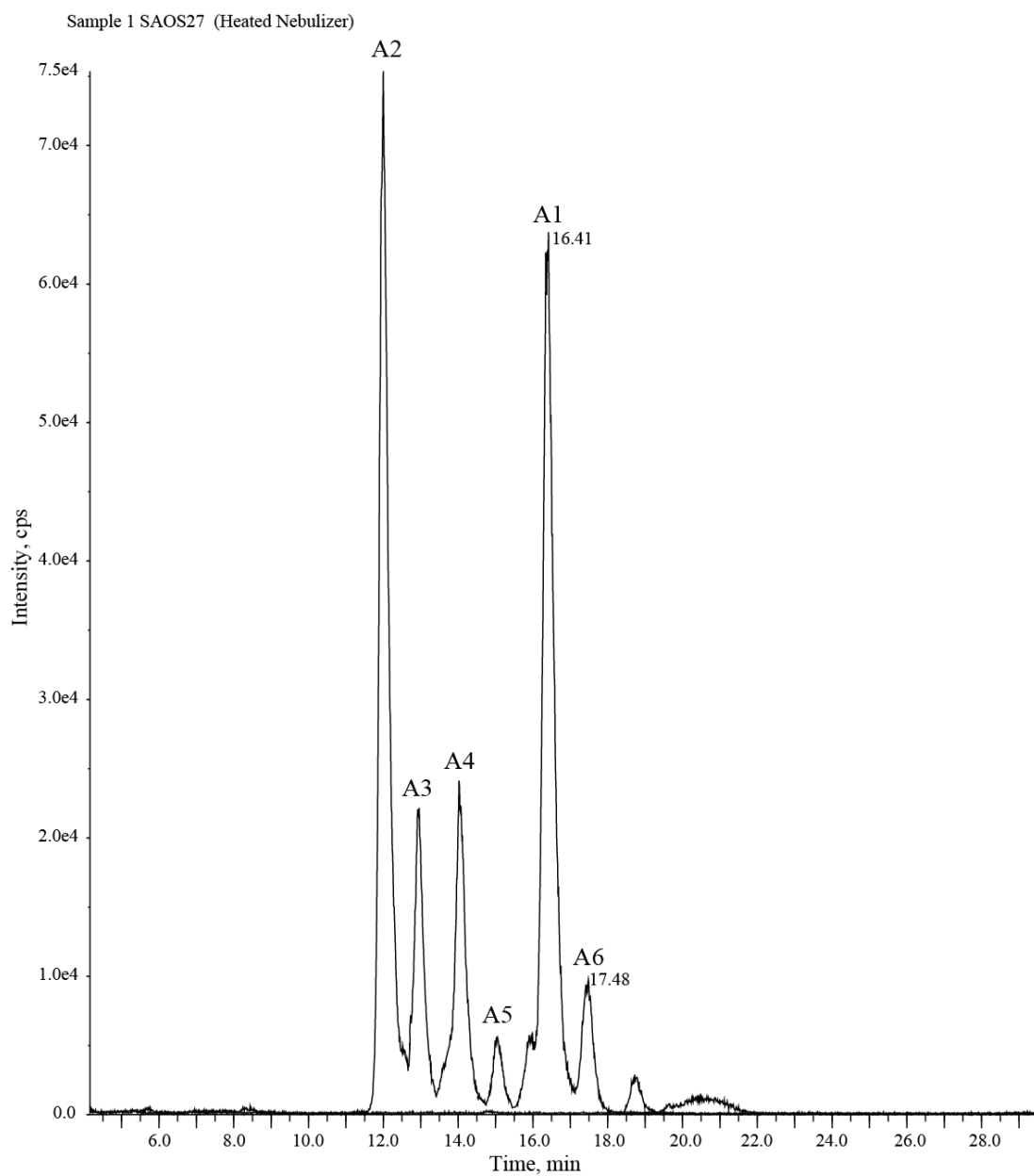
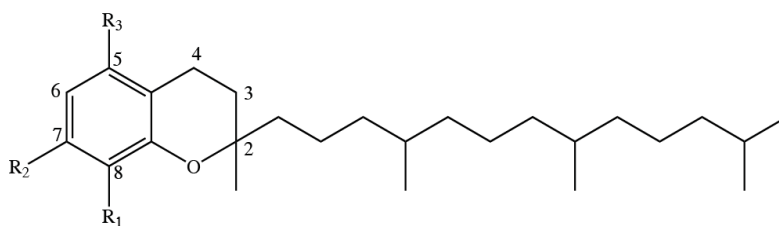


Figure A-1 Typical partial HPLC/MS base peak chromatogram obtained from the analysis of sample SAOS 27 from the Ghareb Formation, Negev/Israel. A1-A6 indicate the structures of the GDGTs.



8-Me-MTTC	$R_1 = \text{CH}_3, R_2 = \text{H}, R_3 = \text{H}$
5,8-diMe-MTTC	$R_1 = \text{CH}_3, R_2 = \text{H}, R_3 = \text{CH}_3$
7,8-diMe-MTTC	$R_1 = \text{CH}_3, R_2 = \text{CH}_3, R_3 = \text{H}$
5,7,8-triMe-MTTC	$R_1 = \text{CH}_3, R_2 = \text{CH}_3, R_3 = \text{H}$

Figure A-2 Structures of Chromanes

Mass spectra of identified biomarkers in the Efe Syncline oil shale

Compound identification is based on mass spectra and/or retention time published in the references written in the brackets.

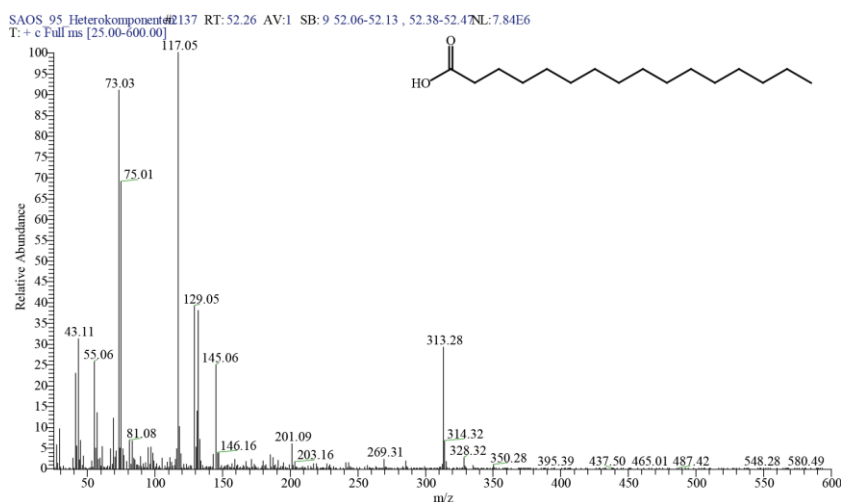


Figure A-3 Mass spectrum of hexadecanoic acid (Wiley Registry, 2008)

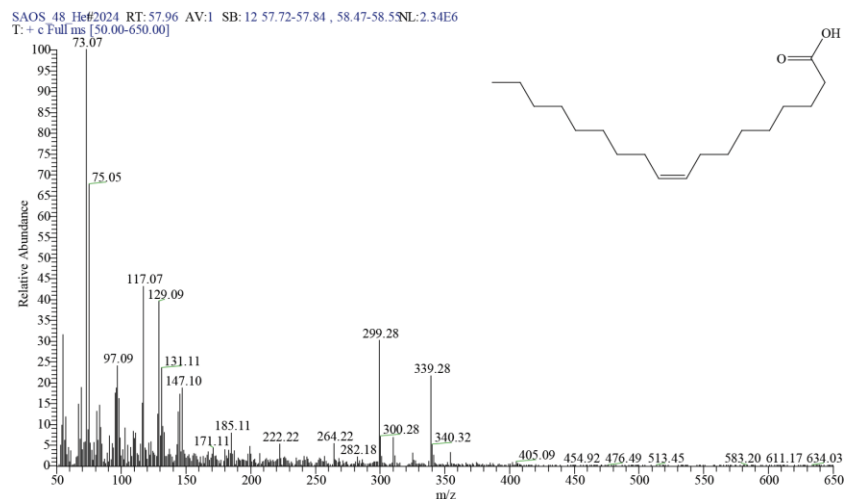


Figure A-4 Mass spectrum of oleic acid (18:1 ω 9) (Elvert et al., 2005; Yang et al., 2009)

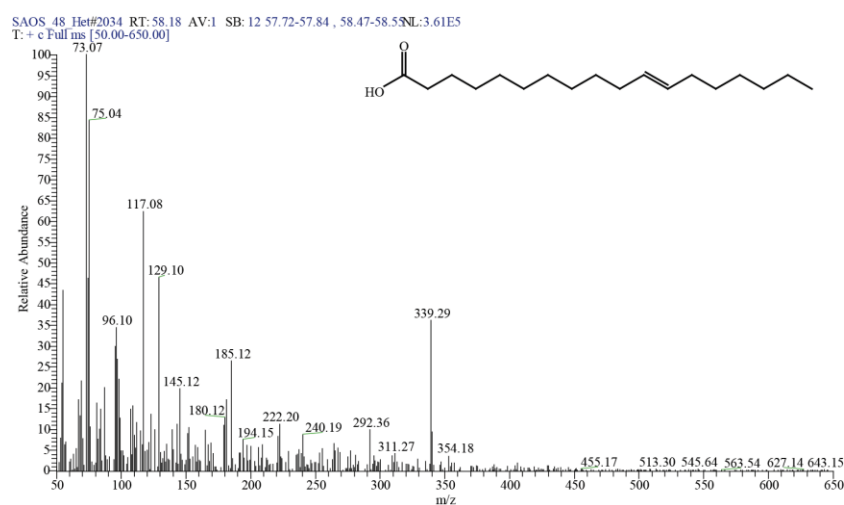


Figure A-5 Mass spectrum of vaccenic acid (18:1 ω 7) (Elvert et al., 2005)

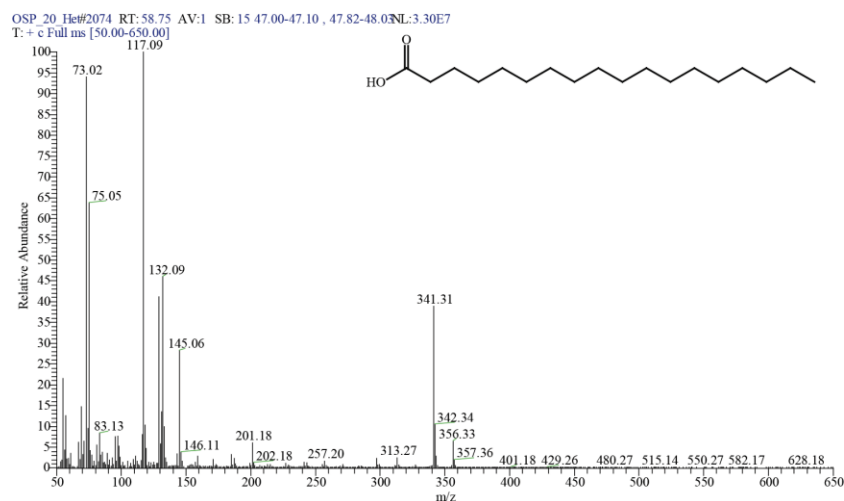


Figure A-6 Mass spectrum of octadecanoic acid (Wiley Registry, 2008)

SAOS 95 Alkane#3228 RT:71.93 AV:1 SB:16 71.63-71.86 , 72.02-72.1 INL:5.01E6
T: + c Full ms [25.00-600.00]

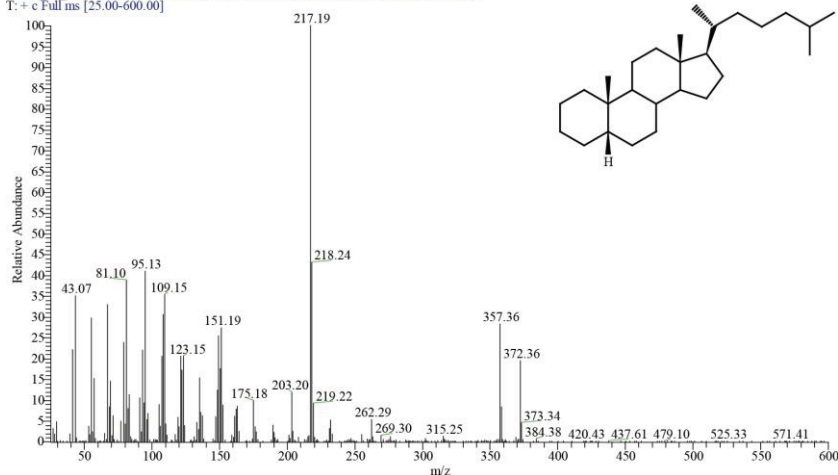


Figure A-7 Mass spectrum of 5 β (H)-cholestane (Rhead et al., 1971)

SAOS 95 Alkane#3268 RT:72.84 AV:1 SB:16 71.63-71.86 , 72.02-72.1 INL:1.17E7
T: + c Full ms [25.00-600.00]

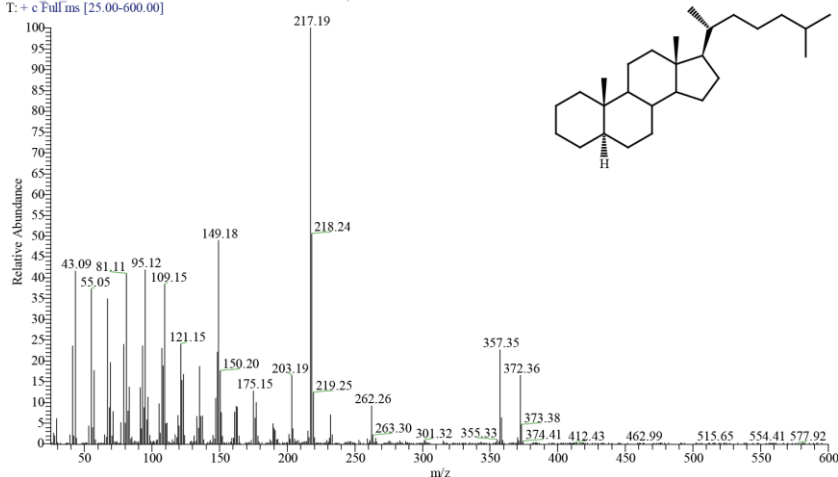


Figure A-8 Mass spectrum of 5 α (H)-cholestane (Rhead et al., 1971)

SAOS 95 Alkane#3333 RT:74.31 AV:1 SB:16 71.63-71.86 , 72.02-72.1 INL:1.03E6
T: + c Full ms [25.00-600.00]

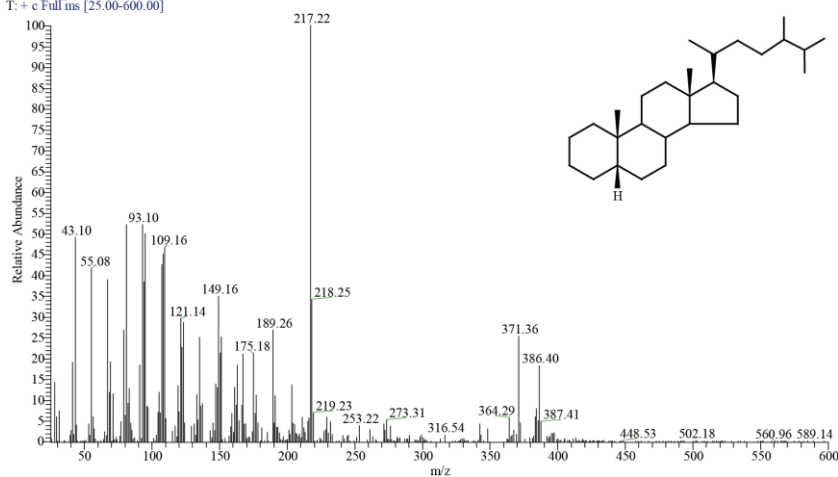


Figure A-9 Mass spectrum of 24-methyl-5 β (H)-cholestane (Philp, 1985)

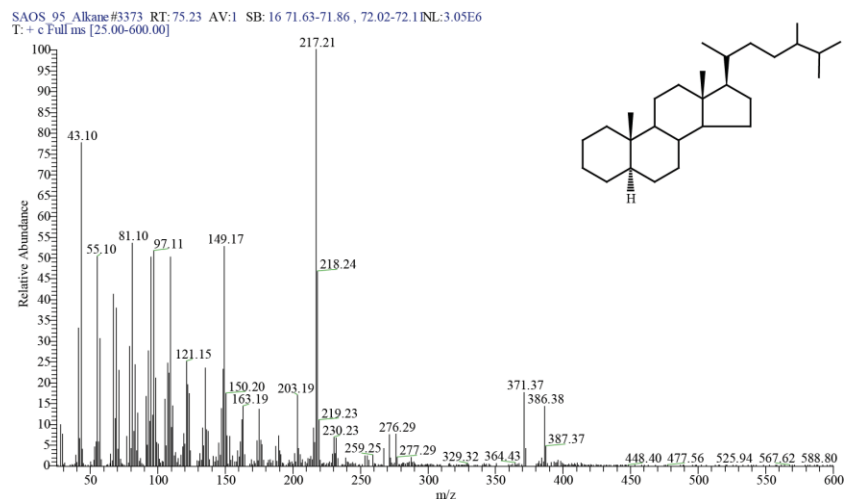


Figure A-10 Mass spectrum of 24-methyl-5 α (H)-cholestane (Philp, 1985)

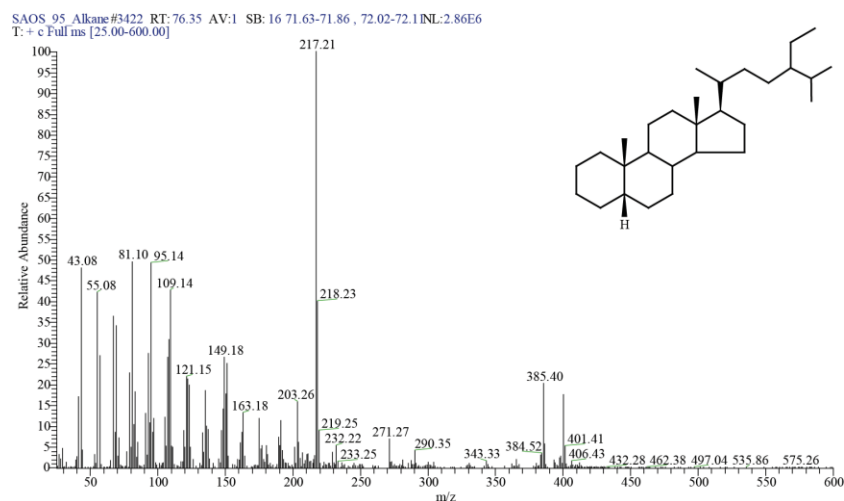


Figure A-11 Mass spectrum of 24-ethyl-5 β (H)-cholestane (Philp, 1985)

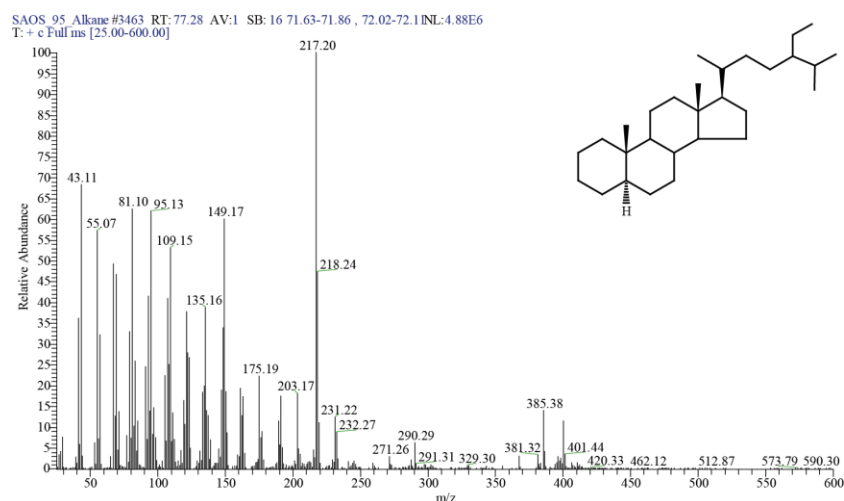


Figure A-12 Mass spectrum of 24-ethyl-5 α (H)-cholestane (Philp, 1985)

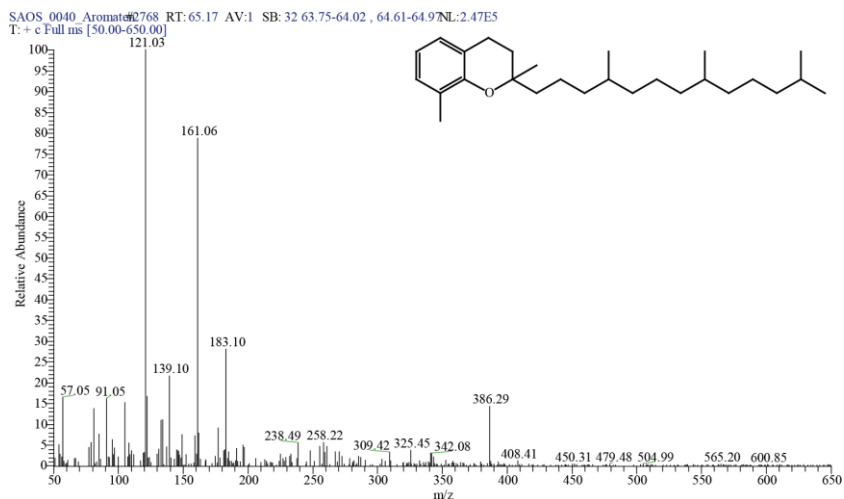


Figure A-13 Mass spectrum of 2,8-dimethyl-2-(4,8,12-trimethyltridecyl)-chroman (8-Me-MTTC) (Sinninghe Damsté et al., 1987a)

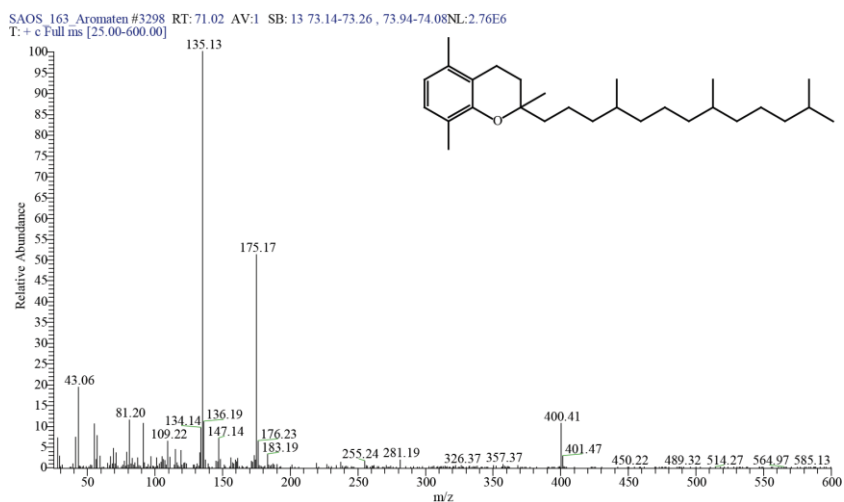


Figure A-14 Mass spectrum of 2,5,8-trimethyl-2-(4,8,12-trimethyltridecyl)-chroman (5,8-diMe-MTTC) (Sinninghe Damsté et al., 1987a)

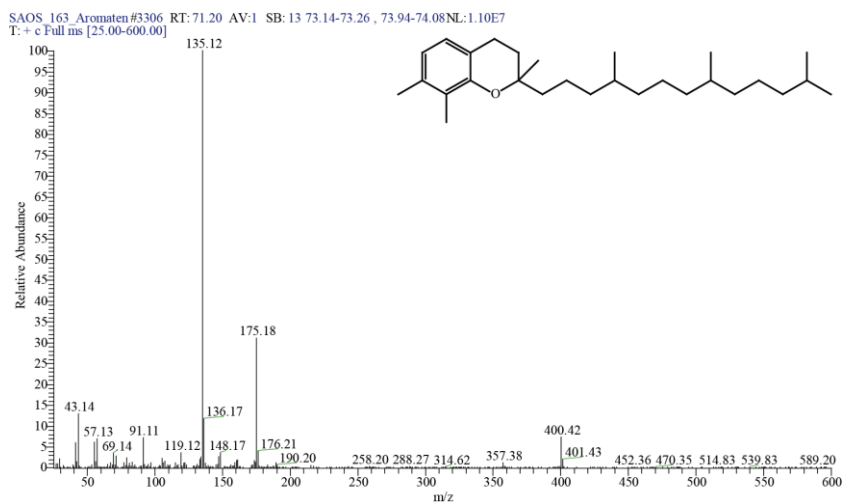


Figure A-15 Mass spectrum of 2,7,8-trimethyl-2-(4,8,12-trimethyltridecyl)-chroman (7,8-diMe-MTTC) (Sinninghe Damsté et al., 1987a)

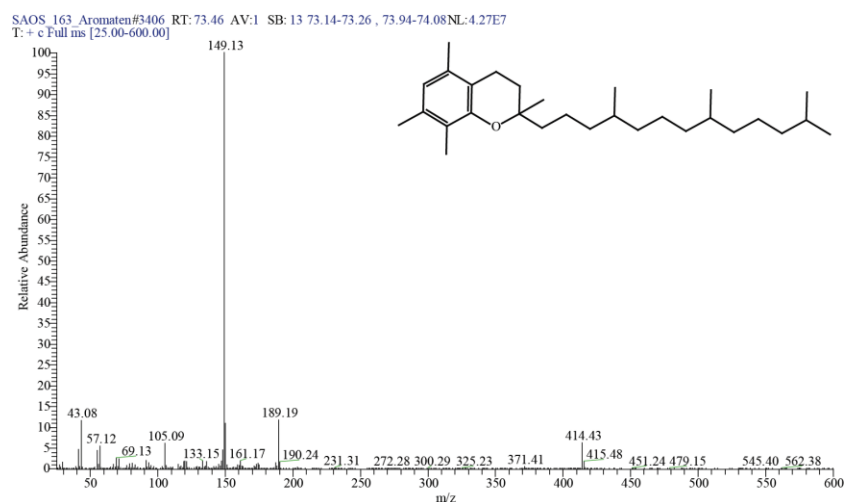


Figure A-16 Mass spectrum of 2,5,7,8-tetramethyl-2-(4,8,12-trimethyltridecyl)-chroman (5,7,8-triMe-MTTC) (Sinninghe Damsté et al., 1987a)

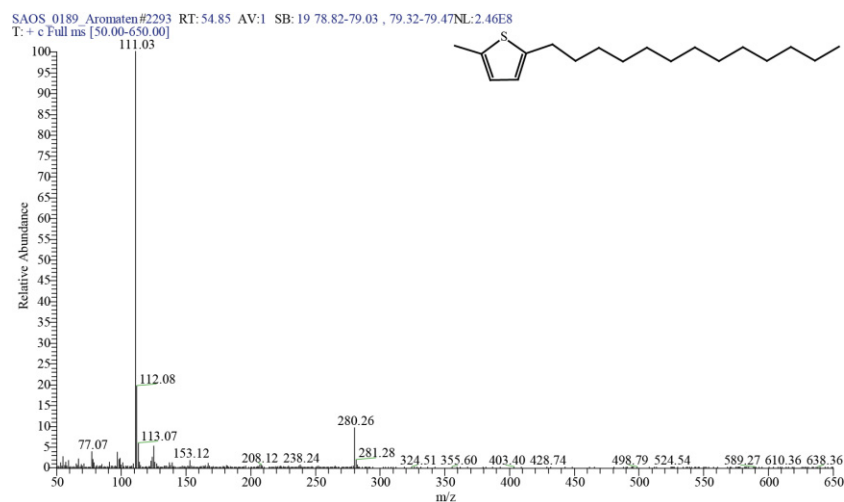


Figure A-17 Mass spectrum of 2-methyl-5-tridecyl-thiophene (Wiley Library)

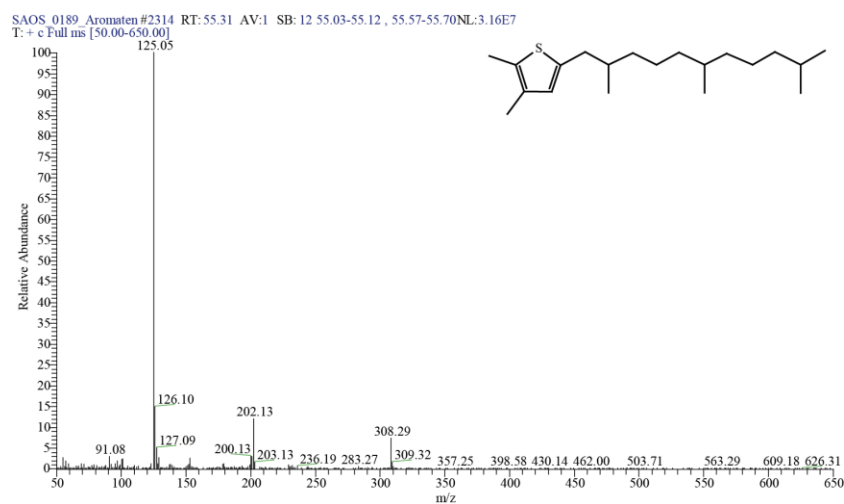


Figure A-18 Mass spectrum of 2,3-dimethyl-5-(2,6,10-trimethylundecyl)-thiophene (Sinninghe Damsté et al., 1987b)

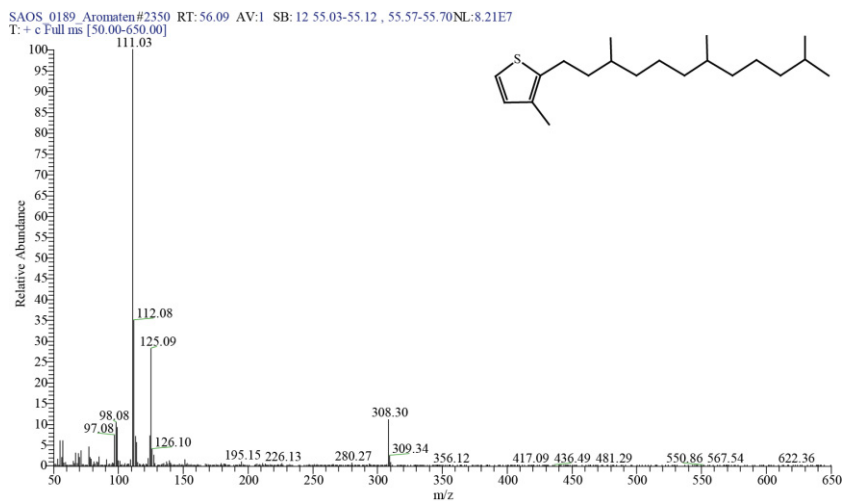


Figure A-19 Mass spectrum of 3-methyl-2-(3,7,11-trimethyldodecyl)-thiophene (Rullkötter et al., 1988)

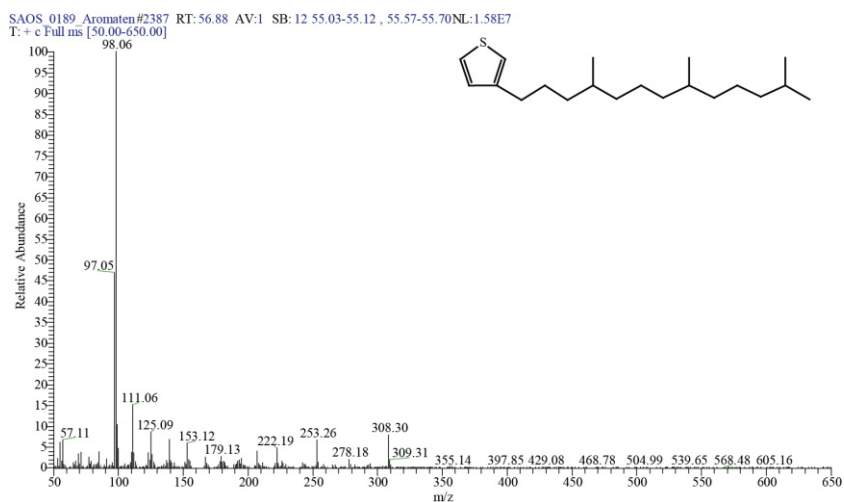


Figure A-20 Mass spectrum of 3-(4,8,12-trimethyltridecyl)-thiophene (Rullkötter et al., 1988)

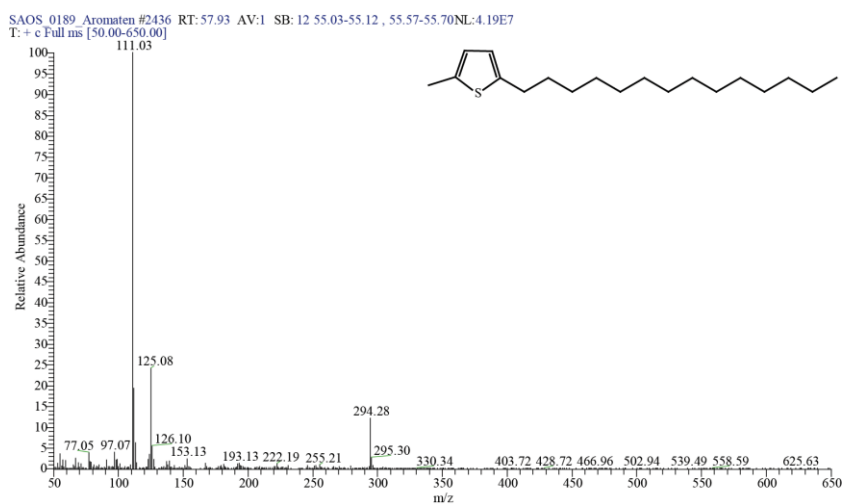


Figure A-21 Mass spectrum of 2-methyl-5-tetradecyl-thiophene (Kohnen et al., 1990a)

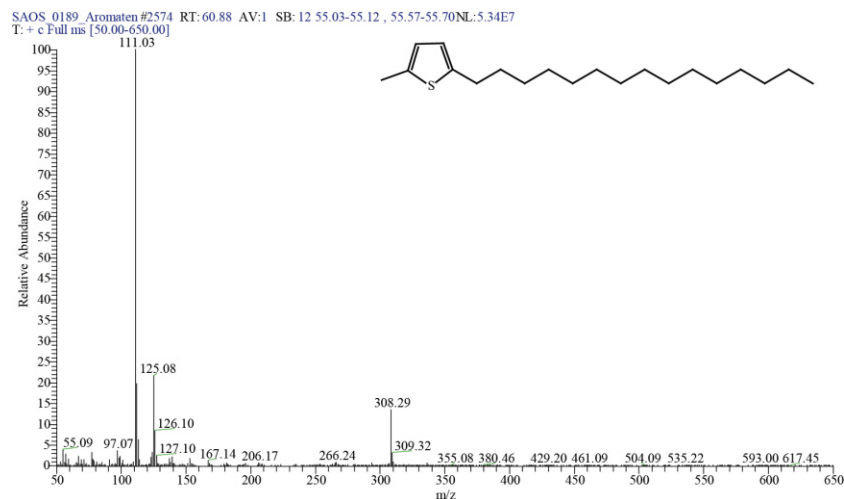


Figure A-22 Mass spectrum of 2-methyl-5-pentadecyl-thiophene (Kohnen et al., 1990a)

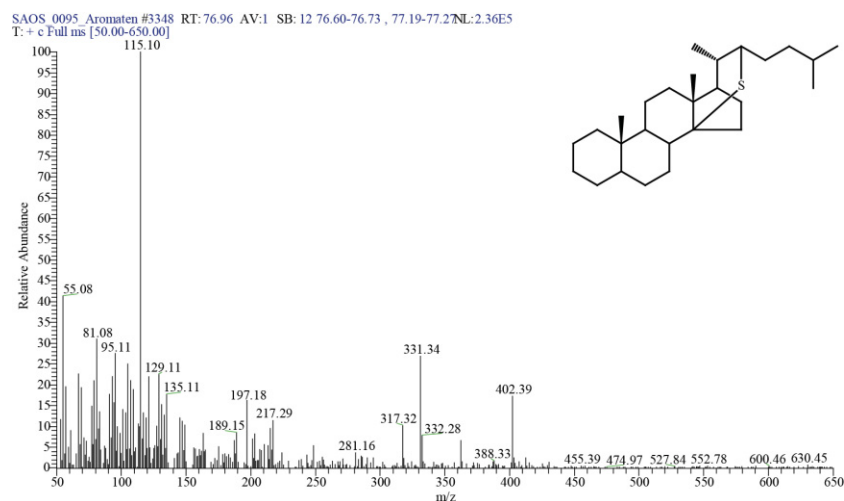


Figure A-23 Mass spectrum of C₂₇-epithiosterane (Behrens et al., 1997)

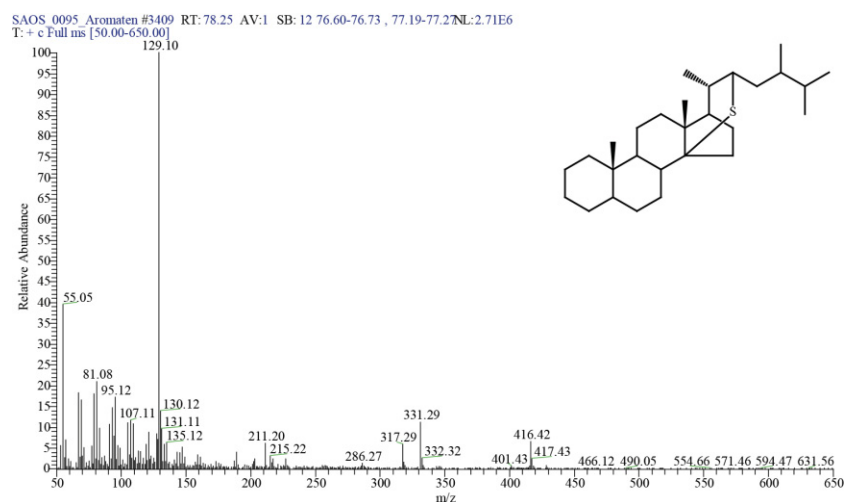
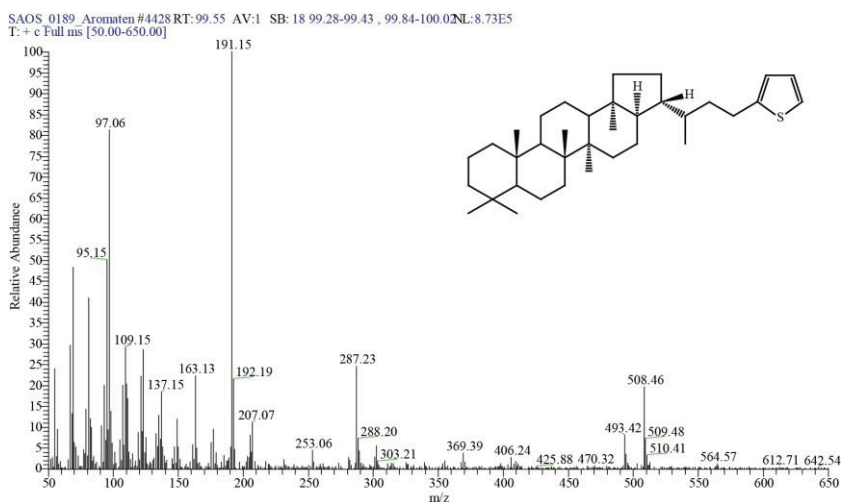
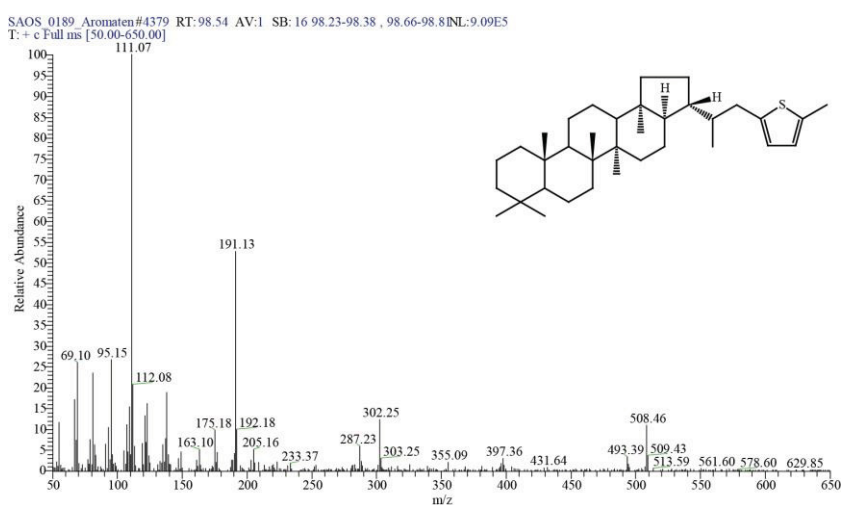
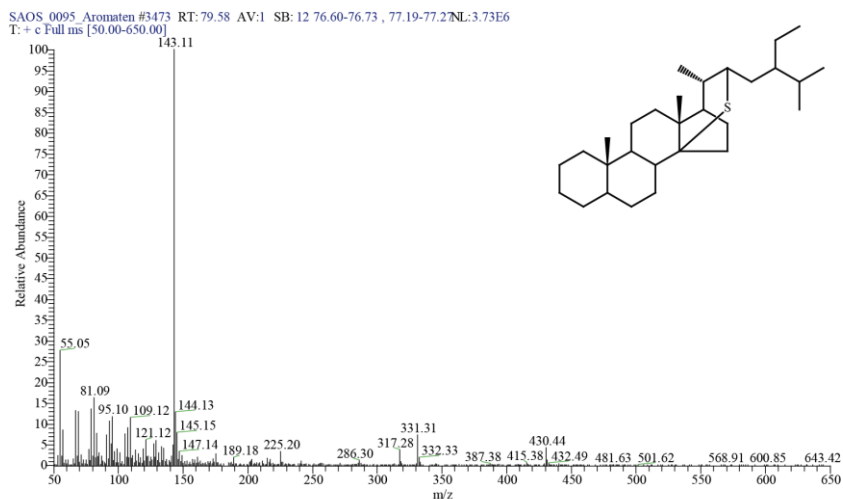


Figure A-24 Mass spectrum of C₂₈-epithiosterane (Behrens et al., 1997)



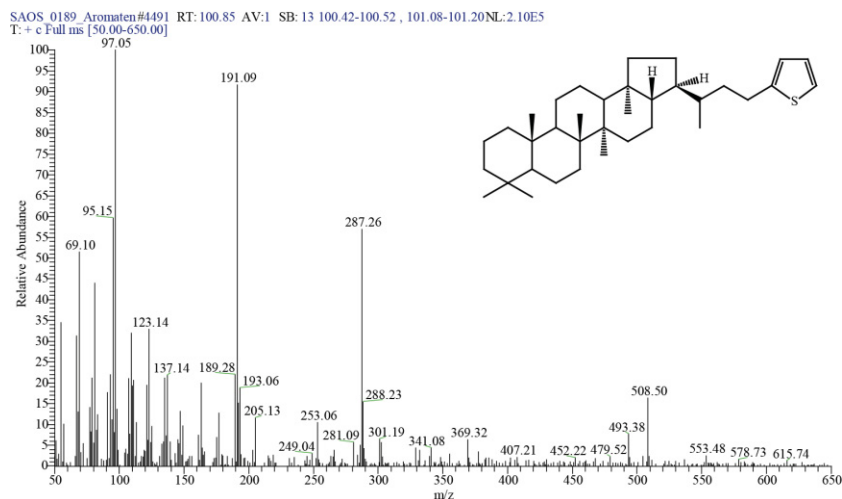


Figure A-28 Mass spectrum of 31-(2'-thienyl)-17 β (H),21 α (H)-homohopane (de las Heras et al., 1997)

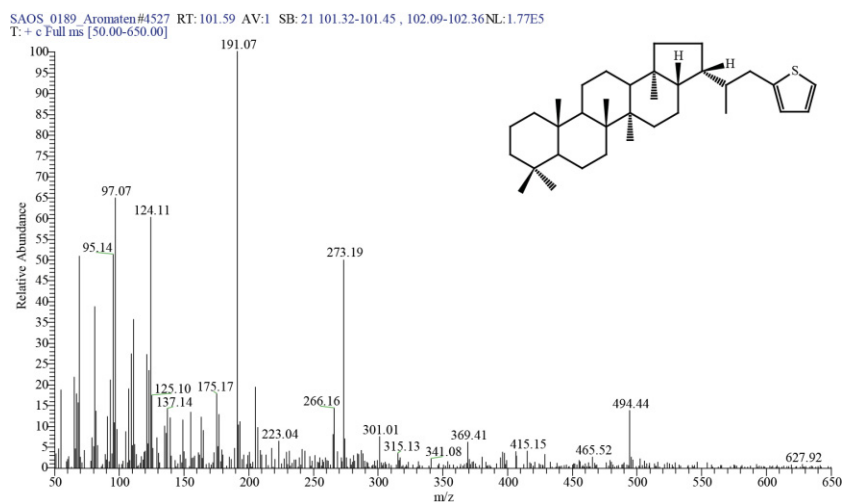


Figure A-29 Mass spectrum of 30-(2'-thienyl)-17 β (H),21 β (H)-hopane (de las Heras et al., 1997)

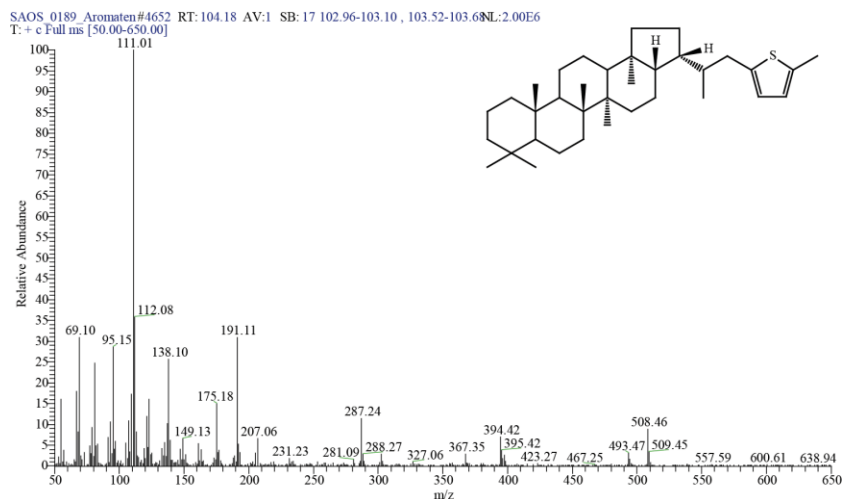


Figure A-30 Mass spectrum of 30-[2'-(5'-methylthienyl)]-17 β (H),21 β (H)-hopane (de las Heras et al., 1997)

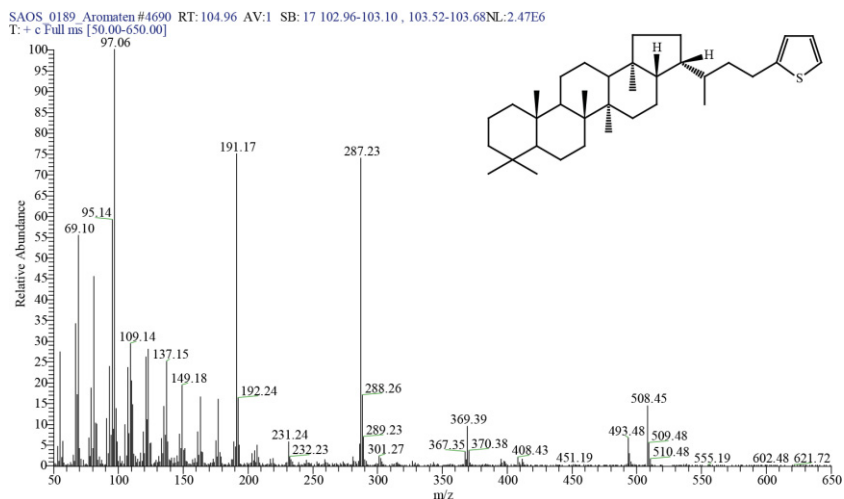


Figure A-31 Mass spectrum of 31-(2'-thienyl)-17 β (H),21 β (H)-homohopane (de las Heras et al., 1997)

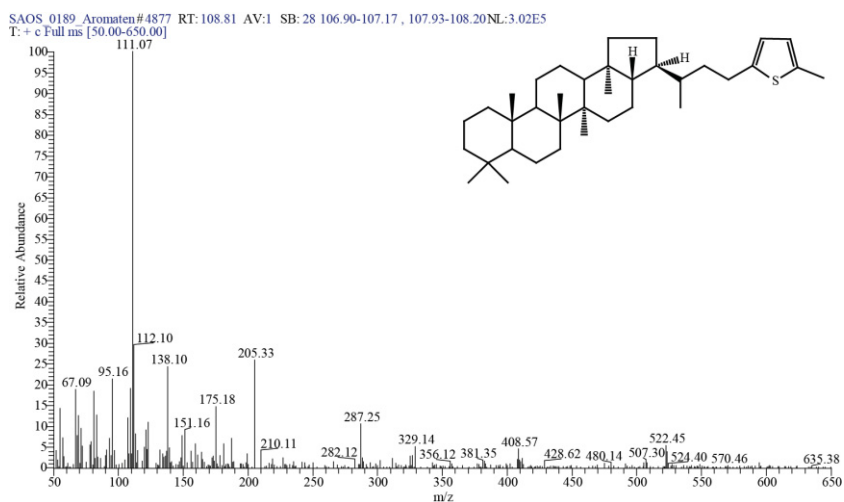


Figure A-32 Mass spectrum of 31-[2'-(5'-methylthienyl)]-17 β (H),21 α (H)-homohopane (Sinninghe Damsté et al., 1989a)

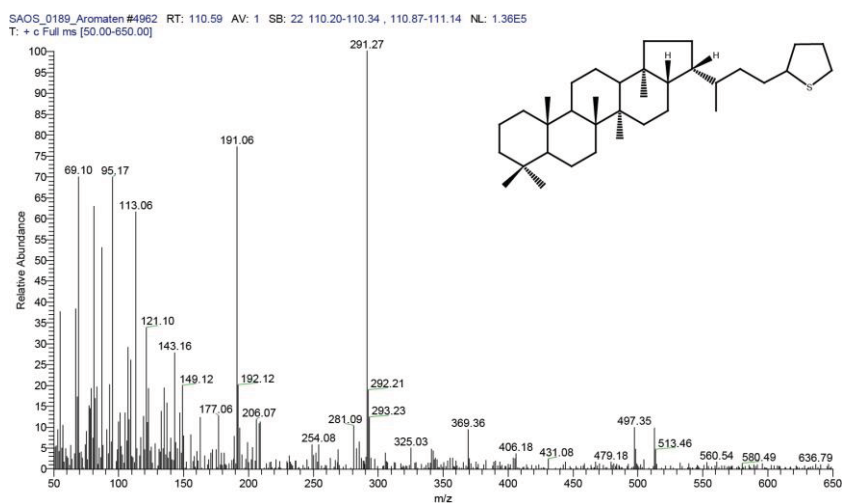


Figure A-33 Mass spectrum of 31-(2'-thiolanyl)-17 β (H),21 β (H)-homohopane (Sinninghe Damsté et al., 1989a)

Table A-1 Sample name and corresponding sample depth [m].

Sample name	Depth [m]	Sample name	Depth [m]	Sample name	Depth [m]	Sample name	Depth [m]
SAM_012	0.0	SAOS_0030	8.00	SAOS_0074	16.80	SAOS_0118	25.60
SAM_011	0.2	SAOS_0031	8.20	SAOS_0075	17.00	SAOS_0119	25.80
SAM_009	0.6	SAOS_0032	8.40	SAOS_0077	17.40	SAOS_0120	26.00
SAM_008	0.8	SAOS_0033	8.60	SAOS_0078	17.60	SAOS_0121	26.20
SAM_007	1.0	SAOS_0034	8.80	SAOS_0079	17.80	SAOS_0122	26.40
SAM_006	1.2	SAOS_0035	9.00	SAOS_0080	18.00	SAOS_0123	26.60
SAM_006	1.2	SAOS_0036	9.20	SAOS_0081	18.20	SAOS_0125	27.00
SAM_005	1.4	SAOS_0037	9.40	SAOS_0082	18.40	SAOS_0126	27.20
SAM_003	1.6	SAOS_0038	9.60	SAOS_0083	18.60	SAOS_0126	27.20
SAM_002	1.8	SAOS_0039	9.80	SAOS_0084	18.80	SAOS_0127	27.40
SAM_001	2.0	SAOS_0040	10.00	SAOS_0084	18.80	SAOS_0128	27.60
SAM_001	2.0	SAOS_0041	10.20	SAOS_0085	19.00	SAOS_0129	27.80
SAOS_0004	2.2	SAOS_0043	10.60	SAOS_0086	19.20	SAOS_0130	28.00
SAOS_0003	2.4	SAOS_0044	10.80	SAOS_0087	19.40	SAOS_0131	28.20
SAOS_0002	2.6	SAOS_0045	11.00	SAOS_0089	19.80	SAOS_0132	28.40
SAOS_0001	2.80	SAOS_0046	11.20	SAOS_0090	20.00	SAOS_0133	28.60
SAOS_0005	3.00	SAOS_0048	11.60	SAOS_0091	20.20	SAOS_0134	28.80
SAOS_0006	3.20	SAOS_0049	11.80	SAOS_0092	20.40	SAOS_0135	29.00
SAOS_0006	3.20	SAOS_0050	12.00	SAOS_0093	20.60	SAOS_0136	29.20
SAOS_0007	3.40	SAOS_0051	12.20	SAOS_0094	20.80	SAOS_0137	29.40
SAOS_0008	3.60	SAOS_0051	12.20	SAOS_0095	21.00	SAOS_0138	29.60
SAOS_0009	3.80	SAOS_0052	12.40	SAOS_0096	21.20	SAOS_0139	29.80
SAOS_0010	4.00	SAOS_0053	12.60	SAOS_0097	21.40	SAOS_0140	30.00
SAOS_0011	4.20	SAOS_0054	12.80	SAOS_0098	21.60	SAOS_0141	30.20
SAOS_0012	4.40	SAOS_0055	13.00	SAOS_0099	21.80	SAOS_0142	30.40
SAOS_0013	4.60	SAOS_0056	13.20	SAOS_0100	22.00	SAOS_0143	30.60
SAOS_0013	4.60	SAOS_0057	13.40	SAOS_0101	22.20	SAOS_0144	30.80
SAOS_0014	4.80	SAOS_0058	13.60	SAOS_0102	22.40	SAOS_0145	31.00
SAOS_0015	5.00	SAOS_0059	13.80	SAOS_0103	22.60	SAOS_0146	31.20
SAOS_0016	5.20	SAOS_0060	14.00	SAOS_0104	22.80	SAOS_0147	31.40
SAOS_0017	5.40	SAOS_0061	14.20	SAOS_0105	23.00	SAOS_0148	31.60
SAOS_0018	5.60	SAOS 60-61	14.30	SAOS_0106	23.20	SAOS_0149	31.80
SAOS_0019	5.80	SAOS_0062	14.40	SAOS_0107	23.40	SAOS_0150	32.00
SAOS_0020	6.00	SAOS_0063	14.60	SAOS_0108	23.60	SAOS_0151	32.20
SAOS_0021	6.20	SAOS_0064	14.80	SAOS_0109	23.80	SAOS_0152	32.40
SAOS_0022	6.40	SAOS_0065	15.00	SAOS_0110	24.00	SAOS_0153	32.60
SAOS_0023	6.60	SAOS_0066	15.20	SAOS_0111	24.20	SAOS_0154	32.80
SAOS_0024	6.80	SAOS_0067	15.40	SAOS_0112	24.40	SAOS_0155	33.00
SAOS_0025	7.00	SAOS_0069	15.80	SAOS_0113	24.60	SAOS_0156	33.20
SAOS_0026	7.20	SAOS_0070	16.00	SAOS_0114	24.80	SAOS_0157	33.40
SAOS_0027	7.40	SAOS_0071	16.20	SAOS_0115	25.00	SAOS_0158	33.60
SAOS_0028	7.60	SAOS_0072	16.40	SAOS_0116	25.20	SAOS_0159	33.80
SAOS_0029	7.80	SAOS_0073	16.60	SAOS_0117	25.40	SAOS_0160	34.00

Sample name	Depth [m]	Sample name	Depth [m]	Sample name	Depth [m]	Sample name	Depth [m]
SAOS_0161	34.20	SAOS_0185	39.00	OSP_013	44.40	SAP12	49.20
SAOS_0162	34.40	SAOS_0186	39.20	OSP_012	44.60	SAP13	49.40
SAOS_0163	34.60	SAOS_0188	39.60	OSP_011	44.80		
SAOS_0164	34.80	SAOS_0189	39.80	OSP_010	45.00		
SAOS_0165	35.00	SAOS_0190	40.00	OSP_009	45.20		
SAOS_0166	35.20	SAOS_0191	40.20	OSP_008	45.40		
SAOS_0167	35.40	SAOS_0192	40.40	OSP_007	45.60		
SAOS_0169	35.80	SAOS_0193	40.60	OSP_006	45.80		
SAOS_0170	36.00	SAOS_0194	40.80	OSP_005	46.00		
SAOS_0171	36.20	SAOS_0195	41.00	OSP_004	46.20		
SAOS_0172	36.40	SAOS_0196	41.20	OSP_003	46.40		
SAOS_0173	36.60	SAOS_0197	41.40	OSP_001	46.80		
SAOS_0174	36.80	SAOS_0198	41.60	SAP1	47.00		
SAOS_0175	37.00	SAOS_0199	41.80	SAP2	47.20		
SAOS 175-176	37.10	SAOS_0200	42.00	SAP3	47.40		
SAOS_0176	37.20	SAOS_0201	42.20	SAP4	47.60		
SAOS_0177	37.40	SAOS_0202	42.40	SAP5	47.80		
SAOS_0177	37.40	SAOS_0203	42.60	SAP6	48.00		
SAOS_0179	37.80	OSP_021	42.80	SAP7	48.20		
SAOS_0180	38.00	OSP_020	43.00	SAP8	48.40		
SAOS_0181	38.20	OSP_019	43.20	SAP8	48.40		
SAOS_0182	38.40	OSP_018	43.40	SAP9	48.60		
SAOS_0183	38.60	OSP_016	43.80	SAP10	48.80		
SAOS_0184	38.80	OSP_015	44.00	SAP11	49.00		

Table A-2 Sampling depth, TEX_{86} , $\log TEX_{86}$ and resulting SST ($^{\circ}C$) calculated according to 1) Schouten et al. (2002) 2) Kim et al. (2008) 3) Schouten et al. (2003) 4) Jenkyns et al. (2004) 5) Kim et al. (2010) 6) Liu et al. (2009) for the Shefela Basin and the Efe Syncline (n.a. not analyzed, n.d. not detected).

Shefela Basin

Depth (m)	TEX_{86}	$\log TEX_{86}$	SST ($^{\circ}C$) ¹⁾	SST ($^{\circ}C$) ²⁾	SST ($^{\circ}C$) ³⁾	SST ($^{\circ}C$) ⁴⁾	SST ($^{\circ}C$) ⁵⁾	SST ($^{\circ}C$) ⁶⁾
265.3	0.701	-0.154	28.1	28.6	25.4	27.4	30.5	27.2
268.2	0.722	-0.141	29.5	29.8	26.1	28.8	32.2	27.9
271.6	0.706	-0.151	28.4	28.9	25.6	27.8	31.0	27.4
274.59	0.715	-0.146	29.0	29.4	25.9	28.3	31.7	27.6
277.55	0.704	-0.152	28.3	28.8	25.5	27.6	30.8	27.3
280.69	0.749	-0.126	31.3	31.3	27.1	30.6	34.4	28.7
283.8	0.705	-0.152	28.3	28.9	25.5	27.7	30.9	27.3
287.79	0.675	-0.170	26.4	27.2	24.4	25.7	28.4	26.3
290.84	0.664	-0.178	25.6	26.5	24.0	24.9	27.5	25.9
293.9	n.a.	n.a.	n.a.	n.a.	n.a.	n.a.	n.a.	n.a.
297	n.a.	n.a.	n.a.	n.a.	n.a.	n.a.	n.a.	n.a.
300.05	0.669	-0.175	25.9	26.8	24.2	25.2	27.9	26.0
303.04	n.a.	n.a.	n.a.	n.a.	n.a.	n.a.	n.a.	n.a.
305.09	n.a.	n.a.	n.a.	n.a.	n.a.	n.a.	n.a.	n.a.
309.2	0.685	-0.164	27.0	27.7	24.8	26.4	29.2	26.6

Appendix

depth (m)	TEX ₈₆	log TEX ₈₆	SST (°C) ¹⁾	SST (°C) ²⁾	SST (°C) ³⁾	SST (°C) ⁴⁾	SST (°C) ⁵⁾	SST (°C) ⁶⁾
312.19	n.a.	n.a.	n.a.	n.a.	n.a.	n.a.	n.a.	n.a.
316.35	0.636	-0.196	23.7	25.0	23.0	23.1	25.2	24.8
320.35	n.a.	n.a.	n.a.	n.a.	n.a.	n.a.	n.a.	n.a.
324.45	0.685	-0.164	27.0	27.7	24.8	26.3	29.2	26.6
327.5	n.a.	n.a.	n.a.	n.a.	n.a.	n.a.	n.a.	n.a.
331.6	0.693	-0.159	27.5	28.2	25.1	26.8	29.9	26.9
334.54	n.a.	n.a.	n.a.	n.a.	n.a.	n.a.	n.a.	n.a.
337.7	n.a.	n.a.	n.a.	n.a.	n.a.	n.a.	n.a.	n.a.
340	n.a.	n.a.	n.a.	n.a.	n.a.	n.a.	n.a.	n.a.
341.69	n.a.	n.a.	n.a.	n.a.	n.a.	n.a.	n.a.	n.a.
344.74	n.a.	n.a.	n.a.	n.a.	n.a.	n.a.	n.a.	n.a.
347.79	n.a.	n.a.	n.a.	n.a.	n.a.	n.a.	n.a.	n.a.
350.76	0.676	-0.170	26.4	27.2	24.4	25.7	28.5	26.3
353.81	0.705	-0.152	28.3	28.8	25.5	27.7	30.8	27.3
356.81	n.a.	n.a.	n.a.	n.a.	n.a.	n.a.	n.a.	n.a.
359.95	0.738	-0.132	30.5	30.7	26.7	29.9	33.5	28.3
363	0.690	-0.161	27.3	28.0	25.0	26.7	29.6	26.8
365.99	0.713	-0.147	28.9	29.3	25.8	28.2	31.5	27.6
369.24	0.706	-0.151	28.4	28.9	25.6	27.7	30.9	27.3
372.3	0.696	-0.157	27.7	28.3	25.2	27.1	30.1	27.0
375.24	0.726	-0.139	29.7	30.0	26.3	29.1	32.6	28.0
378.24	0.745	-0.128	31.0	31.1	27.0	30.3	34.1	28.5
381.3	n.a.	n.a.	n.a.	n.a.	n.a.	n.a.	n.a.	n.a.
384.245	0.706	-0.151	28.4	28.9	25.6	27.7	30.9	27.3
386.98	0.732	-0.135	30.1	30.4	26.5	29.5	33.1	28.2
390.95	0.712	-0.148	28.8	29.2	25.8	28.1	31.4	27.5
394.34	0.710	-0.149	28.7	29.1	25.7	28.0	31.3	27.5
397.1	0.713	-0.147	28.9	29.3	25.8	28.2	31.5	27.6
400.3	0.736	-0.133	30.4	30.6	26.7	29.7	33.4	28.3
403.6	n.a.	n.a.	n.a.	n.a.	n.a.	n.a.	n.a.	n.a.
407	0.744	-0.128	30.9	31.0	27.0	30.3	34.0	28.5
410	0.690	-0.161	27.3	28.0	25.0	26.7	29.6	26.8
412.94	0.713	-0.147	28.9	29.3	25.8	28.2	31.5	27.6
416	0.705	-0.152	28.4	28.9	25.5	27.7	30.9	27.3
419	0.696	-0.157	27.7	28.3	25.2	27.1	30.1	27.0
422	0.726	-0.139	29.7	30.0	26.3	29.1	32.6	28.0
425.94	n.a.	n.a.	n.a.	n.a.	n.a.	n.a.	n.a.	n.a.
428.94	0.692	-0.160	27.5	28.1	25.0	26.8	29.8	26.9
432	0.694	-0.159	27.6	28.2	25.1	26.9	30.0	26.9
435	0.711	-0.148	28.7	29.2	25.7	28.1	31.3	27.5
438	0.719	-0.143	29.3	29.6	26.0	28.6	32.0	27.8
441	0.713	-0.147	28.9	29.3	25.8	28.2	31.5	27.6
443.94	n.a.	n.a.	n.a.	n.a.	n.a.	n.a.	n.a.	n.a.
446.94	0.703	-0.153	28.2	28.7	25.4	27.5	30.7	27.2
450	0.751	-0.124	31.4	31.4	27.2	30.7	34.6	28.7
453	n.a.	n.a.	n.a.	n.a.	n.a.	n.a.	n.a.	n.a.
456	0.724	-0.140	29.6	29.9	26.2	28.9	32.4	27.9
459	n.a.	n.a.	n.a.	n.a.	n.a.	n.a.	n.a.	n.a.
462	0.747	-0.127	31.1	31.2	27.1	30.4	34.3	28.6
465	0.718	-0.144	29.2	29.6	26.0	28.5	31.9	27.7

depth (m)	TEX ₈₆	log TEX ₈₆	SST (°C) ¹⁾	SST (°C) ²⁾	SST (°C) ³⁾	SST (°C) ⁴⁾	SST (°C) ⁵⁾	SST (°C) ⁶⁾
468	0.728	-0.138	29.9	30.1	26.4	29.2	32.7	28.0
471	0.713	-0.147	28.9	29.3	25.8	28.2	31.5	27.6
474.1	n.a.	n.a.	n.a.	n.a.	n.a.	n.a.	n.a.	n.a.
477	0.739	-0.131	30.6	30.8	26.8	30.0	33.7	28.4
480	0.724	-0.140	29.6	29.9	26.2	28.9	32.4	27.9
483	0.725	-0.139	29.7	30.0	26.3	29.0	32.5	28.0
486	n.a.	n.a.	n.a.	n.a.	n.a.	n.a.	n.a.	n.a.
489	0.709	-0.149	28.6	29.1	25.7	27.9	31.2	27.4
492	0.720	-0.143	29.3	29.7	26.1	28.7	32.1	27.8
495.1	0.722	-0.141	29.5	29.8	26.1	28.8	32.2	27.9
498	n.a.	n.a.	n.a.	n.a.	n.a.	n.a.	n.a.	n.a.
504	n.a.	n.a.	n.a.	n.a.	n.a.	n.a.	n.a.	n.a.
507	0.710	-0.149	28.7	29.1	25.7	28.0	31.2	27.5
510.13	0.626	-0.204	23.0	24.4	22.6	22.4	24.4	24.4
513	0.592	-0.228	20.8	22.5	21.3	20.1	21.7	22.9
517	0.739	-0.131	30.6	30.8	26.8	29.9	33.6	28.4
520	0.713	-0.147	28.9	29.3	25.8	28.2	31.5	27.6
523	0.696	-0.157	27.7	28.3	25.2	27.1	30.1	27.0
526	0.714	-0.146	29.0	29.4	25.9	28.3	31.6	27.6
529.16	n.a.	n.a.	n.a.	n.a.	n.a.	n.a.	n.a.	n.a.
535	0.736	-0.133	30.4	30.6	26.7	29.7	33.4	28.3
538	n.a.	n.a.	n.a.	n.a.	n.a.	n.a.	n.a.	n.a.
541	0.745	-0.128	31.0	31.1	27.0	30.3	34.1	28.6
544	n.a.	n.a.	n.a.	n.a.	n.a.	n.a.	n.a.	n.a.
545	n.a.	n.a.	n.a.	n.a.	n.a.	n.a.	n.a.	n.a.
548	0.719	-0.143	29.3	29.6	26.0	28.6	32.0	27.8
550	n.a.	n.a.	n.a.	n.a.	n.a.	n.a.	n.a.	n.a.
553	0.732	-0.135	30.1	30.4	26.5	29.5	33.1	28.2
556	n.a.	n.a.	n.a.	n.a.	n.a.	n.a.	n.a.	n.a.
559	0.774	-0.111	32.9	32.7	28.1	32.3	36.5	29.4
562	n.a.	n.a.	n.a.	n.a.	n.a.	n.a.	n.a.	n.a.
565.07	0.790	-0.102	34.0	33.6	28.7	33.3	37.8	29.8
568.6	n.a.	n.a.	n.a.	n.a.	n.a.	n.a.	n.a.	n.a.
576.75	0.806	-0.094	35.1	34.5	29.3	34.4	39.1	30.2
580	n.a.	n.a.	n.a.	n.a.	n.a.	n.a.	n.a.	n.a.
581.85	0.781	-0.107	33.4	33.1	28.4	32.8	37.1	29.6
585.9	0.797	-0.098	34.5	34.0	28.9	33.8	38.4	30.0
591	0.815	-0.089	35.7	35.0	29.6	35.0	39.8	30.4
595	0.835	-0.079	37.0	36.1	30.3	36.3	41.4	30.9

Efe Syncline

Depth [m]	TEX ₈₆	log TEX ₈₆	SST (°C) ¹⁾	SST (°C) ²⁾	SST (°C) ³⁾	SST (°C) ⁴⁾	SST (°C) ⁵⁾	SST (°C) ⁶⁾
0.0	n.d.	n.d.	n.d.	n.d.	n.d.	n.d.	n.d.	n.d.
0.2	n.d.	n.d.	n.d.	n.d.	n.d.	n.d.	n.d.	n.d.
0.6	n.d.	n.d.	n.d.	n.d.	n.d.	n.d.	n.d.	n.d.
0.8	n.d.	n.d.	n.d.	n.d.	n.d.	n.d.	n.d.	n.d.
1.0	n.d.	n.d.	n.d.	n.d.	n.d.	n.d.	n.d.	n.d.

Appendix

Depth [m]	TEX ₈₆	log TEX ₈₆	SST (°C) ¹⁾	SST (°C) ²⁾	SST (°C) ³⁾	SST (°C) ⁴⁾	SST (°C) ⁵⁾	SST (°C) ⁶⁾
1.2	n.d.	n.d.	n.d.	n.d.	n.d.	n.d.	n.d.	n.d.
1.4	n.d.	n.d.	n.d.	n.d.	n.d.	n.d.	n.d.	n.d.
1.6	n.d.	n.d.	n.d.	n.d.	n.d.	n.d.	n.d.	n.d.
1.8	n.d.	n.d.	n.d.	n.d.	n.d.	n.d.	n.d.	n.d.
2.0	n.d.	n.d.	n.d.	n.d.	n.d.	n.d.	n.d.	n.d.
2.2	n.d.	n.d.	n.d.	n.d.	n.d.	n.d.	n.d.	n.d.
2.4	n.d.	n.d.	n.d.	n.d.	n.d.	n.d.	n.d.	n.d.
2.6	n.d.	n.d.	n.d.	n.d.	n.d.	n.d.	n.d.	n.d.
3.0	n.d.	n.d.	n.d.	n.d.	n.d.	n.d.	n.d.	n.d.
3.2	n.d.	n.d.	n.d.	n.d.	n.d.	n.d.	n.d.	n.d.
3.6	0.610	-0.215	22.0	23.5	22.0	21.3	23.1	23.7
3.8	0.704	-0.152	28.3	28.8	25.5	27.6	30.8	27.3
4.0	n.a.	n.a.	n.a.	n.a.	n.a.	n.a.	n.a.	n.a.
4.2	0.620	-0.207	22.7	24.1	22.4	22.0	24.0	24.2
4.4	n.a.	n.a.	n.a.	n.a.	n.a.	n.a.	n.a.	n.a.
4.6	0.644	-0.191	24.2	25.4	23.2	23.6	25.9	25.1
4.8	n.a.	n.a.	n.a.	n.a.	n.a.	n.a.	n.a.	n.a.
5.2	n.a.	n.a.	n.a.	n.a.	n.a.	n.a.	n.a.	n.a.
5.4	0.645	-0.191	24.3	25.4	23.3	23.6	25.9	25.1
5.6	0.716	-0.145	29.1	29.5	25.9	28.4	31.8	27.7
5.8	n.a.	n.a.	n.a.	n.a.	n.a.	n.a.	n.a.	n.a.
6.0	0.672	-0.173	26.1	27.0	24.3	25.4	28.1	26.2
6.2	0.703	-0.153	28.2	28.7	25.4	27.5	30.7	27.2
6.4	n.a.	n.a.	n.a.	n.a.	n.a.	n.a.	n.a.	n.a.
6.6	0.656	-0.183	25.0	26.1	23.7	24.4	26.8	25.6
6.8	0.695	-0.158	27.7	28.3	25.2	27.0	30.1	27.0
7.0	0.678	-0.169	26.5	27.3	24.5	25.9	28.7	26.4
7.2	n.a.	n.a.	n.a.	n.a.	n.a.	n.a.	n.a.	n.a.
7.4	n.a.	n.a.	n.a.	n.a.	n.a.	n.a.	n.a.	n.a.
7.6	0.650	-0.187	24.7	25.8	23.5	24.0	26.4	25.4
7.8	0.671	-0.174	26.0	26.9	24.2	25.4	28.1	26.1
8.0	n.a.	n.a.	n.a.	n.a.	n.a.	n.a.	n.a.	n.a.
8.2	0.682	-0.166	26.8	27.6	24.7	26.2	29.0	26.5
8.4	0.668	-0.175	25.9	26.8	24.2	25.2	27.9	26.0
8.6	n.a.	n.a.	n.a.	n.a.	n.a.	n.a.	n.a.	n.a.
8.8	0.646	-0.190	24.4	25.5	23.3	23.7	26.1	25.2
9.0	0.683	-0.165	26.9	27.6	24.7	26.2	29.1	26.6
9.2	0.693	-0.159	27.5	28.2	25.1	26.9	29.9	26.9
9.4	0.709	-0.149	28.6	29.1	25.7	27.9	31.2	27.4
9.6	0.683	-0.166	26.9	27.6	24.7	26.2	29.1	26.6
9.8	n.a.	n.a.	n.a.	n.a.	n.a.	n.a.	n.a.	n.a.
10.0	0.689	-0.162	27.3	28.0	24.9	26.6	29.6	26.8
10.2	0.733	-0.135	30.2	30.4	26.6	29.5	33.1	28.2
10.4	0.620	-0.208	22.7	24.1	22.4	22.0	23.9	24.1
10.8	n.a.	n.a.	n.a.	n.a.	n.a.	n.a.	n.a.	n.a.
11.0	n.a.	n.a.	n.a.	n.a.	n.a.	n.a.	n.a.	n.a.

Depth [m]	TEX ₈₆	log TEX ₈₆	SST (°C) ¹⁾	SST (°C) ²⁾	SST (°C) ³⁾	SST (°C) ⁴⁾	SST (°C) ⁵⁾	SST (°C) ⁶⁾
11.2	n.a.	n.a.	n.a.	n.a.	n.a.	n.a.	n.a.	n.a.
11.4	0.667	-0.176	25.8	26.7	24.1	25.1	27.7	26.0
11.8	0.672	-0.172	26.1	27.0	24.3	25.5	28.2	26.2
12.0	n.a.	n.a.	n.a.	n.a.	n.a.	n.a.	n.a.	n.a.
12.2	0.700	-0.155	28.0	28.6	25.3	27.4	30.5	27.2
12.4	n.a.	n.a.	n.a.	n.a.	n.a.	n.a.	n.a.	n.a.
12.6	n.a.	n.a.	n.a.	n.a.	n.a.	n.a.	n.a.	n.a.
12.8	0.673	-0.172	26.2	27.0	24.3	25.5	28.2	26.2
13.0	0.693	-0.159	27.6	28.2	25.1	26.9	29.9	26.9
13.2	0.734	-0.134	30.3	30.5	26.6	29.6	33.2	28.2
13.4	n.a.	n.a.	n.a.	n.a.	n.a.	n.a.	n.a.	n.a.
13.6	n.a.	n.a.	n.a.	n.a.	n.a.	n.a.	n.a.	n.a.
13.8	n.a.	n.a.	n.a.	n.a.	n.a.	n.a.	n.a.	n.a.
14.0	n.a.	n.a.	n.a.	n.a.	n.a.	n.a.	n.a.	n.a.
14.2	0.660	-0.181	25.3	26.3	23.8	24.7	27.2	25.7
14.4	0.689	-0.162	27.3	27.9	24.9	26.6	29.5	26.8
14.6	n.a.	n.a.	n.a.	n.a.	n.a.	n.a.	n.a.	n.a.
14.8	n.a.	n.a.	n.a.	n.a.	n.a.	n.a.	n.a.	n.a.
15.0	n.a.	n.a.	n.a.	n.a.	n.a.	n.a.	n.a.	n.a.
15.2	n.a.	n.a.	n.a.	n.a.	n.a.	n.a.	n.a.	n.a.
15.4	n.a.	n.a.	n.a.	n.a.	n.a.	n.a.	n.a.	n.a.
15.6	n.a.	n.a.	n.a.	n.a.	n.a.	n.a.	n.a.	n.a.
16.0	0.691	-0.160	27.4	28.1	25.0	26.8	29.8	26.9
16.2	0.679	-0.168	26.6	27.4	24.5	25.9	28.7	26.4
16.4	n.a.	n.a.	n.a.	n.a.	n.a.	n.a.	n.a.	n.a.
16.6	n.a.	n.a.	n.a.	n.a.	n.a.	n.a.	n.a.	n.a.
16.8	n.a.	n.a.	n.a.	n.a.	n.a.	n.a.	n.a.	n.a.
17.0	n.a.	n.a.	n.a.	n.a.	n.a.	n.a.	n.a.	n.a.
17.2	n.a.	n.a.	n.a.	n.a.	n.a.	n.a.	n.a.	n.a.
17.6	n.a.	n.a.	n.a.	n.a.	n.a.	n.a.	n.a.	n.a.
17.8	n.a.	n.a.	n.a.	n.a.	n.a.	n.a.	n.a.	n.a.
18.0	0.694	-0.159	27.6	28.2	25.1	26.9	29.9	26.9
18.2	0.661	-0.180	25.4	26.4	23.9	24.7	27.2	25.8
18.4	n.a.	n.a.	n.a.	n.a.	n.a.	n.a.	n.a.	n.a.
18.6	0.662	-0.179	25.5	26.4	23.9	24.8	27.4	25.8
18.8	n.a.	n.a.	n.a.	n.a.	n.a.	n.a.	n.a.	n.a.
19.0	n.a.	n.a.	n.a.	n.a.	n.a.	n.a.	n.a.	n.a.
19.2	n.a.	n.a.	n.a.	n.a.	n.a.	n.a.	n.a.	n.a.
19.4	n.a.	n.a.	n.a.	n.a.	n.a.	n.a.	n.a.	n.a.
19.6	n.a.	n.a.	n.a.	n.a.	n.a.	n.a.	n.a.	n.a.
20.0	n.a.	n.a.	n.a.	n.a.	n.a.	n.a.	n.a.	n.a.
20.2	n.a.	n.a.	n.a.	n.a.	n.a.	n.a.	n.a.	n.a.
20.4	n.a.	n.a.	n.a.	n.a.	n.a.	n.a.	n.a.	n.a.
20.6	0.680	-0.168	26.6	27.4	24.6	26.0	28.8	26.4

Appendix

Depth [m]	TEX ₈₆	log TEX ₈₆	SST (°C) ¹⁾	SST (°C) ²⁾	SST (°C) ³⁾	SST (°C) ⁴⁾	SST (°C) ⁵⁾	SST (°C) ⁶⁾
20.8	n.a.	n.a.	n.a.	n.a.	n.a.	n.a.	n.a.	n.a.
21.0	n.a.	n.a.	n.a.	n.a.	n.a.	n.a.	n.a.	n.a.
21.2	0.703	-0.153	28.2	28.8	25.5	27.6	30.7	27.3
21.4	n.a.	n.a.	n.a.	n.a.	n.a.	n.a.	n.a.	n.a.
21.8	n.a.	n.a.	n.a.	n.a.	n.a.	n.a.	n.a.	n.a.
22.0	0.685	-0.164	27.0	27.7	24.8	26.4	29.3	26.6
22.2	n.a.	n.a.	n.a.	n.a.	n.a.	n.a.	n.a.	n.a.
22.4	0.706	-0.151	28.4	28.9	25.6	27.8	31.0	27.4
22.6	n.a.	n.a.	n.a.	n.a.	n.a.	n.a.	n.a.	n.a.
22.8	n.a.	n.a.	n.a.	n.a.	n.a.	n.a.	n.a.	n.a.
23.0	n.a.	n.a.	n.a.	n.a.	n.a.	n.a.	n.a.	n.a.
23.2	n.a.	n.a.	n.a.	n.a.	n.a.	n.a.	n.a.	n.a.
23.4	n.a.	n.a.	n.a.	n.a.	n.a.	n.a.	n.a.	n.a.
23.6	0.698	-0.156	27.9	28.4	25.3	27.2	30.3	27.1
23.8	n.a.	n.a.	n.a.	n.a.	n.a.	n.a.	n.a.	n.a.
24.0	0.681	-0.167	26.7	27.5	24.6	26.1	28.9	26.5
24.2	n.a.	n.a.	n.a.	n.a.	n.a.	n.a.	n.a.	n.a.
24.4	n.a.	n.a.	n.a.	n.a.	n.a.	n.a.	n.a.	n.a.
24.6	n.a.	n.a.	n.a.	n.a.	n.a.	n.a.	n.a.	n.a.
24.8	0.698	-0.156	27.9	28.5	25.3	27.2	30.3	27.1
25.0	n.a.	n.a.	n.a.	n.a.	n.a.	n.a.	n.a.	n.a.
25.4	0.678	-0.169	26.5	27.3	24.5	25.9	28.7	26.4
25.6	0.667	-0.176	25.8	26.7	24.1	25.1	27.7	26.0
25.8	0.684	-0.165	26.9	27.7	24.7	26.3	29.1	26.6
26.0	0.692	-0.160	27.5	28.1	25.0	26.8	29.8	26.9
26.2	0.687	-0.163	27.1	27.8	24.9	26.5	29.4	26.7
26.4	n.a.	n.a.	n.a.	n.a.	n.a.	n.a.	n.a.	n.a.
26.6	0.680	-0.167	26.7	27.4	24.6	26.0	28.8	26.5
26.8	0.668	-0.175	25.8	26.7	24.1	25.2	27.8	26.0
27.2	0.678	-0.169	26.6	27.3	24.5	25.9	28.7	26.4
27.4	0.675	-0.171	26.3	27.1	24.4	25.6	28.4	26.3
27.6	0.696	-0.158	27.7	28.3	25.2	27.0	30.1	27.0
27.8	0.696	-0.157	27.8	28.4	25.2	27.1	30.2	27.0
28.0	0.686	-0.163	27.1	27.8	24.8	26.4	29.3	26.7
28.2	0.689	-0.162	27.3	28.0	24.9	26.6	29.6	26.8
28.4	0.677	-0.170	26.4	27.2	24.5	25.8	28.5	26.3
28.6	n.a.	n.a.	n.a.	n.a.	n.a.	n.a.	n.a.	n.a.
28.8	0.667	-0.176	25.8	26.7	24.1	25.2	27.8	26.0
29.0	0.699	-0.155	27.9	28.5	25.3	27.3	30.4	27.1
29.4	0.672	-0.173	26.1	27.0	24.3	25.4	28.1	26.2
29.6	0.681	-0.167	26.7	27.5	24.6	26.1	28.9	26.5
29.8	0.725	-0.140	29.6	29.9	26.2	29.0	32.5	27.9
30.0	0.665	-0.177	25.6	26.6	24.0	25.0	27.6	25.9
30.2	n.a.	n.a.	n.a.	n.a.	n.a.	n.a.	n.a.	n.a.
30.4	0.675	-0.171	26.3	27.2	24.4	25.7	28.4	26.3
30.6	n.a.	n.a.	n.a.	n.a.	n.a.	n.a.	n.a.	n.a.
30.8	n.a.	n.a.	n.a.	n.a.	n.a.	n.a.	n.a.	n.a.

Depth [m]	TEX ₈₆	log TEX ₈₆	SST (°C) ¹⁾	SST (°C) ²⁾	SST (°C) ³⁾	SST (°C) ⁴⁾	SST (°C) ⁵⁾	SST (°C) ⁶⁾
31.0	0.698	-0.156	27.9	28.5	25.3	27.2	30.3	27.1
31.2	0.672	-0.172	26.1	27.0	24.3	25.5	28.2	26.2
31.4	0.714	-0.146	29.0	29.4	25.9	28.3	31.6	27.6
31.6	0.684	-0.165	27.0	27.7	24.8	26.3	29.2	26.6
31.8	0.676	-0.170	26.4	27.2	24.5	25.8	28.5	26.3
32.0	n.a.	n.a.	n.a.	n.a.	n.a.	n.a.	n.a.	n.a.
32.2	0.669	-0.175	25.9	26.8	24.2	25.3	27.9	26.1
32.4	0.656	-0.183	25.1	26.1	23.7	24.4	26.9	25.6
32.6	0.690	-0.161	27.3	28.0	25.0	26.7	29.6	26.8
32.8	0.687	-0.163	27.1	27.8	24.8	26.4	29.4	26.7
33.0	0.704	-0.153	28.3	28.8	25.5	27.6	30.8	27.3
33.2	0.711	-0.148	28.7	29.2	25.7	28.1	31.4	27.5
33.4	n.a.	n.a.	n.a.	n.a.	n.a.	n.a.	n.a.	n.a.
33.6	0.683	-0.165	26.9	27.6	24.7	26.2	29.1	26.6
33.8	0.702	-0.154	28.1	28.7	25.4	27.5	30.6	27.2
34.0	0.661	-0.180	25.4	26.4	23.9	24.8	27.3	25.8
34.2	0.725	-0.140	29.7	30.0	26.3	29.0	32.5	28.0
34.4	0.691	-0.160	27.4	28.1	25.0	26.8	29.8	26.9
34.6	0.664	-0.178	25.6	26.6	24.0	25.0	27.6	25.9
34.8	0.695	-0.158	27.7	28.3	25.2	27.0	30.1	27.0
35.0	0.703	-0.153	28.2	28.7	25.4	27.5	30.7	27.2
35.2	n.a.	n.a.	n.a.	n.a.	n.a.	n.a.	n.a.	n.a.
35.4	0.721	-0.142	29.4	29.7	26.1	28.7	32.2	27.8
35.6	0.732	-0.135	30.2	30.4	26.5	29.5	33.1	28.2
36.0	n.a.	n.a.	n.a.	n.a.	n.a.	n.a.	n.a.	n.a.
36.2	n.a.	n.a.	n.a.	n.a.	n.a.	n.a.	n.a.	n.a.
36.6	0.651	-0.186	24.7	25.8	23.5	24.1	26.5	25.4
37.0	0.685	-0.164	27.0	27.7	24.8	26.3	29.2	26.6
37.4	0.660	-0.180	25.3	26.3	23.9	24.7	27.2	25.7
37.6	0.749	-0.126	31.3	31.3	27.1	30.6	34.4	28.7
38.0	n.a.	n.a.	n.a.	n.a.	n.a.	n.a.	n.a.	n.a.
38.4	0.655	-0.183	25.0	26.1	23.7	24.4	26.8	25.6
38.6	0.762	-0.118	32.1	32.0	27.6	31.5	35.5	29.0
38.8	0.687	-0.163	27.1	27.8	24.8	26.4	29.4	26.7
39.0	n.a.	n.a.	n.a.	n.a.	n.a.	n.a.	n.a.	n.a.
39.2	n.a.	n.a.	n.a.	n.a.	n.a.	n.a.	n.a.	n.a.
39.4	0.677	-0.169	26.5	27.3	24.5	25.8	28.6	26.4
39.8	0.713	-0.147	28.9	29.3	25.8	28.2	31.5	27.6
40.0	0.721	-0.142	29.4	29.8	26.1	28.7	32.2	27.8
40.2	n.a.	n.a.	n.a.	n.a.	n.a.	n.a.	n.a.	n.a.
41.0	n.a.	n.a.	n.a.	n.a.	n.a.	n.a.	n.a.	n.a.
41.6	n.a.	n.a.	n.a.	n.a.	n.a.	n.a.	n.a.	n.a.
41.8	n.a.	n.a.	n.a.	n.a.	n.a.	n.a.	n.a.	n.a.
42.0	n.a.	n.a.	n.a.	n.a.	n.a.	n.a.	n.a.	n.a.
42.2	0.701	-0.154	28.1	28.6	25.4	27.4	30.5	27.2
42.4	n.a.	n.a.	n.a.	n.a.	n.a.	n.a.	n.a.	n.a.
42.6	n.a.	n.a.	n.a.	n.a.	n.a.	n.a.	n.a.	n.a.

Appendix

Depth [m]	TEX ₈₆	log TEX ₈₆	SST (°C) ¹⁾	SST (°C) ²⁾	SST (°C) ³⁾	SST (°C) ⁴⁾	SST (°C) ⁵⁾	SST (°C) ⁶⁾
42.8	0.701	-0.154	28.1	28.6	25.4	27.4	30.6	27.2
43.0	n.a.	n.a.	n.a.	n.a.	n.a.	n.a.	n.a.	n.a.
43.2	0.682	-0.166	26.8	27.6	24.7	26.1	29.0	26.5
43.4	0.668	-0.175	25.9	26.8	24.2	25.2	27.9	26.0
43.6	n.a.	n.a.	n.a.	n.a.	n.a.	n.a.	n.a.	n.a.
43.8	0.676	-0.170	26.4	27.2	24.5	25.7	28.5	26.3
44.2	0.681	-0.167	26.7	27.5	24.6	26.0	28.9	26.5
44.4	n.a.	n.a.	n.a.	n.a.	n.a.	n.a.	n.a.	n.a.
44.8	n.a.	n.a.	n.a.	n.a.	n.a.	n.a.	n.a.	n.a.
45.0	n.a.	n.a.	n.a.	n.a.	n.a.	n.a.	n.a.	n.a.
45.2	n.a.	n.a.	n.a.	n.a.	n.a.	n.a.	n.a.	n.a.
45.4	n.a.	n.a.	n.a.	n.a.	n.a.	n.a.	n.a.	n.a.
45.6	n.a.	n.a.	n.a.	n.a.	n.a.	n.a.	n.a.	n.a.
45.8	n.a.	n.a.	n.a.	n.a.	n.a.	n.a.	n.a.	n.a.
46.0	0.634	-0.198	23.6	24.9	22.9	23.0	25.1	24.7
46.2	n.a.	n.a.	n.a.	n.a.	n.a.	n.a.	n.a.	n.a.
46.4	0.677	-0.169	26.5	27.3	24.5	25.8	28.6	26.4
46.8	0.672	-0.172	26.2	27.0	24.3	25.5	28.2	26.2
47.6	n.a.	n.a.	n.a.	n.a.	n.a.	n.a.	n.a.	n.a.
47.8	n.a.	n.a.	n.a.	n.a.	n.a.	n.a.	n.a.	n.a.
48.0	n.a.	n.a.	n.a.	n.a.	n.a.	n.a.	n.a.	n.a.
48.2	0.672	-0.173	26.1	27.0	24.3	25.4	28.1	26.2
48.4	n.a.	n.a.	n.a.	n.a.	n.a.	n.a.	n.a.	n.a.
48.8	n.a.	n.a.	n.a.	n.a.	n.a.	n.a.	n.a.	n.a.
49.0	n.a.	n.a.	n.a.	n.a.	n.a.	n.a.	n.a.	n.a.
49.2	n.a.	n.a.	n.a.	n.a.	n.a.	n.a.	n.a.	n.a.
49.4	n.a.	n.a.	n.a.	n.a.	n.a.	n.a.	n.a.	n.a.
49.6	n.a.	n.a.	n.a.	n.a.	n.a.	n.a.	n.a.	n.a.

Table A-3 Distribution of reconstructed SSTs covering the Santonian to early Maastrichtian from this study and other published data.

- 1) This study: PAMA quarry, Efe Syncline (8-15°N; paleo inner belt)
- 2) This study: Aderet 1 borehole, Shefela basin (8-15°N; paleo outer belt)
- 3) Forster et al. (2007a), SST calculated from TEX₈₆ values of samples from western equatorial Atlantic (ODP Leg 207 Site 1259), 5°N
- 4) Jenkyns et al. (2004), SST calculated from TEX₈₆ values of samples from the Arctic Ocean (FI-437 and FI-533), 80°N
- 5) Liu (2009), SSTs calculated based on the calibration of Erez and Luz (1983) from $\delta^{18}\text{O}$ of bulk material from the Mooreville Chalk of the eastern Gulf Coastal Plain, U.S.A., 30-35°N

	1		2		3		4		5	
Age (Ma)	SST (°C)	Age (Ma)	SST (°C)	Age (Ma)	SST (°C)	Age (Ma)	SST (°C)	Age (Ma)	SST (°C)	
69.83	23.5	68.25	28.6	83.8	32.6	70	15	80.2	24	
69.85	28.8	68.50	29.8	84	33.1			80.3	24	
69.87	24.1	68.75	28.9	84.5	33.7			80.4	24.4	
69.89	25.4	68.80	29.4	84.9	34.7			80.5	24.8	
69.91	25.4	68.85	28.8	85.5	34.4			80.6	25.3	

1		2		5	
Age (Ma)	SST (°C)	Age (Ma)	SST (°C)	Age (Ma)	SST (°C)
69.92	29.5	68.92	31.3	80.7	26.4
69.97	27.0	69.02	28.9	80.8	27
69.98	28.7	69.08	27.2	80.9	27.1
70.00	26.1	69.17	26.5	81	27.2
70.01	28.3	69.25	26.8	81.1	27.2
70.02	27.3	69.26	27.7	81.2	27.2
70.05	25.8	69.42	25.0	81.3	27.6
70.06	26.9	69.44	27.7	81.4	27.6
70.08	27.6	69.52	28.2	81.5	27.5
70.09	26.8	69.60	27.2	81.6	27.7
70.11	25.5	69.70	28.8	81.7	27.7
70.12	27.6	69.75	30.7	81.8	27.8
70.13	28.2	69.83	28.0	81.9	27.8
70.14	29.1	69.93	29.3	82	28.1
70.15	27.6	70.00	28.9	82.1	28.5
70.17	28.0	70.10	28.3	82.2	28.5
70.18	30.4	70.13	30.0	82.3	28.3
70.19	24.1	70.17	31.1	82.4	28.7
70.23	26.7	70.28	28.9	82.5	28.7
70.24	27.0	70.35	30.4	82.6	28.5
70.26	28.6	70.40	29.2	82.7	28.3
70.29	27.0	70.45	29.1	82.8	28.3
70.29	28.2	70.50	29.3	82.9	28.5
70.30	30.5	70.60	30.6	83	28.5
70.35	26.3	70.70	31.0	83.1	28.8
70.36	27.9	70.77	28.0	83.2	29.3
70.43	28.1	70.80	29.3	83.3	29.7
70.44	27.4	70.92	28.9	83.4	30
70.52	28.2	71.00	28.3	83.5	30.3
70.53	26.4	71.05	30.0	83.6	30.8
70.55	26.4	71.10	28.1	83.7	31
70.64	27.4	71.15	28.2	83.8	30.9
70.67	28.8	71.20	29.2	83.9	30
70.70	27.7	71.25	29.6	84	29.3
70.72	28.9	71.30	29.3	84.1	28.6
70.78	28.4	71.45	28.7	84.2	28.7
70.80	27.5	71.50	31.4		
70.84	28.5	72.05	29.9		
70.86	27.3	72.55	31.2		
70.87	26.7	73.00	29.6		
70.88	27.7	73.50	30.1		
70.89	28.1	73.92	29.3		
70.90	27.8	74.66	30.8		
70.92	27.4	74.83	30.0		
70.93	26.7	75.00	29.1		
70.94	27.3	75.30	29.7		
70.95	27.1	75.40	29.8		
70.96	28.3	75.84	29.1		
70.97	28.4	76.16	24.4		

Appendix

1		2	
Age (Ma)	SST (°C)	Age (Ma)	SST (°C)
70.98	27.8	76.50	22.5
70.99	28.0	76.83	30.8
71.00	27.2	77.16	29.3
71.02	26.7	77.50	28.3
71.03	28.5	77.80	29.4
71.04	27.0	78.16	30.6
71.05	27.5	78.40	31.1
71.06	29.9	79.60	29.6
71.07	26.6	80.30	30.4
71.09	27.2	81.10	32.7
71.12	28.5	81.92	33.6
71.13	27.0	82.67	34.5
71.14	29.4	83.50	33.1
71.15	27.7	83.75	34.0
71.16	27.2	83.83	35.0
71.17	26.8	84.00	36.1
71.18	26.1		
71.19	28.0		
71.20	27.8		
71.21	28.8		
71.22	29.2		
71.24	27.6		
71.25	28.7		
71.26	26.4		
71.27	30.0		
71.28	28.1		
71.29	26.6		
71.30	28.3		
71.31	28.7		
71.33	29.7		
71.34	30.4		
71.37	25.8		
71.38	27.7		
71.39	26.3		
71.40	31.3		
71.42	26.1		
71.43	32.0		
71.44	27.8		
71.47	27.3		
71.48	29.3		
71.49	29.8		
71.56	28.6		
71.59	28.6		
71.61	27.6		
71.62	26.8		
71.64	27.2		
71.65	27.5		
71.73	24.9		
71.75	27.3		

1	
Age (Ma)	SST (°C)
71.76	27.0
71.80	27.0

Continuation of Table A-3

- 6) Friedrich et al. (2012), water temperatures from $\delta^{18}\text{O}$ values of benthic foraminifera from the subtropical south Atlantic, Walvis Ridge, Deep Sea Drilling Project (DSDP) 525, 30°S
- 7) Friedrich et al. (2012), water temperatures from $\delta^{18}\text{O}$ values of benthic foraminifera from the South Atlantic (Maud Rise, ODP Leg 113 Site 690 C, 65°S; Falkland Plateau DSDP 511, 51°S) and Indian Ocean, Wombat Plateau, ODP Leg 120 Site 750, 57°S
- 8) Friedrich et al. (2012), SSTs from $\delta^{18}\text{O}$ values of benthic foraminifera from the tropical Pacific Ocean at Shatsky Rise and (DSDP 305 and 463), 10°N and 5°S respectively
- 9) Friedrich et al. (2012), water temperatures from $\delta^{18}\text{O}$ values of benthic foraminifera from the North Atlantic, Demerara Rise, 5°N

6		7		8		9	
Age (Ma)	SST (°C)	Age (Ma)	SST (°C)	Age (Ma)	SST (°C)	Age (Ma)	SST (°C)
65.6	12.5	65.6	10.5	67.2	10.5	65.6	13.5
66.0	11.7	66.0	10.6	67.6	10.5	66	12.3
66.4	11.5	66.4	10.4	68.0	10.5	66.4	11.5
66.8	11.5	66.8	10.4	68.4	11.4	66.8	11.2
67.2	12.0	67.2	10.2	68.8	11.4	67.2	11.2
67.6	12.5	67.6	9.9	69.2	10.5	67.6	11.2
68.0	12.8	68.0	10.0	69.6	9.6	68.0	11.4
68.4	13.5	68.4	9.5	70.0	9.2	68.4	11.6
68.8	13.0	68.8	10.3	70.4	9.2	68.8	12.0
69.2	12.3	69.2	10.4	70.8	10.0	69.2	11.5
69.6	11.4	69.6	9.9	71.2	10.9	69.6	10.7
70.0	11.6	70.0	9.7	71.6	11.6	70.0	10.4
70.4	12	70.4	10.4	72.0	12.4	70.4	9.9
70.8	13.5	70.8	10.7	72.4	12.4	70.8	9.4
71.2	14.5	71.2	11.4	72.8	12.4	71.2	9.9
71.6	14.5	71.6	11.4	73.2	12.7	71.6	11.4
72	14.5	72.0	11.6	73.6	13.2	72	11.5
72.4	14.9	72.4	12.0	74.0	13.2	75.6	12.5
72.8	14.9	72.8	11.5	74.4	13.4	76	13.5
73.2	15.3	73.2	12.3	74.8	13.4	76.4	14.4
73.6	16	73.6	12.8	75.2	13.2	76.8	14.5
		74.0	13.5	75.6	12.7	77.2	14.5
		74.4	13.8	76.0	12.4		
		74.8	14.0	78.0	11.4		
		75.2	14.4	78.4	10.9		
		75.6	14.5	78.8	11.4		
		79.2	15.6	79.2	11.6		
		79.6	15.8	79.6	11.6		
		80.0	16.0	80.0	11.8		
		80.4	16.2	80.4	11.6		
		80.8	16.4	80.8	12.2		

7		8	
Age (Ma)	SST °C	Age (Ma)	SST °C
81.2	16.5	81.2	12.7
81.6	16.6	81.6	13.2
82.0	16.6	82.0	14.0
82.4	16.7	82.4	14.0
82.8	17.4	82.8	14.0
83.2	17.5	83.2	14.0
83.6	17.6	83.6	14.2
84	17.7	84.0	15.2
84.4	17.8	84.4	16.3
84.8	18.0	84.8	16.9
		85.2	18.5
		85.6	18.5
		86	18.5

Continuation of Table A-3

- 10) Friedrich et al. (2004), SSTs from $\delta^{18}\text{O}$ values of planktic foraminifera from the Blake Plateau western Atlantic DSDP Leg 74 Site 390 A, 30°N
- 11) Li and Keller (1999), SSTs range calculated from $\delta^{18}\text{O}$ values of planktic foraminifera and from the equatorial Pacific DSDP Site 463, 5°S
- 12) Wilson and Opdyke (1996) SSTs range calculated from $\delta^{18}\text{O}$ values of planktic foraminifera from Leg 144 of the Ocean Drilling Program (ODP), Hole 877A, equatorial Pacific, 8°S
- 13) Pearson et al. (2001), SSTs range calculated from $\delta^{18}\text{O}$ values of planktic foraminifera from Lindi, Tanzania (19°S)

10		11		12		13	
Age (Ma)	SST (°C)	Age (Ma)	SST (°C)	Age (Ma)	SST (°C)	Age (Ma)	SST (°C)
69.6	16.7	69.15	17.1	69±1 Ma	27-32	67±2	26-32
69.7	17.1	69.2	18.1				
69.8	17.0	69.3	17.8				
69.9	16.6	69.35	17.4				
70.0	16.5	69.4	17.9				
70.1	16.1	69.5	18.0				
70.2	16.8	69.55	17.8				
70.3	16.3	69.7	17.6				
70.4	16.7	69.8	17.4				
70.5	17.1	69.9	17.25				
70.6	16.4	70.0	17.8				
70.7	15.9	70.1	18.5				
70.8	16.8	70.15	17.6				
70.9	16.6	70.2	17.4				
71.0	16.7	70.2	17.4				
71.1	16.8	70.3	18.0				
71.2	16.8	70.4	18.7				
		70.4	17.8				
		70.5	17.9				
		70.6	18.4				
		70.65	18.2				
		70.7	18.2				
		70.8	18.3				

11

Age (Ma)	SST (°C)
70.9	19.2
71.1	18.7
71.3	17.5
71.4	17.6
71.5	18.4
71.6	17.8
71.7	18.2
71.8	17.3
71.9	18.5
72.3	18.2
72.4	18.3
72.5	18.2
72.7	17.5
72.8	19.0
72.9	18.6
74.0	18.1
74.1	18.9
74.2	18.8
74.3	18.0
74.4	18.0
74.5	18.0
74.6	20.2
74.7	19.5
74.8	17.6
75.0	17.3
75.3	17.8
75.3	18.0
75.35	18.8
75.5	17.0
75.6	17.7

Table A-4 Depth and variation in TOC, calculated original TOC (TOC_{OR}), TOC/TOC_{OR} ratio, TFe, TS, TP and CPI (n.d. not detected, n.a. not analyzed).

Depth [m]	TOC [%]	TOC _{OR}	TOC/TOC _{OR}	TFe [%]	TS (%)	TP [%]	CPI*
0.0	1.0	1.0	1.0	1.4	n.a.	1.1	n.d.
0.2	1.0	n.a.	n.a.	n.a.	n.a.	n.a.	n.d.
0.6	0.8	n.a.	n.a.	1.8	n.a.	1.0	n.d.
0.8	0.7	1.1	0.6	1.8	0.3	0.9	n.d.
1.0	0.6	3.9	0.1	1.5	2.9	0.6	n.d.
1.2	0.9	1.2	0.8	1.8	0.3	1.0	n.d.
1.4	0.9	1.2	0.8	1.9	0.2	0.8	n.d.
1.6	0.7	n.a.	n.a.	n.a.	n.a.	n.a.	n.d.
1.8	0.9	1.1	0.8	1.9	0.2	0.8	n.d.
2.0	0.8	2.4	0.3	2.1	1.4	0.5	n.d.
2.2	0.8	1.0	0.9	1.6	0.1	1.2	n.d.
2.4	1.0	1.2	0.9	1.9	0.1	0.8	n.a.
2.6	1.4	n.d.	n.d.	2.1	n.d.	n.d.	1.5
3.0	0.6	n.d.	n.d.	2.3	n.d.	n.d.	n.a.
3.4	7.5	8.9	0.8	2.1	1.2	0.5	n.a.

Appendix

Depth [m]	TOC [%]	TOC _{OR}	TOC/TOC _{OR}	TFe [%]	TS (%)	TP [%]	CPI*
3.6	7.9	n.a.	n.a.	n.a.	n.a.	n.a.	2.6
3.8	8.2	9.5	0.9	2.3	1.2	0.4	2.6
4.0	8.2	9.7	0.8	2.5	1.3	0.5	3.1
4.2	7.2	8.6	0.8	2.5	1.2	0.7	3.0
4.4	9.0	10.6	0.8	2.3	1.4	0.7	3.3
4.6	10.8	12.5	0.9	2.4	1.5	0.6	3.1
4.8	11.5	13.4	0.9	2.6	1.7	0.5	n.a.
5.4	10.2	11.9	0.9	2.4	1.5	0.4	2.7
5.6	9.8	11.5	0.9	2.5	1.5	0.4	2.7
5.8	7.7	9.0	0.9	2.7	1.2	0.5	n.a.
6.0	7.6	9.1	0.8	2.7	1.3	0.5	3.2
6.2	9.3	10.8	0.9	2.6	1.3	0.5	3.2
6.6	10.3	12.0	0.9	2.3	1.5	0.6	3.1
6.8	9.3	10.8	0.9	2.4	1.3	0.6	3.0
7.0	8.7	10.3	0.8	2.5	1.4	0.6	3.3
7.2	8.3	10.0	0.8	3.0	1.5	0.6	n.a.
7.4	7.5	9.0	0.8	2.7	1.3	0.4	n.a.
7.6	7.8	9.2	0.8	2.4	1.2	0.5	2.8
7.8	7.9	9.4	0.8	2.4	1.3	0.5	2.9
8.0	7.5	8.9	0.8	2.2	1.2	0.4	n.a.
8.2	8.3	9.7	0.9	2.1	1.3	0.3	n.a.
8.4	11.6	n.a.	n.a.	n.a.	n.a.	n.a.	3.0
8.6	9.4	11.0	0.9	1.8	1.3	0.6	n.a.
8.8	8.6	10.3	0.8	2.0	1.5	0.5	2.0
9.0	10.6	12.2	0.9	2.0	1.4	0.4	3.1
9.2	7.7	9.0	0.9	1.9	1.1	0.3	3.2
9.4	6.2	7.5	0.8	1.9	1.2	0.4	2.9
9.6	9.9	11.4	0.9	1.6	1.3	0.4	3.1
9.8	7.7	n.a.	n.a.	n.a.	n.a.	n.a.	n.a.
10.0	7.1	8.4	0.8	1.4	1.1	0.3	2.1
10.2	7.8	9.1	0.9	1.6	1.1	0.2	3.0
10.4	8.0	9.5	0.8	1.7	1.3	0.2	2.7
10.8	9.4	10.8	0.9	1.6	1.3	0.3	n.a.
11.0	10.2	11.9	0.9	1.8	1.5	0.3	n.a.
11.2	7.3	8.7	0.8	1.6	1.2	0.4	n.a.
11.4	10.1	11.9	0.9	1.8	1.5	0.4	3.3
11.8	9.3	11.0	0.8	1.7	1.4	0.4	3.1
12.0	10.2	n.a.	n.a.	n.a.	n.a.	n.a.	n.a.
12.2	9.1	10.5	0.9	1.5	1.2	0.3	3.4
12.4	9.4	10.8	0.9	1.7	1.3	0.3	n.a.
12.6	9.1	10.6	0.9	1.8	1.3	0.4	n.a.
12.8	7.1	8.4	0.8	1.7	1.2	0.4	3.3
13.0	7.6	8.8	0.9	1.4	1.0	0.3	3.1
13.2	6.8	7.9	0.9	1.3	0.9	0.3	3.2
13.4	7.6	8.8	0.9	1.7	1.1	0.4	n.a.
13.6	7.5	8.8	0.9	1.7	1.1	0.5	n.a.
13.8	11.5	13.5	0.9	2.3	1.7	0.9	n.a.

Depth [m]	TOC [%]	TOC _{OR}	TOC/TOC _{OR}	TFe [%]	TS (%)	TP [%]	CPI*
14.0	n.a.	n.a.	n.a.	2.2	1.7	0.9	n.a.
14.2	11.5	13.3	0.9	1.9	1.6	0.6	3.0
14.4	11.2	13.1	0.9	2.1	1.7	0.8	n.a.
14.6	12.1	14.0	0.9	1.9	1.6	0.7	2.8
14.8	11.5	13.3	0.9	2.0	1.6	1.0	n.a.
15.0	11.5	13.5	0.9	2.1	1.8	0.9	n.a.
15.2	13.3	15.5	0.9	2.3	1.9	0.9	n.a.
15.4	11.8	13.8	0.9	2.1	1.7	0.9	n.a.
15.6	11.2	13.0	0.9	1.7	1.6	0.8	n.a.
16.0	12.7	14.7	0.9	1.8	1.7	0.8	3.0
16.2	12.5	14.6	0.9	2.2	1.9	1.0	3.2
16.4	12.4	14.5	0.9	2.0	1.8	0.8	n.a.
16.6	12.2	14.3	0.9	2.1	1.8	0.9	n.a.
16.8	12.8	14.8	0.9	2.2	1.8	0.8	n.a.
17.0	13.0	15.2	0.9	2.6	1.9	0.9	n.a.
17.6	13.4	15.5	0.9	2.1	1.8	0.9	n.a.
17.8	6.2	7.7	0.8	1.5	1.3	0.5	n.a.
18.0	13.0	15.3	0.9	2.5	2.0	0.9	2.7
18.2	12.4	14.6	0.9	2.7	1.9	0.9	2.6
18.6	14.6	16.8	0.9	2.1	1.9	0.9	2.8
18.8	13.4	15.7	0.9	2.3	2.0	1.0	n.a.
19.0	6.8	n.a.	n.a.	n.a.	n.a.	n.a.	n.a.
19.4	13.5	15.8	0.9	2.3	2.0	1.1	n.a.
19.6	14.5	16.9	0.9	2.1	2.1	0.9	n.a.
20.0	13.9	16.5	0.8	2.0	2.3	1.2	n.a.
20.2	9.8	11.4	0.9	2.0	1.4	0.8	n.a.
20.4	8.3	10.0	0.8	1.9	1.5	0.7	n.a.
20.6	10.0	11.7	0.9	1.6	1.5	0.8	3.5
20.8	8.6	10.3	0.8	2.0	1.5	0.8	n.a.
21.0	10.5	12.2	0.9	2.4	1.5	0.8	n.a.
21.2	9.3	n.a.	n.a.	n.a.	n.a.	n.a.	2.9
21.4	9.4	10.9	0.9	1.9	1.3	0.6	n.a.
21.8	9.8	11.7	0.8	2.5	1.6	0.9	n.a.
22.0	11.1	13.2	0.8	3.0	1.8	1.0	n.a.
22.4	10.0	12.0	0.8	3.1	1.8	1.0	n.a.
22.6	12.2	14.6	0.8	3.0	2.1	0.9	3.5
22.8	11.8	14.1	0.8	2.9	2.0	1.1	n.a.
23.0	11.8	13.8	0.9	2.4	1.8	1.0	n.a.
23.2	7.6	9.2	0.8	2.2	1.4	0.7	n.a.
23.4	9.7	11.4	0.8	2.3	1.5	0.8	n.a.
23.6	9.2	11.1	0.8	2.1	1.7	0.8	4.0
23.8	12.6	15.0	0.8	2.8	2.1	1.2	n.a.
24.0	10.8	12.8	0.8	2.1	1.8	1.0	n.a.
24.2	10.6	12.8	0.8	2.4	1.9	1.2	n.a.

Appendix

Depth [m]	TOC [%]	TOC _{OR}	TOC/TOC _{OR}	TFe [%]	TS (%)	TP [%]	CPI*
24.4	8.5	n.a.	n.a.	n.a.	n.a.	n.a.	n.a.
24.6	12.7	14.9	0.9	2.3	2.0	1.3	n.a.
24.8	11.2	13.3	0.8	2.1	1.9	1.2	3.8
25.0	13.5	16.0	0.8	1.8	2.2	0.9	n.a.
25.4	11.6	13.7	0.8	1.8	1.8	1.0	3.6
25.6	11.2	13.1	0.9	1.6	1.7	0.7	3.5
25.8	9.7	11.5	0.8	1.6	1.6	0.7	3.2
26.0	10.2	12.6	0.8	1.5	2.1	0.6	3.1
26.2	7.7	9.4	0.8	1.5	1.4	0.5	2.7
26.4	10.2	11.8	0.9	1.4	1.4	0.5	n.a.
26.6	9.7	11.4	0.9	1.9	1.5	0.7	n.a.
26.8	11.4	13.7	0.8	2.0	2.0	0.7	3.5
27.2	10.9	12.8	0.8	2.4	1.7	0.7	2.9
27.4	15.6	18.0	0.9	2.6	2.1	1.1	3.9
27.6	11.4	13.5	0.8	2.7	1.8	0.9	3.1
27.8	10.1	12.1	0.8	2.8	1.7	1.0	3.6
28.0	10.1	12.1	0.8	2.8	1.8	0.9	3.4
28.2	11.2	13.3	0.8	3.1	1.9	1.1	n.a.
28.4	11.6	13.8	0.8	2.2	1.9	1.3	2.3
28.6	11.1	12.9	0.9	2.3	1.6	0.9	n.a.
28.8	10.0	11.9	0.8	2.7	1.7	1.0	2.8
29.0	12.5	15.0	0.8	3.2	2.2	1.2	2.6
29.4	10.6	12.6	0.8	3.0	1.8	0.9	3.1
29.6	12.4	14.6	0.8	2.3	1.9	1.2	2.9
29.8	12.6	14.5	0.9	2.1	1.7	0.9	4.4
30.0	12.1	14.2	0.9	2.3	1.8	1.0	3.3
30.2	7.9	9.8	0.8	2.3	1.6	0.9	n.a.
30.4	11.4	13.4	0.9	2.2	1.7	1.2	2.9
30.6	10.5	12.3	0.9	2.2	1.6	0.7	n.a.
30.8	11.5	13.4	0.9	2.1	1.6	0.9	3.3
31.0	16.2	18.5	0.9	2.4	2.0	0.7	3.4
31.2	14.4	16.6	0.9	2.2	2.0	0.7	3.6
31.4	12.1	n.a.	n.a.	n.a.	n.a.	n.a.	3.8
31.6	11.8	13.8	0.9	1.7	1.7	0.7	3.4
31.8	11.7	13.7	0.9	1.5	1.7	0.6	3.7
32.0	12.7	14.8	0.9	1.8	1.9	1.1	n.a.
32.2	10.4	12.1	0.9	1.7	1.4	1.0	3.6
32.4	10.1	11.7	0.9	1.7	1.4	0.9	3.5
32.6	15.4	17.8	0.9	2.3	2.1	1.6	3.8
32.8	14.8	17.3	0.9	2.3	2.2	1.4	3.5
33.0	12.8	14.8	0.9	1.5	1.8	1.1	2.7
33.2	11.5	13.4	0.9	1.8	1.7	0.8	2.7
33.4	12.6	14.8	0.9	2.0	1.9	1.0	n.a.
33.6	11.6	13.6	0.8	2.6	1.8	0.9	3.0
33.8	13.2	15.7	0.8	2.2	2.1	1.1	2.8
34.0	8.0	9.7	0.8	2.0	1.5	0.8	3.2
34.2	11.7	13.7	0.9	1.9	1.7	0.9	3.4
34.4	5.7	8.4	0.7	1.3	2.3	1.0	3.0
34.6	19.0	21.6	0.9	1.1	2.3	1.0	n.a.

Depth [m]	TOC [%]	TOC _{OR}	TOC/TOC _{OR}	TFe [%]	TS (%)	TP [%]	CPI*
34.8	17.9	20.7	0.9	1.2	2.4	1.2	3.3
35.0	13.7	15.9	0.9	1.4	1.9	1.4	2.7
35.2	13.7	16.2	0.8	1.3	2.2	1.3	n.a.
35.4	20.0	22.8	0.9	1.4	2.5	1.7	2.7
35.6	24.5	28.0	0.9	0.4	3.1	1.6	n.a.
36.0	14.4	16.9	0.9	1.6	2.2	1.5	n.a.
36.2	12.5	14.8	0.8	1.1	2.1	1.6	n.a.
36.6	15.7	18.4	0.9	1.6	2.4	1.7	3.0
37.0	18.3	21.2	0.9	1.4	2.6	1.6	2.9
37.4	17.8	20.6	0.9	0.9	2.4	1.3	3.3
37.6	15.1	17.9	0.8	1.5	2.4	2.0	3.0
38.4	16.6	19.4	0.9	0.7	2.4	2.1	3.1
38.6	19.4	22.5	0.9	0.9	2.7	2.5	1.7
38.8	19.3	22.6	0.9	0.4	2.8	1.6	2.4
39.0	21.5	25.2	0.9	0.5	3.2	1.8	n.a.
39.2	14.1	17.6	0.8	0.6	3.0	1.7	n.a.
39.4	24.2	27.8	0.9	0.4	3.1	1.7	2.8
39.8	19.5	22.7	0.9	0.6	2.8	1.4	2.6
40.0	20.0	23.3	0.9	0.4	2.9	1.5	n.a.
40.2	20.6	24.0	0.9	0.4	3.0	1.6	n.a.
41.0	18.0	21.5	0.8	0.5	3.0	0.9	2.5
41.6	18.8	21.5	0.9	0.9	2.4	1.1	n.a.
41.8	14.4	16.8	0.9	0.4	2.1	2.0	n.a.
42.0	13.5	15.8	0.9	0.4	2.0	1.1	n.a.
42.2	16.5	19.2	0.9	0.4	2.4	1.4	2.2
42.2	15.5	18.2	0.9	0.3	2.3	1.8	n.a.
42.4	20.7	24.1	0.9	0.6	3.0	0.8	n.a.
42.8	22.6	26.5	0.9	0.7	3.4	0.9	2.9
42.8	22.2	26.1	0.9	0.6	3.4	1.0	n.d.
43.0	20.6	23.9	0.9	0.6	2.9	0.9	n.d.
43.2	18.1	21.2	0.9	0.6	2.7	1.0	n.d.
43.4	16.8	19.5	0.9	0.4	2.4	1.3	n.d.
43.6	13.7	16.0	0.9	0.3	2.0	1.8	n.d.
43.8	14.8	17.2	0.9	0.3	2.1	1.3	n.d.
44.2	17.7	20.6	0.9	0.6	2.5	1.5	2.1
44.4	1.9	2.7	0.7	0.2	0.8	9.4	n.d.
44.8	3.1	n.a.	n.a.	n.a.	n.a.	11.2	n.d.
45.0	4.2	5.5	0.8	0.2	1.2	7.4	n.d.
45.2	2.1	2.9	0.7	0.1	0.7	12.9	n.d.
45.4	3.2	4.4	0.7	0.2	1.1	11.9	n.d.
45.6	4.2	5.6	0.8	0.2	1.2	12.8	n.d.
45.8	3.1	4.1	0.7	0.2	0.9	11.7	n.d.
46.0	3.6	4.3	0.8	0.1	0.7	3.9	n.d.
46.2	5.0	6.3	0.8	0.2	1.2	6.0	n.d.
46.4	2.7	3.6	0.7	0.1	0.8	6.7	n.d.
46.8	2.3	3.1	0.7	0.1	0.7	12.9	n.d.

Appendix

Depth [m]	TOC [%]	TOC _{OR}	TOC/TOC _{OR}	TFe [%]	TS (%)	TP [%]	CPI*
47.6	2.5	3.4	0.8	0.1	0.7	12.8	n.d.
47.8	2.8	3.6	0.8	0.1	0.7	14.6	n.d.
48.0	2.3	3.1	0.7	0.1	0.7	14.9	n.d.
48.2	17.2	20.3	0.8	0.6	2.7	5.5	n.d.
48.4	1.0	1.4	0.7	0.0	0.4	11.3	n.d.
48.8	1.2	1.8	0.7	0.0	0.6	12.7	n.d.
49.0	2.0	3.0	0.7	0.1	0.9	14.2	n.d.
49.2	1.9	2.8	0.7	0.1	0.8	14.4	n.d.
49.4	1.9	2.8	0.7	0.0	0.8	15.0	n.d.
49.6	2.3	3.2	0.7	0.1	0.8	13.8	n.d.

Carbon Preference Index (CPI) according to Bray and Evans (1961)

$$* \text{CPI} = \frac{1}{2} \cdot \left[\frac{C_{25} + C_{27} + C_{29} + C_{31} + C_{33}}{C_{24} + C_{26} + C_{28} + C_{30} + C_{32}} + \frac{C_{25} + C_{27} + C_{29} + C_{31} + C_{33}}{C_{26} + C_{28} + C_{30} + C_{32} + C_{34}} \right] \quad \text{Eq.-A1}$$

Table A-5 Distribution of the saturated fatty acids C_{16:0} and C_{18:0} and the monounsaturated fatty acids C_{18:1 ω 7} and C_{18:1 ω 9} over the profile in $\mu\text{g/g}$ TOC.

Depth [m]	C _{16:0}	C _{18:0}	C _{18:1ω9}	C _{18:1ω7}
0.0	n.d.	n.d.	n.d.	n.d.
0.2	n.d.	n.d.	n.d.	n.d.
0.6	n.d.	n.d.	n.d.	n.d.
0.8	n.d.	n.d.	n.d.	n.d.
1.0	n.d.	n.d.	n.d.	n.d.
1.4	n.d.	n.d.	n.d.	n.d.
1.8	n.d.	n.d.	n.d.	n.d.
2.2	n.d.	n.d.	n.d.	n.d.
3.4	n.d.	n.d.	n.d.	n.d.
3.6	10.7	8.1	1.4	0.9
3.8	n.d.	n.d.	n.d.	n.d.
4.0	3.6	4.1	0.8	0.2
4.2	6.1	9.0	0.5	n.d.
4.4	9.4	19.1	1.8	0.7
4.6	29.5	18.0	0.9	0.9
4.8	n.d.	n.d.	n.d.	n.d.
5.4	3.1	2.9	0.2	0.1
6.0	11.4	5.2	0.4	0.1
6.2	16.2	10.8	2.1	0.3
6.6	9.7	4.4	0.3	n.d.
6.8	18.4	8.7	n.d.	n.d.
7.0	16.6	7.1	0.6	0.4
7.6	4.6	3.9	0.3	0.2
7.8	10.2	3.8	0.6	0.3
8.4	21.8	8.9	0.4	n.d.
8.8	8.6	4.2	0.4	0.3
9.0	9.9	5.4	1.2	0.2
9.4	31.9	18.2	6.8	0.7
9.6	23.6	14.3	1.8	n.d.
10.2	13.7	9.4	1.1	0.3
10.4	3.6	2.3	0.4	n.d.
11.4	13.0	4.0	0.4	n.d.
11.8	14.2	8.5	1.4	0.3
12.2	11.8	6.6	1.4	0.2
12.8	25.7	11.4	0.7	n.d.

Depth [m]	C _{16.0}	C _{18.0}	C _{18.109}	C _{18.107}
13.2	20.6	8.7	1.0	n.d.
13.4	n.a.	n.a.	n.a.	n.a.
13.6	n.a.	n.a.	n.a.	n.a.
13.8	n.a.	n.a.	n.a.	n.a.
14.0	n.a.	n.a.	n.a.	n.a.
14.2	4.4	2.2	0.4	n.d.
16.0	3.2	2.5	0.5	n.d.
16.2	5.3	5.7	0.2	0.1
16.6	n.a.	n.a.	n.a.	n.a.
16.8	n.a.	n.a.	n.a.	n.a.
17.0	n.a.	n.a.	n.a.	n.a.
18.0	7.8	8.3	1.6	0.2
18.2	7.9	7.7	0.8	0.2
18.6	n.d.	n.d.	n.d.	n.d.
20.6	1.4	n.d.	n.d.	0.7
21.2	2.6	1.5	0.4	0.2
22.0	4.1	3.9	1.5	n.d.
22.6	3.0	2.0	0.10	n.d.
23.6	5.9	2.6	0.2	n.d.
24.0	3.9	3.2	0.9	0.2
24.8	6.0	2.2	0.50	0.1
25.4	9.8	8.5	1.02	0.7
25.8	8.7	4.5	n.d.	n.d.
26.0	5.5	2.9	n.d.	n.d.
26.6	20.4	13.4	1.03	0.16
26.8	36.3	16.4	1.27	0.63
27.4	11.3	3.7	1.14	0.48
27.6	6.8	2.9	0.24	n.d.
27.8	9.8	5.9	1.3	0.2
28.0	24.3	9.2	n.d.	n.d.
28.2	8.9	4.2	0.4	0.5
28.4	14.3	5.3	n.d.	n.d.
28.8	21.9	8.5	0.6	0.3
29.0	2.6	1.5	0.4	0.2
29.4	13.9	7.2	n.d.	n.d.
29.6	6.7	3.2	n.d.	n.d.
29.8	7.1	5.6	1.4	0.4
30.0	6.7	3.5	1.1	n.d.
30.4	4.1	2.3	0.2	0.1
30.8	8.4	5.3	0.9	n.d.
31.0	5.6	3.3	0.2	0.1
31.2	6.1	3.4	n.d.	0.2
31.4	10.7	8.2	n.d.	0.1
31.6	2.2	1.8	0.3	0.1
31.8	5.0	3.4	0.7	n.d.
32.2	3.7	3.1	0.1	n.d.
32.4	3.4	1.9	0.5	n.d.
32.6	4.5	2.5	n.d.	n.d.
32.8	5.8	4.0	0.4	0.48
33.0	4.6	2.4	n.d.	n.d.
33.2	4.5	4.4	n.d.	n.d.
34.0	4.7	4.5	0.4	n.d.
34.2	3.6	3.9	0.4	n.d.
34.4	11.0	5.5	n.d.	n.d.
34.6	4.0	2.8	n.d.	n.d.
34.8	5.7	3.7	0.6	n.d.
35.0	3.9	3.0	0.3	0.3
35.4	3.0	2.1	0.2	0.3
35.6	23.1	9.9	0.3	0.3
36.6	4.8	3.5	0.4	n.d.
37.0	7.6	4.4	0.4	n.d.
37.4	10.6	6.4	0.7	0.4
37.6	13.1	7.0	0.9	n.d.
38.4	n.d.	n.d.	n.d.	n.d.

Depth [m]	C _{16:0}	C _{18:0}	C _{18:1ω9}	C _{18:1ω7}
39.4	16.2	8.5	n.d.	n.d.
40.0	11.0	11.8	n.d.	0.9
41.0	10.0	7.2	1.5	n.d.
42.2	11.8	7.0	0.7	n.d.
42.8	13.6	8.7	0.8	0.2
43.2	28.2	29.2	1.4	n.d.
43.4	26.9	27.0	2.4	0.8
43.8	1.2	1.0	n.d.	0.4
44.2	3.0	2.1	1.5	n.d.
45.8	54.2	57.8	1.2	n.d.
46	33.1	34.5	0.9	n.d.
46.4	6.5	4.5	4.3	0.6
46.8	10.0	7.1	0.7	0.4
48.2	16.7	16.9	1.3	0.4
48.8	66.7	28.9	3.1	1.2

Table A-6 Distribution and proportion of sum of C₂₇–C₂₉ steranes along the Efe Syncline profile.

Depth [m]	Sum C ₂₇ steranes [μ g/g TOC]	Sum C ₂₈ steranes [μ g/g TOC]	Sum C ₂₉ steranes [μ g/g TOC]
0.0	n.d.	n.d.	n.d.
0.2	n.d.	n.d.	n.d.
0.6	n.d.	n.d.	n.d.
0.8	n.d.	n.d.	n.d.
1.0	n.d.	n.d.	n.d.
1.2	n.d.	n.d.	n.d.
1.4	n.d.	n.d.	n.d.
1.6	n.d.	n.d.	n.d.
1.8	n.d.	n.d.	n.d.
2.0	n.d.	n.d.	n.d.
2.2	n.d.	n.d.	n.d.
2.4	n.d.	n.d.	n.d.
2.6	0.8	0.1	0.4
2.8	n.a.	n.a.	n.a.
3.0	n.d.	n.d.	n.d.
3.4	n.d.	n.d.	n.d.
3.6	2.0	0.5	1.0
3.8	5.5	0.4	2.5
4.0	2.0	0.4	0.9
4.2	5.1	0.8	2.3
4.4	1.8	0.4	0.9
4.6	0.9	0.1	0.4
4.8	n.a.	n.a.	n.a.
5.4	3.0	0.5	1.3
5.6	1.6	0.3	0.7
5.8	n.a.	n.a.	n.a.
6.0	1.0	0.2	0.4
6.2	1.5	0.3	0.6
6.6	3.3	0.7	1.6
6.8	3.4	0.7	1.5
7.0	1.9	0.4	0.8
7.2	n.a.	n.a.	n.a.
7.4	n.a.	n.a.	n.a.
7.6	4.8	1.0	2.2

Depth [m]	Sum C ₂₇ steranes [μg/g TOC]	Sum C ₂₈ steranes [μg/g TOC]	Sum C ₂₉ steranes [μg/g TOC]
7.8	1.8	0.4	0.8
8.0	n.a.	n.a.	n.a.
8.2	1.4	0.3	0.7
8.4	1.1	0.2	0.5
8.6	n.a.	n.a.	n.a.
8.8	1.2	0.2	0.6
9.0	2.7	0.3	1.1
9.2	9.1	1.7	4.2
9.4	2.7	0.5	1.1
9.6	2.2	0.2	0.9
9.8	n.a.	n.a.	n.a.
10.0	1.3	0.2	0.6
10.2	2.9	0.3	1.2
10.4	3.1	0.6	1.3
10.8	n.a.	n.a.	n.a.
11.0	n.a.	n.a.	n.a.
11.2	n.a.	n.a.	n.a.
11.4	3.1	0.3	1.1
11.8	4.7	0.3	1.2
12.0	n.a.	n.a.	n.a.
12.2	2.5	0.4	1.7
12.4	n.a.	n.a.	n.a.
12.6	n.a.	n.a.	n.a.
12.8	0.8	0.1	0.3
13.0	1.1	0.2	0.5
13.2	2.1	0.5	0.9
13.4	n.a.	n.a.	n.a.
13.6	n.a.	n.a.	n.a.
13.8	n.a.	n.a.	n.a.
14.0	n.a.	n.a.	n.a.
14.2	3.6	1.2	1.7
14.4	10.7	3.3	5.0
14.6	n.a.	n.a.	n.a.
14.8	n.a.	n.a.	n.a.
15.0	n.a.	n.a.	n.a.
15.2	n.a.	n.a.	n.a.
15.4	n.a.	n.a.	n.a.
15.6	n.a.	n.a.	n.a.
16.0	3.3	1.1	1.6
16.2	9.6	2.8	4.1
16.4	n.a.	n.a.	n.a.
16.6	n.a.	n.a.	n.a.
16.8	n.a.	n.a.	n.a.
17.0	n.a.	n.a.	n.a.
17.6	n.a.	n.a.	n.a.
17.8	n.a.	n.a.	n.a.
18.0	3.3	1.0	1.4
18.2	4.3	1.3	1.7
18.6	2.2	0.7	0.9
18.8	n.a.	n.a.	n.a.

Appendix

Depth [m]	Sum C ₂₇ steranes [μg/g TOC]	Sum C ₂₈ steranes [μg/g TOC]	Sum C ₂₉ steranes [μg/g TOC]
19.0	n.a.	n.a.	n.a.
19.4	n.a.	n.a.	n.a.
19.6	n.a.	n.a.	n.a.
20.0	n.a.	n.a.	n.a.
20.2	n.a.	n.a.	n.a.
20.4	n.a.	n.a.	n.a.
20.6	3.7	1.0	1.6
20.8	n.a.	n.a.	n.a.
21.0	n.a.	n.a.	n.a.
21.2	4.4	0.4	1.1
21.4	n.a.	n.a.	n.a.
21.8	n.a.	n.a.	n.a.
22.0	n.a.	n.a.	n.a.
22.4	n.a.	n.a.	n.a.
22.6	5.1	1.4	2.2
22.8	n.a.	n.a.	n.a.
23.0	n.a.	n.a.	n.a.
23.2	n.a.	n.a.	n.a.
23.4	n.a.	n.a.	n.a.
23.6	5.8	1.9	2.7
23.8	n.a.	n.a.	n.a.
24.0	n.a.	n.a.	n.a.
24.2	n.a.	n.a.	n.a.
24.4	n.a.	n.a.	n.a.
24.6	n.a.	n.a.	n.a.
24.8	2.9	0.5	1.2
25.0	n.a.	n.a.	n.a.
25.4	2.6	0.4	1.0
25.6	1.4	0.3	0.6
25.8	4.9	0.5	1.9
26.0	4.0	0.4	1.0
26.2	n.a.	n.a.	n.a.
26.4	n.a.	n.a.	n.a.
26.6	2.8	0.3	1.2
26.8	2.6	0.2	1.2
27.2	4.5	0.0	1.5
27.4	1.6	0.3	0.7
27.6	2.9	0.3	1.1
27.8	2.6	0.3	0.9
28.0	0.8	0.1	0.3
28.2	1.0	0.2	0.4
28.4	1.2	0.2	0.5
28.6	n.a.	n.a.	n.a.
28.8	3.6	0.7	1.6
29.0	3.0	0.5	1.1
29.4	2.9	0.5	1.2
29.6	3.4	0.6	1.4
29.8	3.4	0.4	1.3
30.0	2.1	0.2	0.8
30.2	n.a.	n.a.	n.a.

Depth [m]	Sum C ₂₇ steranes [μg/g TOC]	Sum C ₂₈ steranes [μg/g TOC]	Sum C ₂₉ steranes [μg/g TOC]
30.4	3.0	0.3	1.2
30.6	n.a.	n.a.	n.a.
30.8	2.7	0.3	1.0
31.0	2.4	0.3	0.9
31.2	1.9	0.2	0.7
31.4	3.3	0.4	1.4
31.6	3.0	0.3	1.1
31.8	3.6	0.4	1.4
32.0	n.a.	n.a.	n.a.
32.2	3.3	0.4	1.2
32.4	3.6	0.5	1.4
32.6	2.4	0.6	0.9
32.8	3.5	0.9	1.5
33.0	3.1	0.7	1.2
33.2	2.3	0.3	0.9
33.4	n.a.	n.a.	n.a.
33.6	3.9	0.5	1.5
33.8	1.7	0.4	0.7
34.0	3.1	0.4	0.7
34.2	1.5	0.2	0.4
34.4	9.3	1.1	4.1
34.6	n.a.	n.a.	n.a.
34.8	3.2	0.4	1.3
35.0	4.2	0.5	1.6
35.2	n.a.	n.a.	n.a.
35.4	3.8	0.9	1.5
35.6	n.a.	n.a.	n.a.
36.0	n.a.	n.a.	n.a.
36.2	n.a.	n.a.	n.a.
36.6	3.0	0.4	0.7
37.0	2.5	0.3	1.0
37.4	2.5	0.3	1.0
37.6	3.7	0.4	1.5
38.4	3.7	0.3	1.4
38.6	2.1	0.5	0.5
38.8	1.5	0.2	0.8
39.0	n.a.	n.a.	n.a.
39.2	n.a.	n.a.	n.a.
39.4	3.5	0.4	1.5
39.8	1.3	0.2	0.6
40.0	4.5	1.0	2.0
40.2	n.a.	n.a.	n.a.
41	2.0	0.2	0.8
41.6	n.a.	n.a.	n.a.
41.8	n.a.	n.a.	n.a.
42.0	n.a.	n.a.	n.a.
42.2	n.a.	n.a.	n.a.
42.2	2.7	0.3	1.1
42.4	n.a.	n.a.	n.a.
42.8	n.a.	n.a.	n.a.

Appendix

Depth [m]	Sum C ₂₇ steranes [μg/g TOC]	Sum C ₂₈ steranes [μg/g TOC]	Sum C ₂₉ steranes [μg/g TOC]
42.8	1.1	0.1	0.4
43.0	n.a.	n.a.	n.a.
43.2	1.5	0.4	0.6
43.4	0.4	0.2	0.2
43.6	n.a.	n.a.	n.a.
43.8	n.a.	n.a.	n.a.
44.2	n.a.	n.a.	n.a.
44.4	n.d.	n.d.	n.d.
44.8	n.d.	n.d.	n.d.
45.0	n.d.	n.d.	n.d.
45.2	n.a.	n.a.	n.a.
45.4	n.a.	n.a.	n.a.
45.6	n.a.	n.a.	n.a.
45.8	n.d.	n.d.	n.d.
46.0	1.4	0.4	0.6
46.2	n.d.	n.d.	n.d.
46.4	n.d.	n.d.	n.d.
46.8	4.4	0.9	1.2
47.0	n.a.	n.a.	n.a.
47.6	n.a.	n.a.	n.a.
47.8	n.a.	n.a.	n.a.
48.0	n.a.	n.a.	n.a.
48.2	n.d.	n.d.	n.d.
48.4	n.a.	n.a.	n.a.
48.8	4.5	n.d.	1.0
49.0	n.a.	n.a.	n.a.
49.2	n.a.	n.a.	n.a.
49.4	n.a.	n.a.	n.a.
49.6	n.a.	n.a.	n.a.

Table A- 7 Concentration of hopanoid thiophenes along the profile in μg/g TOC I 30-[2'-(5'-methylthienyl)-17α(H),21β(H)-hopane, II 31-(2'-thienyl)-17α(H),21β(H)-homohopane, V 30-[2'-(5'-methylthienyl)-17β(H),21β(H)-hopane, VI 31-(2'-thienyl)-17β(H),21β-(H)-homohopane

Depth[m]	I [μg/g TOC]	II [μg/g TOC]	V [μg/g TOC]	VI [μg/g TOC]
0.0	n.d.	n.d.	n.d.	n.d.
0.2	n.d.	n.d.	n.d.	n.d.
0.6	n.d.	n.d.	n.d.	n.d.
0.8	n.d.	n.d.	n.d.	n.d.
1.0	n.d.	n.d.	n.d.	n.d.
1.2	n.d.	n.d.	n.d.	n.d.
1.4	n.d.	n.d.	n.d.	n.d.
1.6	n.d.	n.d.	n.d.	n.d.
1.8	n.d.	n.d.	n.d.	n.d.
2.0	n.d.	n.d.	n.d.	n.d.
2.2	n.d.	n.d.	n.d.	n.d.
2.4	n.d.	n.d.	n.d.	n.d.
2.6	n.d.	n.d.	n.d.	n.d.

Depth[m]	I [$\mu\text{g/g TOC}$]	II [$\mu\text{g/g TOC}$]	V [$\mu\text{g/g TOC}$]	VI [$\mu\text{g/g TOC}$]
3.0	n.a.	n.a.	n.a.	n.a.
3.4	n.a.	n.a.	n.a.	n.a.
3.6	0.11	0.09	0.45	1.49
3.8	0.17	0.14	0.55	1.93
4.0	0.03	0.05	0.21	0.66
4.2	n.d.	0.03	0.28	0.69
4.4	n.d.	0.10	0.26	0.94
4.6	n.d.	0.03	0.15	0.33
4.8	n.a.	n.a.	n.a.	n.a.
5.4	0.03	0.03	0.09	0.35
5.6	n.d.	0.07	0.38	1.39
5.8	n.a.	n.a.	n.a.	n.a.
6.0	n.d.	0.02	0.13	0.40
6.2	n.d.	0.05	0.26	0.45
6.6	0.02	0.06	0.22	0.67
6.8	n.d.	0.06	0.28	0.93
7.0	n.d.	0.07	0.19	0.60
7.2	n.a.	n.a.	n.a.	n.a.
7.4	n.a.	n.a.	n.a.	n.a.
7.6	0.05	0.07	0.21	0.72
7.8	n.a.	n.a.	n.a.	n.a.
8.0	n.a.	n.a.	n.a.	n.a.
8.2	n.d.	0.07	0.39	1.37
8.4	n.a.	n.a.	n.a.	n.a.
8.6	n.a.	n.a.	n.a.	n.a.
8.8	n.a.	n.a.	n.a.	n.a.
9.0	n.d.	0.08	0.37	1.01
9.2	0.29	0.06	0.52	n.d.
9.4	0.02	0.06	0.08	2.28
9.6	0.04	0.06	0.23	0.67
9.8	n.a.	n.a.	n.a.	n.a.
10.0	n.d.	0.09	0.56	1.59
10.2	n.d.	0.08	0.15	1.01
10.4	0.04	0.04	0.16	0.43
10.8	n.a.	n.a.	n.a.	n.a.
11.0	n.a.	n.a.	n.a.	n.a.
11.2	n.a.	n.a.	n.a.	n.a.
11.4	n.d.	0.10	0.34	1.05
11.8	n.d.	0.12	0.40	1.21
12.0	n.a.	n.a.	n.a.	n.a.
12.2	n.d.	0.13	0.44	1.00
12.4	n.a.	n.a.	n.a.	n.a.
12.6	n.a.	n.a.	n.a.	n.a.
12.8	n.a.	n.a.	n.a.	n.a.
13.0	0.03	0.05	0.43	1.23
13.2	0.05	0.03	0.30	0.66
13.4	n.a.	n.a.	n.a.	n.a.
13.6	n.a.	n.a.	n.a.	n.a.
13.8	n.a.	n.a.	n.a.	n.a.
14.0	n.a.	n.a.	n.a.	n.a.

Appendix

Depth[m]	I [$\mu\text{g/g TOC}$]	II [$\mu\text{g/g TOC}$]	V [$\mu\text{g/g TOC}$]	VI [$\mu\text{g/g TOC}$]
14.2	0.06	0.12	0.23	0.82
14.4	0.09	0.12	0.32	0.92
14.6	n.a.	n.a.	n.a.	n.a.
14.8	n.a.	n.a.	n.a.	n.a.
15.0	n.a.	n.a.	n.a.	n.a.
15.2	n.a.	n.a.	n.a.	n.a.
15.4	n.a.	n.a.	n.a.	n.a.
15.6	n.a.	n.a.	n.a.	n.a.
16.0	0.04	0.12	0.38	1.16
16.2	0.07	0.17	0.56	1.32
16.4	n.a.	n.a.	n.a.	n.a.
16.6	n.a.	n.a.	n.a.	n.a.
16.8	n.a.	n.a.	n.a.	n.a.
17.0	n.a.	n.a.	n.a.	n.a.
17.6	n.a.	n.a.	n.a.	n.a.
17.8	n.a.	n.a.	n.a.	n.a.
18.0	n.d.	0.05	0.19	0.39
18.2	0.08	0.18	0.53	1.43
18.6	n.a.	n.a.	n.a.	n.a.
18.8	n.a.	n.a.	n.a.	n.a.
19.0	n.a.	n.a.	n.a.	n.a.
19.4	n.a.	n.a.	n.a.	n.a.
19.6	n.a.	n.a.	n.a.	n.a.
20.0	n.a.	n.a.	n.a.	n.a.
20.2	n.a.	n.a.	n.a.	n.a.
20.4	n.a.	n.a.	n.a.	n.a.
20.6	0.03	0.05	0.23	#NV
20.8	n.a.	n.a.	n.a.	n.a.
21.0	n.a.	n.a.	n.a.	n.a.
21.2	0.13	0.04	1.02	2.57
21.4	n.a.	n.a.	n.a.	n.a.
21.8	n.a.	n.a.	n.a.	n.a.
22.0	n.a.	n.a.	n.a.	n.a.
22.4	n.a.	n.a.	n.a.	n.a.
22.6	0.08	0.14	0.46	1.20
22.8	n.a.	n.a.	n.a.	n.a.
23.0	n.a.	n.a.	n.a.	n.a.
23.2	n.a.	n.a.	n.a.	n.a.
23.4	n.a.	n.a.	n.a.	n.a.
23.6	0.08	0.12	0.71	1.67
23.8	n.a.	n.a.	n.a.	n.a.
24.0	n.d.	n.d.	n.d.	n.d.
24.2	n.a.	n.a.	n.a.	n.a.
24.4	n.a.	n.a.	n.a.	n.a.
24.6	n.a.	n.a.	n.a.	n.a.
24.8	n.d.	n.d.	n.d.	n.d.
25.0	n.a.	n.a.	n.a.	n.a.
25.4	0.19	0.29	0.96	2.50
25.6	0.06	0.09	1.02	2.37
25.8	0.12	0.16	1.16	3.11

Depth[m]	I [$\mu\text{g/g TOC}$]	II [$\mu\text{g/g TOC}$]	V [$\mu\text{g/g TOC}$]	VI [$\mu\text{g/g TOC}$]
26.0	0.19	0.15	1.36	3.19
26.2	0.29	0.24	1.64	3.80
26.4	n.a.	n.a.	n.a.	n.a.
26.6	n.d.	n.d.	0.48	0.81
26.8	0.06	0.17	0.45	1.00
27.2	0.08	0.11	0.36	0.79
27.4	0.06	0.08	0.22	0.57
27.6	0.09	0.09	0.26	0.64
27.8	0.05	0.07	0.21	0.49
28.0	n.d.	n.d.	n.d.	n.d.
28.2	n.d.	0.05	0.10	0.40
28.4	n.d.	0.06	0.08	0.39
28.6	n.a.	n.a.	n.a.	n.a.
28.8	0.09	0.16	0.46	1.36
29.0	0.10	0.13	0.43	1.12
29.4	0.08	0.11	0.51	1.23
29.6	0.10	0.14	1.06	2.42
29.8	0.13	0.13	0.32	0.89
30.0	0.04	0.13	0.69	1.67
30.2	n.a.	n.a.	n.a.	n.a.
30.4	0.09	0.24	1.03	2.11
30.6	n.a.	n.a.	n.a.	n.a.
30.8	0.09	0.11	0.20	0.52
31.0	0.04	0.08	0.14	0.40
31.2	0.05	0.10	0.64	1.12
31.4	0.06	0.25	0.13	1.72
31.6	0.08	0.08	0.26	0.64
31.8	n.a.	n.a.	n.a.	n.a.
32.0	n.a.	n.a.	n.a.	n.a.
32.2	0.23	0.15	0.49	1.06
32.4	0.17	0.10	0.35	0.86
32.6	0.04	0.08	0.15	0.37
32.8	0.03	0.09	0.21	0.54
33.0	0.13	0.19	0.89	1.86
33.2	0.03	0.05	0.34	0.75
33.4	n.a.	n.a.	n.a.	n.a.
33.6	0.05	0.09	0.16	0.56
33.8	0.10	0.14	0.57	1.48
34.0	0.04	0.05	0.19	0.31
34.2	0.07	0.04	#NV	0.99
34.4	0.15	0.11	1.60	3.55
34.6	0.11	0.15	0.56	1.52
34.8	0.08	0.19	0.54	1.34
35.0	0.12	0.18	0.58	1.21
35.2	n.a.	n.a.	n.a.	n.a.
35.4	0.12	0.26	0.55	1.24
35.6	n.d.	n.d.	0.33	0.28
36.0	n.a.	n.a.	n.a.	n.a.
36.2	n.a.	n.a.	n.a.	n.a.
36.6	0.02	0.04	0.11	0.24

Appendix

Depth[m]	I [$\mu\text{g/g TOC}$]	II [$\mu\text{g/g TOC}$]	V [$\mu\text{g/g TOC}$]	VI [$\mu\text{g/g TOC}$]
37.0	0.07	0.10	0.12	0.32
37.4	0.01	0.04	0.11	0.24
37.6	0.12	0.26	0.72	1.71
38.4	0.03	0.13	0.32	0.69
38.6	0.11	0.23	0.37	0.85
38.8	0.10	0.29	0.71	1.59
39.0	n.a.	n.a.	n.a.	n.a.
39.2	n.a.	n.a.	n.a.	n.a.
39.4	0.18	0.36	0.62	1.39
39.8	0.10	0.26	0.55	1.49
40.0	0.10	0.84	0.28	0.71
40.2	n.a.	n.a.	n.a.	n.a.
41.0	0.22	0.13	1.60	3.32
41.6	n.a.	n.a.	n.a.	n.a.
41.8	n.a.	n.a.	n.a.	n.a.
42.0	n.a.	n.a.	n.a.	n.a.
42.2	n.a.	n.a.	n.a.	n.a.
42.2	0.15	0.29	1.14	2.01
42.4	n.a.	n.a.	n.a.	n.a.
42.8	n.a.	n.a.	n.a.	n.a.
42.8	0.07	0.13	0.20	0.45
43.0	n.a.	n.a.	n.a.	n.a.
43.2	0.07	0.21	1.06	1.99
43.4	n.d.	n.d.	0.15	0.43
43.6	n.d.	n.d.	n.d.	n.d.
43.8	n.d.	n.d.	0.31	0.87
44.2	0.43	n.d.	0.33	0.68
44.4	n.d.	n.d.	n.d.	n.d.
44.8	n.d.	n.d.	n.d.	n.d.
45.0	n.d.	n.d.	n.d.	n.d.
45.2	n.d.	n.d.	n.d.	n.d.
45.4	n.d.	n.d.	n.d.	n.d.
45.6	n.d.	n.d.	n.d.	n.d.
45.8	n.d.	n.d.	n.d.	n.d.
46.0	n.d.	0.06	n.d.	n.d.
46.2	n.d.	n.d.	n.d.	n.d.
46.4	n.d.	n.d.	n.d.	n.d.
46.8	n.d.	0.05	n.d.	n.d.
47.6	n.a.	n.a.	n.a.	n.a.
47.8	n.a.	n.a.	n.a.	n.a.
48.0	n.a.	n.a.	n.a.	n.a.
48.2	n.d.	n.d.	n.d.	n.d.
48.4	n.a.	n.a.	n.a.	n.a.
48.8	n.d.	0.06	n.d.	n.d.
49.0	n.a.	n.a.	n.a.	n.a.
49.2	n.a.	n.a.	n.a.	n.a.
49.4	n.a.	n.a.	n.a.	n.a.
49.6	n.a.	n.a.	n.a.	n.a.

Table A-8 Depth, TON, Pr/Ph, C/N, $\delta^{15}\text{N}_{\text{org}}$ and $\delta^{13}\text{C}_{\text{org}}$ records of the studied sequence.

Depth [m]	TON [wt. %]	C/N	Pr/Ph	$\delta^{15}\text{N}_{\text{org}}$ [‰]	$\delta^{13}\text{C}_{\text{org}}$ [‰]
0,0	n.d.	n.d.	n.d.	n.a.	n.a.
0,2	0,02	6,27	n.d.	6,69	-26,64
0,6	n.d.	n.d.	n.d.	n.a.	n.a.
0,8	n.d.	n.d.	n.d.	n.a.	n.a.
1,0	0,03	6,80	n.d.	6,68	-26,68
1,2	n.a.	n.a.	n.d.	n.a.	n.a.
1,2	n.a.	n.a.	n.d.	n.a.	n.a.
1,4	n.a.	n.a.	1,8	n.a.	n.a.
1,6	n.a.	n.a.	n.d.	n.a.	n.a.
1,8	n.a.	n.a.	n.d.	n.a.	n.a.
2,0	0,03	6,25	n.d.	7,45	-26,53
2,0	n.a.	n.a.	n.a.	n.a.	n.a.
2,2	n.a.	n.a.	n.a.	n.a.	n.a.
2,4	0,06	13,89	n.d.	6,64	-27,90
2,6	n.a.	n.a.	n.a.	n.a.	n.a.
2,80	0,06	9,89	n.d.	6,99	-26,78
3,00	0,23	25,22	n.d.	5,30	-28,49
3,20	n.a.	n.a.	n.d.	n.a.	n.a.
3,20	n.a.	n.a.	n.d.	n.a.	n.a.
3,40		26,46	n.d.	n.a.	n.a.
3,60	n.a.	n.a.	n.a.	n.a.	n.a.
3,80	n.a.	n.a.	0,3	n.a.	n.a.
4,00	0,27	26,04	0,2	5,62	-28,41
4,20	n.a.	n.a.	n.a.	n.a.	n.a.
4,40	0,31	26,89	n.a.	5,01	-28,70
4,60	n.a.	n.a.	n.a.	n.a.	n.a.
4,80	n.a.	n.a.	n.a.	n.a.	n.a.
5,00	0,30	24,03	n.a.	5,28	-28,33
5,20	n.a.	n.a.	0,2	n.a.	n.a.
5,40	n.a.	n.a.	0,6	n.a.	n.a.
5,60	0,32	26,63	n.a.	5,50	-28,67
5,80	n.a.	n.a.	n.a.	n.a.	n.a.
6,00	n.a.	n.a.	0,5	n.a.	n.a.
6,20	n.a.	n.a.	n.a.	n.a.	n.a.
6,40	n.a.	n.a.	n.a.	n.a.	n.a.
6,60	n.a.	n.a.	n.a.	n.a.	n.a.
6,80	n.a.	n.a.	n.a.	n.a.	n.a.
7,00	0,26	27,17	n.a.	5,09	-28,50
7,20	n.a.	n.a.	n.a.	n.a.	n.a.
7,40	n.a.	n.a.	0,3	n.a.	n.a.

Appendix

Depth [m]	TON [wt. %]	C/N	Pr/Ph	$\delta^{15}\text{N}_{\text{org}}$ [‰]	$\delta^{13}\text{C}_{\text{org}}$ [‰]
7,60	n.a.	n.a.	n.a.	n.a.	n.a.
7,80	n.a.	n.a.	n.a.	n.a.	n.a.
8,00	n.a.	n.a.	0,6	n.a.	n.a.
8,20	n.a.	n.a.	n.a.	n.a.	n.a.
8,40	n.a.	n.a.	n.a.	n.a.	n.a.
8,60	n.a.	n.a.	n.a.	n.a.	n.a.
8,80	n.a.	n.a.	0,3	n.a.	n.a.
9,00	0,20	27,77	0,6	5,76	-28,42
9,20	0,22	26,85	0,3	6,55	-28,71
9,40	n.a.	n.a.	n.a.	n.a.	n.a.
9,60	n.a.	n.a.	n.a.	n.a.	n.a.
9,80	0,27	28,09	0,6	5,40	-28,40
10,00	n.a.	n.a.	n.a.	n.a.	n.a.
10,20	n.a.	n.a.	0,2	n.a.	n.a.
10,60	n.a.	n.a.	n.a.	n.a.	n.a.
10,80	n.a.	n.a.	n.a.	n.a.	n.a.
11,00	0,26	27,66	n.a.	5,50	-28,49
11,20	n.a.	n.a.	n.a.	n.a.	n.a.
11,60	n.a.	n.a.	0,5	n.a.	n.a.
11,80	n.a.	n.a.	n.a.	n.a.	n.a.
12,00	n.a.	n.a.	0,4	n.a.	n.a.
12,20	n.a.	n.a.	n.a.	n.a.	n.a.
12,20	n.a.	n.a.	n.a.	n.a.	n.a.
12,40	n.a.	n.a.	n.a.	n.a.	n.a.
12,60	n.a.	n.a.	n.a.	n.a.	n.a.
12,80	n.a.	n.a.	0,5	n.a.	n.a.
13,00	0,20	27,38	0,6	5,16	-28,90
13,20	n.a.	n.a.	n.a.	n.a.	n.a.
13,40	n.a.	n.a.	n.a.	n.a.	n.a.
13,60	n.a.	n.a.	n.a.	n.a.	n.a.
13,80	n.a.	n.a.	n.a.	n.a.	n.a.
14,00	n.a.	n.a.	0,4	n.a.	n.a.
14,20	n.a.	n.a.	0,5	n.a.	n.a.
14,40	0,36	29,29	n.a.	5,59	-29,16
14,60	n.a.	n.a.	n.a.	n.a.	n.a.
14,80	n.a.	n.a.	n.a.	n.a.	n.a.
15,00	0,35	28,97	n.a.	5,50	-28,96
15,20	n.a.	n.a.	n.a.	n.a.	n.a.
15,40	n.a.	n.a.	n.a.	n.a.	n.a.
15,80	n.a.	n.a.	0,5	n.a.	n.a.
16,00	n.a.	n.a.	0,4	n.a.	n.a.
16,20	n.a.	n.a.	n.a.	n.a.	n.a.

Depth [m]	TON [wt. %]	C/N	Pr/Ph	$\delta^{15}\text{N}_{\text{org}}$ [‰]	$\delta^{13}\text{C}_{\text{org}}$ [‰]
16,40	n.a.	n.a.	n.a.	n.a.	n.a.
16,60	n.a.	n.a.	n.a.	n.a.	n.a.
16,80	n.a.	n.a.	n.a.	n.a.	n.a.
17,00	0,40	28,07	n.a.	4,77	-28,91
17,40	n.a.	n.a.	n.a.	n.a.	n.a.
17,60	n.a.	n.a.	n.a.	n.a.	n.a.
17,80	n.a.	n.a.	0,3	n.a.	n.a.
18,00	n.a.	n.a.	0,5	n.a.	n.a.
18,20	n.a.	n.a.	n.a.	n.a.	n.a.
18,40	n.a.	n.a.	0,4	n.a.	n.a.
18,60	n.a.	n.a.	n.a.	n.a.	n.a.
18,80	n.a.	n.a.	n.a.	n.a.	n.a.
18,80	n.a.	n.a.	n.a.	n.a.	n.a.
19,00	0,44	29,39	n.a.	4,87	-28,73
19,20	n.a.	n.a.	n.a.	n.a.	n.a.
19,40	0,41	29,85	n.a.	4,59	-28,67
19,80	n.a.	n.a.	n.a.	n.a.	n.a.
20,00	n.a.	n.a.	n.a.	n.a.	n.a.
20,20	n.a.	n.a.	n.a.	n.a.	n.a.
20,40	n.a.	n.a.	0,5	n.a.	n.a.
20,60	n.a.	n.a.	n.a.	n.a.	n.a.
20,80	n.a.	n.a.	n.a.	n.a.	n.a.
21,00	0,28	28,05	0,6	5,90	-28,72
21,20	n.a.	n.a.	n.a.	n.a.	n.a.
21,40	n.a.	n.a.	n.a.	n.a.	n.a.
21,60	n.a.	n.a.	n.a.	n.a.	n.a.
21,80	n.a.	n.a.	n.a.	n.a.	n.a.
22,00	n.a.	n.a.	n.a.	n.a.	n.a.
22,20	n.a.	n.a.	n.a.	n.a.	n.a.
22,40	n.a.	n.a.	0,5	n.a.	n.a.
22,60	n.a.	n.a.	n.a.	n.a.	n.a.
22,80	n.a.	n.a.	n.a.	n.a.	n.a.
23,00	0,28	29,46	n.a.	4,42	-28,82
23,20	n.a.	n.a.	n.a.	n.a.	n.a.
23,40	n.a.	n.a.	0,5	n.a.	n.a.
23,60	n.a.	n.a.	n.a.	n.a.	n.a.
23,80	n.a.	n.a.	n.a.	n.a.	n.a.
24,00	n.a.	n.a.	n.a.	n.a.	n.a.
24,20	n.a.	n.a.	n.a.	n.a.	n.a.
24,40	n.a.	n.a.	n.a.	n.a.	n.a.
24,60	n.a.	n.a.	0,4	n.a.	n.a.
24,80	n.a.	n.a.	n.a.	n.a.	n.a.

Appendix

Depth [m]	TON [wt. %]	C/N	Pr/Ph	$\delta^{15}\text{N}_{\text{org}}$ [‰]	$\delta^{13}\text{C}_{\text{org}}$ [‰]
25,00	n.a.	n.a.	n.a.	n.a.	n.a.
25,20	0,35	27,55	n.a.	5,06	-28,20
25,40	n.a.	n.a.	0,5	n.a.	n.a.
25,60	n.a.	n.a.	0,6	n.a.	n.a.
25,80	n.a.	n.a.	0,5	n.a.	n.a.
26,00	0,28	28,95	0,6	4,90	-28,36
26,20	n.a.	n.a.	n.a.	n.a.	n.a.
26,40	n.a.	n.a.	n.a.	n.a.	n.a.
26,60	n.a.	n.a.	n.a.	n.a.	n.a.
27,00	0,28	27,56	0,5	5,06	-28,49
27,20	n.a.	n.a.	n.a.	n.a.	n.a.
27,40	n.a.	n.a.	0,7	n.a.	n.a.
27,60	n.a.	n.a.	0,6	n.a.	n.a.
27,80	n.a.	n.a.	n.a.	n.a.	n.a.
28,00	n.a.	n.a.	n.a.	n.a.	n.a.
28,20	0,36	27,81	n.a.	4,59	-28,39
28,40	n.a.	n.a.	n.a.	n.a.	n.a.
28,60	n.a.	n.a.	n.a.	n.a.	n.a.
28,80	n.a.	n.a.	0,6	n.a.	n.a.
29,00	0,27	27,32	n.a.	4,69	-28,30
29,20	0,28	29,12	0,5	4,51	-28,47
29,40	n.a.	n.a.	0,4	n.a.	n.a.
29,60	n.a.	n.a.	0,3	n.a.	n.a.
29,80	n.a.	n.a.	0,4	n.a.	n.a.
30,00	n.a.	n.a.	n.a.	n.a.	n.a.
30,20	n.a.	n.a.	0,5	n.a.	n.a.
30,40	n.a.	n.a.	n.a.	n.a.	n.a.
30,60	n.a.	n.a.	0,4	n.a.	n.a.
30,80	n.a.	n.a.	n.a.	n.a.	n.a.
31,00	0,36	29,72	0,4	5,12	-28,63
31,20	n.a.	n.a.	n.a.	n.a.	n.a.
31,40	n.a.	n.a.	0,6	n.a.	n.a.
31,60	n.a.	n.a.	0,5	n.a.	n.a.
31,80	n.a.	n.a.	n.a.	n.a.	n.a.
32,00	n.a.	n.a.	n.a.	n.a.	n.a.
32,20	n.a.	n.a.	0,4	n.a.	n.a.
32,40	n.a.	n.a.	n.a.	n.a.	n.a.
32,60	n.a.	n.a.	n.a.	n.a.	n.a.
32,80	n.a.	n.a.	0,3	n.a.	n.a.
33,00	0,31	32,69	0,2	4,52	-28,71
33,20	n.a.	n.a.	n.a.	n.a.	n.a.
33,40	n.a.	n.a.	0,5	n.a.	n.a.

Depth [m]	TON [wt. %]	C/N	Pr/Ph	$\delta^{15}\text{N}_{\text{org}}$ [‰]	$\delta^{13}\text{C}_{\text{org}}$ [‰]
33,60	n.a.	n.a.	0,6	n.a.	n.a.
33,80	n.a.	n.a.	0,5	n.a.	n.a.
34,00	n.a.	n.a.	0,5	n.a.	n.a.
34,20	n.a.	n.a.	0,3	n.a.	n.a.
34,40	n.a.	n.a.	n.a.	n.a.	n.a.
34,60	n.a.	n.a.	0,3	n.a.	n.a.
34,80	0,34	31,52	n.a.	5,14	-28,81
35,00	0,30	32,90	n.a.	4,78	-28,61
35,20	n.a.	n.a.	0,3	n.a.	n.a.
35,40	n.a.	n.a.	n.a.	n.a.	n.a.
35,80	n.a.	n.a.	n.a.	n.a.	n.a.
36,00	n.a.	n.a.	n.a.	n.a.	n.a.
36,20	n.a.	n.a.	n.a.	n.a.	n.a.
36,40	n.a.	n.a.	0,3	n.a.	n.a.
36,60	n.a.	n.a.	n.a.	n.a.	n.a.
36,80	n.a.	n.a.	0,4	n.a.	n.a.
37,00	0,40	29,80	n.a.	4,48	-28,35
37,20	n.a.	n.a.	0,4	n.a.	n.a.
37,40	n.a.	n.a.	0,3	n.a.	n.a.
37,40	n.a.	n.a.	0,3	n.a.	n.a.
37,80	n.a.	n.a.	n.a.	n.a.	n.a.
38,00	n.a.	n.a.	n.a.	n.a.	n.a.
38,20	n.a.	n.a.	0,5	n.a.	n.a.
38,40	n.a.	n.a.	0,3	n.a.	n.a.
38,60	n.a.	n.a.	0,3	n.a.	n.a.
38,80	n.a.	n.a.	n.a.	n.a.	n.a.
39,00	0,53	32,30	n.a.	4,74	-29,01
39,20	n.a.	n.a.	0,1	n.a.	n.a.
39,60	n.a.	n.a.	0,2	n.a.	n.a.
39,80	n.a.	n.a.	n.d.	n.a.	n.a.
40,00	0,54	32,22	n.a.	4,72	-29,51
40,20	n.a.	n.a.	n.a.	n.a.	n.a.
40,40	n.a.	n.a.	n.a.	n.a.	n.a.
40,60	n.a.	n.a.	n.a.	n.a.	n.a.
40,80	0,56	32,14	0,2	4,81	-28,31
41,00	0,45	31,74	n.a.	4,66	-28,43
41,20	n.a.	n.a.	n.a.	n.a.	n.a.
41,40	n.a.	n.a.	n.a.	n.a.	n.a.
41,60	n.a.	n.a.	n.a.	n.a.	n.a.
41,60	n.a.	n.a.	n.a.	n.a.	n.a.
41,80	n.a.	n.a.	n.a.	n.a.	n.a.
42,00	n.a.	n.a.	0,3	n.a.	n.a.

Appendix

Depth [m]	TON [wt. %]	C/N	Pr/Ph	$\delta^{15}\text{N}_{\text{org}}$ [‰]	$\delta^{13}\text{C}_{\text{org}}$ [‰]
42,20	n.a.	n.a.	n.a.	n.a.	n.a.
42,40	n.a.	n.a.	n.a.	n.a.	n.a.
42,60	n.a.	n.a.	0,1	n.a.	n.a.
42,80	0,07	31,79	n.d.	3,71	-28,71
43,00	0,39	31,71	n.d.	4,01	-28,97
43,20	n.a.	n.a.	n.d.	n.a.	n.a.
43,40	0,33	26,93	n.d.	4,53	-29,25
43,80	0,05	28,85	0,4	3,33	-29,00
44,00	0,08	29,75	n.d.	3,40	-29,32
44,40	n.a.	n.a.	n.d.	n.a.	n.a.
44,40	0,14	28,65	n.d.	3,54	-29,49
44,60	n.a.	n.a.	n.d.	n.a.	n.a.
44,80	0,09	25,72	n.d.	3,59	-28,47
45,00	n.a.	n.a.	n.d.	n.a.	n.a.
45,20	0,12	24,96	n.d.	3,53	-28,52
45,40	n.a.	n.a.	n.d.	n.a.	n.a.
45,60	n.a.	n.a.	n.d.	n.a.	n.a.
45,80	n.a.	n.a.	n.d.	n.a.	n.a.
46,00	0,06	26,28	n.d.	3,51	-28,59
46,20	0,05	25,55	n.d.	2,96	-28,62
46,40	0,16	28,41	0,5	2,97	-29,00
46,80	0,09	28,51	n.a.	3,18	-28,67
47,00	n.a.	n.a.	n.a.	n.a.	n.a.
47,20	0,08	27,29	n.a.	2,81	-29,06
47,40	0,15	28,47	n.a.	3,57	-28,66
47,60	0,42	24,90	n.a.	2,96	-29,69
47,80	0,04	26,43	n.a.	3,92	-28,62
48,00	n.a.	n.a.	n.a.	n.a.	n.a.
48,20	0,04	27,25	n.a.	3,38	-28,85
48,40	n.a.	n.a.	0,7	n.a.	n.a.
48,40	n.a.	n.a.	0,7	n.a.	n.a.
48,60	n.a.	n.a.	n.a.	n.a.	n.a.
48,80	0,06	28,02	n.a.	2,98	-28,83
49,00	n.a.	n.a.	n.a.	n.a.	n.a.
49,20	n.a.	n.a.	n.a.	n.a.	n.a.
49,40	0,02		n.a.	3,79	-28,07

Publications

Alsenz, H., Zereini, F., Wiseman, C.L.S., Püttmann, W. 2009. Analysis of palladium concentrations in airborne particulate matter with reductive co-precipitation, He collision gas, and ID-ICP-Q-MS. *Anal. Bioanal. Chem.* 395: 1919-1927.

Zereini, F., Alsenz, H., Wiseman, C. & Püttmann, W., Reimer, E., Schleyer, R., Bieber, E., Wallasch, M. 2012. Platinum group elements (Pt, Pd, Rh) in airborne particulate matter in rural vs. urban areas of Germany: Concentrations and spatial patterns of distribution. *Sci. Total Environ.* 416: 261-268.

Schneider-Mor, A., Alsenz, H., Ashckenazi-Polivoda, S., Illner, P., Abramovich, S., Feinstein, S., Almogi-Labin, A., Berner, Z., Püttmann, W. 2012. Paleooceanographic reconstruction of the Late Cretaceous oil shale of the Negev, Israel: integration of geochemical, and stable isotope records of the organic matter. *Paleogeogr. Paleoclimatol. Paleoecol.* 319–320: 46-57.

Alsenz, H., Regnery, J., Ashckenazi-Polivoda, S., Meilijson, A., Ron-Yankovich, L., Abramovich, S., Illner, P., Almogi-Labin, A., Feinstein, S., Berner, Z., Püttmann, W. 2013. Sea surface temperature record of a Late Cretaceous tropical Southern Tethys upwelling system. *Paleogeogr. Paleoclimatol. Paleoecol.* 392: 350-358.

Jacobasch, C., Völker, C., Giebner, S., Völker, J., Alsenz, H., Potouridis, T., Heidenreich, H., Kayser, G., Oehlmann, J., Oetken, M. 2014. Long-term effects of nanoscaled titanium dioxide on the cladoceran *Daphnia magna* over six generations. *Environ. Pollut.* 186: 180-186.

Meilijson, A., Ashckenazi-Polivoda, S., Ron-Yankovich, L., Illner, P., Alsenz, H., Speijer, R.P., Almogi-Labin, A., Feinstein, S., Berner, Z., Püttmann, W., Abramovich, S. 2014. Chronostratigraphy of the Upper Cretaceous high productivity sequence of the southern Tethys, Israel. *Cretaceous Res.* 50: 187-213.

Potouridis, T., Völker, J., Alsenz, H., Oetken, M., Püttmann, W. 2014. Using ICP-qMS to trace the uptake of nanoscale titanium dioxide by microalgae—potential disadvantages of vegetable reference material. *Anal. Bioanal. Chem.* 406: 2495-2502.

Alsenz, H., Illner, P., Ashckenazi-Polivoda, S., Meilijson, A., Abramovich, S., Feinstein, S., Almogi-Labin, A., Berner, Z., Püttmann, W. 2015. Geochemical evidence for the link between sulfate re-duction, sulfide oxidation and phosphate accumulation in a Late Cretaceous upwelling system. *Geochem. Trans.* accepted

Curriculum Vitae

Persönliche Daten

Name: Heiko Alsenz
Geburtsdatum: 25.11.1977
Geburtsort: Bingen am Rhein, Deutschland
Staatsangehörigkeit: deutsch
Familienstand: ledig

Promotion/Studium

02/2008 bis 08/2014 Doktorand am Institut für Atmosphäre und Umwelt,
Abteilung Umweltanalytik an der Goethe-Universität
Frankfurt am Main
Betreuer: Prof. Dr. Wilhelm Püttmann

04/2001 bis 12/2007 Diplomstudiengang Chemie an der Goethe-Universität
Frankfurt am Main
Betreuer: Prof. Dr. Wilhelm Püttmann

10/2000 bis 03/2001 Studium der Informatik an der Goethe-Universität
Frankfurt am Main

Berufstätigkeit

06/2000 bis 08/2000 Mainzer Volksbank eG (Filiale Ingelheim)
Kundenservice und Anlageberatung

Berufsausbildung
08/1998 bis 06/2000 Ausbildung zum Bankkaufmann bei der Mainzer
Volksbank eG

Schule und Wehrdienst

09/1997 bis 06/1998 Grundwehrdienst beim 5. Wachbataillon BMVg

08/1994 bis 6/1997 Sebastian-Münster-Gymnasium in Ingelheim